Dissertation

submitted to the

Combined Faculty of Mathematics, Engineering and Natural Sciences

of Heidelberg University, Germany

for the degree of

Doctor of Natural Sciences

Put forward by

*Daniel Spitz*

born in: *Blaubeuren*

Oral examination: *July, 2023*

**Topological data analysis and geometry in quantum field dynamics**

Referees:                                   *Prof. Dr. Jürgen Berges*
*Prof. Dr. Manfred Salmhofer*

HEIDELBERG UNIVERSITY

DOCTORAL THESIS

# Topological data analysis and geometry in quantum field dynamics

Author: *Daniel Spitz*                    Supervisor: *Prof. Dr. Jürgen Berges*

Dissertation

submitted to the

Combined Faculty of Mathematics, Engineering and Natural Sciences

of Heidelberg University, Germany

for the degree of

Doctor of Natural Sciences

May, 2023

Physics is not the science of the laws of nature.
Physics is mathematical model building to quantitatively
describe the human perception of nature.

# *Abstract*

**Topological data analysis and geometry in quantum field dynamics**

Many non-perturbative phenomena in quantum field theories are driven or accompanied by non-local excitations, whose dynamical effects can be intricate but difficult to study. Amongst others, this includes diverse phases of matter, anomalous chiral behavior, and non-equilibrium phenomena such as non-thermal fixed points and thermalization. Topological data analysis can provide non-local order parameters sensitive to numerous such collective effects, giving access to the topology of a hierarchy of complexes constructed from given data.

This dissertation contributes to the study of topological data analysis and geometry in quantum field dynamics. A first part is devoted to far-from-equilibrium time evolutions and the thermalization of quantum many-body systems. We discuss the observation of dynamical condensation and thermalization of an easy-plane ferromagnet in a spinor Bose gas, which goes along with the build-up of long-range order and superfluidity. In real-time simulations of an over-occupied gluonic plasma we show that observables based on persistent homology provide versatile probes for universal dynamics off equilibrium. Related mathematical effects such as a packing relation between the occurring persistent homology scaling exponents are proven in a probabilistic setting.

In a second part, non-Abelian features of gauge theories are studied via topological data analysis and geometry. The structure of confining and deconfining phases in non-Abelian lattice gauge theory is investigated using persistent homology, which allows for a comprehensive picture of confinement. More fundamentally, four-dimensional space-time geometries are considered within real projective geometry, to which canonical quantum field theory constructions can be extended. This leads to a derivation of much of the particle content of the Standard Model.

The works discussed in this dissertation provide a step towards a geometric understanding of non-perturbative phenomena in quantum field theories, and showcase the promising versatility of topological data analysis for statistical and quantum physics studies.

# *Zusammenfassung*

**Topologische Datenanalyse und Geometrie in der Dynamik von Quantenfeldern**

Nicht-lokale Anregungen sind eine treibende Kraft für zahlreiche nicht-perturbative Phänomene in Quantenfeldtheorien oder deren Begleiterscheinung und können komplexe dynamische Effekte mit sich bringen, jedoch schwer zu untersuchen sein. Unter anderem umfasst dies vielfältige Phasen von Materie, anomales chirales Verhalten und Nicht-gleichgewichtsphänomene wie nicht-thermische Fixpunkte oder Thermalisierung. Die topologische Datenanalyse kann nicht-lokale Ordnungsparameter zur Verfügung stellen, die sensitiv auf zahlreiche solcher kollektiven Effekte reagieren und die Topologie einer Hierarchie von Komplexen zugänglich machen.

Diese Dissertation trägt zum Verständnis der topologischen Datenanalyse und Geometrie in der Dynamik von Quantenfeldern bei. In einem ersten Teil werden Zeitevolutionen fern des Gleichgewichts sowie die Thermalisierung von Quantenvielteilchensystemen behandelt. Wir diskutieren die Beobachtung von dynamischer Kondensation und Thermalisierung eines *easy-plane* (in der Ebene) Ferromagneten in einem Spin-behafteten Bose Gas, die mit dem Aufbau von langreichweitiger Ordnung und Suprafluidität einhergehen. In reell-zeitigen Simulationen eines überbesetzten gluonischen Plasmas zeigen wir, dass Observablen basierend auf persistenter Homologie vielseitige Sensoren für universelles Verhalten außerhalb des Gleichgewichts darstellen. Damit einhergehende mathematische Effekte wie etwa eine Packungsrelation zwischen auftretenden homologischen Skalierungsexponenten werden in probabilistischem Rahmen bewiesen.

Im zweiten Teil werden nicht-Abelsche Besonderheiten von Eichtheorien mittels topologischer Datenanalse und Geometrie untersucht. In nicht-Abelschen Gittereichtheorien wird mit persistenter Homologie die Struktur konfinierender und dekonfinierender Phasen beleuchtet, was ein umfassendes Bild von *confinement* erzeugt. Auf grundlegenderer Ebene können vierdimensionale Raumzeit-Geometrien innerhalb von reeller projektiver Geometrie behandelt werden, auf die kanonische Quantenfeldtheorie-Konstruktionen erweitert werden können. Dies führt zur Herleitung eines Großteils der Teilchen des Standardmodells.

Die Arbeiten, die innerhalb dieser Dissertation diskutiert werden, stellen einen Schritt hin zum geometrischen Verständnis nicht-perturbativer Phänomene in Quantenfeldtheorien dar. Sie zeigen exemplarisch die erfolgversprechende Vielseitigkeit topologischer Datenanalyse für Untersuchungen in statistischer und Quantenphysik.

# *List of publications*

Parts of this dissertation have been published in the following articles:

1. Spitz, D. and Wienhard, A., "The self-similar evolution of stationary point processes via persistent homology", arXiv: 2012.05751 [math.PR].

2. Prüfer, M., Spitz, D., Lannig, S., Strobel, H., Berges, J., and Oberthaler, M. K., "Condensation and thermalization of an easy-plane ferromagnet in a spinor Bose gas", *Nat. Phys.*, vol. 18, no. 12, pp. 1459–1463, 2022. arXiv: 2205.06188 [cond-mat.quant-gas].

3. Spitz, D., Urban, J. M., and Pawlowski, J. M., "Confinement in non-Abelian lattice gauge theory via persistent homology", *Phys. Rev. D*, vol. 107, no. 3, p. 034 506, 2023. arXiv: 2208.03955 [hep-lat].

4. Spitz, D., Boguslavski, K., and Berges, J., "Probing universal dynamics with topological data analysis in a gluonic plasma", *under review in Phys. Rev. D*, arXiv: 2303.08618 [hep-ph].

5. Spitz, D., "Standard Model gauge theory from projective geometries", *in preparation*, 2023.

Wherever content of these articles has been used for the present thesis, it is clearly stated at the beginning of each chapter, including a summary of my contributions to the collaborative research projects.

During my doctoral studies I was involved in the following publications that are not part of this dissertation, of which the first one contains the main results of my Master's thesis, and the second one is a popular scientific account related to Prüfer, Spitz, *et al.* 2022 above:

6. Spitz, D., Berges, J., Oberthaler, M. K., and Wienhard, A., "Finding self-similar behavior in quantum many-body dynamics via persistent homology", *SciPost Phys.*, vol. 11, no. 3, p. 060, 2021. arXiv: 2001.02616 [cond-mat.quant-gas].

7. Prüfer, M., Spitz, D., and Strobel, H., "Supraflüssigkeit mit Spin", *Physik in unserer Zeit*, vol. 54, no. 2, pp. 58–59, 2023.

# Contents

# Chapter 1

# Introduction

## 1.1 Motivation

The inconceivably complex and phenomenologically rich dynamics of physical systems on macroscopic scales provides the basis for many physical experiments. As a unified approach to model the related many-body physics, quantum field theory (QFT) has proven extraordinarily powerful. Its applicability ranges from high-energy particle physics and condensed matter physics to cosmology and astrophysics [8–12]. Quantum field theories can be formulated both for presumably fundamental degrees of freedom and for effective degrees of freedom [13]. This provides twofold challenges: (i) fundamental ingredients of quantum field theories, and (ii) the formation of effective degrees of freedom and their collective, macroscopic dynamics need to be understood.

Among the most successful scientific theories of all times and related to (i), the Standard Model of particle physics [14–16] describes the *status quo* of what has been experimentally verified regarding the elementary subatomic particles making up matter. The Standard Model is constructed from local symmetry principles, which give rise to gauge bosons mediating the strong and the electroweak forces. For instance, on everyday temperature scales the gluons of quantum chromodynamics (QCD) bind quarks into hadrons, and these in turn into atomic nuclei. Unstable atomic nuclei can radioactively decay into others via the weak force. Atomic nuclei are electromagnetically charged and attract electrons via the photons of quantum electrodynamics (QED), thus forming atoms.

The Standard Model cannot explain the observed occurrence of dark matter and comes with a range of theoretical difficulties such as the ultraviolet triviality of the Higgs sector and neutrino masses. All extension attempts, ranging from e.g. supersymmetry [17], grand unified theories [18], axions [19, 20] and sterile neutrinos [21], to the fundamental paradigm changes that string theory proposes [22, 23], have so far escaped experimental validation [24]. Despite the mentioned problems, this might hint at parts of the Standard Model being more fundamental than originally thought. A range of studies explored different possibilities to derive Standard Model structures (without vast extensions) from mathematical constructions with strong ties to space-time geometry, using e.g. non-commutative geometry [25, 26], the octonions [27–30], or Twistor theory [31]. A clarification of the link between space-time geometries and parts of the Standard Model appears crucial, also in light of the demand for a quantum theory of gravity.

Quantum field theories such as the Standard Model can give rise to a plethora of collective phenomena and related dynamics, which motivates (ii). In equilibrium this includes multifarious phases of matter, whose detection often requires non-local order parameters. For instance, strongly interacting nuclear matter can be in the hadronic phase, where quarks are confined into hadrons, or show exotic superconducting and superfluid behavior [32, 33]. The detection of confinement is facilitated, amongst others, by the (non-local) Polyakov loop. Providing another example, in condensed matter physics a zoo of topologically ordered phases is known [34], which come with long-range entanglement. Out of equilibrium the quantum many-body phenomenology is even richer. Instabilities [35–38] and non-thermal fixed points with their characteristic self-similar dynamics can appear [39–49], along with dynamical condensation [43, 44, 50, 51], for which particles transiently condense into (global) zero modes to form a Bose-Einstein condensate (BEC). Moreover, many quantum field theories can thermalize despite their unitary time evolution, steadily approaching thermodynamic expectation values primarily for lower-order correlation functions [52–55]. This goes along with partial memory loss [37] and entanglement growth [56–58].

The prediction of such collective dynamics of quantum particles provides extensive theoretical challenges, often based on the lack of understanding of the relevant, effective degrees of freedom and their dynamics. Yet, a detailed understanding of these is necessary to devise suitable effective theories for their description, ideally based on first principles derivations. An example is given by heavy-ion collisions at collider facilities such as the Large Hadron Collider (LHC) or the Relativistic Heavy-Ion Collider (RHIC). There, quark-gluon plasma (QGP) is created through the collision of atomic nuclei, which provides highly energetic, strongly correlated nuclear matter [59, 60]. Its description throughout the entire collision process calls for different theoretical approaches, from semi-classical to kinetic to hydrodynamic theories [38]. Prominently appearing in the chiral magnetic effect (CME) [61–64], non-local, non-perturbative excitations such as topological configurations can be of relevance for anomalous behavior in heavy-ion collisions. The detection of corresponding experimental signatures remains challenging [65]. This also applies to the identification of topological configurations in lattice simulations of this and related scenarios, which is often based on ambiguous cooling techniques [45, 66].

Versatile non-local probes for mechanisms and signatures of collective quantum field-theoretic phenomena are demanded. Observables based on topological data analysis (TDA) are promising in this regard. TDA provides flexible means to infer scale-resolved topological information from discrete data via a hierarchy of combinatorial objects. Persistent homology, the prevailing TDA tool, is numerically efficiently calculable [67] and comes with desirable mathematical properties such as stability with regard to input data perturbations [68, 69] as well as well-defined statistical limits [70] and large-volume asymptotics [71]. It has proven sensitive to the partly intricate phase structure of diverse physical models and can allow for the identification of corresponding non-local order parameters [72–80]. In particular, this can include strong persistent homology signatures of relevant physical scales with parametric dependences [6, 76–80].

## 1.2 Thesis overview

This dissertation is devoted to topological data analysis and geometry in quantum field dynamics. In a first part we study far-from-equilibrium time evolutions and the thermalization of quantum many-body systems. This includes an experiment-theory effort to understand the dynamics of an ultracold spinor Bose gas, and the study of topological observables in a simulated gluonic plasma out of equilibrium. We investigate dynamical self-similarity in persistent homology from a mathematical viewpoint.

A second part is dedicated to non-Abelian features in the dynamics of gauge theories in conjunction with geometry. Confinement is explored in a non-Abelian lattice gauge theory on Euclidean space-time through the lens of TDA. Further, we extend canonical quantum field-theoretical constructions to projective space-time geometries, which allows for the derivation of much of the particle content of the Standard Model.

In more detail, the individual chapters address the following.

In Chapter 2, *"Key physical concepts"*, a review of the physical concepts of relevance for this thesis is provided. This includes a brief introduction to the formulation of non-equilibrium quantum field theories and to gauge theories. An overview of collective phenomena out of equilibrium is given.

Chapter 3, *"Condensation and thermalization of an easy-plane ferromagnet in a spinor Bose gas"*, is devoted to the study of the thermalization dynamics of an easy-plane ferromagnet employing a homogeneous one-dimensional spinor Bose gas. We demonstrate the dynamic emergence of effective long-range coherence for the spin field and verify spin-superfluidity by experimentally testing Landau's criterion. The structure of one massive and two massless emerging modes is revealed, which is a consequence of explicit and spontaneous symmetry breaking. The experiments allow for the observation of the thermalization of the easy-plane ferromagnetic Bose gas, in agreement with a thermal prediction for the relevant momentum-resolved observables, obtained from an underlying microscopic model within the Bogoliubov approximation.

In Chapter 4, *"Probing universal dynamics with topological data analysis in a gluonic plasma"*, we study the non-equilibrium dynamics of pure $SU(2)$ lattice gauge theory in Minkowski space-time in a classical-statistical regime, where characteristic gluon occupancies are much larger than unity. In this strongly correlated system far from equilibrium, the correlations of energy and topological densities show self-similar behavior related to a turbulent cascade towards higher momentum scales. We employ persistent homology to infer topological features of the gluonic plasma via a hierarchy of simplicial and cubical complexes. All topological observables under investigation are manifestly gauge-invariant and shown to exhibit self-similar time evolution, which relate the spatial and temporal properties of the plasma in terms of universal scaling exponents and functions.

In Chapter 5, *"The self-similar evolution of stationary point processes via persistent homology"*, the persistent homology of point clouds is embedded into a probabilistic setting, exploiting the theory of point processes. We provide variants of ergodicity and investigate measures

on the space of persistence diagrams. In particular, we introduce the notion of self-similar scaling for persistence diagram expectation measures and prove a packing relation for the occurring dynamical scaling exponents. As a byproduct we generalize the strong law of large numbers for persistent Betti numbers, proven in [71] for averages over cubes, to arbitrary convex averaging sequences.

In Chapter 6, *"Confinement in non-Abelian lattice gauge theory via persistent homology"*, we investigate the structure of confining and deconfining phases in $\mathrm{SU}(2)$ lattice gauge theory via persistent homology. Specifically, we use filtrations by traced Polyakov loops, topological densities, holonomy Lie algebra fields, as well as electric and magnetic fields. This allows for a comprehensive picture of confinement. In particular, topological densities form spatial lumps, which show signatures of the classical probability distribution of instanton-dyons. Signatures of well-separated dyons located at random positions are encoded in holonomy Lie algebra fields, following the semi-classical temperature dependence of the instanton appearance probability. Debye screening discriminating between electric and magnetic fields is visible in persistent homology and pronounced at large gauge coupling. All employed constructions are gauge-invariant without a priori assumptions on the configurations under study.

In Chapter 7, *"Standard Model gauge theory from projective geometries"*, four-dimensional space-time geometries are considered within real projective geometry. This provides a mathematically well-defined framework to discuss their deformations and limits without the appearance of coordinate singularities. We introduce quantum fields that transform naturally under deformations and limits of geometries. Connections on the related projective frame bundles provide gauge fields with gauge group $\mathrm{PGL}_5\mathbb{R}$. Causality implies that only $\mathrm{P}(\mathrm{GL}_2\mathbb{R} \times \mathrm{GL}_3\mathbb{R}) \cong \mathbb{R}_{\neq 0} \times \mathrm{PGL}_2\mathbb{R} \times \mathrm{PGL}_3\mathbb{R}$ gauge bosons can interact non-trivially with other quantum fields. $\mathrm{P}(\mathrm{GL}_2\mathbb{R} \times 1) \cong \mathbb{R}_{\neq 0} \times \mathrm{PGL}_2\mathbb{R}$ gauge bosons break physical scale invariance, reminiscent of the Higgs mechanism. Irreducible fermionic quantum fields yield Dirac fermions which transform under the reduced gauge group $\mathrm{P}(\mathrm{GL}_2\mathbb{R} \times \mathrm{GL}_3\mathbb{R})$ analogous to Standard Model fermions under the Standard Model gauge group. It is conjectured that the projective setting facilitates renormalization of the model.

Chapter 8, *"Conclusions"*, provides a *résumé* of the main chapters. We discuss future research prospects. This includes both evident extensions to nearby research questions and proposals for more fundamental applications.

Except for Chapter 3, we employ units with $\hbar = c = k_B = 1$ throughout this thesis. Where applicable and sensible, parts of this dissertation are formulated in full mathematical rigor. In particular, this applies to Chapters 5 and 7.

# Chapter 2

# Key physical concepts

The application of methods from topological data analysis and geometry to quantum field dynamics provides an interdisciplinary research theme. We formulate quantum field theories for general non-equilibrium density operators, followed by gauge theories and related physical phenomena. While this introduction is restricted to the fundamentals, more elaborate introductions to non-equilibrium quantum field theory can be found in [37, 81, 82], which this chapter is based on.

## 2.1 Non-equilibrium quantum field theory

Quantum field theory provides a generic framework to describe quantum many-body systems on Minkowski and other space-times, not limited to finite-dimensional Hilbert spaces. We consider Minkowski space-time here, and refer to Chapter 7 for a more formal discussion of general space-time geometries. In the Heisenberg picture of quantum mechanics a state in the Hilbert space $\mathcal{H}$ of the quantum system under investigation can be described by a fixed density operator[1] $\hat{\varrho}_0 : \mathcal{H} \to \mathcal{H}$, and may be mixed ($\mathrm{Tr}\,(\hat{\varrho}_0^2) < 1$) or pure ($\mathrm{Tr}\,(\hat{\varrho}_0^2) = 1$). Examples of density operators include vacuum and thermal density operators, but the following discussion is not restricted to these.

Let $\hat{\Phi}(x)$ be a complex (Heisenberg) quantum field, which provides linear operators $\mathcal{H} \to \mathcal{H}$ for every point $x$ in Minkowski space-time. Measurable in experiments are the expectation values of observables, i.e., of self-adjoint operators $\hat{\mathcal{O}} = \hat{\mathcal{O}}^\dagger$,

$$\langle \hat{\mathcal{O}} \rangle := \mathrm{Tr}\,[\hat{\varrho}_0\,\hat{\mathcal{O}}]\,, \tag{2.1}$$

with a trace over the Hilbert space $\mathcal{H}$. Of particular interest are expectation values of field operator correlators such as one- and connected two-point correlation functions,

$$\phi(x) := \mathrm{Tr}\,[\hat{\varrho}_0\,\hat{\Phi}(x)]\,, \qquad \mathrm{Tr}\,[\hat{\varrho}_0\,(\hat{\Phi}(x) - \phi(x))(\hat{\Phi}(y) - \phi(y))]\,. \tag{2.2}$$

In fact, all correlation functions of quantum fields in a certain sense completely specify the QFT at any point in space-time.[2]

---

[1]A density operator is a linear operator acting on the Hilbert space $\mathcal{H}$ of the QFT and fulfils positive semi-definiteness, $\hat{\varrho}_0 \geq 0$, is self-adjoint, $\hat{\varrho}_0^\dagger = \hat{\varrho}_0$, and has unit trace, $\mathrm{Tr}\,(\hat{\varrho}_0) = 1$.

[2]In algebraic QFT the Reeh-Schlieder theorem goes even further, stating that all correlation functions with arguments within an arbitrarily small open space-time neighborhood suffice for this [83, 84].

The field $\hat{\Phi}(x)$ transforms unitarily under a Poincaré transformation $(\Lambda, a)$, which consists of a homogeneous Lorentz transformation $\Lambda \in O(1,3)$ and a translation $a \in \mathbb{R}^4$ in Minkowski space-time,

$$\hat{\Phi}(x) \mapsto U(\Lambda, a)\hat{\Phi}(x)U^{\dagger}(\Lambda, a) = \sigma(\Lambda^{-1})\hat{\Phi}(\Lambda x + a), \tag{2.3}$$

where $\hat{U}$ denotes a projective unitary representation of the Poincaré group on $\mathcal{H}$, and $\sigma$ is a finite-dimensional complex representation of the homogeneous Lorentz group. This type of transformation behavior originates from the unitary representations of the universal cover of the Poincaré group, all of which decompose into direct sums or, more generally, direct integrals of irreducible unitary representations [85]. The latter are induced from the little group, which is the homogeneous Lorentz group [8]. We can use Equation (2.3) to evolve the quantum field $\hat{\Phi}(x) \equiv \hat{\Phi}(t, \mathbf{x})$, $\mathbf{x} = (x^1, x^2, x^3)$, in time:

$$\hat{\Phi}(t', \mathbf{x}) = U(1_{4\times 4}, (t'-t, \mathbf{0}))\hat{\Phi}(t, \mathbf{x})U^{\dagger}(1_{4\times 4}, (t'-t, \mathbf{0})) = e^{i\hat{H}(t'-t)}\hat{\Phi}(t, \mathbf{x})e^{-i\hat{H}(t'-t)}. \tag{2.4}$$

Here, the Hamiltonian $\hat{H}$ appears as the Lie algebra generator of time translations on the representation level.[3]

For closed quantum systems, the density operator $\hat{\varrho}_0$ together with the Hamiltonian $\hat{H}$ allow in principle for the computation of any observable at arbitrary time. The time evolution of a closed quantum system to later times provides an initial value problem. Frequently, non-equilibrium expectation values of quantum field correlators evolve towards thermal equilibrium in the course of time, as we discuss later. Although not considered in this work, we note that often the dynamics of open quantum systems can be suitably described by stochastic approaches [86, 87].

In light of special relativity, we require quantum fields to preserve causality. Let two points $x, y$ in Minkowski space-time be space-like separated, i.e., their Minkowski distance $(\Delta x^0)^2 - (\Delta x^1)^2 - (\Delta x^2)^2 - (\Delta x^3)^2 < 0$ with $\Delta x^{\mu} = y^{\mu} - x^{\mu}$. Then, for $\sigma$ an integer spin (bosonic) Lorentz group representation, causality preservation requires that on operator level the commutator fulfils

$$[\hat{\Phi}(x), \hat{\Phi}(y)] = 0. \tag{2.5}$$

Else, intuitively quantum fields could transmit information faster than the speed of light, thus breaking causality. Causality implies that a given QFT contains particles and their anti-particles with the same spins and masses [9]. For the related discussion of fermionic representations of the Poincaré group and the symmetry groups of other space-time geometries which admit a notion of causality, we refer to Chapter 7.

If we consider the non-relativistic (Galilei) limit of a relativistic QFT, causality cannot be required anymore. Indeed, for Galilei geometry all points $x, y$ with $x^0 \neq y^0$ are time-like separated. For instance, this applies to the ultracold atom experiment described in Chapter 3. Such a limit is conventionally taken by explicitly reinserting factors of the speed of light $c$ and sending $c \to \infty$, which corresponds to a Lie algebra contraction [88].

---

[3]We employ physics conventions for Lie algebras in this dissertation, such that a simply connected Lie group $G$ with Lie algebra $\mathfrak{g}$ fulfils $G = \exp(i\mathfrak{g})$.
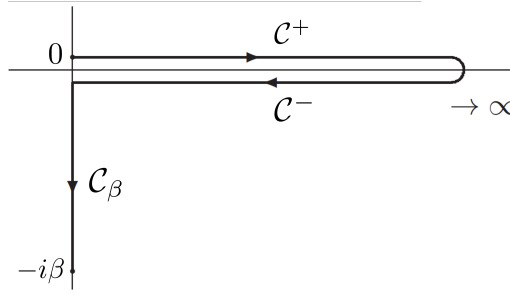
**FIGURE 2.1:** Schwinger-Keldysh contour with the thermal branch $\mathcal{C}_\beta$.

In Chapter 7 we describe a more canonical method to take such limits of space-time geometries.

To allow for the computation of two-point correlation functions of *arbitrary* order in time from *time-ordered* field operator correlations, we introduce the Schwinger-Keldysh contour $\mathcal{C}$. This is necessary to be able to apply the versatile functional (path) integral formalism, which gives access to time-ordered correlation functions. The contour $\mathcal{C}$ is sketched in Figure 2.1 and consists out of equilibrium of two time branches:[4] the forward branch $\mathcal{C}^+$ from time 0 to time $\infty$, and the backward branch $\mathcal{C}^-$ from time $\infty$ to time 0, identifying $0 \in \mathcal{C}^+$ with $0 \in \mathcal{C}^-$. In thermal equilibrium with inverse temperature $\beta$, before the latter identification the contour $\mathcal{C}$ is augmented by a third, imaginary time branch $\mathcal{C}_\beta$ from 0 to $-\mathrm{i}\beta$, then identifying $-\mathrm{i}\beta \in \mathcal{C}_\beta$ with $0 \in \mathcal{C}^+$. If field operator correlators are considered with all time arguments in $\mathcal{C}_\beta$, i.e., on a Euclidean space-time, this identification leads to the discrete Matsubara frequencies of equilibrium systems. We denote time ordering along the contour $\mathcal{C}$ by $\mathrm{T}_\mathcal{C}$.

All information on contour time-ordered correlation functions of the QFT is contained in the non-equilibrium generating functional

$$Z[J; \hat{\varrho}_0] = \mathrm{Tr}\left[\hat{\varrho}_0\, \mathrm{T}_\mathcal{C} \exp\left\{\mathrm{i}\int_{x,\mathcal{C}} [J^\dagger(x)\hat{\Phi}(x) + \hat{\Phi}^\dagger(x)J(x)]\right\}\right], \tag{2.6}$$

where $\int_{x,\mathcal{C}} := \int_\mathcal{C} \mathrm{d}x^0 \int \mathrm{d}^3\mathbf{x}$, and the source $J$ is a $\dim(\sigma)$-vector of complex functions with contour time arguments. Out of equilibrium, for $x = (x^0, \mathbf{x})$ with $x^0 \in \mathcal{C}$ we denote the time $x^0$ after forgetting the branch by $t(x^0)$. For $x_0 \in \mathcal{C}_\beta$ we set $t(x^0) := x^0$. Field operators $\hat{\Phi}(x^0, \mathbf{x})$ with $x^0 \in \mathcal{C}$ as in Equation (2.6) are defined from two independent copies $\hat{\Phi}^\pm(t(x^0), \mathbf{x})$ of the original field operators on Minkowski space-time, one for each of the two branches $\mathcal{C}^\pm$. To implement the thermal branch $\mathcal{C}_\beta$, these are augmented by a third independent copy $\hat{\Phi}^\beta(t(x^0), \mathbf{x})$, analytically continued to imaginary times $t(x^0) \in [0, -\mathrm{i}\beta]$. Similarly, we can decompose the source $J(x^0, \mathbf{x})$ into $J^\pm(t(x^0), \mathbf{x})$ and $J^\beta(t(x^0), \mathbf{x})$ according to whether $x^0 \in \mathcal{C}^+$, $x^0 \in \mathcal{C}^-$ or $x^0 \in \mathcal{C}_\beta$. Out of equilibrium, we then have

$$\int_{x,\mathcal{C}} J^\dagger(x)\hat{\Phi}(x) \equiv \int_0^\infty \mathrm{d}t \int \mathrm{d}^3\mathbf{x}\, [J^{+,\dagger}(t,\mathbf{x})\hat{\Phi}^+(t,\mathbf{x}) - J^{-,\dagger}(t,\mathbf{x})\hat{\Phi}^-(t,\mathbf{x})], \tag{2.7}$$

---

[4]We assume the time arguments of all real-time correlation functions of interest to be in $[0, \infty)$.

and analogously for $\int_{x,\mathcal{C}} \hat{\Phi}^\dagger(x) J(x)$. Functional derivatives of $Z[J; \hat{\varrho}_0]$ with respect to the source $J$ yield all contour time-ordered correlation functions, e.g.

$$\phi_J(x) := \langle T_\mathcal{C} \hat{\Phi}(x) \rangle_J = \text{Tr} \left[ \hat{\varrho}_0\, T_\mathcal{C} \hat{\Phi}(x) \exp \left\{ i \int_{x,\mathcal{C}} [J^\dagger(x)\hat{\Phi}(x) + \hat{\Phi}^\dagger(x)J(x)] \right\} \right]$$

$$= \frac{1}{Z[J; \hat{\varrho}_0]} \frac{\delta}{i\,\delta J(x)} Z[J; \hat{\varrho}_0] \,, \tag{2.8}$$

$$\langle T_\mathcal{C} \hat{\Phi}(x) \hat{\Phi}(y) \rangle_J = \text{Tr} \left[ \hat{\varrho}_0\, T_\mathcal{C} \hat{\Phi}(x) \hat{\Phi}(y) \exp \left\{ i \int_{x,\mathcal{C}} [J^\dagger(x)\hat{\Phi}(x) + \hat{\Phi}^\dagger(x)J(x)] \right\} \right]$$

$$= \frac{1}{Z[J; \hat{\varrho}_0]} \frac{\delta}{i\,\delta J^\dagger(x)} \frac{\delta}{i\,\delta J^\dagger(y)} Z[J; \hat{\varrho}_0] \,, \tag{2.9}$$

where the subscript $J$ denotes the expectation value in the presence of the source $J$. Expectation values without the source $J$ can be computed by setting $J = 0$.

The Schwinger functional is defined as

$$W[J; \hat{\varrho}_0] = -i \log Z[J; \hat{\varrho}_0] \,. \tag{2.10}$$

Its functional derivatives with respect to the source $J$ yield the *connected* contour time-ordered correlation functions such as the propagator

$$\mathcal{G}_J(x, y) := \langle T_\mathcal{C} \hat{\Phi}(x) \hat{\Phi}(y) \rangle_J - \phi_J(x)\phi_J(y) = -i \frac{\delta}{\delta J^\dagger(x)} \frac{\delta}{\delta J^\dagger(y)} W[J; \hat{\varrho}_0] \,. \tag{2.11}$$

In comparison to Equation (2.9) we note that here the disconnected contribution $\phi_J(x)\phi_J(y)$ has been subtracted.

In order to rewrite the generating functional $Z[J; \hat{\varrho}_0]$ out of equilibrium in the functional integral formalism, we evaluate the trace $\text{Tr}$ using eigenstates $|\varphi^\pm\rangle$ of the field operators $\hat{\Phi}^\pm(0, \mathbf{x})$:

$$\hat{\Phi}^\pm(0, \mathbf{x})|\varphi^\pm\rangle = \varphi_0^\pm(\mathbf{x})|\varphi^\pm\rangle \,, \tag{2.12}$$

where the $\varphi_0^\pm(\mathbf{x})$ are $\dim(\sigma)$-vectors of complex functions on $\mathbb{R}^3$. Formally, we introduce the integration measure

$$\int [\mathrm{d}\varphi_0^\pm] := \int \prod_{\mathbf{x} \in \mathbb{R}^3} \mathrm{d}\varphi_0^\pm(\mathbf{x}) \,. \tag{2.13}$$

The Hilbert space identity operator admits a decomposition as

$$\mathbb{1}_\mathcal{H} = \int [\mathrm{d}\varphi_0^-]\, |\varphi^-\rangle\langle\varphi^-| \,. \tag{2.14}$$

A number of derivation steps [37] yields

$$Z[J; \hat{\varrho}_0] = \int [\mathrm{d}\varphi_0^+][\mathrm{d}\varphi_0^-]\, \langle\varphi^+|\hat{\varrho}_0|\varphi^-\rangle \int_{\varphi_0^+}^{\varphi_0^-} \mathscr{D}'\varphi \, \exp \left\{ iS_\mathcal{C}[\varphi] + i \int_{x,\mathcal{C}} [J^\dagger(x)\varphi(x) + \varphi^\dagger J(x)] \right\} \,, \tag{2.15}$$

where $\int_{\varphi_0^+}^{\varphi_0^-} \mathscr{D}'\varphi$ is the functional integral over all fields $\varphi(x^0, \mathbf{x})$ with time arguments $x^0 \in \mathcal{C}$, which are consistent with the boundary conditions $\varphi^\pm(0, \mathbf{x}) = \varphi_0^\pm(\mathbf{x})$. The action

$S_{\mathcal{C}}[\varphi]$ is of the form

$$S_{\mathcal{C}}[\varphi] = \int_{\mathcal{C}} \mathrm{d}x^0 \int \mathrm{d}^3\mathbf{x}\, \mathcal{L}(\varphi(x^0, \mathbf{x}), \partial_\mu \varphi(x^0, \mathbf{x}), \dots) \tag{2.16}$$

with $\mathcal{L}(\varphi(x^0, \mathbf{x}), \partial_\mu \varphi(x^0, \mathbf{x}), \dots)$ the Lagrangian of the QFT, which can be computed from the Hamiltonian $\hat{H}$. The functional integral expression (2.15) for the generating functional consists of two parts: the initial conditions, which give boundary conditions for the space-time functional integral, and the latter integral itself. This encodes the non-equilibrium initial value problem in the functional integral formalism: for given initial conditions $\hat{\varrho}_0$, the knowledge of the action $S_{\mathcal{C}}[\varphi]$ suffices to compute any contour time-ordered correlation function. Depending on the problem under investigation, the Hamiltonian operator formalism or the functional integral formalism can both be beneficial with regard to computational efficiency. We will encounter both approaches in this dissertation.

For completeness we note that upon inclusion of the thermal branch $\mathcal{C}_\beta$ in $\mathcal{C}$ the derivation proceeds analogously.

## 2.2 Gauge theories

A central pillar of contemporary particle physics and the topic of Chapters 4, 6 and 7 are gauge theories, which obey local symmetry principles. Their construction is particularly transparent in the functional integral approach. We provide a brief introduction to gauge theories formulated on Minkowski space-time, considering a unitary matrix gauge group $G$ with Lie algebra $\mathfrak{g}$. Prominent examples for such gauge groups are $\mathrm{U}(1)$ and $\mathrm{SU}(N_c)$ for a number of colours $N_c$, or a direct product of these. We focus on a physical viewpoint on gauge theories, based on [9]. For a mathematical introduction to the construction of gauge fields from connections on principal bundles we refer to [89], in this dissertation appearing in Chapter 7.

Let us assume that under a gauge transformation $V(x)$, i.e., a smooth map of space-time points into $G$, the field $\hat{\Phi}(x)$ and its adjoint transform as

$$\hat{\Phi}(x) \mapsto V(x)\hat{\Phi}(x), \qquad \hat{\Phi}^\dagger(x) \mapsto \hat{\Phi}^\dagger(x)V^\dagger(x). \tag{2.17}$$

This implies that the corresponding fields $\varphi(x)$ and $\varphi^\dagger(x)$ as in Equation (2.15) transform analogously. We aim to construct a Lagrangian for the gauge theory that is invariant under such gauge transformations. For this, we first note that kinetic contributions with partial derivatives of $\varphi(x)$ do not gauge-transform as $\varphi(x)$, since

$$\partial_\mu \varphi(x) \mapsto (\partial_\mu V(x))\varphi(x) + V(x)\partial_\mu \varphi(x). \tag{2.18}$$

If instead we replace $\partial_\mu$ by the covariant derivative

$$\nabla_\mu(x) = \partial_\mu - \mathrm{i}g A_\mu(x), \tag{2.19}$$

for a coupling constant $g$ and a (classical) $\mathfrak{g}$-valued vector field $A_\mu(x)$ which gauge-transforms as

$$A_\mu(x) \mapsto V(x)A_\mu(x)V^\dagger(x) + \frac{\mathrm{i}}{g}V(x)\partial_\mu V^\dagger(x)\,, \tag{2.20}$$

then we find

$$\nabla_\mu(x)\varphi(x) \mapsto V(x)\nabla_\mu(x)\varphi(x)\,. \tag{2.21}$$

Expressions such as $(\nabla^\mu\varphi(x))^\dagger\nabla_\mu(x)\varphi(x)$ are gauge-invariant and provide both a space-time derivative of the field $\varphi(x)$ and interactions with the gauge field $A_\mu(x)$, if considered part of a Lagrangian.

Gauge bosons propagate in the gauge theory, if a gauge-invariant kinetic term for the gauge field $A_\mu(x)$ is included in the Lagrangian. Define the $\mathfrak{g}$-valued field strength tensor

$$F_{\mu\nu}(x) := \frac{\mathrm{i}}{g}[\nabla_\mu(x), \nabla_\nu(x)] = \partial_\mu A_\nu(x) - \partial_\nu A_\mu(x) - \mathrm{i}g[A_\mu(x), A_\nu(x)]\,, \tag{2.22}$$

which is antisymmetric in the indices $\mu, \nu$. If $G$ is Abelian, the commutator contribution $[A_\mu(x), A_\nu(x)]$ is absent, as for QED. The field strength tensor transforms covariantly under the gauge transformation $V(x)$:

$$F_{\mu\nu}(x) \mapsto V(x)F_{\mu\nu}(x)V^\dagger(x)\,. \tag{2.23}$$

Unitarity of $G$ implies that the gauge-invariant Lie algebra trace $\mathrm{tr}(F_{\mu\nu}(x)) \in \mathrm{i}\mathbb{R}$, or $\mathrm{tr}(F_{\mu\nu}(x)) = 0$ for unit-determinant gauge groups such as $\mathrm{SU}(N_c)$. Thus, this expression cannot be used to construct a real-valued kinetic Lagrangian term for the gauge bosons. Instead, the second order trace

$$-\frac{1}{2}\mathrm{tr}(F_{\mu\nu}(x)F^{\mu\nu}(x)) \tag{2.24}$$

is readily Lorentz and gauge-invariant. Here, upper indices are obtained by contraction with the inverse Minkowski metric $\eta^{\mu\nu} = (\mathrm{diag}(+1, -1, -1, -1))^{\mu\nu}$, and summation over repeated indices is implied. In fact, for $G$ a direct product of compact simple factors such as $\mathrm{SU}(N_c)$ and $\mathrm{U}(1)$ factors, the term $\mathrm{tr}(F_{\mu\nu}(x)F^{\mu\nu}(x))$ is positive-definite, due to properties of the quadratic Casimir of the Lie algebra $\mathfrak{g}$ [90]. As such, the Lagrangian kinetic term (2.24) contributes negative-definitely to the corresponding Lagrangian. This is required for the eigenvalues of the corresponding Hamiltonian (energies) to be bounded from below, such that the quantum system maintains stability in this regard.

Finally, a minimal-coupling Lagrangian for the gauge theory can read

$$\mathcal{L}(\varphi(x), A_\mu(x)) = -\frac{1}{2}\mathrm{tr}(F_{\mu\nu}(x)F^{\mu\nu}(x)) + (\nabla^\mu\varphi(x))^\dagger\nabla_\mu(x)\varphi(x) + \mathcal{L}_{\mathrm{pot}}(\varphi(x))\,, \tag{2.25}$$

with $\mathcal{L}_{\mathrm{pot}}(\varphi(x))$ a potential term for the field $\varphi(x)$, which can include a mass term for suitable $\sigma$. If multiple matter fields similar to $\hat{\Phi}(x)$ are included, one may simply sum over the last two terms with $\varphi(x)$ replaced by these. For Dirac fermions the second term may be suitably replaced by a corresponding kinetic term which involves the Dirac $\gamma$-matrices. Based on renormalization group arguments, higher-order contributions to $\mathcal{L}(\varphi(x), A_\mu(x))$

polynomial in the field operators, other than those already included in Equation (2.25), are highly suppressed at ordinary energies by negative powers of a very large mass [90]. These are hence commonly and in this dissertation ignored.

So far, we discussed the *classical* gauge field $A_\mu(x)$ interacting with the quantum field $\hat{\Phi}(x)$. The quantization of $A_\mu(x)$ can be efficiently accomplished in the functional integral formalism. We assume the Hilbert space $\mathcal{H}$ encompasses now excited states of both fields $\hat{\Phi}(x)$ and $\hat{A}_\mu(x)$. We proceed analogously to the construction of the functional integral for $\hat{\Phi}(x)$ correlators, Equation (2.15), and consider time arguments on the Schwinger-Keldysh contour $\mathcal{C}$. Focusing on non-equilibrium situations here, we note that the inclusion of a thermal branch $\mathcal{C}_\beta$ is again straight-forward. As is usual in light of its canonical commutation relations, we assume that the quantized gauge field $\hat{A}_\mu(t, \mathbf{x})$ commutes with the quantum field $\hat{\Phi}(t, \mathbf{x})$ at the same time. To this end, we can choose a common basis of eigenstates $|A^\pm, \varphi^\pm\rangle$ for both field operators $\hat{A}^\pm(0, \mathbf{x})$ and $\hat{\Phi}(0, \mathbf{x})$:

$$\hat{\Phi}^\pm(0, \mathbf{x})|A^\pm, \varphi^\pm\rangle = \varphi_0^\pm(\mathbf{x})|A^\pm, \varphi^\pm\rangle, \qquad \hat{A}_\mu^\pm(0, \mathbf{x})|A^\pm, \varphi^\pm\rangle = A_{\mu,0}^\pm(\mathbf{x})|A^\pm, \varphi^\pm\rangle. \quad (2.26)$$

The Hilbert space identity operator $1_\mathcal{H}$ changes to

$$1_\mathcal{H} = \int [\mathrm{d}\varphi_0^-][\mathrm{d}A_0^-]\,|A^-, \varphi^-\rangle\langle A^-, \varphi^-|, \quad (2.27)$$

where

$$\int [\mathrm{d}A_0^\pm] := \int \prod_{\mu,\mathbf{x}} \mathrm{d}A_{\mu,0}^\pm(\mathbf{x}). \quad (2.28)$$

Similar to before, we find for the corresponding generating functional with density operator $\hat{\varrho}_0$ and sources $J_\varphi$ and $J_A^\mu$ for the fields $\hat{\Phi}$ and $\hat{A}_\mu$:

$$\begin{aligned}
Z&[J_\varphi, J_A; \hat{\varrho}_0] \\
&:= \mathrm{Tr}\left[\hat{\varrho}_0\, \mathrm{T}_\mathcal{C} \exp\left\{\mathrm{i}\int_{x,\mathcal{C}}[J_\varphi^\dagger(x)\hat{\Phi}(x) + J_A^{\mu,\dagger}(x)\hat{A}_\mu(x) + \mathrm{h.c.}]\right\}\right] \\
&= \int [\mathrm{d}\varphi_0^+][\mathrm{d}\varphi_0^-][\mathrm{d}A_0^+][\mathrm{d}A_0^-]\,\langle A^+, \varphi^+|\hat{\varrho}_0|A^-, \varphi^-\rangle \\
&\quad \times \int_{\varphi_0^+}^{\varphi_0^-} \mathscr{D}'\varphi \int_{A_0^+}^{A_0^-} \mathscr{D}'A \exp\left\{\mathrm{i}S_\mathcal{C}[A, \varphi] + \mathrm{i}\int_{x,\mathcal{C}}[J_\varphi^\dagger(x)\varphi(x) + J_A^{\mu,\dagger}(x)A_\mu(x) + \mathrm{h.c.}]\right\},
\end{aligned}$$
$$(2.29)$$

with the functional integral $\int_{A_0^+}^{A_0^-} \mathscr{D}'A$ over all fields $A_\mu(x^0, \mathbf{x})$, $x^0 \in \mathcal{C}$, which are consistent with the boundary conditions $A_\mu^\pm(0, \mathbf{x}) = A_{\mu,0}^\pm(\mathbf{x})$.

The functional integral (2.29) can be readily applied to (formally) compute gauge-invariant observables. For these no gauge fixing is required. This is different if gauge dependent quantities such as gauge boson propagators $\sim \langle A_\mu A_\nu\rangle$ are computed, where full gauge fixing must be applied. Quantization can then be accomplished with the inclusion of Faddeev-Popov ghosts, see e.g. [9, 90]. The physical Hilbert space of perturbation theory containing only transversely polarized gauge bosons is singled out as the cohomology of the Becchi-Rouet-Stora-Tyutin (BRST) operator [9, 90]. Let us remark that gauge-invariant

observables can equivalently be computed with or without gauge fixing. While the formulation of classical-statistical simulations in Chapter 4 for Minkowski space-time makes use of temporal-axial gauge fixing with the additional fixation of Gauss' law, the Monte Carlo simulations of Chapter 6 do not employ any gauge fixing. Both approaches are equally valid to compute the gauge-invariant observables under investigation in these chapters.

The Standard Model of particle physics provides a gauge theory with gauge group

$$G_{\mathrm{SM}} = (\mathrm{U}(1) \times \mathrm{SU}(2) \times \mathrm{SU}(3))/\mathbb{Z}_6 \,, \tag{2.30}$$

with the cyclic $\mathbb{Z}_6$ subgroup generated by [91]

$$(\exp(\pi\mathrm{i}/3), -1_{2\times2}, \exp(2\pi\mathrm{i}/3) \cdot 1_{3\times3}) \,. \tag{2.31}$$

In the Standard Model, Dirac fermions interact non-trivially with the gauge bosons of $G_{\mathrm{SM}}$ gauge theory. The gauge theory including the fermions can be subdivided into different theories for particular gauge subgroups. $\mathrm{U}(1) \times \mathrm{SU}(2)$ yields the electroweak interactions involved in radioactive decays, and $\mathrm{SU}(3)$ gives QCD, which includes the strong interactions binding atomic nuclei, for instance. After electroweak symmetry breaking, the $\mathrm{U}(1)_{\mathrm{em}}$ gauge subgroup of $\mathrm{U}(1) \times \mathrm{SU}(2)$ corresponds to QED. Yet, the origin of the specific gauge group structure of $G_{\mathrm{SM}}$ remains unknown. We provide a corresponding space-time geometry-based proposal in Chapter 7, which also yields the observed behavior of fermions as they interact with the Standard Model gauge bosons.

We note that in Equation (2.24) cubic and quartic self-interactions of the gauge bosons appear for non-Abelian gauge groups. These are responsible for a plethora of non-perturbative physical phenomena even at everyday energy scales, and render computations in non-Abelian gauge theories complicated and in general intractable. Prominently, non-Abelian gauge theories give rise to color confinement and asymptotic freedom. At low energies quarks and gluons are confined, such that the physically observed Hilbert space contains only states which transform trivially under gauge transformations for the full gauge group $G$. This includes the observed mesons, baryons, tetra- and pentaquarks [92], for instance. At higher energies, lattice simulations suggest a cross-over which renders the quarks and gluons deconfined. Signatures of free quarks can appear for instance in the QGP.

Typically, deconfinement is accompanied by the spontaneous breaking of center symmetry, i.e., elements of the center $Z(G)$ of $G$ can act non-trivially on physical states. As an example consider $G = \mathrm{SU}(N_c)$ with center $Z(\mathrm{SU}(N_c)) \cong \mathbb{Z}_{N_c}$, which is generated by $\exp(2\pi\mathrm{i}/N_c) \cdot 1_{N_c \times N_c}$. Let $V(x)$ be a center gauge transformation, i.e., $V(x) \in Z(\mathrm{SU}(N_c))$ for all space-time points $x$. Continuity of $V(x)$ implies that $V(x) = c$ for a constant $c \in Z(\mathrm{SU}(N_c))$. The center gauge transformation is thus actually a *global* gauge transformation, and the breaking of center symmetry is the breaking of a global symmetry. The gauge symmetry is not spontaneously broken as a *local* symmetry, which would not be possible anyhow due to Elitzur's theorem [93]. To date, the rigorous mathematical

origin of confinement remains elusive [94]. We discuss confinement and center symmetry breaking in light of topological data analysis in Chapter 6.

At the highest energies, quarks and gluons become asymptotically free. This is due to the effective running of the gauge coupling, which changes depending on the probed energy scale. Based on quantum effects, at low energies the gauge coupling can become non-perturbatively large, while being perturbative at high energies and approaching zero asymptotically. Analytical computations are mostly restricted to perturbative high energy regimes. In part, the non-perturbative regime can be accessed with numerical lattice methods. In equilibrium and for imaginary times, for instance, importance sampling techniques such as Monte Carlo simulations, carried out in Chapter 6, often allow for numerical investigations [95], although finite baryon densities can cause a sign problem due to an uncontrollably oscillating functional integral measure. Out of equilibrium, the sign problem is more severe, since the functional integral measure $\sim \exp(\mathrm{i}S)$ oscillates vastly even without chemical potentials. Yet, at early times weakly coupled classical-statistical regimes can be accessed, for which quantum effects are suppressed, and at late times kinetic approaches can facilitate the numerical analysis [38, 96]. For the classical-statistical real-time simulations of Chapter 4 the former applies. Not conclusively established methods to study non-perturbative regimes at finite baryon densities include amongst others complex Langevin approaches [97] and Lefshetz thimbles [98].

The requirement of gauge-invariance puts strong constraints on the types of observables that one can measure in experiments. A particularly interesting class is given by Wilson loops, which can be formulated also for pure gauge theories. Let $\gamma$ be a continuous space-time path with parameters in $[0, 1]$. We define the Wilson line along $\gamma$ as

$$W[\gamma] := \mathrm{P} \exp \left\{ \mathrm{i}g \int_\gamma \mathrm{d}x^\mu A_\mu(x) \right\}, \tag{2.32}$$

where P denotes path ordering along $\gamma$ from $\gamma(0)$ to $\gamma(1)$. It gauge-transforms as

$$W[\gamma] \mapsto V(\gamma(1))W[\gamma]V^\dagger(\gamma(0)). \tag{2.33}$$

If $\gamma$ is a closed loop, i.e., $\gamma(0) = \gamma(1)$, we can construct the Wilson loop as the gauge-invariant observable

$$\mathrm{tr}\, W[\gamma]. \tag{2.34}$$

Polyakov loops, which are Wilson loops for particular lattice-encircling paths $\gamma$, will be studied explicitly in Section 6.2. Wilson lines facilitate the efficient formulation of gauge theories on discretized space-time lattices. There, the independent field degrees of freedom are not taken to be the gauge fields themselves but instead Wilson lines between neighboring lattice sites, called link variables [95]. Lattice gauge theories will be investigated in Chapters 4 and 6, which contain non-equilibrium and equilibrium formulations, respectively.

## 2.3    Collective phenomena out of equilibrium

Despite their unitary time evolution, generic isolated out-of-equilibrium quantum many-body systems steadily approach thermal equilibrium during their time evolution. The dynamics of quantum fields and their late time thermalization can accommodate a variety of collective phenomena, an overview of which we deliver in this section with emphasis on the phenomena of relevance for this dissertation. This excludes phenomena such as dynamical quantum phase transitions [99, 100], which come with non-analyticities on transient time scales. This section is in parts based on [37, 81].

Isolated quantum many-body systems with far-from-equilibrium initial conditions appear in a wide range of physical scenarios. Notably, this encompasses the post-inflationary early universe, the early stages of ultrarelativistic collisions of heavy or not quite so heavy [101] atomic nuclei for instance at the LHC or RHIC, or table-top experiment with ultracold quantum gases. While typical energy scales differ vastly for these systems, their subsequent dynamics can show similarities.

In the early time regime the non-equilibrium dynamics of a QFT can give rise to instabilities, of specific relevance e.g. for the (pre-)heating of the early universe [35] or for heavy-ion collisions [38]. They are based on parametric resonance effects, which amplify quantum fluctuations and lead to particle production even for small couplings [36]. This can be due to effective mass terms interacting with two-point correlation functions, similar to parametric resonances in classical mechanics. In the subsequent non-linear regime, when characteristic occupancies become of order one or larger, secondary instabilities can occur. For these, loop corrections can lead to further non-linear amplifications.

At some point the explosive particle production stops, having led to over-occupations at characteristic momenta if compared to a thermal equilibrium state for the same conserved quantities. At this stage there is often an infinite number of order-one loop corrections; the quantum many-body system is strongly correlated, even for a possibly small coupling. A regime of universal behavior can set in, related to non-equilibrium attractor solutions to the (quantum-)dynamical equations of motion. It is governed by self-similar time evolutions, which share similarities with critical scaling phenomena in equilibrium. Specifically, for a distribution function $f(t, \mathbf{p})$ of particles or quasi-particles in a homogeneous and isotropic system, the self-similar dynamics is described by a characteristic scaling function $f_S$ and a pair of scaling exponents $\alpha, \beta$, such that

$$f(t, \mathbf{p}) = t^\alpha f_S(t^\beta |\mathbf{p}|) \,, \tag{2.35}$$

for all times $t$ in the self-similar scaling regime, measured in suitable dimensionless units. In Chapter 4 we discuss self-similarity in classical-statistical Yang-Mills theory using gauge-invariant observables, in part constructed with tools from topological data analysis. In Chapter 5 we consider self-similar time evolutions in persistent homology from a mathematical viewpoint.

Dynamical self-similar behavior as in Equation (2.35) is often related to (turbulent) transport processes for conserved quantities. Isolated many-body systems feature energy conservation, and additional conserved quantities can appear. For instance, for
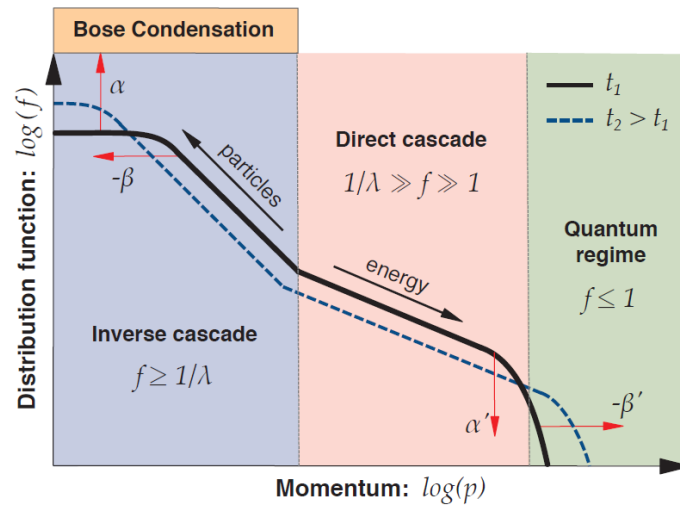
**FIGURE 2.2:** A dual cascade with related self-similar dynamics in the vicinity of non-thermal fixed points in scalar field theory, schematically. The inverse particle cascade is characterized by scaling exponents $\alpha, \beta$, the direct energy cascade by $\alpha', \beta'$. Figure reprinted from [44].

both relativistic and non-relativistic scalar field theories an effective mass is dynamically generated [44], which results in the effective conservation of the total particle number, transiently for the relativistic theory. As such, multiple conservation laws need to be met. This can result in dual cascades as shown schematically in Figure 2.2. Energy is transported in a direct cascade towards higher momenta, and total particle number is transported in an inverse cascade towards the infrared. Both transport processes can come with different pairs of scaling exponents $\alpha, \beta$ and $\alpha', \beta'$. The direct energy cascade can often be understood from perturbative weak wave turbulence [39, 102]. Due to typical occupations much larger than one, the non-perturbative inverse particle cascade in scalar field theories requires the introduction of strong wave turbulence [40, 103].

Self-similar behavior far from equilibrium can be remarkably *universal* across different physical systems, energy scales and initial conditions. For instance, this includes the example of relativistic and non-relativistic scalar field theories giving rise to the same scaling function $f_S$ and the same scaling exponents $\alpha, \beta$ for the inverse particle cascade [44]. Numerical agreement with these scaling exponents has also been found for spatial Wilson loops in non-Abelian gauge theory [46]. As for the direct cascade, non-Abelian gauge theories and relativistic scalar fields give rise to similar scaling exponents [39, 41, 45]. For longitudinally expanding spatial lattices, agreement has been observed for simulations of non-Abelian gauge theories and relativistic scalar fields [42, 43]. In recent years, dynamical self-similarity has been found experimentally for ultracold Bose gases [47–49], which includes evidence for its universality across very different initial conditions. In particular, the scaling exponent $\beta$ observed in [47] matches the one found for the inverse particle cascade in the simulations of scalar fields [44]. The conclusive grouping of many-body systems into non-equilibrium universality classes based on their dynamical behavior in the vicinity of non-thermal fixed points, similar to the Hohenberg-Halperin classification scheme based on critical behavior in equilibrium [104], is outstanding.

The inverse cascade with particle number transported towards the infrared can result in the dynamical formation of a BEC off equilibrium [50]. In relativistic QFTs the condensate is not stable and later decays due to particle number-changing processes [50]. In non-relativistic quantum many-body systems such as ultracold quantum gases this can be different, since total particle number is conserved. Indeed, for such systems the formation of an equilibrium condensate is expected for large particle densities at sufficiently low temperatures [105].

For non-moving systems, a condensate can be characterized by zero mode occupations scaling extensively with volume [106]. This criterion can be readily employed to examine the presence of out-of-equilibrium condensates in terms of volume scaling, employed e.g. in [43, 44, 50, 51]. Related to this, condensates also feature off-diagonal long-range order (ODLRO) [106, 107]. The spatial asymptotics of coherence functions, which are normalized correlation functions in position space, contains information on the corresponding condensate fraction, i.e., the quotient of the number of particles in the condensate divided by the total particle number [108]. To this end, the formation of a condensate out of equilibrium can be transparently followed with such correlators, which probe the related ODLRO. We employ this method in Chapter 3 to study the emergent non-equilibrium condensation of magnetizations in a spinor Bose gas.

As a specific phenomenon for non-Abelian gauge theories, initial states with gluonic over-occupations in the infrared can give rise to dynamical condensation [51], which is *not* accompanied by an inverse cascade. Typically, solely a direct cascade appears in simulations, see e.g. [109] and Chapter 4 of this thesis. We briefly provide an argument for this based on large-$N_c$ dynamics. Let $\gamma, \gamma'$ be two spatial loops. An inverse cascade related to the condensation dynamics of Wilson loops can be expected to show up in the connected Wilson loop correlator,

$$\langle \text{tr}(W[\gamma])\text{tr}(W[\gamma']) \rangle - \langle \text{tr}(W[\gamma]) \rangle \langle \text{tr}(W[\gamma']) \rangle \,, \tag{2.36}$$

which is gauge-invariant. Agreement of the condensation dynamics of spatial Wilson loops for both $\text{SU}(N_c)$ gauge theory with $N_c = 2$ and $N_c = 3$ has been observed [46]. It can thus be expected that the non-equilibrium condensation dynamics of [51] can be extrapolated to large $N_c \gg 1$. At large $N_c$ the expectation values of Wilson loop correlators behave as [110–112]

$$\langle \text{tr}(W[\gamma])\text{tr}(W[\gamma']) \rangle = \langle \text{tr}(W[\gamma]) \rangle \langle \text{tr}(W[\gamma']) \rangle + \mathcal{O}(1/N_c^2) \,. \tag{2.37}$$

The potential appearance of a related inverse glue cascade in connected Wilson loop correlators such as (2.36) can thus be largely suppressed due the large-$N_c$ Wilson loop factorization, Equation (2.37).

Ultimately, generic quantum many-body systems thermalize. Although overall governed by unitary and thus reversible time evolution, at late times particular local observables such as low-order correlation functions approach their equilibrium expectation values computed for a thermal ensemble consistent with the conserved quantities [52–55]. For the equilibration of local observables, entanglement can provide a driving force

[56–58]. At increasingly late times local observables resemble thermal equilibrium on larger and larger length scales due to correlations which spread with finite speed through the quantum many-body system [113, 114], and progressively entangle more degrees of freedom. Varying the system size, in Chapter 3 we utilize the volume-dependence of thermalization times for specific observables in order to be able to study a spinor Bose gas until its eventual thermalization.

To conclude, quantum many-body systems in and out of equilibrium, in particular gauge theories, provide a phenomenologically fertile ground. Much is known in this regard, but crucial open problems remain. In this dissertation we address some these through the lens of topological data analysis and geometry.

# Part I

# Far-from-equilibrium time evolutions and thermalization
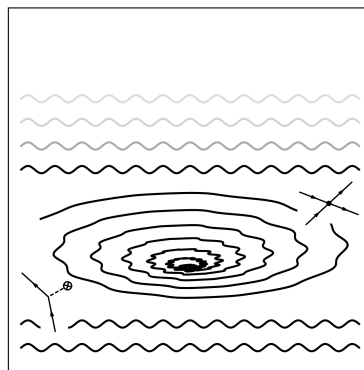
Starting from initial conditions far from equilibrium, quantum field theories can thermalize in the course of time. We report about a corresponding experiment with ultracold atoms. A study on self-similar dynamics in the gluonic plasma follows, leading to a mathematical analysis of related persistent homology phenomena.

# Chapter 3

# Condensation and thermalization of an easy-plane ferromagnet in a spinor Bose gas

This chapter is based on the following article:

- Prüfer, M., Spitz, D., Lannig, S., Strobel, H., Berges, J., and Oberthaler, M. K., "Condensation and thermalization of an easy-plane ferromagnet in a spinor Bose gas", *Nat. Phys.*, vol. 18, no. 12, pp. 1459–1463, 2022. arXiv: 2205.06188 [cond-mat.quant-gas].

Most of the present chapter is taken from this publication, where I contributed to the text, to the discussion of the measurement results, participated in the data analysis and predominantly elaborated the theoretical framework.

This work has been reported about in the following popular scientific account, which is not part of this dissertation:

- Prüfer, M., Spitz, D., and Strobel, H., "Supraflüssigkeit mit Spin", *Physik in unserer Zeit*, vol. 54, no. 2, pp. 58–59, 2023.

## 3.1 Overview

Bose-Einstein condensates are an ideal platform to experimentally explore dynamical phenomena emerging in the many-body limit, such as the build-up of long-range coherence, superfluidity or spontaneous symmetry breaking. In Bose-Einstein condensates [115] the macroscopic occupation of the ground state together with a spontaneously broken symmetry manifests itself in a globally well-defined phase of the complex-valued order parameter in each realization. This phase can be probed experimentally by interferometric measurements, which has been demonstrated with different platforms [116–118]. In an easy-plane ferromagnetic system the order parameter is characterized by a well-defined magnitude in the transversal plane, and all orientations in the plane are equally likely. Theoretically, this is due to a spatial anisotropy, breaking the full rotational $SO(3)$ symmetric part of the Hamiltonian down to a transversal $SO(2)$ symmetry. In condensed matter physics prototype models include the XXZ model [119], which has also been realized with ultracold atoms in lattice systems [120] and Rydberg atoms [121, 122].

In recent years analog quantum simulators with ultracold atoms allowed for unprecedented insights by implementing building blocks of complex condensed matter systems [123, 124]. This opens up new possibilities for studying pressing questions concerning quantum many-body dynamics and thermalization [125–133]. For probing these phenomena in macroscopic systems, often either the time-scales are too short or the control to extract information is not given such that direct observation of the dynamical processes is not possible.

We study the thermalization dynamics of an easy-plane ferromagnet in a homogeneous one-dimensional spinor Bose gas. The dynamic emergence of effective long-range coherence for the transversal magnetization field is demonstrated, and spin-superfluidity is verified by experimentally testing Landau's criterion. We reveal the structure of one massive and two massless emerging quasi-particle modes, which appear as a consequence of explicit and spontaneous symmetry breaking. Our experiments allow us to observe the thermalization of the easy-plane ferromagnetic Bose gas, for the relevant momentum-resolved observables in agreement with a thermal prediction obtained from an underlying microscopic model within the Bogoliubov approximation.

This chapter is structured as follows. In Section 3.2 we describe the experimental setup. Subsequently, in Section 3.3 we demonstrate the emergence of a condensate in the transversal spin degree of freedom, and test for superfluidity. In Section 3.4 we derive the structure of quasi-particles for the system via Bogoliubov theory, and experimentally probe their infrared behavior using local perturbations. To characterize the system at late times, in Section 3.5 we compare a variety of structure factors and local observables with thermal predictions obtained in the Bogoliubov approximation. In Section 3.6 we provide a summary.

## 3.2   The experimental setup

We realize a spinor BEC of $^{87}$Rb with easy-plane ferromagnetic properties [134, 135] in a quasi-one-dimensional box trap [136], see Figure 3.1(a). It consists of three internal states, labelled by their magnetic quantum number $m \in \{0, \pm 1\}$. The system features rotationally invariant ferromagnetic spin-spin interactions described by $\hat{H}_s = c_1 \int \mathrm{d}^3\mathbf{x}\, \hat{\mathbf{F}}^2/2$, where $c_1 < 0$ is the spin-spin interaction constant and $\hat{\mathbf{F}}$ denotes the spin operator (see Equation (3.4)). A quadratic Zeeman shift $q$ induced by the magnetic field plays the role of the isotropy-breaking term; it shifts the energy of the $m = \pm 1$ levels (see Figure 3.1(b)) and is explicitly given by $\hat{H}_q = q \int \mathrm{d}^3\mathbf{x}\,(\hat{N}_{+1} + \hat{N}_{-1})$, $\hat{N}_\pm$ the atom number density operators of the $m = \pm 1$ levels. We adjust $q$ by using off-resonant microwave dressing [137] such that the mean-field ground-state exhibits easy-plane ferromagnetic properties ($0 < q < 2n|c_1|$ with $n$ the atomic density) and our initial conditions restrict the dynamics to the spatially averaged longitudinal ($z$-) spin being zero. In addition to the spin interactions, our system exhibits SO(3)-invariant density-density interactions described by $\hat{H}_d = c_0 \int \mathrm{d}^3\mathbf{x}\, \hat{N}^2/2$, with interaction constant $c_0$ and $|c_0/c_1| \approx 200$ [134].

To implement the box-like trapping potential we use a weakly focused red-detuned laser beam creating a quasi-one-dimensional trapping potential with longitudinal frequency $\omega_l \approx 2\pi \times 1.7\,\text{Hz}$ and transversal frequency $\omega_r \approx 2\pi \times 170\,\text{Hz}$. This corresponds to a transversal harmonic oscillator length of $\sqrt{\hbar/M\omega_r} \approx 0.8\,\mu\text{m}$, with $M$ the atomic mass. Repulsive potential walls are created by two blue-detuned laser beams which results in a trapping volume of adjustable size around the centre of the harmonic trap. The longitudinal harmonic potential is in good approximation constant over the employed sizes and, thus, effectively leads to a one-dimensional box-like confinement for the atomic cloud.

The capability to extract the relevant order-parameter field [138] allows us to study the build-up of effective long-range coherence in a time- and space-resolved fashion. Accessing the full structure factors of the observables defining the Hamiltonian will also be the handle to faithfully witness thermalization. Details concerning the preparation and readout of the transversal spin can be found in [138–141].

We experimentally examine the order parameter, which is the transversal spin degree of freedom, by acquiring many realizations of the complex-valued field $F_\perp(y) = F_x(y) + iF_y(y)$ depending on the longitudinal position $y$, using spatially resolved joint measurements based on positive operator valued measures (POVM) [138, 140]. Specifically, after the evolution time $t$ we image the atomic densities using spatially resolved absorption imaging. Employing a Stern-Gerlach magnetic field gradient followed by a short time-of-flight (TOF; $2\,\text{ms}$), we are able to image the atomic densities of all 8 magnetic sublevels of the $F = 1$ and $F = 2$ hyperfine manifolds of the electronic ground state. Additional coherent microwave and radio-frequency manipulations before the imaging allow us to map the two spin projections $F_x$ and $F_y$ of the transversal spin [140] onto measurable densities. In every experimental realization $(i)$ we infer single shot realizations $O^{(i)}$ of different observables $\hat{O}$ from the atomic densities. The quantum expectation value is approximated by averaging over many realizations as

$$\langle \hat{O} \rangle \simeq O = \frac{1}{N_S} \sum_{i=1}^{N_S} O^{(i)}, \tag{3.1}$$

where $N_S$ is the number of realizations. This way, we obtain the complex-valued transversal spin $F_\perp(y) = F_x(y) + iF_y(y) = |F_\perp|(y) \exp(-i\phi_\text{L}(y))$ with length $|F_\perp|$ and orientation in the plane $\phi_L$ as a function of the position $y$. The discretized position $y$ is the centre of a spatial bin which contains $\sim 500$ atoms and has a spatial extension of $\sim 1.2\,\mu\text{m}$ along the cloud.[1] In each typical imaging volume we infer the spin from an average over $\sim 500$ atoms which are described by a spin field, i.e., taking nearly continuous values as illustrated schematically in Figure 3.1(c). This provides a macroscopic order-parameter field, which is sensitive to spin condensation.

For studying the spin condensation dynamics, we initialize the system far from equilibrium with $|F_\perp|$ near zero [142]. For the detailed observation of the emergence of spin coherence we prepare the atoms in the state $|F, m\rangle = |1, 0\rangle$, the so-called polar state. We

---

[1]We bin three adjacent camera pixels where each pixel corresponds to $420\,\mu\text{m}$ in the atom plane.
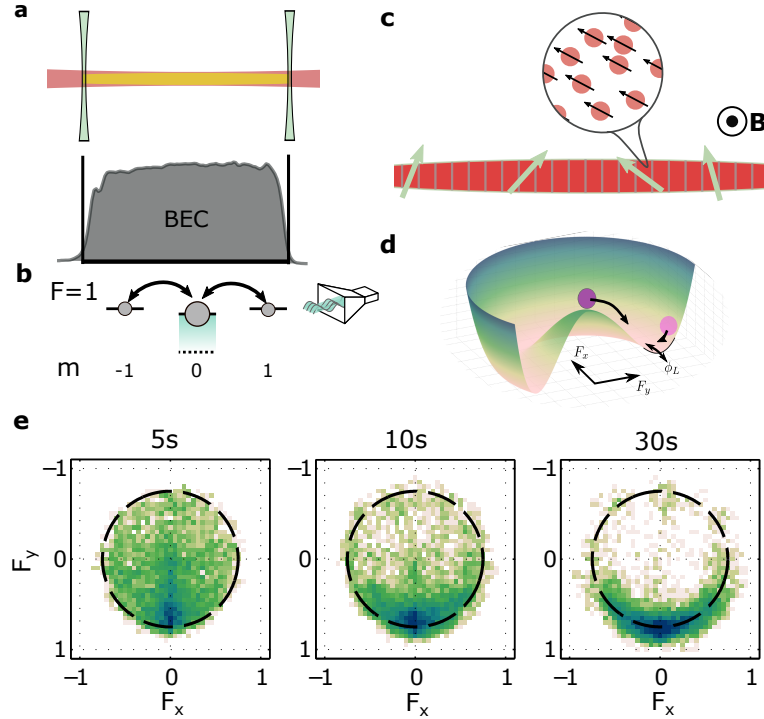
**FIGURE 3.1:** Homogeneous spinor Bose gas and easy-plane ferromagnetic properties. (a): We realize a homogeneous spinor BEC of $^{87}$Rb in a box-like trapping potential by a combination of an elongated attractive potential (red) and two repulsive end caps (green). The total density (grey shading) is flat over the extent of the cloud. (b): Level structure of the $F = 1$ hyperfine manifold. We control the offset energy between the $m$-states by microwave dressing (blue shading) such that the system features easy-plane ferromagnetic properties in its ground state. (c): The spatial degree of freedom is continuous, however, in the analysis discretized by the finite pixel size of the camera and the imaging resolution ($\approx 1.2\,\mu$m). Each imaging volume (boxes) contains $\approx 500$ atoms which are described by continuous fields for density and spin. The spins orient themselves in the (easy-)plane orthogonal to the external magnetic field **B**. (d): The transversal spin features two different types of excitations: A Goldstone mode and a Higgs mode related to the excitation of the orientation $\phi_{\mathrm{L}}$ and length $|F_{\perp}|$, respectively. (e): Histogram of the local spin normalized by the atom number, combining all spatial points and experimental realizations. In every realization the phase of the central spatial point is subtracted fixing the spin in the center to the $y$-direction. The dashed line is a guide to the eye and indicates $|F_{\perp}| = 0.75$.

visualize the emergence of a spin field expectation value $|F_{\perp}|$ by evaluating the histogram of local $F_{\perp}^{(i)}(y)$ values, taking into account all spatial positions and realizations, and given in Figure 3.1(e). After $5\,$s, which corresponds to approximately 10 times the typical time scale of the spin interaction energy $t_s = h/(n|c_1|)$, the spin is still far from equilibrium and shows large fluctuations in orientation and length. After $30\,$s (approximately $60\,t_s$) of evolution time we find that the fluctuations settle around a well-defined spin length $|F_{\perp}|$ and the phase $\phi_{\mathrm{L}}$ becomes well-defined over the whole sample, i.e., effective long-range order emerges. This is expected for a thermal state incorporating spontaneous symmetry breaking in the transversal spin degree of freedom and, intuitively, can be grasped by looking at the underlying mexican-hat-like free-energy potential, see Figure 3.1(d) and [143].
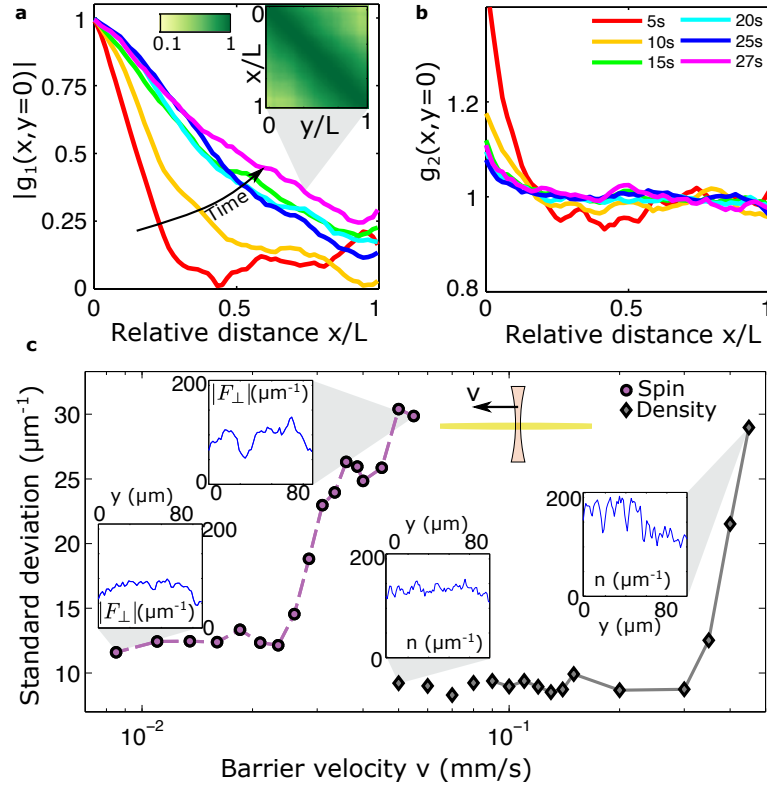
**FIGURE 3.2:** Emergence of effective long-range coherence in the transversal spin and superfluidity. (a): Absolute value of first order coherence $|g_1(x, y = 0)|$ of transversal spin $F_\perp$; reference point $(y = 0)$ is chosen at the left edge of the cloud with system size $L = 74\,\mu$m. We observe a build-up of effective long-range order, i.e., for long times the system features non-zero coherence over its whole size. Inset: Two-dimensional coherence function $|g_1(x, y)|$ after $27$ s evolution time. For long times we find the correlations to be approximately translation invariant. (b): Second order coherence of the transversal spin showing the evolution and character of spin length fluctuations. (c): Superfluid properties of the spin condensate. Standard deviation along the cloud of spin length (purple) and density (grey) for different barrier velocities $v$. The rapid increase at non-zero speeds indicates superfluid properties of spin and density. Insets show representative single realizations of the spin length and total density in the different regimes.

## 3.3 Spin condensation and superfluidity

To test for eventual spin condensation, we characterize the coherence properties of the transversal spin by evaluating first and second order coherence functions [108]. These are explicitly given by

$$g_1(x, y) = \frac{\langle \hat{F}_\perp^\dagger(x)\hat{F}_\perp(y)\rangle}{\sqrt{\langle \hat{F}_\perp^\dagger(x)\hat{F}_\perp(x)\rangle\,\langle \hat{F}_\perp^\dagger(y)\hat{F}_\perp(y)\rangle}} \tag{3.2}$$

and

$$g_2(x, y) = \frac{\langle \hat{F}_\perp^\dagger(x)\hat{F}_\perp^\dagger(y)\hat{F}_\perp(x)\hat{F}_\perp(y)\rangle}{\langle \hat{F}_\perp^\dagger(x)\hat{F}_\perp(x)\rangle\,\langle \hat{F}_\perp^\dagger(y)\hat{F}_\perp(y)\rangle}\,. \tag{3.3}$$

For the inferred single shot results of the transversal spin $F_\perp^{(i)}(y)$ the $^\dagger$ is treated as the complex conjugate. In contrast to earlier experiments observing the emergence of long-range coherence in one-component BECs [116, 144, 145], we do not rely on spatial

interference as we access the relevant spin field directly by joint measurements entailing interference in the internal degrees of freedom [138, 141]. We find that coherence is built up dynamically and the system finally features long-range order, i.e., non-zero $|g_1(x, y)|$ over the whole extent of the atomic cloud, see Figure 3.2(a). At the same time the spin length fluctuations, quantified by $g_2(x, y)$ as shown in Figure 3.2(b), settle close to unity at zero distance as expected for a weakly interacting Bose-Einstein condensate [146–150].

To characterize the final state, we first test for superfluidity of the spin as well as the density. In the spirit of Landau [151], we drag a well-localized obstacle coupling to density and spin through the BEC [152–154], and measure the response of the system, see Appendix 3.A for experimental details. We quantify the response by evaluating the mean standard deviation of the total density and the transversal spin length along the cloud. The breakdown of superfluidity is signalled by a rapid increase of the response at a non-zero critical velocity. We find two different critical velocities for spin and density in Figure 3.2(c). While the spin shows superfluidity up to $v_{c,s} \simeq 3 \times 10^{-2}$ mm/s, the density tolerates a moving barrier for up to 10 times faster speeds. This is consistent with the interaction strengths and the corresponding *stiffness* of the degrees of freedom.

## 3.4 Bogoliubov quasi-particles

We address the underlying quasi-particle structures in more detail. With two spontaneously broken symmetries, the $U(1)$ symmetry of the total density and the $SO(2)$ symmetry of the spin orientation, we anticipate two Goldstone-like modes with linear dispersions in the infrared. The different energy scales of density and spin interactions are reflected in the two associated sound speeds. They are theoretically expected to differ by more than an order of magnitude, which is consistent with the observed critical velocities. Additionally, the symmetry explicitly broken by $\hat{H}_s + \hat{H}_q$ leads to a Higgs-like gapped mode, see Figure 3.3(a). Compared to two-component BECs we find an additional quasi-particle mode due to the increased number of degrees of freedom [155, 156]. This behavior of the Bogoliubov quasi-particles can be inferred from their dispersion relations. These come with related Bogoliubov transformations, which we employ later to compute correlation functions for a thermal ensemble.

### 3.4.1 Bogoliubov transformations in the easy-plane ferromagnetic phase

We explicitly derive the Bogoliubov transformations in the easy-plane ferromagnetic phase ($0 < q/(n|c_1|) < 2$). Here we set $\hbar = 1$. In terms of the total density and spin operators

$$\hat{N}(\mathbf{x}) = \sum_{m=-1}^{1} \hat{N}_m(\mathbf{x}) = \sum_{m=-1}^{1} \hat{\psi}_m^\dagger(\mathbf{x})\hat{\psi}_m(\mathbf{x}), \quad \hat{F}_\nu(\mathbf{x}) = \sum_{m,m'=-1}^{1} \hat{\psi}_m^\dagger(\mathbf{x})(f^\nu)_{mm'}\hat{\psi}_{m'}(\mathbf{x}),$$

$$(3.4)$$

with the spin-1 matrices

$$
f^x = \frac{1}{\sqrt{2}} \begin{pmatrix} 0 & 1 & 0 \\ 1 & 0 & 1 \\ 0 & 1 & 0 \end{pmatrix}, \qquad f^y = \frac{i}{\sqrt{2}} \begin{pmatrix} 0 & -1 & 0 \\ 1 & 0 & -1 \\ 0 & 1 & 0 \end{pmatrix}, \qquad f^z = \begin{pmatrix} 1 & 0 & 0 \\ 0 & 0 & 0 \\ 0 & 0 & -1 \end{pmatrix}, \quad (3.5)
$$

the system Hamiltonian reads

$$
\hat{H} = \int \mathrm{d}^3\mathbf{x} \left[ \sum_{m=-1}^{1} \hat{\psi}_m^\dagger(\mathbf{x}) \left( -\frac{\nabla^2}{2M} + qm^2 \right) \hat{\psi}_m(\mathbf{x}) + \frac{c_0}{2} : \hat{N}^2(\mathbf{x}) : + \frac{c_1}{2} \sum_{\nu=x,y,z} : \hat{F}_\nu^2(\mathbf{x}) : \right],
$$
$$(3.6)$$

where $: \cdot :$ indicates normal ordering. With the momentum-space creation and annihilation operators

$$
\hat{a}_{\mathbf{k},m}^\dagger = \frac{1}{\sqrt{V}} \int \mathrm{d}^3\mathbf{x}\, \hat{\psi}_m^\dagger(\mathbf{x}) e^{i\mathbf{k}\mathbf{x}}, \qquad \hat{a}_{\mathbf{k},m} = \frac{1}{\sqrt{V}} \int \mathrm{d}^3\mathbf{x}\, \hat{\psi}_m(\mathbf{x}) e^{-i\mathbf{k}\mathbf{x}}, \qquad (3.7)
$$

the Hamiltonian becomes in the number-conserving Bogoliubov approximation [143]

$$
\begin{aligned}
\hat{H}_B = E_0 &+ \sum_{\mathbf{k}\neq\mathbf{0},m} (\epsilon_{\mathbf{k}} + qm^2 - \mu)\hat{n}_{\mathbf{k},m} \\
&+ \frac{N}{V} \sum_{j,j',m,m'} \sum_{\mathbf{k}\neq\mathbf{0}} (\Gamma_{jj',m'm} + \Gamma_{jm,m'j'})\zeta_{j'}\zeta_{m'}^* \hat{a}_{\mathbf{k},j}^\dagger \hat{a}_{\mathbf{k},m} \\
&+ \frac{N}{2V} \sum_{j,j',m,m'} \sum_{\mathbf{k}\neq\mathbf{0}} \Gamma_{jj',mm'} \left( \zeta_j^* \zeta_m^* \hat{a}_{-\mathbf{k},m'} \hat{a}_{\mathbf{k},j'} + \zeta_{m'}\zeta_{j'} \hat{a}_{\mathbf{k},j}^\dagger \hat{a}_{-\mathbf{k},m}^\dagger \right), \qquad (3.8)
\end{aligned}
$$

with $\epsilon_{\mathbf{k}} = \mathbf{k}^2/(2M)$, atom mass $M$, total atom number $N$, system volume $V$, and $\hat{n}_{\mathbf{k},m} = \hat{a}_{\mathbf{k},m}^\dagger \hat{a}_{\mathbf{k},m}$. The momentum scale $|\mathbf{k}|$ corresponds to the wavelength $\lambda = 2\pi/|\mathbf{k}|$. The spinor $(\zeta_m)$ specifies the normalized condensate configuration, and we have set $\hat{a}_{\mathbf{k}=0,m} = \sqrt{N}\zeta_m$. $\Gamma_{jj',mm'}$ denotes density and spin interactions,

$$
\Gamma_{jj',mm'} \equiv c_0 \delta_{jj'} \delta_{mm'} + c_1 \sum_{\nu=x,y,z} f_{jj'}^\nu f_{mm'}^\nu . \qquad (3.9)
$$

The ground state energy is in the Bogoliubov approximation given by

$$
E_0 \equiv N \left[ \sum_m qm^2 |\zeta_m|^2 + \frac{N-1}{2V} \sum_{j,j',m,m'} \Gamma_{jj',mm'} \zeta_j^* \zeta_m^* \zeta_{m'} \zeta_{j'} \right], \qquad (3.10)
$$

the chemical potential reads

$$
\mu \equiv \sum_m qm^2 |\zeta_m|^2 + \frac{2N-1}{2V} \sum_{j,j',m,m'} \Gamma_{jj',mm'} \zeta_j^* \zeta_m^* \zeta_{m'} \zeta_{j'} . \qquad (3.11)
$$

We set $\sin\theta = \sqrt{1/2 - q/(4n|c_1|)}$, such that the mean-field ground state is $\zeta = (\sin\theta/\sqrt{2}, \cos\theta, \sin\theta/\sqrt{2})$ [157]. The initial orthogonal transformation of creation and

annihilation operators, given by

$$
\begin{pmatrix} \hat{a}_{\mathbf{k},d} \\ \hat{a}_{\mathbf{k},\theta} \\ \hat{a}_{\mathbf{k},f_z} \end{pmatrix} = \begin{pmatrix} \sin\theta/\sqrt{2} & \cos\theta & \sin\theta/\sqrt{2} \\ \cos\theta/\sqrt{2} & -\sin\theta & \cos\theta/\sqrt{2} \\ 1/\sqrt{2} & 0 & -1/\sqrt{2} \end{pmatrix} \begin{pmatrix} \hat{a}_{\mathbf{k},1} \\ \hat{a}_{\mathbf{k},0} \\ \hat{a}_{\mathbf{k},-1} \end{pmatrix} \equiv A(\theta) \begin{pmatrix} \hat{a}_{\mathbf{k},1} \\ \hat{a}_{\mathbf{k},0} \\ \hat{a}_{\mathbf{k},-1} \end{pmatrix} , \tag{3.12}
$$

leads to a description of the system in terms of longitudinal and transversal spin fluctuations.

The longitudinal ($z$-)spin fluctuations can be diagonalized using the Bogoliubov transformation [157]

$$
\hat{b}_{\mathbf{k},f_z} = u_{\mathbf{k},f_z} \hat{a}_{\mathbf{k},f_z} + v_{\mathbf{k},f_z} \hat{a}^{\dagger}_{-\mathbf{k},f_z} , \tag{3.13}
$$

where

$$
u_{\mathbf{k},f_z} \equiv \sqrt{\frac{\epsilon_{\mathbf{k}} + q/2 + E_{\mathbf{k},f_z}}{2E_{\mathbf{k},f_z}}} , \qquad v_{\mathbf{k},f_z} \equiv \sqrt{\frac{\epsilon_{\mathbf{k}} + q/2 - E_{\mathbf{k},f_z}}{2E_{\mathbf{k},f_z}}} , \tag{3.14}
$$

with the dispersion

$$
E_{\mathbf{k},f_z} = \sqrt{\epsilon_{\mathbf{k}}(\epsilon_{\mathbf{k}} + q)} . \tag{3.15}
$$

To diagonalize transversal spin fluctuations we follow the procedure outlined in [143]. We obtain mode energies $\pm E_{\mathbf{k},+}$ and $\pm E_{\mathbf{k},-}$ as in [143], explicitly given by

$$
E_{\mathbf{k},\pm} = \sqrt{\epsilon_{\mathbf{k}}^2 + n(c_0 - c_1)\epsilon_{\mathbf{k}} + 2n^2 c_1(c_1 - c_q) \pm E_1(\mathbf{k})} , \tag{3.16}
$$

with

$$
E_1(\mathbf{k}) = \big([n^2(c_0 + 3c_1)^2 + 4n^2 c_q(c_0 + 2c_1)]\epsilon_{\mathbf{k}}^2 - 4n^3 c_1(c_0 + 3c_1)(c_1 - c_q)\epsilon_{\mathbf{k}}
$$
$$
+ [2n^2 c_1(c_1 - c_q)]^2\big)^{1/2} . \tag{3.17}
$$

The dispersions $E_{\mathbf{k},f_z}$ and $E_{\mathbf{k},\pm}$ are sketched in Figure 3.3(a). Defining

$$
h_{00} \equiv n(c_0 + c_1 - c_1) , \quad h_{01} \equiv q\sin(2\theta)/2 , \quad h_{11} \equiv -2nc_1 + nc_q , \quad h_{211} \equiv nc_q , \tag{3.18}
$$

and

$$
u_{\mathbf{k},\pm,1} = - \big(h_{01}\big[\pm 2E_1 + 4\epsilon_{\mathbf{k}}^2 + 2\epsilon_{\mathbf{k}}(2E_{\mathbf{k},\pm} + h_{00} + 2h_{11} - h_{211})
$$
$$
+ (h_{11} - h_{211})(2E_{\mathbf{k},\pm} + h_{11} + h_{211})\big]\big)\big/\big(4\epsilon_{\mathbf{k}}h_{01}^2 + 2\epsilon_{\mathbf{k}}(h_{11} - h_{00})h_{211}
$$
$$
+ h_{211}(\pm 2E_1 + h_{11}^2 - h_{211}^2)\big) , \tag{3.19a}
$$
$$
u_{\mathbf{k},\pm,2} = \big(4\epsilon_{\mathbf{k}}^2(h_{00} - h_{11}) - 2(E_{\mathbf{k},\pm} + h_{11})(\pm 2E_1 + h_{11}^2 - h_{211}^2)
$$
$$
- 2\epsilon_{\mathbf{k}}(\pm 2E_1 + 4h_{01}^2 - 2E_{\mathbf{k},\pm}(h_{00} - h_{11}) - 2h_{00}h_{11} + 3h_{11}^2
$$
$$
- h_{211}^2)\big)\big/\big(8\epsilon_{\mathbf{k}}h_{01}^2 + 4\epsilon_{\mathbf{k}}(h_{11} - h_{00})h_{211} + 2h_{211}(\pm 2E_1 + h_{11}^2 - h_{211}^2)\big) , \tag{3.19b}
$$
$$
v_{\mathbf{k},\pm,1} = \frac{h_{01}\big[\pm 2E_1 + 2\epsilon_{\mathbf{k}}(h_{00} + h_{211}) + (h_{11} - h_{211})(2E_{\mathbf{k},\pm} + h_{11} + h_{211})\big]}{4\epsilon_{\mathbf{k}}h_{01}^2 + 2\epsilon_{\mathbf{k}}(h_{11} - h_{00})h_{211} + h_{211}(\pm 2E_1 + h_{11}^2 - h_{211}^2)} , \tag{3.19c}
$$
$$
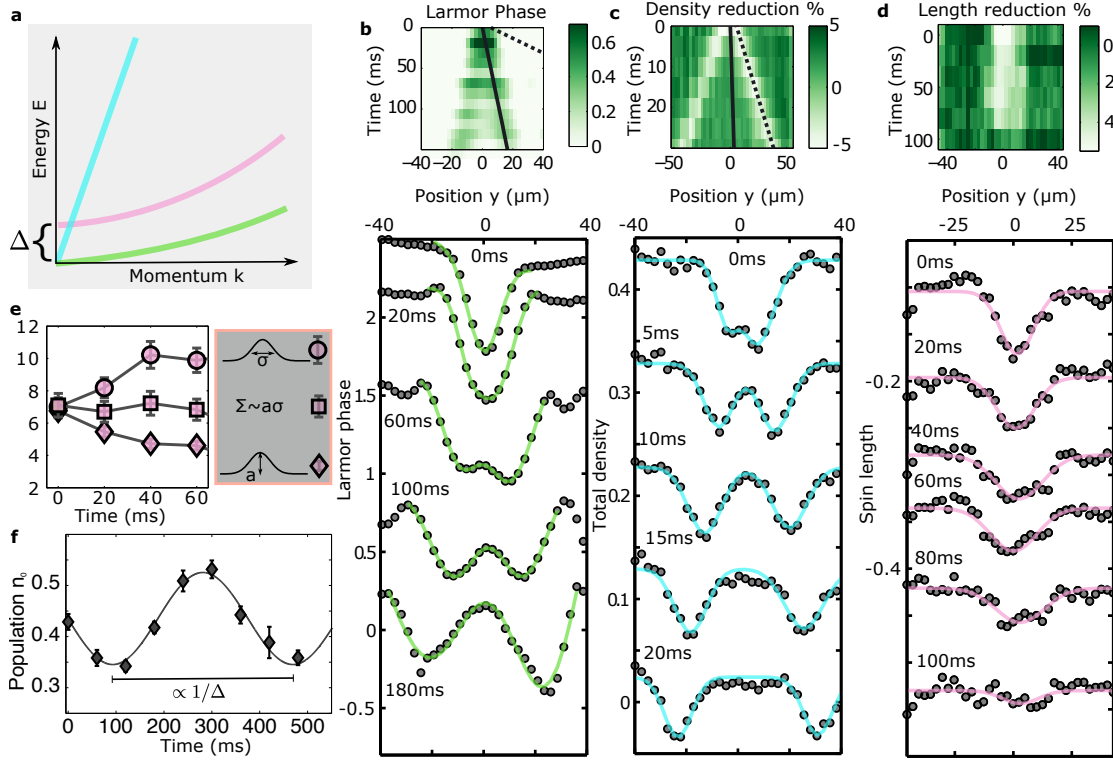v_{\mathbf{k},\pm,2} = 1 , \tag{3.19d}
$$

**FIGURE 3.3:** Local spin and density control enables probing of quasi-particle properties. (a): Schematics of the three Bogoliubov dispersion relations. (b-d): Time evolution of transversal spin orientation (b), total density (c) and spin length (d) after local perturbation of the spin condensate. The upper panels show all evolution times and lower panels selected 1D cuts. We find a splitting of the imprinted wavepacket for phase and total density according to the expected linear dispersion relations (green and blue); solid lines are Gaussian fits. Strikingly, the speed of sound differs by one order of magnitude reflecting the energy scales (solid black line corresponds to $v = 110\mu\text{m/s}$ and dashed line to $v = 1100\mu\text{m/s}$). In contrast, the spin length excitation disperses. (e): Results of Gaussian fits to spin length excitations. $1\sigma$ width (circles), the amplitude $a$ (diamonds) and the integral $\propto a\sigma$ (squares) are shown. We find an increasing (decreasing) width (amplitude) while the product stays nearly constant; this is in accordance with an underlying gapped quadratic dispersion. (f): Oscillation of the $m = 0$ population after perturbing the $k = 0$ mode of the spin length. The oscillation frequency is a measure of the gap $\Delta$ of the quadratic mode identified in (d). All shown error bars are 1 s.d. of the mean.

together with the normalization factors

$$\mathcal{N}_{\mathbf{k},\pm} \equiv \sqrt{u_{\mathbf{k},\pm,1}^2 + u_{\mathbf{k},\pm,2}^2 - v_{\mathbf{k},\pm,1}^2 - v_{\mathbf{k},\pm,2}^2}\,, \tag{3.20}$$

we find the Bogoliubov transformation matrices for transversal excitations (in the parametrization of [157]):

$$U_{\mathbf{k},d\theta} = \begin{pmatrix} u_{\mathbf{k},+,1}/\mathcal{N}_{\mathbf{k},+} & u_{\mathbf{k},+,2}/\mathcal{N}_{\mathbf{k},+} \\ u_{\mathbf{k},-,1}/\mathcal{N}_{\mathbf{k},-} & u_{\mathbf{k},-,2}/\mathcal{N}_{\mathbf{k},-} \end{pmatrix}, \quad V_{\mathbf{k},d\theta} = \begin{pmatrix} -v_{\mathbf{k},+,1}/\mathcal{N}_{\mathbf{k},+} & -v_{\mathbf{k},+,2}/\mathcal{N}_{\mathbf{k},+} \\ -v_{\mathbf{k},-,1}/\mathcal{N}_{\mathbf{k},-} & -v_{\mathbf{k},-,2}/\mathcal{N}_{\mathbf{k},-} \end{pmatrix}. \tag{3.21}$$

These fulfil the identities

$$U_{\mathbf{k},d\theta} U_{\mathbf{k},d\theta}^\dagger - V_{\mathbf{k},d\theta} V_{\mathbf{k},d\theta}^\dagger = 1\,, \qquad U_{\mathbf{k},d\theta}^* V_{\mathbf{k},d\theta}^\dagger - V_{\mathbf{k},d\theta}^* U_{\mathbf{k},d\theta}^\dagger = 0\,, \tag{3.22}$$

as required for the transformations to preserve canonical commutation relations. This requirement is not fulfilled for the transformations given in [157].

The complete transformation matrices diagonalizing the Bogoliubov Hamiltonian (3.8) read

$$U_{\mathbf{k}} = \begin{pmatrix} U_{\mathbf{k},d\theta} & 0 \\ 0 & u_{\mathbf{k},f_z} \end{pmatrix} A(\theta) \,, \qquad V_{\mathbf{k}} = \begin{pmatrix} V_{\mathbf{k},d\theta} & 0 \\ 0 & v_{\mathbf{k},f_z} \end{pmatrix} A(\theta) \,. \tag{3.23}$$

### 3.4.2   Local spin and density perturbations probing quasi-particle properties

Experimentally, we probe the three different modes with dispersions $E_{\mathbf{k},f_z}$ and $E_{\mathbf{k},\pm}$ by applying local perturbations. Experimental details for this can be found in Appendix 3.A. After the perturbation we observe and analyze the temporal evolution, to learn about the underlying structure of the dispersion relations. First, we probe the linear mode associated with the spin orientation by imprinting a spatially varying orientation pattern in $\phi_L$ onto the thermalized state. The probing scheme is based on our capabilities to combine global and local radio frequency spin rotations with fixed relative phases. The initially imprinted Gaussian wavepacket splits up into two wavepackets travelling with velocities of $\pm v_s$, see Figure 3.3(b). This provides a clear indication for a linear dispersion relation.

To access the density degree of freedom we imprint a Gaussian-shaped density reduction of $\sim 5\%$ and observe again a splitting of the initially prepared wave packet, see Figure 3.3(c). The difference in energy scales of density and spin is reflected in the two observed sound speeds $v_d$ and $v_s$ which yield $v_d/v_s \approx 10 \approx \sqrt{|c_0/c_1|}$.

Finally, the gapped mode is associated with excitations of the spin length, which we perturb with a Gaussian length modulation. Strikingly, in Figure 3.3(d) we observe no splitting but a decaying amplitude and growing width of the prepared perturbation. Additionally, we measure the gap of this mode, which manifests as a finite oscillation frequency when exciting the $k = 0$ mode, see Figure 3.3(f). We find a $q$-dependent, non-zero oscillation frequency consistent with expectations concerning the nature of the underlying Bogoliubov mode in the easy-plane ferromagnetic phase.

## 3.5   Thermal comparison

In order to characterize the experimental spinor Bose gas at late times, we compare structure factors of multiple experimentally accessible atom and spin densities with predictions obtained within the Bogoliubov approximation for a thermal ensemble with a single temperature for all Bogoliubov quasi-particles. We describe the latter in Section 3.5.1, before dicussing the experimental protocol and results in Section 3.5.2. A comparison of experimental local density histograms with results for Bogoliubov theory samples is provided in Section 3.5.3, and Section 3.5.4 gives indications for long-lived non-linear excitations in other parameter regimes.

### 3.5.1 Thermal structure factors from Bogoliubov theory

Employing the Bogoliubov theory for the spinor Bose gas, we are interested in correlators of the form

$$\langle \hat{C}^\dagger(\mathbf{x})\hat{C}(\mathbf{y})\rangle_{\beta,s} \tag{3.24}$$

for a composite field $\hat{C}(\mathbf{x})$ given by

$$\hat{C}(\mathbf{x}) = \sum_{m,m'=-1}^{+1} \hat{\psi}_m^\dagger(\mathbf{x})c_{mm'}\hat{\psi}_{m'}(\mathbf{x}) \tag{3.25}$$

with $c_{mm'}$ a $3 \times 3$ matrix corresponding to the type of structure factor under investigation; $c = f^x + \mathrm{i}f^y$ leads to the transversal magnetization structure factor, $c = f^z$ describes the structure factor of magnetization in the $z$-direction, $c = \mathrm{diag}(1,1,1)$ describes the total density structure factor. In Equation (3.24) $\langle \cdot \rangle_{\beta,s}$ indicates the thermal expectation value at inverse temperature $\beta = 1/(k_B T)$ with symmetrically (Weyl-)ordered arguments. We compare with symmetrically ordered predictions since expectation values of experimental observables are inferred from realizations of observables $O^{(i)}$ given by polynomials of complex numbers (cf. [158] for a similar normal-ordered computation). Fourier-transforming Equation (3.24) with respect to the relative coordinate $\mathbf{x} - \mathbf{y}$, we obtain the structure factor

$$\langle \hat{C}^\dagger(\mathbf{k})\hat{C}(\mathbf{k})\rangle_{\beta,s} = \int \mathrm{d}^3(\mathbf{x} - \mathbf{y}) \, \langle \hat{C}^\dagger(\mathbf{x})\hat{C}(\mathbf{y})\rangle_{\beta,s} \, e^{-\mathrm{i}\mathbf{k}(\mathbf{x}-\mathbf{y})}$$

$$= \frac{1}{V} \sum_{m,m',n,n'} c_{mm'}^\dagger c_{nn'} \sum_{\mathbf{p},\mathbf{q}} \langle \hat{a}_{\mathbf{p}+\mathbf{k},m}^\dagger \hat{a}_{\mathbf{p},m'} \hat{a}_{\mathbf{q},n}^\dagger \hat{a}_{\mathbf{q}+\mathbf{k},n'}\rangle_{\beta,s}. \tag{3.26}$$

In the Bogoliubov approximation Equation (3.26) simplifies as follows. We replace zero modes of creation and annihilation operators by numbers, $\hat{a}_{\mathbf{0},m} = \sqrt{N_{\mathrm{cond}}}\zeta_m$, $N_{\mathrm{cond}}$ the total number of condensate atoms. Contributions from fluctuating modes $\hat{a}_{\mathbf{k}\neq\mathbf{0},m}$ are computed from propagators via Wick's theorem. The symmetrically ordered propagators are defined as

$$G_{mm'}^{11}(\mathbf{k}) \equiv \langle \hat{a}_{\mathbf{k},m}\hat{a}_{\mathbf{k},m'}^\dagger\rangle_{\beta,s}, \qquad G_{mm'}^{22}(\mathbf{k}) \equiv \langle \hat{a}_{\mathbf{k},m}^\dagger \hat{a}_{\mathbf{k},m'}\rangle_{\beta,s},$$

$$G_{mm'}^{12}(\mathbf{k}) \equiv \langle \hat{a}_{\mathbf{k},m}\hat{a}_{-\mathbf{k},m'}\rangle_{\beta,s}, \qquad G_{mm'}^{21}(\mathbf{k}) \equiv \langle \hat{a}_{\mathbf{k},m}^\dagger \hat{a}_{-\mathbf{k},m'}^\dagger\rangle_{\beta,s}. \tag{3.27}$$

The first two of these we refer to as normal propagators, the second two as anomalous propagators. Any normal propagator evaluated for non-diagonal momenta such as $\langle \hat{a}_{\mathbf{k},m}^\dagger \hat{a}_{\mathbf{k}',m'}\rangle_{\beta,s}$ for $\mathbf{k}' \neq \mathbf{k}$ and any anomalous propagator evaluated for non-anti-diagonal momenta such as $\langle \hat{a}_{\mathbf{k},m}\hat{a}_{-\mathbf{k}',m'}\rangle_{\beta,s}$ for $\mathbf{k}' \neq \mathbf{k}$ equates to zero. We then find for $\mathbf{k} = \mathbf{0}$,

$$\langle \hat{C}^\dagger(\mathbf{0})\hat{C}(\mathbf{0})\rangle_{\beta,s} = \frac{N_{\mathrm{cond}}(N_{\mathrm{cond}}-1)}{V} \sum_{m,m',n,n'} c_{mm'}^\dagger c_{nn'} \zeta_m^* \zeta_n^* \zeta_{m'} \zeta_{n'} + \mathcal{O}(N_{\mathrm{cond}}), \tag{3.28}$$

and for the non-zero modes $\mathbf{k} \neq \mathbf{0}$,

$$\langle \hat{C}^\dagger(\mathbf{k})\hat{C}(\mathbf{k})\rangle_{\beta,s} = \frac{N_{\text{cond}}}{V} \sum_{m,m',n,n'} c^\dagger_{mm'} c_{nn'} \left[ \zeta_m^* \zeta_n^* G^{12}_{m'n'}(\mathbf{k}) + \zeta_m^* \zeta_{n'} G^{11}_{m'n}(\mathbf{k}) \right.$$
$$\left. + \zeta_n^* \zeta_{m'} G^{22}_{mn'}(\mathbf{k}) + \zeta_{m'} \zeta_{n'} G^{21}_{mn}(\mathbf{k}) \right] + \mathcal{O}(1), \qquad (3.29)$$

where we have used that the propagators $G^{ab}_{mm'}(\mathbf{k})$ only depend on the absolute value of the momentum, $|\mathbf{k}|$. Thus, to leading order in $N_{\text{cond}}$ they are independent from the trap geometry, since no sum over momenta occurs for given $\mathbf{k}$. Normalized experimental structure factors are compared to $\langle \hat{C}^\dagger(\mathbf{k})\hat{C}(\mathbf{k})\rangle_{\beta,s}/n_{\text{cond}}$, $n_{\text{cond}} = N_{\text{cond}}/V$ the total condensate atom density. The photon shot noise of the absorption imaging is determined to be $0.6$ after normalization and is added on the thermal prediction of the total density fluctuations.

In the easy-plane ferromagnetic phase thermal propagators $G^{ab}_{mm'}(\mathbf{k} \neq \mathbf{0})$ can be computed from the Bogoliubov transformations derived in Section 3.4.1. Bogoliubov quasi-particle excitations $f_z$ and $\pm$ are expressed in terms of fundamental magnetic sublevel excitations as

$$\begin{pmatrix} \hat{b}_{\mathbf{k},j} \\ \hat{b}^\dagger_{-\mathbf{k},j} \end{pmatrix} = \sum_{m=-1}^{+1} \begin{pmatrix} U_{\mathbf{k},jm} & V_{\mathbf{k},jm} \\ V^*_{-\mathbf{k},jm} & U^*_{-\mathbf{k},jm} \end{pmatrix} \begin{pmatrix} \hat{a}_{\mathbf{k},m} \\ \hat{a}^\dagger_{-\mathbf{k},m} \end{pmatrix}, \qquad (3.30)$$

for $j \in \{f_z, \pm\}$. Inverting this, we obtain [143]

$$\begin{pmatrix} \hat{a}_{\mathbf{k},m} \\ \hat{a}^\dagger_{-\mathbf{k},m} \end{pmatrix} = \sum_{j \in \{f_z, \pm\}} \begin{pmatrix} U^\dagger_{\mathbf{k},mj} & -V^T_{\mathbf{k},mj} \\ -V^\dagger_{-\mathbf{k},mj} & U^T_{-\mathbf{k},mj} \end{pmatrix} \begin{pmatrix} \hat{b}_{\mathbf{k},j} \\ \hat{b}^\dagger_{-\mathbf{k},j} \end{pmatrix}. \qquad (3.31)$$

The propagators can efficiently be computed from the tensor product

$$\begin{pmatrix} G^{12}_{mm'}(\mathbf{k}) & G^{11}_{mm'}(\mathbf{k}) \\ G^{22}_{mm'}(-\mathbf{k}) & G^{21}_{mm'}(-\mathbf{k}) \end{pmatrix} = \langle \begin{pmatrix} \hat{a}_{\mathbf{k},m} \\ \hat{a}^\dagger_{-\mathbf{k},m} \end{pmatrix} \otimes \begin{pmatrix} \hat{a}_{-\mathbf{k},m'}, \hat{a}^\dagger_{\mathbf{k},m'} \end{pmatrix} \rangle_{\beta,s}$$
$$= \sum_{j,j' \in \{f_z, \pm\}} \begin{pmatrix} U^\dagger_{\mathbf{k},mj} & -V^T_{\mathbf{k},mj} \\ -V^\dagger_{-\mathbf{k},mj} & U^T_{-\mathbf{k},mj} \end{pmatrix} \begin{pmatrix} \langle \hat{b}_{\mathbf{k},j}\hat{b}_{-\mathbf{k},j'}\rangle_{\beta,s} & \langle \hat{b}_{\mathbf{k},j}\hat{b}^\dagger_{\mathbf{k},j'}\rangle_{\beta,s} \\ \langle \hat{b}^\dagger_{-\mathbf{k},j}\hat{b}_{-\mathbf{k},j'}\rangle_{\beta,s} & \langle \hat{b}^\dagger_{-\mathbf{k},j}\hat{b}^\dagger_{\mathbf{k},j'}\rangle_{\beta,s} \end{pmatrix}$$
$$\times \begin{pmatrix} U^*_{-\mathbf{k},j'm'} & -V^*_{-\mathbf{k},j'm'} \\ -V_{\mathbf{k},j'm'} & U_{\mathbf{k},j'm'} \end{pmatrix}. \qquad (3.32)$$

The Bogoliubov quasi-particle modes $\hat{b}_{\mathbf{k},j}$ are occupied thermally,

$$\langle \hat{b}^\dagger_{\mathbf{k},j}\hat{b}_{\mathbf{k},j'}\rangle_\beta = \delta_{jj'} n_\beta(E_{\mathbf{k},j}), \qquad \langle \hat{b}_{\mathbf{k},j}\hat{b}^\dagger_{\mathbf{k},j'}\rangle_\beta = \delta_{jj'}(n_\beta(E_{\mathbf{k},j}) + 1), \qquad (3.33)$$

with the Bose-Einstein distribution $n_\beta(E_{\mathbf{k},j}) \equiv 1/(\exp(\beta E_{\mathbf{k},j}) - 1)$. Anomalous propagators of $\hat{b}_{\mathbf{k},j}$-modes are zero. Insertion of Equation (3.33) into Equation (3.32) and using that

$U_{\mathbf{k},mj}$ and $V_{\mathbf{k},mj}$ only depend on $|\mathbf{k}|$ leads to

$$G^{11}_{mm'}(\mathbf{k}) = \sum_{j\in\{f_z,\pm\}} \left[ U^{\dagger}_{\mathbf{k},mj} \left( n_\beta(E_{\mathbf{k},j}) + \frac{1}{2} \right) U_{\mathbf{k},jm'} + V^T_{\mathbf{k},mj} \left( n_\beta(E_{\mathbf{k},j}) + \frac{1}{2} \right) V^*_{\mathbf{k},jm'} \right],$$

(3.34a)

$$G^{22}_{mm'}(\mathbf{k}) = \sum_{j\in\{f_z,\pm\}} \left[ V^{\dagger}_{\mathbf{k},mj} \left( n_\beta(E_{\mathbf{k},j}) + \frac{1}{2} \right) V_{\mathbf{k},jm'} + U^T_{\mathbf{k},mj} \left( n_\beta(E_{\mathbf{k},j}) + \frac{1}{2} \right) U^*_{\mathbf{k},jm'} \right],$$

(3.34b)

$$G^{12}_{mm'}(\mathbf{k}) = -\sum_{j\in\{f_z,\pm\}} \left[ U^{\dagger}_{\mathbf{k},mj} \left( n_\beta(E_{\mathbf{k},j}) + \frac{1}{2} \right) V_{\mathbf{k},jm'} + V^T_{\mathbf{k},mj} \left( n_\beta(E_{\mathbf{k},j}) + \frac{1}{2} \right) U^*_{\mathbf{k},jm'} \right],$$

(3.34c)

$$G^{21}_{mm'}(\mathbf{k}) = -\sum_{j\in\{f_z,\pm\}} \left[ V^{\dagger}_{\mathbf{k},mj} \left( n_\beta(E_{\mathbf{k},j}) + \frac{1}{2} \right) U_{\mathbf{k},jm'} + U^T_{\mathbf{k},mj} \left( n_\beta(E_{\mathbf{k},j}) + \frac{1}{2} \right) V^*_{\mathbf{k},jm'} \right].$$

(3.34d)

With these expressions thermal structure factors can be readily computed from Equation (3.29).

### 3.5.2 Experimental structure factors

We now turn to the question if we experimentally realized a thermal ensemble. To ease its realization we prepare an elongated spin initial condition and evolve it for $30\,\mathrm{s}$. For this we apply a $\pi/2$-rf rotation with the atoms initially prepared in the state $|F,m\rangle = |1,-1\rangle$. Experimentally, we characterize the thermalized state of our system by using different structure factors, such as those of the spin in transversal as well as in longitudinal ($z$-) direction and the densities of the three $m$-components, see Figure 3.4. For the measurements of the thermalized state we utilize a box size of $\sim 100\,\mu\mathrm{m}$. The position of the walls fluctuates $\sim 0.4\,\mu\mathrm{m}$ from realization to realization. The final characterized state has on average $N_{\mathrm{tot}} = 65,000$ atoms (initially starting with $160,000$ atoms). To separate the single components we employ a Stern-Gerlach magnetic field gradient and a short TOF ($2\,\mathrm{ms}$). We are able to extract momentum-resolved structure factors by Fourier-transforming the spatial profiles, i.e., as functions of the spatial momentum $k$ the structure factors are computed as

$$\langle |\hat{O}(k)|^2 \rangle \simeq |O(k)|^2 = \frac{1}{N_{\mathrm{tot}}} \frac{1}{N_S} \sum_{i=1}^{N_S} \left| \mathrm{DFT}_{x\to k} \left( O^{(i)}(x) - O(x) \right) \right|^2, \tag{3.35}$$

where $\mathrm{DFT}_{x\to k}$ is the discrete Fourier transform, $k = 1/\lambda$ the spatial momentum. The structure factors have been divided by $N_{\mathrm{tot}}$ to obtain an atom number independent measure for the fluctuations and facilitate the comparison between experiment and theory. As a reference noise level for the thermalized structure factor, we prepare a coherent spin state by performing the rotation after holding the atoms in $|1,-1\rangle$ for $30\,\mathrm{s}$ (grey diamonds in Figure 3.4 and Figure 3.6).
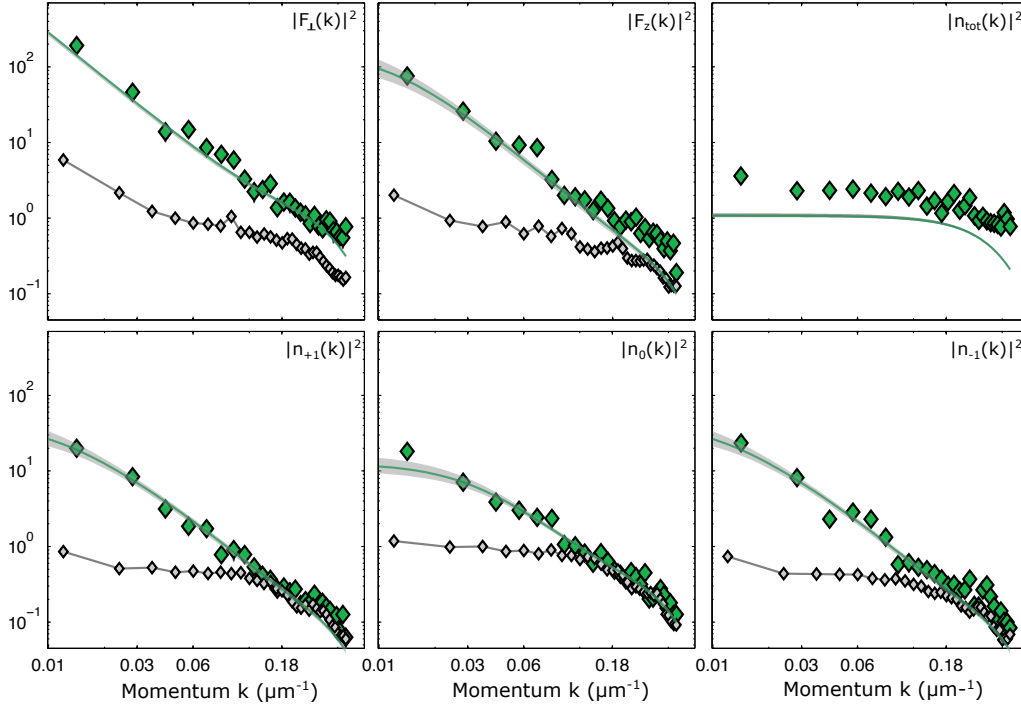
**FIGURE 3.4:** Structure factors of different observables at late times. We show experimental structure factors (green diamonds; error bars smaller than plot markers) after $30\,\text{s}$ evolution time where the system behaves approximately stationary. Experimental uncertainties are smaller than marker size. We compare to a thermal prediction within number-conserving Bogoliubov theory (green line; grey band indicates 68% confidence interval of statistical and systematic uncertainties). Grey diamonds indicate reference noise level of a coherent spin state prepared from a single component gas by a global spin rotation.

For the total density structure factor $|N_{\text{tot}}|^2(k)$ a value of one corresponds to the atomic shot noise level. Special care has to be applied here since phase fluctuations are transformed into density fluctuations during any TOF, leading to a strongly enhanced structure factor for the total atom densities [159, 160]. For its measurement we take in-situ images without spin resolution (without Stern-Gerlach separation). It is important to note that the observed increased fluctuations compared to the spin coherent state by a factor of two can be a result of only one particle per $k$-mode. For the spin observables and the single densities we checked that the enhanced fluctuations due to the TOF are negligible.

The structure factors of all observables are consistently described using a thermal prediction, displayed in Figure 3.4. The latter is obtained for the spinor Bose gas with contact interactions within the Bogoliubov approximation [157, 161], using a single temperature for all three quasi-particle modes and detailed in the previous subsection. We thus conclude that the system has evolved to a thermal state within experimentally accessible time-scales. The found temperature is $(57 \pm 3)\,\text{Hz}$ ($\sim 3\,\text{nK}$) and thus approximately five times smaller than the density-density interaction energy scale ($nc_0 = (252 \pm 54)\,\text{Hz}$) and more than one order of magnitude larger than the spin-spin interaction energy scale ($|nc_1| = (1.17 \pm 0.25)\,\text{Hz}$). The effective energy scales have been obtained from fitting the thermal Bogoliubov theory structure factors to the experimental data as detailed in Appendix 3.B. The temperature is consistent with theoretical estimates for the critical
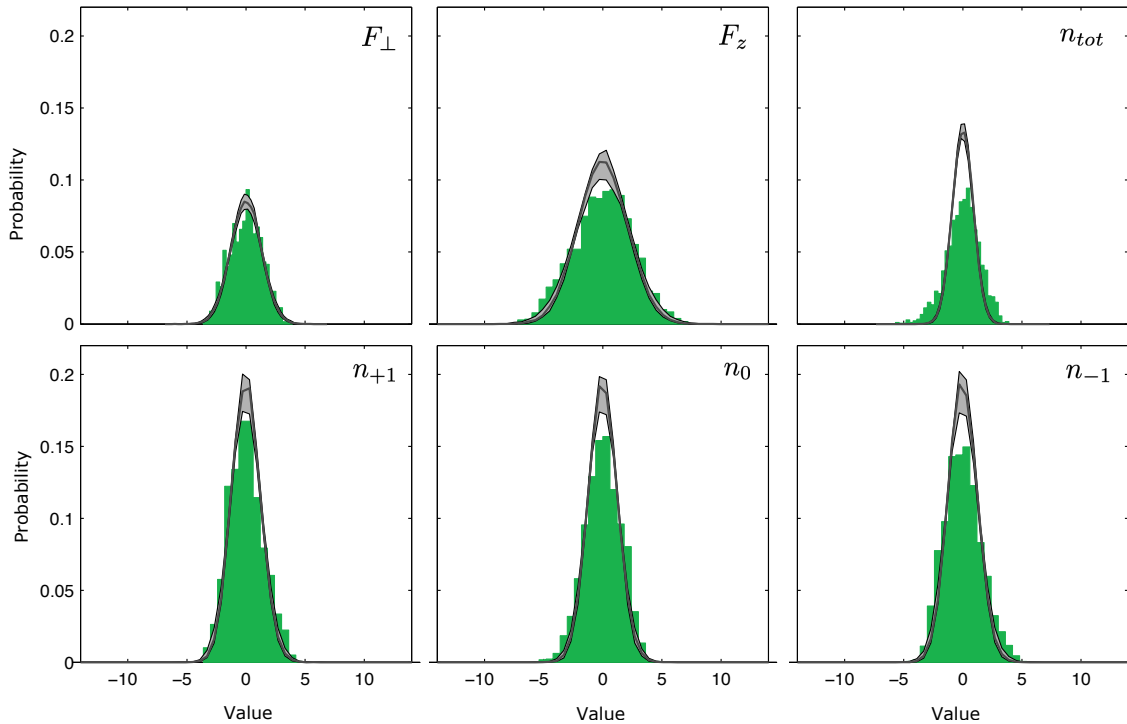
**FIGURE 3.5:** Histograms of local observables in the thermalized state. Histograms obtained from evaluating the local observations of the experimental data presented in Figure 3.4 (green bars). Here, each local observable is normalized to the square-root of the local mean of the total atom number. On top we display theoretical estimates from 1000 samples generated according to thermal Bogoliubov theory with parameters as in Figure 3.4 (grey line; grey band indicates 68% confidence interval including statistical and systematic uncertainties). The mean value of each local observable is subtracted.

temperature related to the emergence of the easy-plane ferromagnetic phase [162, 163]. Interestingly, the single $m$-densities feature high fluctuations also in comparison with three independent single-component condensates at corresponding density, interaction and temperature.

### 3.5.3 Local fluctuations

As a further consistency check with the thermal ensemble, though not independent from the structure factors, we study local density histograms as shown in Figure 3.5. In order to access these within Bogoliubov theory, we devise a sampling scheme for drawing individual samples according to thermal Bogoliubov theory, detailed in Appendix 3.C. We find consistency up to deviations comparable to those for the structure factors displayed in Figure 3.4.

### 3.5.4 Indications for long-lived non-linear excitations

We repeat our measurement close to the phase boundary at $q = 0$ and find structures beyond thermal Bogoliubov theory, see Figure 3.6. The observed enhanced fluctuations can be signatures of long-lived non-linear excitations of the spin [164], which are energetically
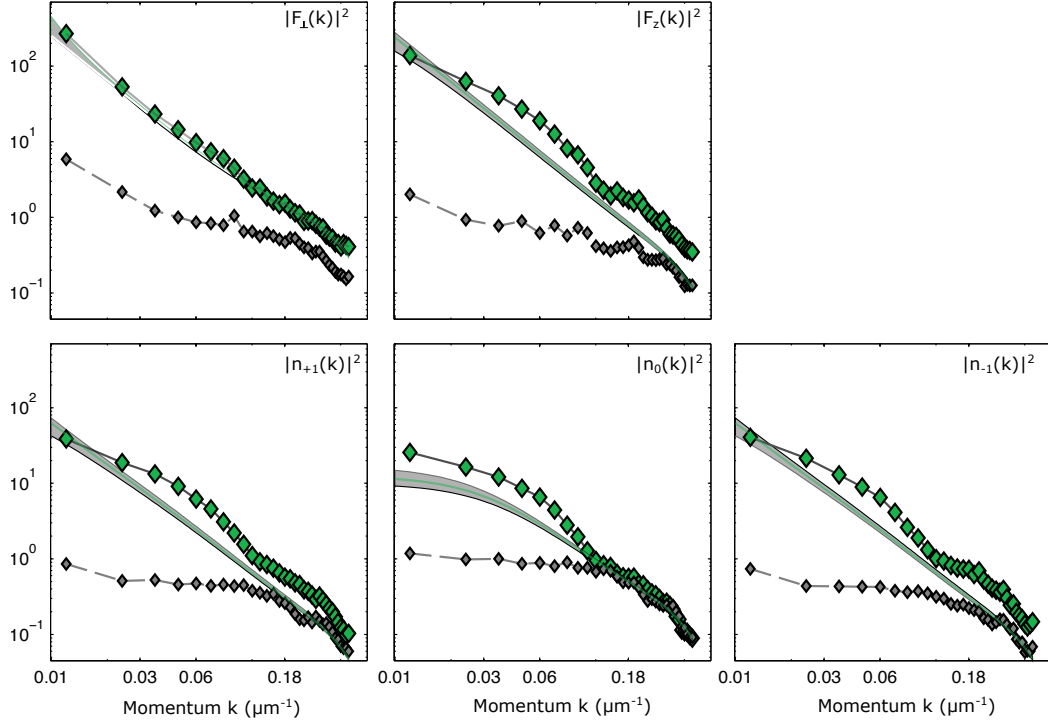
**FIGURE 3.6:** Structure factor close to $q = 0$. We show experimental power spectra of different spin and density degrees of freedom close to $q = 0$ (green diamonds). The grey diamonds represent the fluctuations of a coherent spin state with comparable atom numbers. We compare to thermal Bogoliubov theory predictions for the same parameters as displayed in Figure 3.4 but with $q = 0$ (green line; grey band indicates 68% confidence interval of statistical and systematic uncertainties). Experimentally, we find that for momenta in the range of $0.02\,\mu m^{-1}$ to $0.1\,\mu m^{-1}$ the fluctuations are higher than for the thermal Bogoliubov theory predictions for all observables (except the transversal spin $F_\perp$). The length scale of these fluctuations is in accordance with observable localized long-lived non-linear excitations which are not present in the thermalized data of Figure 3.4.

less suppressed for lower $q$. These excitations can delay equilibration, as discussed for polar core vortices in two spatial dimensions [165].

## 3.6   Summary

We have observed the emergence of effective long-range coherence in a quasi one-dimensional spinor Bose gas. For this we have initialized the system in the polar phase, and have let it evolve for system parameters corresponding to the easy-plane ferromagnetic phase. The built-up condensate has given rise to superfluidity in spin and density degrees of freedom. This we have verified experimentally by dragging an obstacle through the BEC, which couples to both spin and density, and measuring the response of the system. By means of local perturbations of the Larmor phase, the total density and the spin length we have accessed the infrared limit of corresponding dispersion relations. We have shown that these are in accordance with Bogoliubov theory predictions for corresponding quasi-particles.

For this we have derived the extensive Bogoliubov transformations which diagonalize the Hamiltonian corresponding to the spinor Bose gas in the Bogoliubov approximation, assuming a large condensate fraction. This has allowed us to compare diverse experimental structure factors at late times with thermal structure factors obtained from Bogoliubov theory. Agreement has been revealed for a temperature of $\sim 3\,\mathrm{nK}$, obtained from fits to the data. Moreover, local fluctuations of the corresponding observables could be consistently described using a Bogoliubov theory sampling scheme which we have devised.

Proceeding related research questions will be discussed in Chapter 8.

# Appendix

## 3.A    Local perturbations of total density and transversal spin length

To access the superfluid properties of the spin and density degrees of freedom we use a localized perturbation (r.m.s. width $\sim 5\,\mu\mathrm{m}$) that we drag through the thermalized system. Specifically, we use a blue detuned, steerable laser beam ($760\,\mathrm{nm}$) whose position is controlled by an acusto-optical deflector. Using a linear frequency ramp we implement a sweep over the cloud with fixed velocity, which we change over two orders of magnitude. The density is probed after $35\,\mathrm{s}$ and the spin after $20\,\mathrm{s}$ evolution time. The ramp duration for the lowest speed is approximately $18\,\mathrm{s}$.

**Local perturbation of the Larmor phase.**    We use a combination of global and local rf rotations (see [166] for details on local rf rotations). A first global $\pi/2$-rf rotation around the $x$-axis maps the $z$-axis onto the $y$-axis. Using a local rotation with a well-defined phase with respect to the global rotation we perform a rotation with variable angle around the $y$-axis. Because of the performed mapping this effectively leads to a rotation around the $z$-axis in the original coordinate system. At the time $\Delta\tau = 210\,\mu\mathrm{s}$ after the first global rf pulse we apply a global rf $\pi$-pulse followed by a second global rf $\pi/2$-pulse after another time delay of $\Delta\tau$, where all pulses rotate around the same axis. This constitutes a spin echo sequence which additionally executes a full $2\pi$ spin rotation and ensures that the global rotation pulses do not excite the system. The last $\pi/2$-pulse maps the local rotation axis back to the $z$-axis in the original system. The perturbation has an approximate Gaussian shape with a r. m. s. width of $\sim 5\,\mu\mathrm{m}$ according to the shape of the used laser beam.

**Local perturbation of the total density.**    We reduce the total density locally by $\sim 5\%$ by shining a blue detuned laser beam ($760\,\mathrm{nm}$) onto the centre of the cloud. We adiabatically ramp up the potential in $100\,\mathrm{ms}$ such that we get no further excitations in the density; after the ramp the potential is instantaneously switched off to generate the wavepacket.

**Local perturbation of the transversal spin length $|F_\perp|$.**    We induce a local density reduction by applying the same blue-detuned laser beam. During the evolution time of $30\,\mathrm{s}$ we

let the system thermalize subject to the local density reduction. This effectively leads to a spatially dependent mean-field ground state spin length. We linearly ramp down the potential over $50\,\mathrm{ms}$. This implements an adiabatic ramp for the total density and a rapid switch off for the spin.

For experimentally accessing the gap we excite the $k = 0$ mode of the spin length by changing the phase of the $m = 0$ component (spinor phase) globally. For this we use two microwave $\pi$-pulses between $|1, 0\rangle$ and $|2, 0\rangle$, where the second pulse is phase-shifted by $\Delta\phi$. We record the subsequent oscillations of the $m = 0$ population and fit a sinusoidal function to extract the frequency. The theoretical prediction for the gap $\Delta$, deduced from Bogoliubov theory ($E_{\mathbf{k},+}$ as in Equation (3.16)), and the $m = 0$ ground state population $n_0$ in the easy-plane ferromagnetic phase are [157]:

$$\Delta = \sqrt{4n^2 c_1^2 - q^2}\,, \qquad\qquad n_0 = \frac{1}{2} - \frac{q}{4nc_1}\,. \qquad (3.36)$$

Assuming $n_{+1} = n_{-1}$, these formulae also hold for $0 > q > 2nc_1$.

## 3.B   Fitting thermal Bogoliubov theory structure factors

Using a least-squares fitting procedure and Gibbs sampling, systematic as well as statistical uncertainties on the optimal set of parameters for the thermal Bogoliubov theory prediction fits to the experimental structure factors are estimated. Given experimental structure factors $S_{\hat{C},\mathrm{exp}}(k) = \langle \hat{C}^\dagger(k) \hat{C}(k) \rangle$ with $\hat{C} \in \mathcal{S} := \{\hat{N}_{+1}, \hat{N}_0, \hat{N}_{-1}, \hat{F}_z, \hat{F}_\perp\}$, we determine an optimal set of parameters $T, q, nc_1$ by minimizing

$$\chi^2(T, q, nc_1; k_{\mathrm{max}}) = \sum_{\hat{C} \in \mathcal{S}} \sum_{k}^{k_{\mathrm{max}}} \frac{(S_{\hat{C},\mathrm{exp}}(k) - S_{\hat{C},\mathrm{Bog}}(k; T, q, nc_1))^2}{\Delta S_{\hat{C},\mathrm{exp}}(k)^2}\,, \qquad (3.37)$$

with $S_{\hat{C},\mathrm{Bog}}(k; T, q, nc_1) = \langle \hat{C}^\dagger(k) \hat{C}(k) \rangle_{1/(k_B T),s}/n_{\mathrm{cond}}$ the Bogoliubov theory structure factor computed for parameters $T, q, nc_1$, and $\Delta S_{\hat{C},\mathrm{exp}}(k)$ the standard deviation of $S_{\hat{C},\mathrm{exp}}(k)$ computed from experimental realizations. Technical correlations of the absorption imaging are described by real-space signals convoluted with a Gaussian of r. m. s. width $w = 5.0\,\mu\mathrm{m}$, taken into account by the multiplication of momentum-space structure factors with a Gaussian of width $2\pi/w$ [167]. Throughout the fitting procedure we set $c_0/c_1 \simeq -216$ in accordance with [134]. In the definition of $\chi^2$ we did not include the structure factor of the total density.

We define a distribution of parameters for a specific $k_{\mathrm{max}}$,

$$W(T, q, nc_1; k_{\mathrm{max}}) \sim \exp\left(-\chi^2(T, q, nc_1; k_{\mathrm{max}})/2\right)\,. \qquad (3.38)$$

We exploit Gibbs sampling to draw $i = 1, \ldots, 100$ approximately i.i.d. samples $(T^{(i)}(k_{\mathrm{max}}), q^{(i)}(k_{\mathrm{max}}), nc_1^{(i)}(k_{\mathrm{max}}))$ from $W(T, q, nc_1; k_{\mathrm{max}})$, which only requires corresponding conditional distributions normalized individually. For a given $k_{\mathrm{max}}$ we compute their means $(\overline{T}(k_{\mathrm{max}}), \overline{q}(k_{\mathrm{max}}), \overline{nc_1}(k_{\mathrm{max}}))$. We repeat this for 5 values of $k_{\mathrm{max}}$ evenly spaced between $0.1 \cdot 2\pi/\mu\mathrm{m}$ and $0.2 \cdot 2\pi/\mu\mathrm{m}$. Collecting all $5 \cdot 100$ samples in a single array, we take the

mean values $\overline{T}, \overline{q}, \overline{nc_1}$ of all samples as final parameter estimates and their distances to the boundaries of $68\%$ confidence intervals as corresponding error estimates. Errors include systematic fit uncertainties. We obtain the final fit parameters

$$T = (57.4 \pm 2.9)\,\mathrm{Hz}\,, \quad q = (0.30 \pm 0.08)\,\mathrm{Hz}\,, \quad nc_1 = (-1.17 \pm 0.25)\,\mathrm{Hz}\,, \tag{3.39}$$

such that $nc_0 = (252 \pm 54)\,\mathrm{Hz}$ and $q/(nc_1) = (-0.26 \pm 0.09)$.

## 3.C   Drawing Bogoliubov theory samples

Bogoliubov theory being quadratic in fluctuating field creation and annihilation operators, it is fully described by zero modes and a suitable covariance matrix of fluctuations. The latter can be constructed from the propagators $G^{ij}_{mm'}(\mathbf{k})$.

Given a one-dimensional position space lattice $\{-\mathcal{N}, \ldots, \mathcal{N}\} \cdot a$ with lattice spacing $a = L/(2\mathcal{N})$, the corresponding momentum space lattice reads $\{-\mathcal{N}, \ldots, \mathcal{N}\} \cdot \pi/(\mathcal{N}a)$. With $\Delta z = z_1 - z_2 \in \{-2\mathcal{N}, \ldots, 2\mathcal{N}\}$ for $z_i \in \{-\mathcal{N}, \ldots, \mathcal{N}\}$ we compute the real-space propagators via

$$\tilde{G}^{ij}_{mm'}(\Delta z) = \frac{1}{L} \sum_{p=-\mathcal{N}}^{\mathcal{N}} G^{ij}_{mm'}(p) \exp\left(\frac{2\pi \mathrm{i} p \Delta z}{2\mathcal{N}+1}\right). \tag{3.40}$$

We assemble these into magnetic sublevel-specific covariance matrices,

$$\mathrm{Cov}_{mm'} = \langle \begin{pmatrix} \hat{\psi}_m(-\mathcal{N}) \\ \vdots \\ \hat{\psi}_m(\mathcal{N}) \\ \hat{\psi}_m^\dagger(-\mathcal{N}) \\ \vdots \\ \hat{\psi}_m^\dagger(\mathcal{N}) \end{pmatrix} \left(\hat{\psi}_{m'}(-\mathcal{N}), \ldots, \hat{\psi}_{m'}(\mathcal{N}), \hat{\psi}_{m'}^\dagger(-\mathcal{N}), \ldots, \hat{\psi}_{m'}^\dagger(\mathcal{N})\right)\rangle_{\beta,s} \tag{3.41}$$

$$= \begin{pmatrix} \tilde{G}^{12}_{mm'}(0) & \tilde{G}^{12}_{mm'}(-1) & \cdots & \tilde{G}^{12}_{mm'}(-2\mathcal{N}) & \tilde{G}^{11}_{mm'}(0) & \tilde{G}^{11}_{mm'}(-1) & \cdots & \tilde{G}^{11}_{mm'}(-2\mathcal{N}) \\ \tilde{G}^{12}_{mm'}(1) & \tilde{G}^{12}_{mm'}(0) & \cdots & \tilde{G}^{12}_{mm'}(-2\mathcal{N}+1) & \tilde{G}^{11}_{mm'}(1) & \tilde{G}^{11}_{mm'}(0) & \cdots & \tilde{G}^{11}_{mm'}(-2\mathcal{N}+1) \\ \vdots & \vdots & \ddots & \vdots & \vdots & \vdots & \ddots & \vdots \\ \tilde{G}^{12}_{mm'}(2\mathcal{N}) & \tilde{G}^{12}_{mm'}(2\mathcal{N}-1) & \cdots & \tilde{G}^{12}_{mm'}(0) & \tilde{G}^{11}_{mm'}(2\mathcal{N}) & \tilde{G}^{11}_{mm'}(2\mathcal{N}-1) & \cdots & \tilde{G}^{11}_{mm'}(0) \\ \tilde{G}^{22}_{mm'}(0) & \tilde{G}^{22}_{mm'}(-1) & \cdots & \tilde{G}^{22}_{mm'}(-2\mathcal{N}) & \tilde{G}^{21}_{mm'}(0) & \tilde{G}^{21}_{mm'}(-1) & \cdots & \tilde{G}^{21}_{mm'}(-2\mathcal{N}) \\ \tilde{G}^{22}_{mm'}(1) & \tilde{G}^{22}_{mm'}(0) & \cdots & \tilde{G}^{22}_{mm'}(-2\mathcal{N}+1) & \tilde{G}^{21}_{mm'}(1) & \tilde{G}^{21}_{mm'}(0) & \cdots & \tilde{G}^{21}_{mm'}(-2\mathcal{N}+1) \\ \vdots & \vdots & \ddots & \vdots & \vdots & \vdots & \ddots & \vdots \\ \tilde{G}^{22}_{mm'}(2\mathcal{N}) & \tilde{G}^{22}_{mm'}(2\mathcal{N}-1) & \cdots & \tilde{G}^{22}_{mm'}(0) & \tilde{G}^{21}_{mm'}(2\mathcal{N}) & \tilde{G}^{21}_{mm'}(2\mathcal{N}-1) & \cdots & \tilde{G}^{21}_{mm'}(0) \end{pmatrix}, \tag{3.42}$$

exploiting spatial homogeneity. We decompose complex field operators into real components, $\hat{\psi}(x) = \frac{1}{\sqrt{2}}(\hat{\psi}_1(x) + \mathrm{i}\hat{\psi}_2(x))$, translating into the unitary transformation

$$\begin{pmatrix} \hat{\psi}_{m,1}(-\mathcal{N}) \\ \vdots \\ \hat{\psi}_{m,1}(\mathcal{N}) \\ \hat{\psi}_{m,2}(-\mathcal{N}) \\ \vdots \\ \hat{\psi}_{m,2}(\mathcal{N}) \end{pmatrix} = A \begin{pmatrix} \hat{\psi}_m(-\mathcal{N}) \\ \vdots \\ \hat{\psi}_m(\mathcal{N}) \\ \hat{\psi}_m^\dagger(-\mathcal{N}) \\ \vdots \\ \hat{\psi}_m^\dagger(\mathcal{N}) \end{pmatrix}, \qquad A = \frac{1}{\sqrt{2}} \begin{pmatrix} I & I \\ -\mathrm{i}I & \mathrm{i}I \end{pmatrix}, \tag{3.43}$$

with $I$ the $(2\mathcal{N}+1) \times (2\mathcal{N}+1)$-dimensional identity matrix. We define the final covariance matrix of the theory as

$$\text{Cov} = \begin{pmatrix} A\,\text{Cov}_{+1,+1}A^T & A\,\text{Cov}_{+1,0}A^T & A\,\text{Cov}_{+1,-1}A^T \\ A\,\text{Cov}_{0,+1}A^T & A\,\text{Cov}_{0,0}A^T & A\,\text{Cov}_{0,-1}A^T \\ A\,\text{Cov}_{-1,+1}A^T & A\,\text{Cov}_{-1,0}A^T & A\,\text{Cov}_{-1,-1}A^T \end{pmatrix}. \tag{3.44}$$

Finally, we sample $i = 1, \ldots, N_{\text{sample}}$ field realizations

$$\psi^{(i)} = \begin{pmatrix} \psi^{(i)}_{+1} \\ \psi^{(i)}_{0} \\ \psi^{(i)}_{-1} \end{pmatrix},$$

$$\psi^{(i)}_m = \left( \psi^{(i)}_{m,1}(-\mathcal{N}), \quad \cdots, \quad \psi^{(i)}_{m,1}(\mathcal{N}), \quad \psi^{(i)}_{m,2}(-\mathcal{N}), \quad \cdots, \quad \psi^{(i)}_{m,2}(\mathcal{N}) \right)^T, \tag{3.45}$$

from the multivariate Gaussian distribution with zero mean vector and covariance matrix Cov. This corresponds to samples from the Wigner distribution of the symmetrically ordered Bogoliubov theory of fluctuating modes at inverse temperature $\beta$. We sample fields in position space instead of momentum space, since in momentum space, having decomposed the operators $\hat{a}_{k,m}$ into $\hat{a}_{k,m} = (\hat{a}_{k,m,1} + \mathrm{i}\hat{a}_{k,m,2})/\sqrt{2}$, the components $\hat{a}_{k,m,j}$ need to satisfy $\hat{a}^{\dagger}_{k,m,j} = \hat{a}_{-k,m,j}$, such that samples of individual momentum modes cannot be drawn independently. From the fluctuating realizations $\psi^{(i)}$ we can compute realizations of the individual spin sublevel fields in real space,

$$\psi^{(i)}_m(x) = \frac{1}{\sqrt{2}}[\psi^{(i)}_{m,1}(x) + \mathrm{i}\psi^{(i)}_{m,2}(x)] + \sqrt{n_{\text{cond}}}\zeta_m, \tag{3.46}$$

with $n_{\text{cond}}$ the condensate density. We explicitly checked that for increasing sample numbers structure factors computed from the samples $\psi^{(i)}_m(x)$ converge towards their expectation values $G^{ij}_{mm'}(k)$.

The composite operator histograms displayed in Figure 3.5 are computed from composite profiles of individual realizations, given by

$$\sum_{m,m'=-1}^{+1} (\psi^{(i)}_m(x))^* c_{mm'} \psi^{(i)}_{m'}(x)/\sqrt{n_{\text{cond}}}, \tag{3.47}$$

with the matrices $c$ as denoted in Section 3.5.1.

# Chapter 4

# Probing universal dynamics with topological data analysis in a gluonic plasma

This chapter is based on the following article:

- Spitz, D., Boguslavski, K., and Berges, J., "Probing universal dynamics with topological data analysis in a gluonic plasma", *under review in Phys. Rev. D*, arXiv: 2303.08618 [hep-ph].

Most of the present chapter is taken from this preprint, to which I contributed major parts of the manuscript, ran the numerical simulations and analyzed the data, and carried out the data analysis.

## 4.1   Introduction

Collective phenomena are ubiquitous during the thermalization of the quark-gluon plasma generated in ultrarelativistic collisions of heavy nuclei at the LHC or RHIC [38, 59, 60]. Most of the freed quarks and gluons during the first yoctosecond of the collision originate from the small-$x$ regime, giving rise to the notion of gluon saturation and large gluon occupations [168, 169]. The 'bottom-up' scenario provides a systematic description for the subsequent thermalization of the pre-equilibrium QGP [170]. Its early stage is governed by gluon over-occupation at low momenta, such that the weakly coupled system can be accurately mapped onto classical-statistical Yang-Mills theory [109, 171–175], which sets the model for this study. For simplicity we focus on homogeneous initial states in non-expanding Minkowski geometry, while more realistic extensions feature also longitudinal expansion [176].

In this chapter we compute the non-equilibrium time evolution of an initially over-occupied gluonic plasma. For a real-time $SU(2)$ lattice gauge theory in 3+1 dimensions in the classical-statistical regime, we analyze gauge-invariant observables using energy and topological densities and their fluctuations, which evade the typical drawbacks of using gauge-fixed field correlation functions. In order to infer non-local geometric information about the plasma's evolution, we use persistent homology [67, 177, 178]. Persistent homology computes topological structures that appear in a hierarchy of simplicial or

cubical complexes constructed from the field data and features measures of their dominance (persistence). It behaves stable with respect to perturbations on the data, and can be efficiently calculated [67, 177, 178]. We devise gauge-invariant persistent homology observables and demonstrate that they exhibit self-similar evolution in terms of universal scaling exponents and functions.

Identifying universal phenomena in the time evolution of the QGP off equilibrium provides a rich line of understanding the otherwise complicated and theoretically challenging relaxation dynamics of strongly interacting nuclei [38]. For the gluonic plasma these include universal time dependences related to non-thermal fixed points [41, 42, 179], and the universal approach to local thermal equilibrium governed by viscous hydrodynamics [180–182]. Non-thermal fixed points provide far-from-equilibrium attractor solutions characterized by universal dynamical self-similarity, as described earlier in Section 2.3. They have first been discussed for relativistic and non-relativistic scalar theories, partly in the context of reheating of the early universe after inflation [39, 40, 44, 96, 102]. In recent years, dynamical self-similarity has been found experimentally for ultracold Bose gases [47–49].

For the gluonic plasma a dynamically separating hierarchy of momentum scales characterizes transport processes related to non-thermal fixed points. In the infrared, the string tension scale encodes the area dependence of spatial Wilson loops [45, 46], going along with condensation far from equilibrium [51]. The Debye mass describing the electric screening scale evolves dynamically towards the infrared, too [45, 109], and the hard scale indicates energy transport towards the ultraviolet in a universal self-similar process [41, 45, 109, 183–189].

Such universal behavior is typically probed using variants of occupation numbers. These are constructed as two-point correlation functions of gluon fields, which are not gauge-invariant and contain limited information on the plasma. Therefore, it is instrumental to go beyond this description using gauge-invariant observables. Energy densities and their fluctuations are relevant quantities for the hydrodynamical description of the later fluid dynamics of the QGP in heavy ion collisions [190, 191]. Topological densities are of importance for the structure of the QCD vacuum, linked to chiral properties of quarks in the QGP via anomalies and of central relevance for topological effects such as sphaleron transitions [45]. For these reasons the study of two-point correlation functions of energy and topological (charge) densities is promising, which involve gauge-invariant four-point correlation functions in the gluon fields.

A complementary viewpoint on universal dynamics beyond local correlation functions can be based on persistent homology [67, 177, 178]. A first study of persistent homology dynamics in the vicinity of a non-thermal fixed point in scalar field theory demonstrated its ability to reveal self-similar behavior [6]. Persistent homology has been applied in the related context of critical phenomena [72–79], notably confinement in non-Abelian gauge theory [3, 80] and corresponding effective models [192, 193].

This chapter is organized as follows. In Section 4.2 we provide details on the lattice setup and discuss energy and topological density correlations, which show clear manifestations of the direct cascade related to energy transport. We argue that dynamical scaling

exponents can be understood from occupation numbers and the energy-momentum conservation Ward identity. We suggest an explanation for the accurate matching of energy and topological density correlations. In Section 4.3 we introduce persistent homology, and discuss the self-similarity of Betti number distributions. We explain how this can heuristically be understood from the behavior of correlation functions in conjunction with the bounded packing of topological features in the constant lattice volume. Finally, in Section 4.4 we summarize the results of this chapter.

## 4.2 Direct cascade in energy and topological density correlators

Energy and topological density correlators show dynamical self-similarity indicative of an energy cascade. In this section we first describe the lattice simulations and the examined observables, and proceed with an analysis of energy and topological density correlators.

### 4.2.1 Real-time non-Abelian gauge theory on the lattice

We consider $\mathrm{SU}(N_c)$ gauge theory for $N_c = 2$ on a cubic lattice with Minkowski metric, spatial extent $N_s^3$, and temporal and spatial lattice spacings $\mathrm{d}t$ and $a_s$, respectively. Spatially periodic boundary conditions are applied. The volume of the spatial lattice $\Lambda_s$ is $V = a_s^3 N_s^3$. We study the theory in temporal-axial gauge, $A_0 \equiv 0$, and formulate it in terms of $\mathfrak{su}(N_c)$-valued (chromo-)electric fields $\mathbf{E}(t, \mathbf{x})$ and $\mathrm{SU}(N_c)$-valued link variables $U_i(t, \mathbf{x})$, $i = 1, 2, 3$. The latter are related to the gauge fields $A_i(t, \mathbf{x})$ via $U_i(t, \mathbf{x}) \approx \exp(\mathrm{i}g a_s A_i(t, \mathbf{x}))$ up to lattice corrections, with $g$ the gauge coupling.

We study the system in the weakly coupled regime, $g \ll 1$, and consider highly occupied gluonic initial conditions. Then, at sufficiently early times the full quantum dynamics is accurately described by the classical-statistical approximation [96, 109, 171–175]. Specifically, we sample over Gaussian initial conditions with variances

$$\langle AA\rangle(t{=}0, \mathbf{p}) = \frac{Q}{g^2|\mathbf{p}|^2}\,\theta(Q - |\mathbf{p}|)\,, \tag{4.1a}$$

$$\langle EE\rangle(t{=}0, \mathbf{p}) = \frac{Q}{g^2}\,\theta(Q - |\mathbf{p}|)\,, \tag{4.1b}$$

where averages over transverse polarizations and color degrees are implied. Here the momentum scale $Q$ determines the width of the initial momentum-space distribution. In particular, these correlation functions are related to the distribution function of gluonic quasiparticles as $f(t{=}0, \mathbf{p}) \simeq |\mathbf{p}|\langle AA\rangle(t{=}0, \mathbf{p}) \simeq \langle EE\rangle(t{=}0, \mathbf{p})/|\mathbf{p}|$, see Appendix 4.B. Such gluon over-occupation up to a gluon saturation scale is characteristic for a state shortly after the collision of heavy ions [38]. More details on how initial conditions are generated can be found in [41, 188]. The time evolution for the lattice fields $\mathbf{E}(t, \mathbf{x})$ and $U_i(t, \mathbf{x})$ results from solving the classical equations of motion. These are the Hamilton equations for the instantaneous classical lattice Hamiltonian

$$H(t) = \frac{1}{2g^2}\sum_{\mathbf{x}\in\Lambda_s}\left[\mathrm{Tr}\left(\mathbf{E}(t, \mathbf{x})^2\right) + \frac{4}{a_s^4}\sum_{j>k}[N_c - \mathrm{Re}\,\mathrm{Tr}\left(U_{jk}(t, \mathbf{x})\right)]\right] =: \sum_{\mathbf{x}\in\Lambda_s} T^{00}(t, \mathbf{x})\,, \tag{4.2}$$

with elementary spatial plaquette variables

$$U_{jk}(t, \mathbf{x}) = U_j(t, \mathbf{x}) U_k(t, \mathbf{x} + \hat{\mathbf{j}}) U_j^\dagger(t, \mathbf{x} + \hat{\mathbf{k}}) U_k^\dagger(t, \mathbf{x}), \tag{4.3}$$

and $\hat{\mathbf{j}}$, $\hat{\mathbf{k}}$ unit lattice vectors in directions $j, k$. We refer to $T^{00}(t, \mathbf{x})$ as the energy density, and emphasize its gauge-invariance. Specifically, the discretized lattice equations of motion derived from the classical Hamiltonian (4.2) read [188]

$$U_j(t + \mathrm{d}t/2, \mathbf{x}) = e^{\mathrm{i}\,\mathrm{d}t\,a_s g E_j(t, \mathbf{x})} U_j(t - \mathrm{d}t/2, \mathbf{x}), \tag{4.4a}$$

$$g E_i(t + \mathrm{d}t, \mathbf{x}) = g E_i(t, \mathbf{x}) - \frac{\mathrm{d}t}{a_s^3} \sum_{j \neq i} \left[ U_{ij}(t - \mathrm{d}t/2, \mathbf{x}) + U_{i(-j)}(t - \mathrm{d}t/2, \mathbf{x}) \right]_{\mathrm{ah}}, \tag{4.4b}$$

where

$$U_{i(-j)}(t, \mathbf{x}) = U_i(t, \mathbf{x}) U_j^\dagger(t, \mathbf{x} + \hat{\mathbf{i}} - \hat{\mathbf{j}}) U_i^\dagger(\mathbf{x} - \hat{\mathbf{j}}) U_j(\mathbf{x} - \hat{\mathbf{j}}). \tag{4.5}$$

The anti-Hermitian part of a matrix $U$ is defined as

$$[U]_{\mathrm{ah}} = -\frac{\mathrm{i}}{2} \left( U - U^\dagger - \frac{1}{N_c} \mathrm{Tr}\left( U - U^\dagger \right) \right). \tag{4.6}$$

Additionally, Gauss' law has to be satisfied. Once fixed initially, which is accomplished using a projection algorithm onto the constraint surface [194], it is preserved by the time evolution of Equation (4.4).

Finally, observables are computed as the average over sampled initial conditions. We set $N_s = 512$, $\mathrm{d}t/a_s = 0.05$ and $Q a_s = 0.125$, and explicitly verified approximate independence of our results from unphysical lattice parameters. Accordingly, no renormalization is applied to any of the computed observables. Results are shown for a single run, which for our large lattice agree with results averaged over multiple runs up to statistical fluctuations. Rescaling the fields $A_i \to g A_i$ and $E_i \to g E_i$, the equations of motion and initial conditions become independent of the coupling $g$. This formally corresponds to the classical field limit $g \to 0$ while keeping $g^2 f$ fixed. For more details on the lattice formulation we refer to [188]. Based on [46, 195, 196], we expect similar results as in this work for $\mathrm{SU}(N_c)$ theories with $N_c \geq 2$.

In conjunction with energy densities, we study the dynamics of topological densities $q(t, \mathbf{x})$, which are space-time integrands of Chern-Simons numbers. In the continuum, we have $q \sim \mathrm{Tr}\left( \mathbf{E} \cdot \mathbf{B} \right)$, with the (chromo-)magnetic field $\mathbf{B}$.

On the lattice we define a topological density as

$$q(t, \mathbf{x}) := -\frac{1}{32\pi^2} \mathrm{Tr}\left( \mathbf{E}^{\mathrm{av}}(t, \mathbf{x}) \cdot \mathbf{B}^{\mathrm{av}}(t, \mathbf{x}) \right), \tag{4.7}$$

where $\mathbf{E}^{\mathrm{av}}(t, \mathbf{x})$ and $\mathbf{B}^{\mathrm{av}}(t, \mathbf{x})$ are $\mathrm{SU}(N_c)$-valued clover-leaf variants of lattice electric and magnetic fields, averaging contributions of neighboring lattice sites. This expression coincides with [197] and is symmetric under parity transformations due to the employed clover-leaf electric and magnetic fields. We emphasize that $q(t, \mathbf{x})$ defined through Equation (4.7) is gauge-invariant. Expression (4.7) is identical to the spatially symmetrized

(thus clover-leaf) version of the topological density usually employed in lattice studies [95, 198]:

$$q(x) = -\frac{1}{2^9 \pi^2} \sum_{\mu\nu\rho\sigma=\pm0}^{\pm3} \tilde{\epsilon}^{\mu\nu\rho\sigma} \text{Tr} \left( U_{\mu\nu}(x) U_{\rho\sigma}(x) \right). \tag{4.8}$$

Here, the fully antisymmetric $\tilde{\epsilon}^{\mu\nu\rho\sigma} = \tilde{\epsilon}_{\mu\nu\rho\sigma}$ is defined through $1 = \tilde{\epsilon}_{0123} = -\tilde{\epsilon}_{1023} = -\tilde{\epsilon}_{(-0)123}$. Explicitly, in temporal-axial gauge the clover-leaf electric field $\mathbf{E}^{\text{av}}$ is defined from the electric fields $E_i(t, \mathbf{x})$ as the Lie algebra element

$$E_i^{\text{av}}(t, \mathbf{x}) := \frac{1}{4} \Big[ E_i(t + \mathrm{d}t\,/2, \mathbf{x}) + U_i^\dagger(t, \mathbf{x} - \hat{i}) E_i(t + \mathrm{d}t\,/2, \mathbf{x} - \hat{i}) U_i(t, \mathbf{x} - \hat{i})$$
$$+ E_i(t - \mathrm{d}t\,/2, \mathbf{x}) + U_i^\dagger(t - \mathrm{d}t\,, \mathbf{x} - \hat{i}) E_i(t - \mathrm{d}t\,/2, \mathbf{x} - \hat{i}) U_i(t - \mathrm{d}t\,, \mathbf{x} - \hat{i}) \Big]_{\text{ah}}. \tag{4.9}$$

Numerically, due to small deviations $\mathcal{O}(\mathrm{d}t\,)$ compared to the full definition (4.9), we employ the following electric field variant

$$E_i^{\text{av}}(t, \mathbf{x}) = \frac{1}{2} \Big[ E_i(t + \mathrm{d}t\,/2, \mathbf{x}) + U_i^\dagger(t, \mathbf{x} - \hat{i}) E_i(t + \mathrm{d}t\,/2, \mathbf{x} - \hat{i}) U_i(t, \mathbf{x} - \hat{i}) \Big]_{\text{ah}}, \tag{4.10}$$

which transforms under a gauge transformation $V$ as $E_i^{\text{av}}(t, \mathbf{x}) \mapsto V(t, \mathbf{x}) E_i^{\text{av}}(t, \mathbf{x}) V^\dagger(t, \mathbf{x})$. We define a clover-leaf magnetic field as the Lie algebra element

$$B^{\text{av},i}(t, \mathbf{x})$$
$$= \frac{1}{4} \epsilon^{ijk} \Big[ U_{jk}(t, \mathbf{x}) + U_j^\dagger(t, \mathbf{x} - \hat{j}) U_{jk}(t, \mathbf{x} - \hat{j}) U_j(t, \mathbf{x} - \hat{j})$$
$$+ U_k^\dagger(t, \mathbf{x} - \hat{k}) U_{jk}(t, \mathbf{x} - \hat{k}) U_k(t, \mathbf{x} - \hat{k})$$
$$+ U_k^\dagger(t, \mathbf{x} - \hat{k}) U_j^\dagger(t, \mathbf{x} - \hat{j} - \hat{k}) U_{jk}(t, \mathbf{x} - \hat{j} - \hat{k}) U_j(t, \mathbf{x} - \hat{j} - \hat{k}) U_k(t, \mathbf{x} - \hat{k}) \Big]_{\text{ah}}, \tag{4.11}$$

which also transforms gauge covariantly under a gauge transformation $V$ as $B^{\text{av},i}(t, \mathbf{x}) \mapsto V(t, \mathbf{x}) B^{\text{av},i}(t, \mathbf{x}) V^\dagger(t, \mathbf{x})$.

### 4.2.2 Correlations of energy and topological densities

Connected two-point correlation functions of the energy density $T^{00}(t, \mathbf{x})$ are constructed via

$$C_{T^{00}}(t, \Delta\mathbf{x}) := \sum_{\mathbf{x} \in \Lambda_s} \langle T^{00}(t, \mathbf{x} + \Delta\mathbf{x}) T^{00}(t, \mathbf{x}) \rangle_c$$
$$= \sum_{\mathbf{x} \in \Lambda_s} \langle (T^{00}(t, \mathbf{x} + \Delta\mathbf{x}) - \bar{T}^{00})(T^{00}(t, \mathbf{x}) - \bar{T}^{00}) \rangle \tag{4.12}$$

with the volume-averaged energy density

$$\bar{T}^{00} = \frac{1}{N_s^3} \sum_{\mathbf{y} \in \Lambda_s} \langle T^{00}(t, \mathbf{y}) \rangle, \tag{4.13}$$
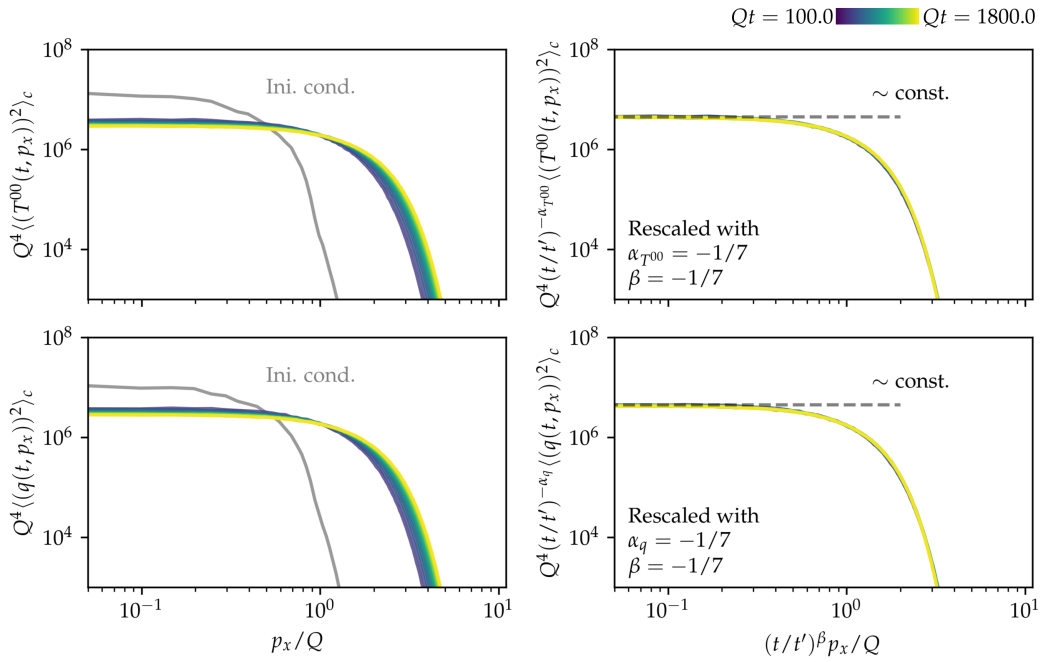
**FIGURE 4.2.1:** Connected two-point correlation functions of energy density $T^{00}(t, p_x)$ (top) and topological density $q(t, p_x)$ (bottom). Variants without (left) and with dynamical rescaling (right) are shown. Gray: Initial condition.

which remains constant in time in the simulations as required by total energy conservation. We Fourier-transform to lattice momentum space in $x$-direction,

$$C_{T^{00}}(t, \tilde{p}_x) = \sum_{\Delta x=0}^{N_s-1} C(t, \Delta\mathbf{x}=(\Delta x, 0, 0))\, e^{-i\tilde{p}_x \Delta x}\,, \qquad (4.14)$$

with $\tilde{p}_x \in 2\pi/(a_s N_s)\{-N_s/2, \dots, N_s/2 - 1\}$ lattice momentum, corresponding to physical momentum $p_x = (2/a_s)\sin(\tilde{p}_x a_s/2)$. Finally, we set

$$\langle (T^{00}(t, p_x))^2 \rangle_c := C_{T^{00}}(t, \tilde{p}_x)\,. \qquad (4.15)$$

In continuum this correlator corresponds to

$$\langle (T^{00}(t, p_x))^2 \rangle_c = \int_{p_y, p_z} \langle T^{00}(t, \mathbf{p})(T^{00}(t, \mathbf{p}))^* \rangle_c\,, \qquad (4.16)$$

where $T^{00}(t, \mathbf{p}) = \int_{\mathbf{x}} T^{00}(t, \mathbf{x}) \exp(-i\mathbf{px})$, with $\int_{\mathbf{x}} = \int_V d^3x$ and $\int_{p_i} = \int dp_i/(2\pi)$. The topological density two-point correlation function $\langle (q(t, p_x))^2 \rangle_c$ is defined analogously.

In Figure 4.2.1 we show results for energy and topological density correlators, compared across times. We find that they start off flat in momentum space and rapidly decay above the momentum scale $Q$. This indicates an equidistribution of low momentum fluctuations of energy and topological densities in momentum space. After a short early-time dynamics (not displayed), the correlators remain constant in shape for times above $Qt = 100$ and solely decrease in overall numbers while shifting to larger momenta. This is indicative of a non-thermal fixed point. We test for the characteristic dynamical self-similar

scaling according to the scaling ansatz

$$\langle (T^{00}(t, p_x))^2 \rangle_c = (t/t')^{\alpha_{T^{00}}} \langle (T^{00}(t', (t/t')^\beta p_x))^2 \rangle_c, \tag{4.17}$$

for suitably chosen scaling exponents $\alpha_{T^{00}}, \beta$ and a reference time $t'$ in the time interval when Equation (4.17) describes the dynamics accurately. In the right column of Figure 4.2.1 we display correlations rescaled according to the scaling ansatz (4.17), where we suggestively set $\beta = -1/7$ and $\alpha_{T^{00}} = -1/7$. We find accurate matching of the rescaled correlations for the entire considered time range from $Qt = 100$ to $Qt = 1800$. The same observations apply to topological density correlations. In fact, both types of correlations agree with each other nearly exactly. We argue for this at the end of this subsection, and primarily discuss $T^{00}$ correlations in the following, noting that similar arguments apply for topological density correlations.

One can heuristically motivate the scaling ansatz (4.17) by following a kinetic quasi-particle picture. The Fourier-transformed local energy density fluctuations for sample $i$ can be approximated on an individual sample level as

$$T_i^{00}(t, \mathbf{p}) \sim \omega_\mathbf{p} \, f_i(t, \mathbf{p}) \, . \tag{4.18}$$

Here, $\omega_\mathbf{p} \simeq |\mathbf{p}|$ is the gluon dispersion and $f_i(t, \mathbf{p})$ denotes a distribution function of gluon occupation numbers computed for a single classical-statistical sample. It has previously been demonstrated that the gluon occupancy $\langle f_i(t, \mathbf{p}) \rangle$ shows dynamical self-similarity for initial conditions similar to ours, scaling as [41, 109, 186–188]

$$\langle f_i(t, \mathbf{p}) \rangle = (t/t')^{-4/7} \langle f_i(t', (t/t')^{-1/7} \mathbf{p}) \rangle \, , \tag{4.19}$$

even for single samples as for our simulations, see Appendix 4.B. The scaling is reminiscent of a direct energy cascade to higher momenta since the momenta of hard modes grow during this process as $(t/t')^{1/7}Q$, while the energy (density) remains constant, $\langle \int_\mathbf{p} T_i^{00}(t, \mathbf{p}) \rangle = \text{const.}$ Due to Equation (4.18) one expects that the exponent $\beta = -1/7$ governs the dynamics at hard momenta also for $\langle (T^{00}(t, p_x))^2 \rangle_c$.

The scaling exponent $\alpha_{T^{00}}$ can be understood from the energy-momentum conservation Ward identity. For the derivation we work in a continuum space-time with spatial volume $V$ in a general spatial dimension $d$. By means of metric variations, in [199] the identity

$$0 = \langle \partial_{x_1, \nu} T^{0\nu}(x_1) T^{00}(x_2) \rangle_c \tag{4.20}$$

has been derived for correlations of the stress-energy tensor $T^{\mu\nu}(x)$, connected in the $T^{\mu\nu}(x_i)$. Integrating $x_1$ over $V$, we find using Gauss' theorem and periodic boundary conditions, such that no spatial boundary terms occur,

$$0 = \partial_{t_1} \int_\mathbf{x} \langle T^{00}(t_1, \mathbf{x}) T^{00}(t_2, \mathbf{y}) \rangle_c \, . \tag{4.21}$$

Expectation values in our simulations exhibit approximate homogeneity and isotropy in space, such that

$$\int_{\mathbf{x}} \langle T^{00}(t_1, \mathbf{x})T^{00}(t_2, \mathbf{y})\rangle_c = \int_{\Delta \mathbf{y}} \langle T^{00}(t_1, \mathbf{0})T^{00}(t_2, \Delta \mathbf{y})\rangle_c$$
$$= \int_{\Delta \mathbf{x}} \langle T^{00}(t_1, \Delta \mathbf{x})T^{00}(t_2, \mathbf{0})\rangle_c, \qquad (4.22)$$

where $\Delta \mathbf{x} = \mathbf{x} - \mathbf{y}$ and $\Delta \mathbf{y} = \mathbf{y} - \mathbf{x}$. We note that

$$\partial_t \langle T^{00}(t, \mathbf{x})T^{00}(t, \mathbf{y})\rangle_c = (\partial_{t_1} + \partial_{t_2})|_{t_1=t_2=t} \langle T^{00}(t_1, \mathbf{x})T^{00}(t_2, \mathbf{y})\rangle_c. \qquad (4.23)$$

Analogous to Equation (4.17) we assume a scaling ansatz in position space for $T^{00}$-correlations,

$$\langle T^{00}(t, \mathbf{x})T^{00}(t, \mathbf{y})\rangle_c = (t/t')^{\alpha'} \langle T^{00}(t', (t/t')^{-\beta}\mathbf{x})T^{00}(t', (t/t')^{-\beta}\mathbf{y})\rangle_c. \qquad (4.24)$$

Together with classical-statistical simulations corresponding to symmetric operator ordering, denoted $\langle \cdot \rangle_s$, this yields

$$0 = (\partial_{t_1} + \partial_{t_2})|_{t_1=t_2=t} \int_{\mathbf{x}} \langle T^{00}(t_1, \mathbf{x})T^{00}(t_2, \mathbf{y})\rangle_{c,s}$$
$$= \partial_t \int_{\mathbf{x}} \langle T^{00}(t, \mathbf{x})T^{00}(t, \mathbf{y})\rangle_{c,s}$$
$$= \partial_t \int_{\Delta \mathbf{x}} \langle T^{00}(t, \Delta \mathbf{x})T^{00}(t, \mathbf{0})\rangle_{c,s}$$
$$= \partial_t \left[ (t/t')^{\alpha'+d\beta} \int_{\Delta \mathbf{x}'} \langle T^{00}(t', \Delta \mathbf{x}')T^{00}(t', \mathbf{0})\rangle_{c,s} \right]$$
$$= \frac{\alpha' + d\beta}{t'} (t/t')^{\alpha'+d\beta-1} \int_{\Delta \mathbf{x}'} \langle T^{00}(t', \Delta \mathbf{x}')T^{00}(t', \mathbf{0})\rangle_{c,s}, \qquad (4.25)$$

with the substitution $\Delta \mathbf{x}' = (t/t')^{-\beta} \Delta \mathbf{x}$ and exploiting the empty boundary of the lattice torus due to periodic boundary conditions. This is solved by $\alpha' = -d\beta$. We obtain the scaling behavior of $\langle (T^{00}(t, p_x))^2 \rangle_c$ via momentum integration over directions $2, \dots, d$ and a Fourier transformation:

$$\langle (T^{00}(t, p_x))^2 \rangle_c = \int_{p_2, \dots, p_d} \int_{\Delta \mathbf{x}} \int_{\mathbf{x}} \langle T^{00}(t, \mathbf{x} + \Delta \mathbf{x})T^{00}(t, \mathbf{x})\rangle_{c,s} e^{-i\mathbf{p}\Delta \mathbf{x}}$$
$$= (t/t')^{\beta} \langle (T^{00}(t', (t/t')^{\beta} p_x))^2 \rangle_c, \qquad (4.26)$$

such that $\alpha_{T^{00}} = \beta$, which is consistent with Figure 4.2.1.

It remains to discuss the similarity of energy density $T^{00} \sim \mathrm{Tr}\,(\mathbf{E}^2 + \mathbf{B}^2)$ and topological density $q \sim \mathrm{Tr}\,(\mathbf{E} \cdot \mathbf{B})$ correlations visible in Figure 4.2.1 and giving rise to identical dynamical scaling behavior. While their one-point functions are different,

$$\bar{T}^{00} = (0.106 \pm 8.4 \cdot 10^{-8})/Q^4, \qquad \bar{q} = (2.2 \cdot 10^{-5} \pm 3.3 \cdot 10^{-5})/Q^4, \qquad (4.27)$$

where the error indicates fluctuations in time, their variances agree. This suggests that

the colour and spatial directions of $\mathbf{E}(t, \mathbf{x})$ and $\mathbf{B}(t, \mathbf{x})$ are statistically independent and, by spatial homogeneity, identically distributed (i.i.d.). This is consistent with the observed $\langle \mathrm{Tr}\,(\mathbf{E}^2 + \mathbf{B}^2) \rangle > 0$, $\langle \mathrm{Tr}\,(\mathbf{E} \cdot \mathbf{B}) \rangle = 0$, and identical higher-order connected correlation functions. Phrased differently, the space-time and colour components of the field strength tensor $F^{\mu\nu}(t, \mathbf{x})$ are i.i.d. up to antisymmetry of the indices. Similar observations have been reported for two-point correlation functions of electric and magnetic fields [186]. Note that this indicates suppressed contributions from non-trivial topological excitations such as sphalerons [45].

The agreement of energy and topological densities provides further evidence for the universality of the non-thermal fixed point across different observables $\mathcal{O}$ with respect to its scaling exponent $\beta$. The amplitude exponent $\alpha_{\mathcal{O}}$ is linked to $\beta$ by constraints such as energy-momentum conservation. In the next section we provide a complementary study of this universality by analyzing non-local geometric observables instead of correlation functions.

## 4.3 Direct cascade in persistent homology

Persistent homology provides a quantitative means to extract topological structures from point clouds of data, and is based on the construction of a hierarchy of combinatorial objects like simplicial or cubical complexes. We will start this section with an intuitive introduction to the utilized alpha complexes and their persistent homology in Section 4.3.1, followed by a discussion of dynamical self-similarity in persistent homology in Section 4.3.2. We then study the dynamics of topological structures in point clouds computed from energy and topological densities in Section 4.3.3. We find clear indications for self-similar scaling associated to the energy cascade, which again reveals universality across observables. Moreover, we confirm a geometric relation between appearing exponents in persistent homology. In Section 4.3.4 we discuss persistence ratios of topological structures, i.e., spatially scale-invariant measures of their dominance, which form a set of dynamical invariants beyond self-similarity in the gluonic plasma.

Similarly to the findings for alpha complexes reported in this section, in Appendix 4.D we discuss so-called cubical complexes, which give access to the persistent homology of level sets without spatial metric information entering the analysis, and are particularly suitable for pixelized data. In this approach the application of coarse-graining is inevitable to exclude lattice artefacts. Again, we find evidence for self-similarity associated to the energy cascade. Hence, the universal dynamics also encompasses the persistent homology of cubical complexes.

### 4.3.1 Introducing alpha complexes and persistent homology

Let $X \subset \mathbb{R}^3$ be a point cloud, i.e., a finite set of distinct points. [1] Alpha complexes of $X$ are computationally useful geometric simplicial complexes describing $X$. Their topology can

---

[1]We assume the point cloud to be in general position, i.e., that no three points are collinear, that no four points lie on a single circle, and that no five points lie on a sphere.
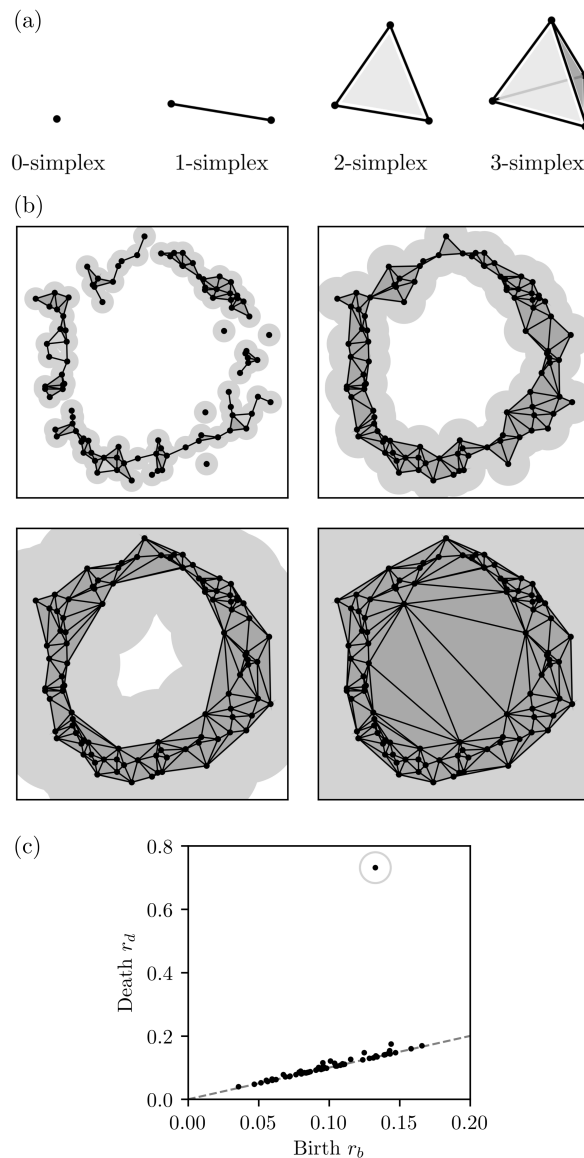
**FIGURE 4.3.1:** (a): Simplices of different dimensions; the 3-simplex is to be regarded as filled. (b): Alpha complexes of increasing radii. The point cloud in (b) consists of points sampled randomly from a circle with Gaussian noise added on their positions. (c): Persistence diagram of dimension one holes of the point cloud. Dashed line: the diagonal $r_b = r_d$.

be extracted algorithmically, which is facilitated by their combinatorial properties. Here we focus on an intuitive description, and in Appendix 4.A we deliver more mathematical details related to persistent homology. For a thorough introduction to topological data analysis we refer to the literature [67, 177, 178, 200], similarly for general introductions to algebraic topology [201, 202].

Simplices of different dimensions are illustrated in Figure 4.3.1(a). We refer to a point as a 0-simplex, a line as a 1-simplex, a triangle as a 2-simplex, and a filled tetrahedron as a 3-simplex. A simplicial complex is a collection of simplices closed under taking boundaries. We construct alpha complexes of $X$. Trivially, we can connect two points in $X$ by a straight line, i.e., a 1-simplex. Similarly, through any three points in $X$ we can draw

a unique circle and through any four points in $X$ we can draw a unique sphere. We call a circle or sphere empty if all points of $X$ lie on or outside of it. We can associate to any two, three and four points a 1-, 2- or 3-simplex connecting them, and a radius parameter. The latter can be defined as half of the length of the line between the two points, as the radius of the unique circle through the three points, or as the radius of the unique sphere through the four points, respectively. We finally define the alpha complex $\alpha_r(X)$ of $X$ with radius $r$ to consist of empty simplices of arbitrary dimension $\leq 3$ with radius $\leq r$. The construction works analogously in an arbitrary number of dimensions. Alpha complexes are simplicial complexes.

In Figure 4.3.1(b) we give two-dimensional examples of alpha complexes of increasing radii (indicated by gray disks around the points) for a cloud consisting of points sampled randomly from a circle with Gaussian noise added to their positions. We note that simplices which enter at larger radii have visually larger area. For a finite point cloud there are finitely many different alpha complexes $\alpha_{r_i}(X)$ with $r_i < r_j$ for $i < j$, $i, j = 1, \ldots, K$ for an integer $K$. They form a filtration:

$$\alpha_0(X) = \emptyset \subsetneq \alpha_1(X) \subsetneq \cdots \subsetneq \alpha_K(X) = \mathrm{Del}(X) \,. \tag{4.28}$$

The final, 'full' alpha complex $\mathrm{Del}(X)$ is also known as the Delaunay complex or Delaunay triangulation. That alpha complexes of increasing radii are nested can be seen in Figure 4.3.1(b).

As we sweep through the filtration of alpha complexes $\alpha_r(X)$, topology changes appear. We observe in Figure 4.3.1(b) that for the lowest radius the alpha complex consists of many distinct connected components. Upon increasing the radius, the connected components successively merge with each other, such that the large loop gets born in the alpha complex. The large loop persists for a comparably large range of radii, until it dies when filled entirely by triangles. Its topology does not 'see' its thickening upon increasing the radius. We describe the topology of $\alpha_r(X)$ for a specific radius $r$ by homology, which can be algorithmically computed. Homology can describe holes of different dimensions in complexes. A dimension zero hole is a connected component, a dimension one hole is an unfilled, planar-like loop, and a dimension two hole is an empty void in the complex.

Persistent homology describes the changing topology of the entire filtration of alpha complexes at once. It associates to a dimension-$k$ hole a birth radius $r_b$ and a death radius $r_d > r_b$, such that the hole is present in the alpha complexes for all radii $r \in [r_b, r_d)$, with $r_b$ minimal and $r_d$ maximal. We can describe the persistent homology of the filtration of alpha complexes $\{\alpha_r(X)\}_r$ by the collection of all birth-death pairs $(r_b, r_d)$, which we call the persistence diagram, denoted $\mathrm{Dgm}_k(X)$. In Figure 4.3.1(c) we display the dimension one persistence diagram of the noisy, approximately circular point cloud. We note that many features appear near the diagonal $r_b = r_d$, i.e., have persistence ratio $r_d/r_b$ near 1, represented by the tiny, short-lived unfilled loops which appear at smaller radii in Figure 4.3.1(b). One prominent feature appears at large $r_d$, highlighted in Figure 4.3.1(c). Having a high persistence ratio $r_d/r_b \simeq 5$, this feature is represented by the large circular structure present in the point cloud. In summary, persistent homology

provides a quantitative means to extract topological structures from point cloud data, and incorporates persistence measures of their dominance.

Persistent homology has a number of useful theoretical properties. It is stable, i.e., perturbations of the input point cloud result in only slight changes of corresponding persistence diagrams with respect to suitable metrics [68, 69]. Furthermore, most observables computed with persistent homology behave well with regard to statistical limits, and also large volume asymptotics exist, including notions of ergodicity, see [71] and Chapter 5. The efficient computation of persistent homology is facilitated by a variety of suitable libraries for different programming languages, see [67] for an overview. We employ the versatile GUDHI library [203], and compute periodic alpha complexes to take the spatially periodic boundary conditions of our lattice into account.

### 4.3.2   Self-similarity in persistent homology

How can dynamical self-similarity manifest itself in persistent homology? Let $X(t) \subset \mathbb{R}^d$ be a family of time-dependent point clouds. In [6] the dimension-$k$ persistence pair distribution has been introduced as

$$\mathfrak{P}_k(t, r_b, r_d) = \sum_{(r_b', r_d') \in \mathrm{Dgm}_k(X(t))} \delta(r_b - r_b') \, \delta(r_d - r_d') \,. \tag{4.29}$$

In general, its expectation value $\langle \mathfrak{P}_k \rangle(t, r_b, r_d)$ exists and is not a sum of Dirac $\delta$-functions anymore, see [204] and Chapter 5. We note that $\langle \mathfrak{P}_k \rangle(t, r_b, r_d)$ has support only for $r_d > r_b$. We say that the expected persistence pair distribution $\langle \mathfrak{P}_k \rangle(t, r_b, r_d)$ scales self-similarly in time if

$$\langle \mathfrak{P}_k \rangle(t, r_b, r_d) = (t/t')^{-\eta_2} \langle \mathfrak{P}_k \rangle(t', (t/t')^{-\eta_1} r_b, (t/t')^{-\eta_1} r_d) \,, \tag{4.30}$$

for suitable scaling exponents $\eta_1, \eta_2$ and arbitrary reference time $t'$ in the self-similar regime. This scaling ansatz is similar to the position space scaling ansatz for the $T^{00}$-correlator given in Equation (4.24).

From $\langle \mathfrak{P}_k \rangle$ we can compute many persistent homology descriptors. For instance, the expected number of dimension-$k$ holes at radius $r$, known as the Betti number, can be computed as

$$\beta_k(t, r) = \int_0^r \mathrm{d}r_b \int_r^\infty \mathrm{d}r_d \, \langle \mathfrak{P}_k \rangle(t, r_b, r_d) \,. \tag{4.31}$$

With Equation (4.30) Betti numbers scale as

$$\beta_k(t, r) = (t/t')^{2\eta_1 - \eta_2} \beta_k(t', (t/t')^{-\eta_1} r) \,. \tag{4.32}$$

$\langle \mathfrak{P}_k \rangle$ also yields the total number of homology classes that appear in the filtration at arbitrary radius:

$$n_k(t) = \int_0^\infty \mathrm{d}r_b \int_0^\infty \mathrm{d}r_d \, \langle \mathfrak{P}_k \rangle(t, r_b, r_d) \,, \tag{4.33}$$

which scales as

$$n_k(t) = (t/t')^{2\eta_1 - \eta_2} n_k(t') \,. \tag{4.34}$$

**FIGURE 4.3.2:** Betti number distributions of the alpha complex filtration for $T^{00}(t, \mathbf{x})$ (top) and $q(t, \mathbf{x})$ sublevel sets (bottom), with limiting values $\nu_{T^{00}} = -0.081/Q^4$ and $\nu_q = -0.13/Q^4$. Scaling exponents are set to $\eta_1 = -1/7$ and $\eta_2 = 5\eta_1 = -5/7$ in accordance with the packing relation. Insets show figures without rescaling. Distributions at initial time are displayed in gray.

The exponent $\eta_2$ encodes the power-law decline of the number of persistent homology classes for given birth and death radii $r_b, r_d$. Similarly, we can compute from $\langle \mathfrak{P}_k \rangle$ the average death radius of dimension-$k$ holes as

$$\langle r_{d,k} \rangle(t) = \frac{1}{n_k(t)} \int_0^\infty \mathrm{d}r_b \int_0^\infty \mathrm{d}r_d \, r_d \, \langle \mathfrak{P}_k \rangle(t, r_b, r_d) = (t/t')^{\eta_1} \langle r_{d,k} \rangle(t') \,. \tag{4.35}$$

The exponent $\eta_1$ describes the dynamical power-law blow-up of length scales associated to persistent homology. For later use we note that the normalized distribution of persistence ratios $\pi = r_d/r_b$ can be computed from $\langle \mathfrak{P}_k \rangle$ as

$$\Pi_k(t, \pi) = \frac{1}{n_k(t)} \int_0^\infty \mathrm{d}r_b \, r_b \, \langle \mathfrak{P}_k \rangle(t, r_b, \pi r_b) \,. \tag{4.36}$$

For self-similar time evolutions all $\Pi_k(t, \pi)$ constitute invariants of motion. It has been conjectured in [205] that the distributions $\Pi_k(t, \pi)$ are in fact universal across different processes to generate i.i.d. point clouds, thus invariant beyond self-similar time evolutions. We will confirm this in Section 4.3.4.

### 4.3.3 Dynamics of homology classes in Betti numbers

Alpha complexes and their persistent homology require point clouds as input. Motivated by the findings of Section 4.2.2, we examine sublevel sets of energy and topological

densities, constructed for $T_i^{00}(t, \mathbf{x})$ and $q_i(t, \mathbf{x})$, and computed from an individual classical-statistical sample $i$ as

$$X_{T^{00}, \nu_{T^{00}}, i}(t) := \{\mathbf{x} \in \Lambda_s \mid T_i^{00}(t, \mathbf{x}) - \bar{T}^{00} \leq \nu_{T^{00}}\}, \qquad (4.37\text{a})$$

$$X_{q, \nu_q, i}(t) := \{\mathbf{x} \in \Lambda_s \mid q_i(t, \mathbf{x}) \leq \nu_q\}. \qquad (4.37\text{b})$$

For each such point cloud at time $t$ we compute the persistent homology of its filtration of alpha complexes. In the classical-statistical approximation we approximate expectation values of persistent homology descriptors as ensemble averages of observables computed for individual samples [6].

In Figure 4.3.2 we show results for Betti number distributions of energy and topological density sublevel sets. We set $\nu_{T^{00}} = -0.081/Q^4$ and $\nu_q = -0.13/Q^4$, such that the point clouds comprise $20,000 - 50,000$ points which reflect the dynamics of local minima. For comparison, $\bar{T}^{00}$ and $\bar{q}$ have been given in Equation (4.27). We notice that dimension zero Betti numbers monotonously decrease with increasing radii, which originates from connected components merging and thus decreasing in number. Dimension one and two Betti numbers show distinct peaks. We observe peaks appearing at larger radii the larger the dimension of the holes is. Dimension zero holes are present at lowest radii, required to merge with each other to form dimension one holes, which in turn need to die (getting filled with triangles) to form dimension two holes, and thus giving rise to the hierarchy. Focusing on the inset figures for $T_i^{00}$ and $q_i$ sublevel sets, we notice a continuous motion of holes to lower radii with time, across all dimensions. The numbers of holes increase, while the shapes of Betti number distributions qualitatively remain invariant. This suggests that topological structures in the alpha complexes decrease in size in the course of time.

The main figures are rescaled according to Equation (4.32). We propose the exponents $\eta_1 = -1/7$, $\eta_2 = -5/7$. For these we observe that the rescaled distributions coincide to good accuracy, which is indicative of the validity of the self-similar scaling ansatz for persistent homology, given in Equation (4.30). The relation $\eta_2 = 5\eta_1$ is an example of the general packing relation first observed in [6] and rigorously proven in Chapter 5 of this dissertation. It originates from the geometric bound that the constant volume puts on the number of holes. If holes decrease in size, more of them fit on the lattice.

We explicitly checked for the independence of the scaling behavior and qualitative shapes of Betti number distributions from the choice of $\nu_{T^{00}}$ and $\nu_q$ in nearby regimes. We verified an approximate insensitivity from infrared and ultraviolet lattice cutoffs, such that the non-local features that persistent homology captures are well-resolved and sufficiently dense.

We conclude that the persistent homology of sublevel sets of energy and topological densities reveals self-similar scaling related to the energy cascade with the same spatial scaling exponent $\eta_1 = \beta$ as for correlation functions. Yet, while energy densities are bounded by positivity, $T_i^{00} \geq 0$, this is not the case for topological densities. This generally results in different functional shapes through the involved point cloud construction. This is to be contrasted with correlation functions. Still, with regard to scaling exponents, we find that the universality of the self-similar dynamics related to the energy cascade
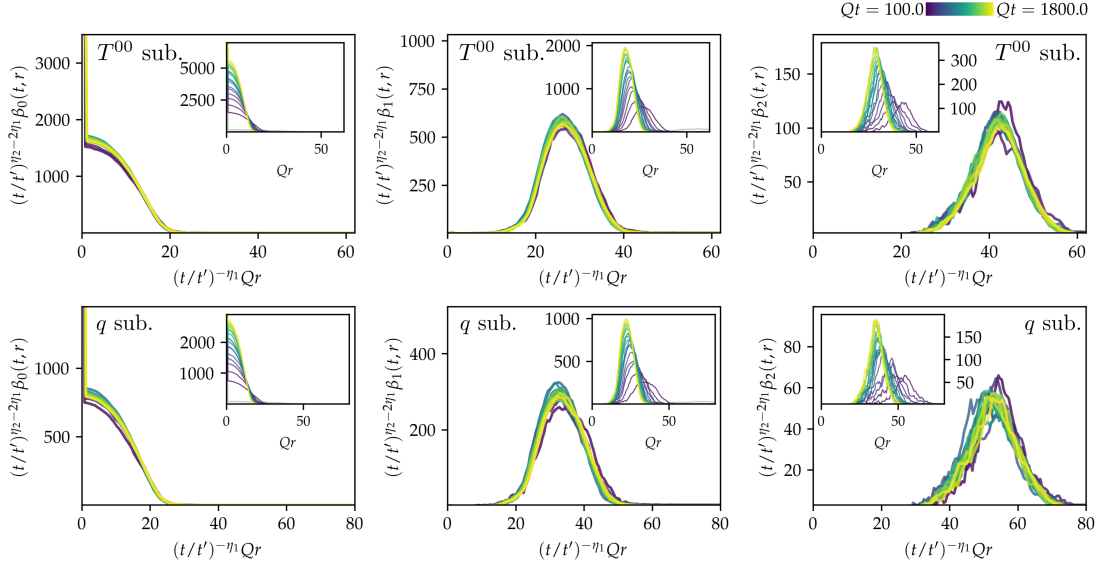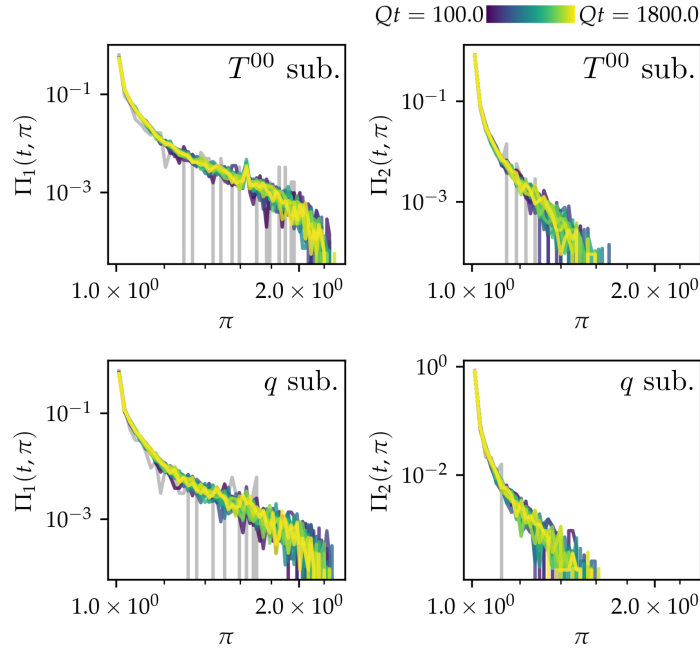
**FIGURE 4.3.3:** Normalized persistence ratio distributions of the alpha complex filtration for $T^{00}(t, \mathbf{x})$ (top) and $q(t, \mathbf{x})$ sublevel sets (bottom), with $\nu_{T^{00}} = -0.081/Q^4$ and $\nu_q = -0.13/Q^4$. Distributions at the initial time are displayed in gray.

encompasses persistent homology observables.

### 4.3.4 Persistence ratio distributions

In Figure 4.3.3 we display distributions of persistence ratios, $\Pi_k(t, \pi)$, for the energy and topological density sublevel sets $X_{T^{00}, \nu_{T^{00}}, i}(t)$ and $X_{q, \nu_q, i}(t)$. The distributions $\Pi_k(t, \pi)$ are particularly sensitive to lattice artefacts. We explicitly removed the two most prominent lattice artefacts from the computed distributions by excluding in dimension 1 holes with $\pi = \sqrt{2}$ and $\pi = \sqrt{4/3}$, and in dimension 2 holes with $\pi = \sqrt{3/2}$ and $\pi = \sqrt{9/8}$. Square roots of quotients of small integers are unique to specific point configurations on the lattice originating from vertices of one up to few elementary lattice voxels. We checked that further lattice artifacts in this sense do not contribute significantly to the distributions shown in Figure 4.3.3.

The distributions $\Pi_k(t, \pi)$ decrease fast and have support roughly up to $\pi \approx 2$ in dimension 1 and up to $\pi \approx 1.6$ in dimension 2. Crucially, the distributions remain constant in time up to statistical fluctuations. Although showing more fluctuations at smaller $\Pi_k(t, \pi)$-values, this also applies to the initial time (indicated in gray). Thus, the time translation invariance of $\Pi_k(t, \pi)$ is not due to the specifics of a self-similar time evolution. The persistence ratio distributions $\Pi_k(t, \pi)$ rather constitute approximate invariants of motion for all $\pi$.

As already mentioned in Section 4.3.2, it has been conjectured that persistence ratio distributions are universal across i.i.d. point cloud generation processes [205]. We regard the constancy in time of $\Pi_k(t, \pi)$ in Figure 4.3.3 as a manifestation of this. An even stronger

universality conjecture for a distribution of transformed $\pi$-values has been provided in the same work [205]. This applies to our data, too, as we detail in Appendix 4.C.

## 4.4   Summary

Energy and topological densities have been studied in real-time $SU(2)$ lattice gauge theory simulations in the classical-statistical regime with over-occupied initial conditions. We have found that energy and topological density correlation functions reveal self-similarity related to a direct energy cascade. Corresponding scaling exponents could be understood from a kinetic quasi-particle picture ($\beta$) and the energy-momentum conservation Ward identity ($\alpha(\beta)$).

The approximate agreement of energy and topological density correlations hints at independently and identically distributed colour and space directions of $\mathbf{E}(t, \mathbf{x})$ and $\mathbf{B}(t, \mathbf{x})$. Differences between energy and topological density correlations could have been due to topological excitations such as sphalerons. While topological excitations typically manifest themselves in coarsening dynamics due to their mutual annihilation, in our study both energy and topological density correlations instead have shown a dynamical refinement of associated structures. This suggests that topological excitations are barely of relevance for the dynamics in gluonic plasmas at the length scales probed by the energy and topological densities for the examined over-occupied initial conditions.

In order to look for self-similar dynamics beyond local correlation functions, we have constructed non-local observables based on persistent homology. Specifically, we have examined the filtration of alpha complexes of energy and topological density sublevel sets, and the filtration of cubical complexes of energy and topological densities (in Appendix 4.D). Even for topological observables like Betti number distributions we have observed self-similarity. The associated scaling exponents could be understood from the correlation functions ($\eta_1 = \beta$) and the packing relation ($\eta_2(\eta_1)$), which follows from the bounded number of topological features for a given non-expanding lattice volume and is, amongst others, the topic of Chapter 5. All investigated observables have been gauge-invariant, and the universality related to the direct energy cascade has encompassed local and non-local observables.

For prospective related research questions we refer to Chapter 8.

## Appendix

## 4.A   The mathematics of persistent homology

In this appendix we describe the construction of persistent homology groups from a more mathematical perspective. We begin with homology groups, subsequently leading to persistent homology. Mathematical aspects of persistent homology in a probabilistic framework will be the topic of Chapter 5. Some of the constructions described here in brevity are described there more concisely.

### 4.A.1   Homology groups

Let $\mathcal{C}$ be a simplicial complex such as the alpha complexes $\alpha_r(X)$ constructed in the main text; the same constructions apply for cubical complexes. We consider chain complexes and homology groups with coefficients in $\mathbb{Z}_2$, such that the $k$-th chain complex $C_k(\mathcal{C})$ of $\mathcal{C}$ consists of formal sums of chains of $k$-simplices with $\mathbb{Z}_2$-coefficients. The boundary operator $\partial_k : C_k(\mathcal{C}) \to C_{k-1}(\mathcal{C})$ is defined to map a chain of $k$-simplices to its boundary, which is a $(k-1)$-chain. Since boundaries of chain boundaries are empty, one has $\partial_{k-1} \circ \partial_k = 0$. We define the cycle group $Z_k(\mathcal{C}) := \ker(\partial_k)$ to consist of all closed $k$-chains, i.e., $k$-chains without boundary. We further define the boundary group $B_k(\mathcal{C}) := \mathrm{im}(\partial_{k+1})$ consisting of all $k$-chains which are boundaries of $(k+1)$-chains. We find $B_k(\mathcal{C}) \subseteq Z_k(\mathcal{C})$ as subgroups, such that we can define their quotient groups,

$$H_k(\mathcal{C}) := Z_k(\mathcal{C})/B_k(\mathcal{C}) \,, \tag{4.38}$$

called homology groups.

We can study the topology of $\mathcal{C}$ using the homology groups $H_k(\mathcal{C})$, which capture similar topological information compared to the homotopy groups of $\mathcal{C}$, but are in general not the same. Technically, elements of $H_k(\mathcal{C})$, called homology classes, are equivalence classes of $k$-cycles modulo higher-dimensional boundary contributions. We may intuitively think of homology classes as independent holes. Their number is the $\mathbb{Z}_2$-dimension of $H_k(\mathcal{C})$, called $k$-th Betti number,

$$\beta_k(\mathcal{C}) := \dim_{\mathbb{Z}_2}(H_k(\mathcal{C})) \,. \tag{4.39}$$

### 4.A.2   Persistent homology groups

Let $\{\mathcal{C}_r\}_{r \geq 0}$ be a filtration of complexes, such as the alpha complex filtration considered in the main text of this chapter. We compute all their individual homology groups $\{H_k(\mathcal{C}_r)\}_r$. In addition, the filtration contains inclusion maps $\mathcal{C}_r \hookrightarrow \mathcal{C}_s$ for all $r \leq s$. These induce maps on homology groups,

$$\iota_k^{r,s} : H_k(\mathcal{C}_r) \to H_k(\mathcal{C}_s) \,. \tag{4.40}$$

The $\iota_k^{r,s}$ map a homology class in $H_k(\mathcal{C}_r)$ either to one in $H_k(\mathcal{C}_s)$, if it is still present for $\mathcal{C}_s$, or to zero, if corresponding (potentially deformed) cycles appear as boundaries in $H_k(\mathcal{C}_s)$. Further, non-trivial cokernels can appear for $\iota_k^{r,s}$: new homology classes may appear in $\mathcal{C}_s$, which are not present in $\mathcal{C}_r$. Then, $s$ can be chosen such that for sufficiently small $\epsilon > 0$,

$$H_k(\mathcal{C}_{s-\epsilon}) \subsetneq H_k(\mathcal{C}_s) \,. \tag{4.41}$$

We call the collection $\{(H_k(\mathcal{C}_r), \iota_k^{r,s})\}_{r \leq s}$ a persistence module. It is tame, if Equation (4.41) holds only for finitely many distinct $s$-values.

By the structure theorem of persistent homology [206, 207], any tame persistence module is isomorphic to its persistence diagram, i.e., the collection of all its birth-death pairs $(r_b, r_d)$, $r_b < r_d \in \mathbb{R} \cup \{\infty\}$. Persistence diagrams form multisets, since the same birth-death pair can appear multiple times.
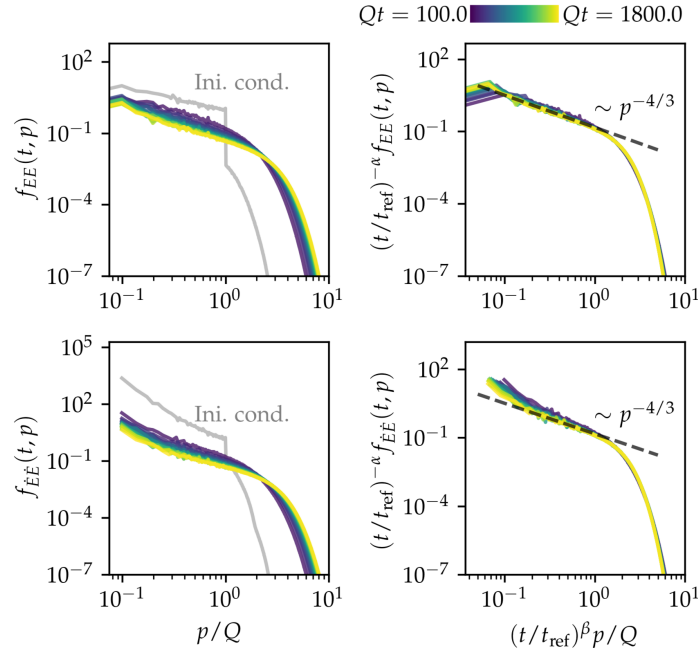
**FIGURE 4.B.1:** Occupation numbers (left) with dynamical rescaling (right) employing $\beta = -1/7$, $\alpha = 4\beta = -4/7$ in accordance with energy conservation. Top row shows occupation numbers for the $f_{EE}$ definition, bottom row for the $f_{\dot{E}\dot{E}}$ definition. Initial time displayed in gray. Dashed lines indicate $\sim p^{-4/3}$ power-laws.

## 4.B    Self-similarity in occupation numbers

One typically investigates dynamical scaling behavior in the vicinity of non-thermal fixed points using occupation numbers. In a non-Abelian gauge theory, the definition of occupation numbers suffers from ambiguities. We focus on occupation numbers defined from electric fields as [188]

$$f_{EE}(t,p) = \frac{1}{(N_c^2 - 1)Vp} P_T^{ij}(\mathbf{p})\langle E_i^a(t,\mathbf{p})(E_j^a(t,\mathbf{p}))^* \rangle \,, \tag{4.42a}$$

$$f_{\dot{E}\dot{E}}(t,p) = \frac{1}{(N_c^2 - 1)Vp^3} P_T^{ij}(\mathbf{p})\langle (\partial_t E_i^a(t,\mathbf{p}))(\partial_t E_j^a(t,\mathbf{p}))^* \rangle \,, \tag{4.42b}$$

with color decomposition $E_j(t, \mathbf{p}) = E_j^a(t, \mathbf{p})T^a$ of the Fourier-transformed electric field, $T^a$ generators of $\mathfrak{su}(N_c)$, $p \equiv |\mathbf{p}|$, and the transversal polarization projector $P_T^{ij}(\mathbf{p})$ defined as in [188]. For simplicity we ignore effects from hard thermal loop self-energies, in particular screening masses, since we focus on hard momentum modes while they would alter correlators primarily at soft momenta.

In Figure 4.B.1 we display the occupation numbers for both definitions in Equation (4.42) across the entire time range investigated. Without dynamical rescaling, we observe an approximate power-law decline $\sim p^{-4/3}$ in momentum space at lower momenta, which for $f_{\dot{E}\dot{E}}$ appears overlaid by an approximate $\sim p^{-2}$ behavior of the correlator. Above $Q$, a steep decline towards zero appears for all times. We note that for both definitions occupations shift towards larger momenta in the course of time. For dynamical rescaling we suggestively set exponents $\beta = -1/7$ and $\alpha = -4/7 = 4\beta$, consistent with
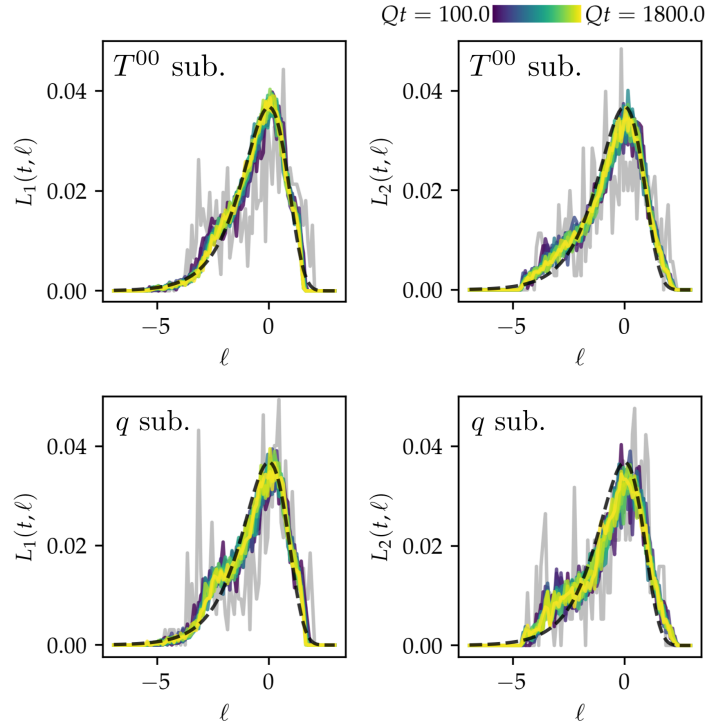
**FIGURE 4.C.1:** $\ell$-transformed distributions of persistence ratios of the alpha complex filtration for $T^{00}(t, \mathbf{x})$ (top) and $q(t, \mathbf{x})$ sublevel sets (bottom), with filtration parameters $\nu_{T^{00}} = -0.081/Q^4$ and $\nu_q = -0.13/Q^4$. Curves at initial time are displayed in gray. The black dashed line indicates the left-skewed Gumbel probability distribution $\sim \exp(\ell - \exp(\ell))$.

Equation (4.19). In particular, the same $\beta$ describes occupation numbers and all dynamical observables considered in the main text.

## 4.C   Strong universality in persistent homology

In this appendix we discuss transformed persistence ratios for alpha complexes of energy and topological density sublevel sets, based on the findings in [205]. There, for a point cloud $X$ and the persistent homology of its alpha complexes[2] it has been proposed to investigate the normalized distribution $L_k(\ell(\pi))$ of

$$\ell(\pi) = \frac{1}{2} \log \log \pi - \lambda - \frac{1}{2}\bar{L}, \qquad (4.43)$$

where $\lambda = 0.577216...$ is the Euler-Mascheroni constant and

$$\bar{L} = \frac{1}{|\mathrm{Dgm}_k(X)|} \sum_{(r_b, r_d) \in \mathrm{Dgm}_k(X)} \log \log \frac{r_d}{r_b}, \qquad (4.44)$$

$|\mathrm{Dgm}_k(X)|$ denoting the total number of holes described by $\mathrm{Dgm}_k(X)$. In Figure 4.C.1 we show the distributions $L_k(t, \ell)$, again with the two leading lattice artefacts removed as

---

[2]Strictly speaking, in [205] the filtration of so-called Čech complexes of $X$ has been considered, which for point clouds in general position has isomorphic persistent homology to the filtration of alpha complexes.

described in Section 4.3.4. We note that distributions look the same for dimensions 1 and 2. Furthermore, up to statistical fluctuations they remain constant in time, including the initial time. This provides evidence for the universality of $L_k(t, \ell)$ conjectured in [205], in which the authors suggest that the $L_k(t, \ell)$ are independent from dimensions of both the ambient space of the point clouds and the holes, and independent from the point cloud generation process, even beyond i.i.d. processes. In particular, it is suggested that the distributions follow the left-skewed Gumbel distribution,

$$L_k(t, \ell) \sim e^{\ell - e^\ell}, \tag{4.45}$$

also shown in Figure 4.C.1 as dashed curves. We find that our numerical distributions are consistent with Equation (4.45). Remaining differences may be a consequence of sub-leading lattice artefacts that we have not removed and thus may still enter $L_k(t, \ell)$, though not visible in the persistence ratio distributions $\Pi_k(t, \pi)$ shown in Figure 4.3.3.

## 4.D  Persistent homology of cubical complexes

In the main text of this chapter we have shown results for the persistent homology of the alpha complex filtration for fixed sublevel sets, which give rise to dynamical self-similar scaling. Here, we discuss results for the filtration of superlevel set cubical complexes, with persistent homology describing persistence properties of topological structures as function values are swept through. We expect similar results for the sublevel set filtration.

First, we introduce cubical complexes as an alternative to alpha complexes. We then discuss Betti numbers and persistence distributions, and find indications of self-similar scaling behavior. We conclude that the universal behavior stemming from the direct energy cascade also encompasses the persistent homology of cubical complexes for the superlevel set filtration.

The homology of sub- or superlevel set cubical complexes of lattice observables does not discriminate between different length scales. Therefore, lattice artefacts enter these in general. Since self-similar scaling associated to non-thermal fixed points requires a sufficient momentum space distance to lattice cutoffs, we employ spatial coarse-graining by a factor of 8 to $T_i^{00}(t, \mathbf{x})$ and $q_i(t, \mathbf{x})$ before computing the persistent homology of their superlevel set cubical complexes. Thus, higher lattice momentum scales than $\pi/(8a_s)$ do not enter the persistent homology analysis. Concerning the infrared, we have verified an approximate extensive scaling of Betti numbers and other persistent homology quantifiers with respect to the lattice volume.

### 4.D.1  Cubical complexes

A cubical complex is a collection of cubes of different dimensions, which is closed under taking boundaries, similarly to simplicial complexes. We explicitly construct the filtration of cubical complexes for sub- and superlevel sets of lattice functions at a given time $t$. Cubical complexes are well-suited to describe sub- and superlevel sets of lattice functions, or pixelized data more generally.

Let $\mathfrak{C}$ be the full cubical complex of the lattice, consisting of one 3-cube $\mathbf{x} + [-1/2, 1/2]^3$ for each spatial lattice point $\mathbf{x} \in \Lambda_s$. Such a 3-cube comes with all its faces, edges and vertices, as required to have $\mathfrak{C}$ closed under taking boundaries. On our lattice, a 3-cube is a cube of side length $a_s$, a 2-cube is a square of side length $a_s$, a 1-cube is an edge of length $a_s$, and a 0-cube is a point. In the literature, such cubes are called elementary [208].

We equip $\mathfrak{C}$ with the information contained in $T_i^{00}(t, \mathbf{x})$ by inductively constructing a map $T_{t,i} : \mathfrak{C} \to \mathbb{R}$. By construction of $\mathfrak{C}$, any 3-cube has a unique lattice point $\mathbf{x} \in \Lambda_s$ at its center. For any 3-cube $C \in \mathfrak{C}$ we set $T_{t,i}(C) := T_i^{00}(t, \mathbf{x})$, $\mathbf{x}$ the center point of $C$. Any 2-cube $D \in \mathfrak{C}$ is contained in the boundaries of two 3-cubes. For all 2-cubes $D \in \mathfrak{C}$, we set

$$T_{t,i}(D) := \min\{T_{t,i}(C) \mid D \subset \partial C, \, C \in \mathfrak{C} \text{ 3-cube}\} . \tag{4.46}$$

Analogously, any 1-cube is contained in the boundaries of four 2-cubes, and any 0-cube is contained in the boundaries of six 1-cubes. We inductively apply Equation (4.46) to construct $T_{t,i}$ for lower-dimensional cubes from higher-dimensional ones, until $T_{t,i}$ is defined on all $\mathfrak{C}$. This construction is called the lower star filtration.

We define cubical complexes corresponding to lattice sublevel sets of $T_i^{00}(t, \mathbf{x})$ at time $t$ as

$$\mathfrak{C}_{T_i^{00}}(t, \nu) := T_{t,i}^{-1}(-\infty, \nu] . \tag{4.47}$$

These are closed under taking boundaries, thus indeed cubical complexes. We define superlevel set cubical complexes as

$$\mathfrak{D}_{T_i^{00}}(t, \nu) := \mathfrak{C}_{-T_i^{00}}(t, -\nu) , \tag{4.48}$$

reflecting the structure of lattice superlevel sets. For topological densities the construction is the same; simply replace $T_i^{00}(t, \mathbf{x})$ by $q_i(t, \mathbf{x})$.

We are interested in the persistent homology of the filtrations of complexes $\{\mathfrak{C}_{T_i^{00}}(t, \nu)\}_\nu$ and $\{\mathfrak{D}_{T_i^{00}}(t, \nu)\}_\nu$, as $\nu$ is swept through. Indeed, we notice that they define filtrations, e.g. $\mathfrak{C}_{T_i^{00}}(t, \nu) \subseteq \mathfrak{C}_{T_i^{00}}(t, \mu)$ whenever $\nu \leq \mu$. The previous constructions of persistent homology apply also in this setting. The persistent homology of cubical complex filtrations can be efficiently calculated [208]. We again use GUDHI [203] to compute persistent homology of the cubical complex filtration, and use periodic cubical complexes to take spatially periodic boundary conditions into account.

Displayed in Chapter 6, in Figure 6.3.1(a) we illustrate the meaning of cubical complex homology classes. In Figure 6.3.1(b) we sketch the meaning of birth $b$ and death $d$ of homology classes as the filtration of superlevel sets is swept through. We note that the birth of dimension zero homology classes happens at function values of local maxima. Their persistences quantify their dominances, dying when merging at saddle points with tails of other local maxima. Dimension one homology classes can be thought of as describing potentially deformed volcano-like features in function landscapes, and analogously for higher-dimensional homology classes.

**FIGURE 4.D.1:** Betti number distributions of the $T^{00}(t, \mathbf{x})$ (top) and the $q(t, \mathbf{x})$ super-level set filtrations (bottom) using cubical complexes. The initial time is displayed in gray. The scaling exponents are set to $\eta_1 = -1/7$ and $\eta_2 = 3\eta_1 = -3/7$. The insets show the original distributions without rescaling; the inset axes have the same ranges as the axes in the main plots.

## 4.D.2  Betti number distributions

In Figure 4.D.1 we show results for Betti number distributions of all dimensions for both the energy and the topological density superlevel set filtrations, using cubical complexes. Insets show numbers without, main plots with dynamical rescaling. Note that energy densities are shown with the average subtracted. We notice from the unrescaled figures that topological features of both energy and topological densities give rise to a hierarchy of peaks between dimensions. For superlevel sets of a function whose values scatter approximately symmetrically around zero, connected components appear first at positive filtration parameters. Multiple such need to merge, to form a dimension one feature, born around zero. Typically at negative filtration parameters, multiple dimension one features die to give birth to a dimension two feature.

In the course of time, throughout dimensions and energy and topological densities topological features shift towards zero filtration parameters, suggesting a homogenization of structures. Further, their number increases, indicative of their dynamical refinement. In the main plots we suggestively rescaled the figures with $\eta_1 = -1/7$ and $\eta_2 = -3/7 = 3\eta_1$. We notice approximate matching of the rescaled curves. Notice that aside of the initial condition we here show data from $Qt = 300$ onwards, while in the main text of this chapter we have shown data starting with $Qt = 100$. Betti number distributions do not allow sufficiently consistent rescaling before $Qt = 300$ (not displayed).

The exponent $\eta_1 = -1/7$ is consistent with the earlier findings of $\eta_1$ for alpha complexes and $\beta$ for correlation functions. However, here it describes the dynamical refinement of structures in the space of function values, not with respect to spatial sizes of structures. How can the exponents still agree? We recall from Section 4.2.2 that the correlators $\langle (T^{00}(t, p_x))^2 \rangle_c$ and $\langle (q(t, p_x))^2 \rangle_c$ scale overall as $\sim t^\beta$ for spatial scaling exponent
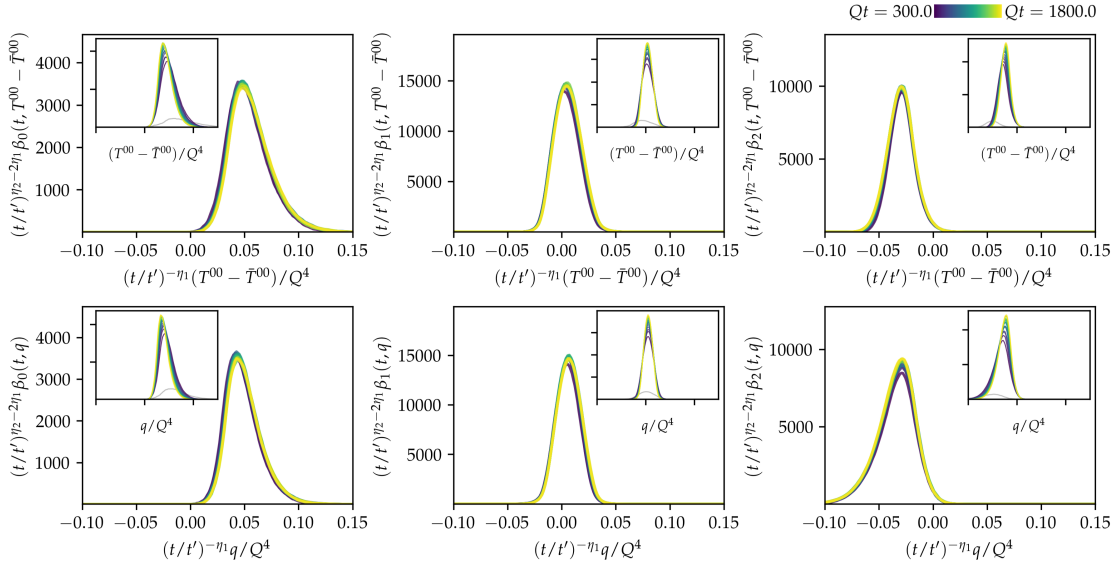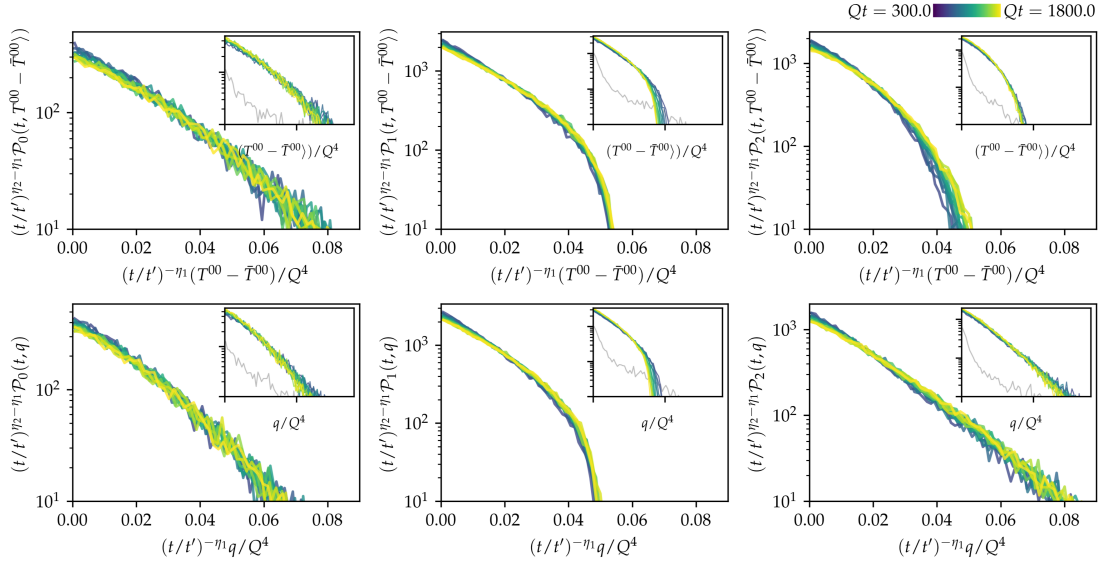
**FIGURE 4.D.2:** Persistence distributions of the $T^{00}(t, \mathbf{x})$ (top) and the $q(t, \mathbf{x})$ super-level set filtrations (bottom) using cubical complexes. The initial time is displayed in gray. The scaling exponents are set to $\eta_1 = -1/7$ and $\eta_2 = 3\eta_1 = -3/7$. The insets show the distributions without rescaling; the inset axes have the same ranges as the main plots.

$\beta = -1/7$. If such correlators contribute predominantly to local fluctuations in $T_i^{00}(t, \mathbf{x})$ and $q_i(t, \mathbf{x})$, we can heuristically find that topological features scale in the space of function values as $\sim t^\beta$, too. We take our observation of $\eta_1 = -1/7$ for the superlevel set filtration as an indication for this.

The number of topological features which appear in $T_i^{00}$ superlevel sets is bounded by total energy conservation in a similar way that the number of topological features for alpha complexes is bounded by the constant system volume. This effectively provides a one-dimensional constraint for the persistent homology of the superlevel set filtration. Then, for cubical complexes of $T_i^{00}$ superlevel sets the packing relation yields $\eta_2 = 3\eta_1$, see [6] and Chapter 5. This is consistent with the data.

The apparent similarity of energy and topological density cubical complexes in persistent homology can again be understood from independent spatial and colour directions of $\mathbf{E}(t, \mathbf{x})$ and $\mathbf{B}(t, \mathbf{x})$ as proposed in Section 4.2.2. Yet, differences are visible in particular for the left-sided tail of dimension two Betti numbers, where the Betti number distribution has larger support for topological rather than energy densities.

### 4.D.3 Persistence distributions

In Figure 4.D.2 we display the distribution of absolute persistences, $d - b$, for energy and topological density superlevel sets. Again, insets show figures without rescaling, which we discuss first. We notice that dimension zero distributions decline approximately exponentially with persistence values. Dimension one distributions have more restricted support only up to $T^{00} - \bar{T}^{00}, q \simeq 0.05\,Q^4$. Persistence distributions of dimension two features of energy densities have more restricted support compared to topological densities, whose dimension two persistence distributions moreover show approximate exponential

behavior. This indicates that energy density persistences have an upper bound due to the positivity of $T_i^{00}$, which is not the case for $q_i$. There, the approximate symmetry among dimension zero and two features hints at a symmetric distribution of topological density values around zero, which in particular features local lumps, similarly to the deductions in Chapter 6 of this dissertation.

Let us now consider absolute persistences defined as integrals of the averaged dimension-$k$ persistence pair distributions over the death parameter,

$$\mathcal{P}_k(t, p) = \int_0^\infty \mathrm{d}d \, \langle \mathfrak{P}_k \rangle (t, d - p, d) \,. \tag{4.49}$$

The scaling ansatz Equation (4.30) then leads to the self-similar scaling

$$\mathcal{P}_k(t, p) = (t/t')^{\eta_1 - \eta_2} \mathcal{P}_k(t', (t/t')^{-\eta_1} p) \,. \tag{4.50}$$

Accordingly, we have rescaled the curves in the main plots in Figure 4.D.2 using the same exponents $\eta_1 = -1/7$ and $\eta_2 = -3/7$ as for the Betti numbers shown in Figure 4.D.1. We observe approximate agreement among the rescaled curves mostly up to statistical fluctuations, which is indicative of dynamical self-similarity. We suggest that the deviations for dimension two persistences of energy density sublevel sets are due to the positivity bound.

# Chapter 5

# The self-similar evolution of stationary point processes via persistent homology

This chapter is based on the following article:

- Spitz, D. and Wienhard, A., "The self-similar evolution of stationary point processes via persistent homology", arXiv: 2012.05751 [math.PR].

Most of the present chapter is taken from this preprint, where I predominantly wrote the text, designed and elaborated the mathematical framework, and derived the results.

While this dissertation contains in Chapters 4 and 6 two persistent homology applications, this chapter is devoted to mathematical explorations of the persistent homology of point clouds in a statistical context. As such, this chapter is kept in mathematically rigorous language.

## 5.1 Introduction

Persistent homology allows one to infer topological structure from finite data. It was developed over the past two decades into a robust and versatile methodology, see for example [67, 178, 209–212]. In recent years there has been a lot of interest in bringing together the classical machinery from algebraic topology with probabilistic approaches, leading to the investigation of random geometric complexes and their limiting behavior, based on random fields and point processes [71, 213–220], see [221] for a survey. In particular, in [204] the density of expected persistence diagrams and its kernel based estimation have been discussed.

In this chapter we follow a similar route. We consider point processes and their persistence diagrams. We describe measures on the space of persistence diagrams. Under certain ergodicity assumptions we show the existence of persistence diagram expectation measures. These persistence diagram expectation measures are maps from the set of bounded Borel sets in $\mathbb{R}^n$ to the space of Radon measures on the set $\Delta = \{b, d \in \mathbb{R}^2 \,|\, b < d\}$.

Strong laws of large numbers for topological descriptors such as (persistent) Betti numbers are of special interest with multifarious results already established [71, 222–225]. Here, as a byproduct we extend the strong law of large numbers for persistent Betti

numbers, proven in [71] for asymptotically large cubes, to more general convex averaging sequences.

With the persistence diagram expectation measures at hand, we introduce the notion of self-similar scaling for time-dependent persistence diagram expectation measures.

**Definition 5.1.1.** *Let $(\mathfrak{p}(t))_{t\in(T_0,T_1)}$ be a family of existing non-zero persistence diagram expectation measures, $0 < T_0 < T_1$. For $t \in (T_0, T_1)$ and $A \subset \mathbb{R}^n$ a bounded Borel set, we set $\mathfrak{p}(t,A) := \mathfrak{p}(t)(A)$. We say that $(\mathfrak{p}(t))_{t\in(T_0,T_1)}$* scales self-similarly between times $T_0$ and $T_1$ *with exponents $\eta_1, \eta_2 \in \mathbb{R}$, if for all $t, t' \in (T_0, T_1)$ and $B$ an element of the Borel $\sigma$-algebra of $\Delta$:*

$$\mathfrak{p}(t,A)(B) = (t/t')^{-\eta_2}\mathfrak{p}(t',A)((t/t')^{-\eta_1}B)\,, \tag{5.1}$$

*where $\kappa B := \{(\kappa b, \kappa d) \mid (b,d) \in B\}$ for $\kappa \in [0, \infty)$.*

We prove a packing relation for the exponents $\eta_1$ and $\eta_2$ in the self-similar scaling approach, which results from bounded total persistence [69].

**Theorem 5.1.2.** *Let $(\xi(t))_{t\in(T_0,T_1)}$, $0 < T_0 < T_1$, be a family of stationary and ergodic simple point processes on $\mathbb{R}^n$ having all finite moments. Let $(\mathfrak{p}(t))_t$ be the family of persistence diagram expectation measures associated to $(\xi(t))_t$. Assume that all $(\mathfrak{p}(t))_t$ exist, are non-zero and that the family scales self-similarly between times $T_0$ and $T_1$ with exponents $\eta_1, \eta_2 \in \mathbb{R}$. Then, if the interval $(T_0, T_1)$ is sufficiently extended, almost surely*

$$\eta_2 = n\eta_1\,. \tag{5.2}$$

In the proof of Theorem 5.1.2 we specify what sufficiently extended means.

Self-similarity is usually exhibited by fractals. We prove that, under a weak assumption on large-volume asymptotics, processes that admit self-similar scaling in fact have constant fractal dimension in the persistent sense of [226].

The motivation for this work originates from applications of the concept of self-similar scaling of time-dependent persistence diagrams to quantum physical systems in [6] and Chapter 4 of this dissertation. This chapter provides a more rigorous mathematical framework for some of the heuristic arguments in [6] and Chapter 4.

It is structured as follows. In Section 5.2 we embed persistence diagrams into the framework of point processes, introduce notions of ergodicity, in order to define persistence diagram measures and related geometric quantities. The existence of limiting Radon measures for large point clouds and the strong law of large numbers for persistent Betti numbers are shown for general convex averaging sequences. In Section 5.3 we introduce the notion of self-similar scaling of persistence diagram expectation measures and prove the packing relation. Section 5.4 is devoted to examples constructed from different point processes. Finally, in Section 5.5 we provide a summary and state further mathematical questions.

**Remark 5.1.3.** *We derive our results for Čech complexes, though they are easily extendable to other types of simplicial complexes. Under the assumption of point clouds being in general position,*

*the filtrations of Čech complexes and of alpha and Wrap complexes have isomorphic persistent homology groups [227]. Thus, all results developed in this work can be directly extended to these.[1]*

*In [71] a fairly general family of complexes defined through specific measurable functions on finite sets of points is introduced, covering both the filtrations of Čech complexes and of Vietoris-Rips complexes. Care is required regarding the extension of our results to this family since for instance Lemma 5.2.15 only applies to filtered complexes with persistent homology groups isomorphic to those of the filtration of Čech complexes.*

## 5.2 Point processes and persistence diagram measures

### 5.2.1 Background on point processes and persistent homology

**Point processes.** Point processes are random collections of at most countably many points, identified with random counting measures. We review notions from the theory of point processes [228–230].

Let $S$ be a complete and separable metric space, $\mathcal{B}(S)$ its Borel $\sigma$-algebra and $\mathcal{R}(S)$ the space of Radon measures[2] on $S$. We define $\mathcal{B}^n = \mathcal{B}(\mathbb{R}^n)$ and denote the set of bounded Borel subsets of $\mathbb{R}^n$ by $\mathcal{B}_b^n$. The space of all boundedly finite measures on $\mathbb{R}^n$ is denoted by $\mathcal{M}^n$ and of the integer-valued ones by $\mathcal{N}^n \subset \mathcal{M}^n$. We denote by $\lambda_n$ the $n$-dimensional Lebesgue measure.

Let $(\Omega, \mathcal{E}, \mathbb{P})$ be a probability space. A random measure on $\mathbb{R}^n$ is a measurable map $\mu : (\Omega, \mathcal{E}, \mathbb{P}) \to (\mathcal{M}^n, \mathcal{B}(\mathcal{M}^n))$. A point process on $\mathbb{R}^n$ is a measurable map $\xi : (\Omega, \mathcal{E}, \mathbb{P}) \to (\mathcal{N}^n, \mathcal{B}(\mathcal{N}^n))$.

A point process $\xi$ is simple, if a.s. all its atoms are distinct; it has all finite moments, if for all $k \geq 1$ and $A \in \mathcal{B}_b^n$: $\mathbb{E}[\xi(A)^k] < \infty$. We assume that all point processes studied in this work have non-zero first moments, $\mathbb{E}[\xi(A)] > 0$ for $A \in \mathcal{B}_b^n$ with $\lambda_n(A) > 0$. For a simple point process $\xi$ on $\mathbb{R}^n$ we define the set of atoms in $A \in \mathcal{B}_b^n$ as

$$X_{\xi_\omega}(A) = \left\{ x_i \;\middle|\; \xi_\omega(A) = \sum_i \delta_{x_i}(A) \right\}, \tag{5.3}$$

where $\delta_{x_i}(A) = 1$ if $x_i \in A$, else $\delta_{x_i}(A) = 0$. The sets $X_{\xi_\omega}(A)$ form point clouds[3] for $A \in \mathcal{B}_b^n$. We often omit the sample $\omega$ from notations.

**Filtered simplicial complexes and persistent homology.** We briefly review notions from persistent homology. For a general introduction to algebraic topology we refer to [201, 202, 231]; for a thorough introduction to computational topology the interested reader may consult [67, 178].

---

[1]The proof of Lemma 5.2.4 actually employs this argument.
[2]A measure $\mu$ on $(S, \mathcal{B}(S))$ is called a Radon measure, if $\mu(A) < \infty$ for every relatively compact $A \in \mathcal{B}(S)$. In particular, since $S$ is a complete, separable metric space, a thus defined Radon measure is regular [228].
[3]A point cloud $X \subset \mathbb{R}^n$ is a finite subset of $\mathbb{R}^n$.

Let $X \subset \mathbb{R}^n$ be a point cloud. The Čech complex of radius $r$ is defined as the abstract simplicial complex

$$\check{C}_r(X) := \left\{ \sigma \subseteq X \,\middle|\, \bigcap_{x \in \sigma} B_r(x) \neq \emptyset \right\}, \tag{5.4}$$

$B_r(x)$ denoting the closed ball of radius $r$ around $x \in \mathbb{R}^n$. We denote the $m$-skeleton of $\check{C}_r(X)$ by $\check{C}_r(X)^m$, which consists of all simplices of $\check{C}_r(X)$ up to and including dimension $m$.

The Čech complexes form a filtration of simplicial complexes: $\check{C}_r(X) \subseteq \check{C}_s(X)$ if $s \geq r$. We set $\mathcal{C}(X) := \{\check{C}_r(X) \,|\, r \geq 0\}$. As in Section 4.A.2, the map of homology groups induced by the inclusion $\check{C}_r(X) \hookrightarrow \check{C}_s(X)$ is denoted by $\iota_\ell^{r,s} : H_\ell(\check{C}_r(X)) \to H_\ell(\check{C}_s(X))$, where we can more generally consider homology with coefficients in an arbitrary field $\mathbb{F}$. The $\ell$-th persistence module is the collection of homology groups with corresponding induced linear maps, $H_\ell(\mathcal{C}(X)) = (H_\ell(\check{C}_r(X)), \iota_\ell^{r,s})_{s \geq r}$. The $\ell$-th persistent Betti numbers are defined as $\beta_\ell^{r,s}(\mathcal{C}(X)) := \mathrm{rk}(\mathrm{im}(\iota_\ell^{r,s}))$. All persistence modules studied in this work are by construction tame,[4] since the underlying point clouds are finite.

Due to the structure theorem [212], tame persistence modules such as $H_\ell(\mathcal{C}(X))$ are up to isomorphism in one-to-one correspondence with persistence diagrams, i.e., finite multisets of pairs $(b, d)$ with $b, d \in \mathbb{R}^2$ and $b < d$. We set $\Delta := \{(b, d) \in \mathbb{R}^2 \,|\, b < d\}$ and denote the space of persistence diagrams by $\mathscr{D}$, which is the space of finite multisets of pairs $(b, d)$ with $b, d \in \mathbb{R}^2$ and $b < d$. A persistence pair $(b, d)$ in the persistence diagram $\mathrm{Dgm}_\ell(X)$ of $H_\ell(\mathcal{C}(X))$ corresponds to an $\ell$-dimensional homology class being present in Čech complexes of all radii within $[b, d)$. We call $b$ the birth radius of the corresponding homological feature, $d$ its death radius and $\mathrm{pers}((b, d)) := d - b$ its persistence. We ignore persistence pairs with zero persistence in persistence diagrams. While this is consistent for our work, persistence pairs with zero persistence can be important e.g. for the computation of the bottleneck distance.

Let $\xi$ be a simple point process on $\mathbb{R}^n$. In this work we are interested in persistence diagrams of the filtration of Čech complexes, $\mathrm{Dgm}_\ell(X_{\xi_\omega}(A))$ for $A \in \mathcal{B}_b^n$ and $\omega \in \Omega$. In particular, then $\bigcup_{\ell=0}^{n-1} \mathrm{Dgm}_\ell(X_\xi(\cdot))$ defines a point process on $\mathscr{D}$.

### 5.2.2 Ergodicity in persistent homology

A random measure $\mu$ on $\mathbb{R}^n$ is stationary, if for all $x \in \mathbb{R}^n$ the distributions of $\mu$ and $\theta_x \mu$ coincide. Here, $(\theta_x \mu)(A) := \mu(A + x)$ for all $A \in \mathcal{B}_b^n$. A stationary random measure $\mu$ is ergodic, if $\mathbb{P}(\mu \in \mathcal{A}) \in \{0, 1\}$ for all Borel sets $\mathcal{A}$ of $\mathcal{M}^n$ that are invariant under translation by $x$ for all $x \in \mathbb{R}^n$. A sequence $\{A_k\} \subset \mathcal{B}_b^n$ is called a convex averaging sequence if

(i) each $A_k$ is convex ,     (ii) $A_k \subseteq A_{k+1}$ for all $k$,     (iii) $\lim_{k \to \infty} r(A_k) = \infty$ ,

(iv) $W_{n-1}(A_k) = O(\lambda_n(A_k)^{1/n})$ for sufficiently large $k$ ,  $\qquad$ (5.5)

---

[4] A value $r > 0$ is a homologically critical value of $H_\ell(\mathcal{C}(X))$, if the map $\iota_\ell^{r-\epsilon, r+\epsilon} : H_\ell(\check{C}_{r-\epsilon}(X)) \to H_\ell(\check{C}_{r+\epsilon}(X))$ is not an isomorphism for sufficiently small $\epsilon > 0$. The persistence module $H_\ell(\mathcal{C}(X))$ is called tame, if $\dim(H_\ell(\check{C}_r(X))) < \infty$ for all $r \geq 0$ and only finitely many homologically critical values occur.

where $r(A) := \sup\{r \mid A \text{ contains a ball of radius } r\}$ and $W_{n-1}$ denotes the $(n-1)$-st quermassintegral. The quermassintegrals $W_i(C)$, $i = 0, \ldots, n$, of a convex body $C$ in $\mathbb{R}^n$ are given by [232]

$$W_i(C) = V(\underbrace{C, \ldots, C}_{n-i}, \underbrace{B_1(0), \ldots, B_1(0)}_{i}), \tag{5.6}$$

where $V$ denotes the mixed volume of $n$ convex bodies in $\mathbb{R}^n$. They are further used in Appendix 5.C.

**Remark 5.2.1.** *The scaling property (iv) is similar to the vanishing relative boundary condition for sequences of Borel subsets of $\mathbb{R}^n$ in [233]. Though not contained in the usual construction of convex averaging sequences, property (iv) is fairly general. For instance, sequences of growing cubes, simplices, polyhedra or balls fulfill this property. Property (iv) is required in the proof of Theorem 5.2.10 in order to exclude sequences of increasingly flat convex bodies for which the ratio of surface area to volume does not converge to zero for $k \to \infty$ [234].*

**Proposition 5.2.2** (Corollary 12.2.V in [229]). *Let $\{A_k\}$ be a convex averaging sequence. When a random measure $\xi$ on $\mathbb{R}^n$ is stationary, ergodic and has finite expectation measure with mean density $m = \mathbb{E}[\xi([0,1]^n)] = m\lambda_n([0,1]^n)$, then $\xi(A_k)/\lambda_n(A_k) \to m$ a.s. as $k \to \infty$, where $\lambda_n$ denotes the Lebesgue measure.*

We define a notion of ergodicity for point processes on the space of persistence diagrams.

**Definition 5.2.3.** *Let $\xi$ be a stationary simple point process on $\mathbb{R}^n$ with finite expectation measure, $\{A_k\}$ a convex averaging sequence, and $n(X_k) := \#\bigcup_{\ell=0}^{n-1} \mathrm{Dgm}_\ell(X_\xi(A_k))$ for all $k$. We say that $\xi$ is ergodic in persistence if a.s. for any $\epsilon > 0$ there exists $N \in \mathbb{N}$ such that for all $k, l \geq N$,*

$$\left| 1 - \frac{n(X_l)}{n(X_k)} \frac{\lambda_n(A_k)}{\lambda_n(A_l)} \right| < \epsilon. \tag{5.7}$$

**Lemma 5.2.4.** *Let $\xi$ be a simple point process on $\mathbb{R}^n$ having all finite moments. If $\xi$ is stationary and ergodic, then $\xi$ is ergodic in persistence.*

*Proof.* Let $\{A_k\}$ be a convex averaging sequence and set $X_k := X_\xi(A_k)$. We find by means of Proposition 5.2.2 that for any $\varepsilon > 0$ there exists an $N \in \mathbb{N}$ such that a.s. for all $k, l \geq N$:

$$\left| 1 - \frac{\#X_l}{\#X_k} \frac{\lambda_n(A_k)}{\lambda_n(A_l)} \right| < \varepsilon. \tag{5.8}$$

Next, we show that $n(X_k)/\#X_k$ converges as $k \to \infty$. Given that $\xi$ is stationary, its first moment measure is proportional to the Lebesgue measure [229], i.e., for $A \in \mathcal{B}_b^n$:

$$\mathbb{E}[\xi(A)] = \mathbb{E}[\xi([0,1]^n)]\lambda_n(A). \tag{5.9}$$

Now, any $k$-dimensional hyperplane and any $k$-dimensional hypersphere for $k < n$ is a set of Lebesgue measure zero. It directly follows a.s. that the affine hull of any subset of $n+1$ atoms of a sample $X$ of $\xi$ is the entire[5] $\mathbb{R}^n$. Let $P \subset X$ be a subset of $k \leq n+1$

---

[5]Else, with non-vanishing probability a Lebesgue-zero set would contain one or more points, in contradiction to Equation (5.9).

points. Analogously, a.s. no point of $X \setminus P$ lies on the smallest circumsphere of $P$, given that circumspheres are Lebesgue-zero sets. Thus, a.s. $X$ is in general position.[6]

To this end, a.s. the number of persistent homology classes $n(X_k)$ computed via Čech complexes is equal to the number of persistent homology classes computed via the family of Delaunay complexes[7] $(\mathrm{Del}_r(X_k))_r$, denoted $n_{\mathrm{Del}}(X_k)$. Indeed, by [227] Čech and Delaunay complexes are even simple-homotopy equivalent for point clouds in general position.

We show that in the limit of large $X_k$, $n_{\mathrm{Del}}(X_k)$ scales proportional to $\#X_k$, using results of [235]. First, the sets $\mathrm{Conv}(X_k)$ define polyhedra in the sense of [235]. It can be shown that $\xi$ a.s. generates point clouds $X_k$ for which $\lambda, \epsilon \in \mathbb{R}$ exist such that the $X_k$ are $\lambda$-sparse $\epsilon$-samples of $\mathrm{Conv}(X_k)$ [235], i.e., (i) a.s. every point $x \in \mathrm{Conv}(X_k)$ has a distance $\epsilon$ or less to a point in $X_k$ of $\mathrm{Conv}(X_k)$, and (ii) a.s. every closed $n$-ball with radius $5n\epsilon$ contains at most $\lambda$ points of $X_k$. To show (i) assume there exists with non-zero probability $x \in \mathrm{Conv}(X_k)$ such that for all $\epsilon > 0$, $s \in X_k$: $|x - s| > \epsilon$. Then, with non-zero probability a ball of arbitrary radius $r > 0$ around $x$ exists, such that $\xi(B_r(x)) = 0$. With non-zero probability this then leads for a sample $\xi$ and $r \to \infty$ to

$$\frac{\xi(B_r(x))}{\lambda_n(B_r(x))} \to 0 \,. \tag{5.10}$$

Since $\xi$ is ergodic, via Proposition 5.2.2 we can conclude with non-zero probability for such a sample $\xi$ that $\mathbb{E}[\xi([0,1]^n)] = 0$, in contradiction to the assumption of $\xi$ having non-zero first moment. Thus, an $\epsilon$ exists such that a.s. for all $x \in \mathrm{Conv}(X_k)$ there exists $s \in X_k$: $|x - s| < \epsilon$.

To show (ii) assume that with non-zero probability there exists an $n$-ball $B$ with radius $5n\epsilon$, such that for all $\lambda > 0$: $\xi(B) > \lambda$. Then, $\xi(B) = \infty$ with non-zero probability, in contradiction to $\xi$ having all finite moments. Thus, every closed $n$-ball with radius $5n\epsilon$ contains at most $\lambda$ points of $X_k$.

Indeed, Theorem 1 of [235] can be applied and we find that the Delaunay triangulation of $X_k$ is a.s. of size $\Theta(\#X_k)$. Denoting the $\ell$-th persistence diagram of $(\mathrm{Del}_r(X_k))_r$ as $\mathrm{Dgm}_{\ell,\mathrm{Del}}(X_k)$, we find

$$n_{\mathrm{Del}}(X_k) = \# \bigcup_{\ell=0}^{n-1} \mathrm{Dgm}_{\ell,\mathrm{Del}}(X_k) \leq \sum_{\ell=0}^{n} \dim_{\mathbb{F}} \left( C_\ell(\mathrm{Del}_\infty(X_k)) \right) = \#\mathrm{Del}_\infty(X_k) \,, \tag{5.11}$$

with $C_\ell(\mathrm{Del}_\infty(X_k))$ the $\ell$-th chain group of $\mathrm{Del}_\infty(X_k)$ with $\mathbb{F}$-coefficients. On the other hand, $n_{\mathrm{Del}}(X_k) \geq \#X_k$ for all $k$.

Thus, for any $\varepsilon > 0$ there a.s. exist constants $c > 0$ and $N' \in \mathbb{N}$, such that for all $k \geq N'$,

$$\left| \frac{n(X_k)}{c \, \#X_k} - 1 \right| < \varepsilon \,. \tag{5.12}$$

---

[6]Employing the definition of [227], $X \subset \mathbb{R}^n$ is in general position if for every $P \subseteq X$ of at most $n+1$ points (i) $P$ is affinely independent, and (ii) no point of $X \setminus P$ lies on the smallest circumsphere of $P$.

[7]The Delaunay complex of a point cloud $X \subset \mathbb{R}^n$ is defined as $\mathrm{Del}_r(X) = \{Q \subseteq X \mid \bigcap_{x \in Q} \mathrm{Vor}_r(x, X) \neq \emptyset\}$ with $\mathrm{Vor}_r(x, X) = B_r(x) \cap \{y \in \mathbb{R}^n \mid |y - x| \leq |y - p| \, \forall \, p \in X\}$ the Voronoi ball around $x \in X$ [227].

Inversion yields

$$\left| \frac{c \, \# X_k}{n(X_k)} - 1 \right| < \varepsilon + O(\varepsilon^2) \,. \tag{5.13}$$

For any $k, l \geq \max(N, N')$ we a.s. obtain from Equations (5.8), (5.12) and (5.13):

$$
\begin{aligned}
\left| 1 - \frac{\lambda_n(A_k)}{\lambda_n(A_l)} \frac{n(X_l)}{n(X_k)} \right| &\leq \left| 1 - \frac{\lambda_n(A_k)}{\lambda_n(A_l)} \frac{c \# X_l}{c \# X_k} \right| + \left| \frac{\lambda_n(A_k)}{\lambda_n(A_l)} \frac{\# X_l}{\# X_k} - \frac{\lambda_n(A_k)}{\lambda_n(A_l)} \frac{n(X_l)}{n(X_k)} \right| \\
&< \varepsilon + \frac{\lambda_n(A_k)}{\lambda_n(A_l)} \frac{n(X_l)}{n(X_k)} \left| 1 - \frac{\# X_l}{\# X_k} \frac{n(X_k)}{n(X_l)} \right| \\
&< \left( 1 + \frac{\lambda_n(A_k)}{\lambda_n(A_l)} \frac{n(X_l)}{n(X_k)} \right) \varepsilon + O(\varepsilon^2) \,.
\end{aligned} \tag{5.14}
$$

Exploiting stationarity of $\xi$ and Theorem 5.2.10 given below and proven independently from Lemma 5.2.4, the prefactor to $\varepsilon$ on the right-hand side of the last inequality converges to a constant $c^* > 0$. This leads to ergodicity in persistence. $\qquad\square$

### 5.2.3 Persistence diagram measures

In this section we consider point processes on $\mathscr{D}$ constructed from persistence diagrams such as $\bigcup_{\ell=0}^{n-1} \mathrm{Dgm}_\ell(X_\xi(\cdot))$.

Let $\xi$ be a simple point process on $\mathbb{R}^n$. Then for any $A \in \mathcal{B}_b^n$ and $\omega \in \Omega$ we consider the point cloud $X_{\xi_\omega}(A)$. We denote by $D_A(X_{\xi_\omega}(A)) := \bigcup_{\ell=0}^{n-1} \mathrm{Dgm}_\ell(X_{\xi_\omega}(A))$ the corresponding persistence diagram of the filtration of the Čech complexes.

**Definition 5.2.5.** *Given a simple point process $\xi$ and $A \in \mathcal{B}_b^n$, the map*

$$\rho_\omega(A) := \sum_{x \in D_A(X_{\xi_\omega}(A))} \delta_x \qquad \text{for all } \omega \in \Omega \tag{5.15}$$

*defines a point process $\rho_\cdot(A)$ on $\Delta$. The map $\rho_\cdot : \Omega \times \mathcal{B}_b^n \to \mathcal{N}(\Delta)$ is called the* persistence diagram measure. *If the measure exists, its first moment measure defines*

$$\mathfrak{p}(A) := \mathbb{E}[\rho_\omega(A)] \,. \tag{5.16}$$

*The map $\mathfrak{p} : \mathcal{B}_b^n \to \mathcal{R}(\Delta)$, $A \mapsto \mathfrak{p}(A)$ is called the* persistence diagram expectation measure.

**Proposition 5.2.6.** *Let $\rho$ be a persistence diagram measure, $\mathfrak{p}$ the corresponding persistence diagram expectation measure and $A \in \mathcal{B}_b^n$, $\omega \in \Omega$. Then, there exist Borel measurable functions $\tilde{\rho}_{\omega,A}, \tilde{\mathfrak{p}}_A : \Delta \to \mathbb{R}_+$ and singular measures $\rho_{\omega,s}(A), \mathfrak{p}_s(A)$, such that for all $B \in \mathcal{B}(\Delta)$,*

$$\rho_\omega(A)(B) = \int_B \tilde{\rho}_{\omega,A}(x) \lambda_2(\mathrm{d}x) + \rho_{\omega,s}(A)(B) \,, \tag{5.17a}$$

$$\mathfrak{p}(A)(B) = \int_B \tilde{\mathfrak{p}}_A(x) \lambda_2(\mathrm{d}x) + \mathfrak{p}_s(A)(B) \,. \tag{5.17b}$$

*Proof.* This is a direct consequence of applying first the Lebesgue decomposition theorem and then the Radon-Nikodym theorem for absolutely continuous measures [236].

Focussing on $\mathfrak{p}(A)$, we explicitly set

$$\tilde{\mathfrak{p}}_A(x) := \lim_{r \searrow 0} \frac{\mathfrak{p}(A)(B_r(x))}{\lambda_2(B_r(x))} \tag{5.18}$$

and

$$S := \left\{ x : \lim_{r \searrow 0} \frac{\mathfrak{p}(A)(B_r(x))}{\lambda_2(B_r(x))} = \infty \right\} . \tag{5.19}$$

Then, we set $\mathfrak{p}_s(A)(B) = \mathfrak{p}(A)(B \cap S)$, and find $\lambda_2(S) = 0$. Fully analogous constructions lead to the decomposition of $\rho_\omega(A)$. $\qquad\square$

**Remark 5.2.7.** *In [204] it is shown that under particular assumptions on the simplicial complex filtration, covering for instance the filtration of Čech complexes, the singular contribution $\mathfrak{p}_s$ to the persistence diagram expectation measure $\mathfrak{p}$ can be absorbed into the density $\tilde{\mathfrak{p}}$.*

**Remark 5.2.8.** *The measurable Lebesgue density corresponding to the non-singular contribution to the persistence diagram (expectation) measure appearing in Proposition 5.2.6 can be identified with the so-called (asymptotic) persistence pair distribution defined in [6] and employed in Section 4.3.2 of this dissertation. In particular, if the persistence diagram (expectation) measure exists, then the density exists as well, though it might be zero.*

The persistence diagram expectation measure exists for stationary and ergodic point processes on $\mathbb{R}^n$, as the following lemma shows.

**Lemma 5.2.9.** *Let $\xi$ be a simple stationary and ergodic point process on $\mathbb{R}^n$ having all finite moments. Then the corresponding persistence diagram expectation measure exists.*

*Proof.* Let $A \in \mathcal{B}_b^n$ and $B \in \mathcal{B}(\Delta)$ be bounded, $\omega \in \Omega$. Let $F_\ell(X_{\xi_\omega}(A), r)$ be the number of $\ell$-simplices in $\check{C}_r(X_{\xi_\omega}(A))$ and $F_\ell(\xi, r; A)$ the number of $\ell$-simplices in $\check{C}_r(X_{\xi_\omega}(\mathbb{R}^n))$ with at least one vertex in $A$. We compute, with $r \geq 0$ sufficiently large, the $n$-skeleton of the Čech complex, $\check{C}_r(X_{\xi_\omega}(A))^n$, and $\#K$ denoting the number of simplices in a simplicial complex $K$,

$$\rho_\omega(A)(B) \leq n(X_{\xi_\omega}(A)) \leq \#(\check{C}_r(X_{\xi_\omega}(A))^n) \tag{5.20}$$

$$= \sum_{\ell=0}^{n} F_\ell(X_{\xi_\omega}(A), r) \tag{5.21}$$

$$\leq \sum_{\ell=0}^{n} F_\ell(\xi, r; A) \leq \sum_{\ell=0}^{n} \sum_{x \in X_{\xi_\omega}(A)} \binom{\xi(B_{2\ell r}(x))}{\ell + 1}, \tag{5.22}$$

which holds since all vertices of an $\ell$-simplex containing a vertex $x \in A$ are contained in $X_{\xi_\omega}(\mathbb{R}^n) \cap B_{2\ell r}(x)$, and all $\ell$-simplices are constructed from $\ell + 1$ points in this intersection. If $\ell + 1 > \xi(B_{2\ell r}(x))$, the binomial coefficient is zero. Let $R(\xi_\omega, A) < \infty$ be the maximum $r > 0$, such that for any $\epsilon > 0$, $\epsilon < r$,

$$\check{C}_r(X_{\xi_\omega}(A)) \neq \check{C}_{r-\epsilon}(X_{\xi_\omega}(A)) . \tag{5.23}$$

Indeed, $R(\xi_\omega, A)$ is well-defined and exists, since the point clouds $X_{\xi_\omega}(A)$ are always finite, hence the Čech complex $\check{C}_r(X_{\xi_\omega}(A))$ changes only finitely often as $r$ increases. Then, we

find

$$\rho_\omega(A)(B) \le n(X_{\xi_\omega}(A)) \le \#(\check{C}_\infty(X_{\xi_\omega}(A))^n) \le \sum_{\ell=0}^{n} \sum_{x \in X_{\xi_\omega}(A)} \binom{\xi(B_{2\ell R(\xi_\omega, A)}(x))}{\ell+1}. \quad (5.24)$$

Taking expectations yields

$$\mathfrak{p}(A)(B) \le \sum_{\ell=0}^{n} \mathbb{E}\left[ \sum_{x \in X_{\xi_\omega}(A)} \binom{\xi(B_{2\ell R(\xi_\omega, A)}(x))}{\ell+1} \right]. \quad (5.25)$$

The expectation value on the right-hand side of this expression exists and is finite for bounded $A$, since $\xi$ is stationary, ergodic and has all finite moments. Thus, $\mathfrak{p}(A)(B)$ is finite and in particular exists. $\qquad\square$

### 5.2.4 The strong law for persistent Betti numbers

In this section we state an extension of the strong law of large numbers for persistent Betti numbers of stationary point processes, established in [71, Theorem 1.11] for averaging along cubes, to general convex averaging sequences. The proofs are given in Appendix 5.C. They make use of the results for cubical averaging sequences [71], and exploit results from convex geometry.

The extension to general convex averaging sequences is of interest for applications in the natural sciences, where large volume asymptotics are not only taken via nested sequences of cubes. An example is given by thermodynamic limits of spherically shaped systems in quantum many-body physics [237, 238].

The following theorem establishes the existence of a limiting Radon measure, towards which volume-averaged persistence diagram expectation measures for convex averaging sequences converge.

**Theorem 5.2.10.** *Let $\xi$ be a simple point process on $\mathbb{R}^n$ having all finite moments and $\{A_k\}$ a convex averaging sequence. If $\xi$ is stationary, then there exists a unique Radon measure $\mathfrak{P} \in \mathcal{R}(\Delta)$, such that*

$$\frac{\mathfrak{p}(A_k)}{\lambda_n(A_k)} \xrightarrow{v} \mathfrak{P} \quad \text{for } k \to \infty, \quad (5.26)$$

*where $\mathfrak{p}$ is the persistence diagram expectation measure corresponding to $\xi$ and $\xrightarrow{v}$ denotes convergence in the vague topology.*

A stronger statement can be established for persistent Betti numbers.

**Theorem 5.2.11** (Strong law of large numbers for persistent Betti numbers)**.** *Let $\xi$ be a stationary simple point process having all finite moments and $\{A_k\}$ a convex averaging sequence. Given $\omega \in \Omega$, we set $X_k := X_{\xi_\omega}(A_k)$. Then, for any $0 \le r \le s < \infty$ and $\ell = 0, 1, \dots, n$ there exists a constant $\hat{\beta}_\ell^{r,s}$, such that*

$$\frac{\mathbb{E}[\beta_\ell^{r,s}(\mathcal{C}(X_k))]}{\lambda_n(A_k)} \to \hat{\beta}_\ell^{r,s} \qquad \text{for } k \to \infty. \quad (5.27)$$

*Additionally, if $\xi$ is ergodic, then a.s.*

$$\frac{\beta_\ell^{r,s}(\mathcal{C}(X_k))}{\lambda_n(A_k)} \to \hat{\beta}_\ell^{r,s} \qquad \text{for } k \to \infty. \tag{5.28}$$

In the spirit of Theorem 5.2.10 and Theorem 5.2.11, several related and also stronger results have been established for particular point processes [222–225, 239].

### 5.2.5   Geometric quantities and a packing lemma

Different geometric quantities may be computed from persistence diagram (expectation) measures, linked by a relation deduced from the notion of bounded total persistence, i.e., a bound on sums of persistences to some power. These quantities are of relevance e.g. for applications in many-body physics, see again [6].

**Definition 5.2.12.** *Let $\rho$ be a persistence diagram measure and $A \in \mathcal{B}_b^n$. Assume that the corresponding persistence diagram expectation measure $\mathfrak{p}$ exists and is non-zero. Let $\omega \in \Omega$. We define the* number of persistent homology classes *as*

$$n_\omega(A) := \int_\Delta \rho_\omega(A)(\mathrm{d}x) = \rho_\omega(A)(\Delta) \tag{5.29}$$

*and the* expected number of persistent homology classes *as*

$$\mathfrak{n}(A) := \int_\Delta \mathfrak{p}(A)(\mathrm{d}x) = \mathfrak{p}(A)(\Delta). \tag{5.30}$$

*Let $q > 0$. The* degree-$q$ persistence *is defined as*

$$l_{q,\omega}(A) := \left[\frac{1}{n_\omega(A)} \int_\Delta \mathrm{pers}(x)^q \, \rho_\omega(A)(\mathrm{d}x)\right]^{1/q}, \tag{5.31}$$

*and the corresponding* expected degree-$q$ persistence *as*

$$\mathfrak{l}_q(A) := \left[\frac{1}{\mathfrak{n}(A)} \int_\Delta \mathrm{pers}(x)^q \, \mathfrak{p}(A)(\mathrm{d}x)\right]^{1/q}. \tag{5.32}$$

*With $Y_\omega(A) \subset \Delta$ the multiset of atoms of $\rho_\omega(A)$, we define the* maximum death *as*

$$d_{\max,\omega}(A) := \max\{d \,|\, (b,d) \in Y_\omega(A)\} = \lim_{p \to \infty} \left[\int_\Delta d(x)^p \, \rho_\omega(A)(\mathrm{d}x)\right]^{1/p}, \tag{5.33}$$

*where the last equality is a general result for $p$-norms in finite dimensions. We define the* expected maximum death *as*

$$\mathfrak{d}_{\max}(A) := \lim_{p \to \infty} \left[\int_\Delta d(x)^p \, \mathfrak{p}(A)(\mathrm{d}x)\right]^{1/p}. \tag{5.34}$$

The following two propositions justify the nomenclature used in Definition 5.2.12.

**Proposition 5.2.13.** *Let $\mathfrak{p}$ be an existing non-zero persistence diagram expectation measure and $A \in \mathcal{B}_b^n$. We find that*

$$\mathfrak{n}(A) = \mathbb{E}[n_\omega(A)]. \tag{5.35}$$

*If the measure $\mathfrak{p}(A)$ is boundedly finite, then $\mathfrak{n}(A) < \infty$.*

We get similar statements for $\mathfrak{d}_{\max}(A)$ and $\mathfrak{l}_q(A)$ for sufficiently large point clouds.

**Proposition 5.2.14.** *Let $\xi$ be a stationary and ergodic simple point process on $\mathbb{R}^n$ having all finite moments. Let $\mathfrak{p}$ be the persistence diagram expectation measure computed from $\xi$, assumed to exist and to be non-zero. Let $\{A_k\}$ be a convex averaging sequence and $\epsilon > 0$. We find for $k$ sufficiently large,*

$$|\mathfrak{d}_{\max}(A_k) - \mathbb{E}[d_{\max,\omega}(A_k)]| < \epsilon. \tag{5.36}$$

*We find for all $q > 0$ and $k$ sufficiently large that*

$$|\mathfrak{l}_q(A_k) - \mathbb{E}[l_{q,\omega}(A_k)]| < \epsilon. \tag{5.37}$$

*Almost surely, for any $p, q \neq 0$ and $\omega \in \Omega$ we find for sufficiently large $k$*

$$\left| \mathbb{E}\left[ \frac{d_{\max,\omega}(A_k)^p}{l_{q,\omega}(A_k)^q} \right] - \lim_{k' \to \infty} \frac{d_{\max,\omega}(A_{k'})^p}{l_{q,\omega}(A_{k'})^q} \right| < \epsilon. \tag{5.38}$$

*In particular, this a.s. implies with Equations (5.36) and (5.37) for sufficiently large $k$*

$$\left| \mathfrak{d}_{\max}(A_k) - \lim_{k' \to \infty} d_{\max,\omega}(A_{k'}) \right| < \epsilon, \tag{5.39}$$

*and for all $q > 0$,*

$$\left| \mathfrak{l}_q(A_k) - \lim_{k' \to \infty} l_{q,\omega}(A_{k'}) \right| < \epsilon. \tag{5.40}$$

*Let $A \in \mathcal{B}_b^n$. If the measure $\mathfrak{p}(A)$ is boundedly finite and $\operatorname{supp}(\mathfrak{p}(A)) \subset \Delta$ is bounded, then $\mathfrak{d}_{\max}(A) < \infty$ and $\mathfrak{l}_q(A) < \infty$ for all $q > 0$.*

The proofs of Proposition 5.2.13 and Proposition 5.2.14 are postponed to Appendix Section 5.B.3.

A link between the geometric quantities is provided by bounded total persistence as introduced in Appendix 5.A, which results in an upper bound for the number of persistent homology classes in a given volume.

**Lemma 5.2.15** (The packing lemma). *Let $\xi$ be a simple point process on $\mathbb{R}^n$ and $n_\omega(\cdot), d_{\max,\omega}(\cdot)$ and $l_{q,\omega}(\cdot)$ be computed from the sample $\xi_\omega, \omega \in \Omega$. Then there exists a constant $c > 0$, such that for any $\delta > 0$ and $A \in \mathcal{B}_b^n$,*

$$n_\omega(A) \leq \frac{c(n + 2\delta)}{\delta} \frac{d_{\max,\omega}(A)^\delta}{l_{n+\delta,\omega}(A)^{n+\delta}}. \tag{5.41}$$

*Proof.* Let $A \in \mathcal{B}_b^n$ and $X := X_{\xi_\omega}(A)$. For all $x \in \operatorname{Conv}(X)$ we set

$$d_X(x) := \min_{p \in X} d(x, p). \tag{5.42}$$

Clearly, $d_X$ is Lipschitz with Lipschitz constant 1. By the nerve theorem [240], for any $r > 0$ the sublevel set $d_X^{-1}[0, r]$ and the Čech complex $\check{C}_r(X)$ have isomorphic homology

groups with homology groups of $d_X^{-1}[0, r]$ computed via singular homology. In particular, the persistence modules of both corresponding filtrations are isomorphic. $\mathrm{Conv}(X)$ being bounded implies bounded degree-$(n + \delta)$ total persistence of the filtration $(d_X^{-1}[0, r])_r$ for all $\delta > 0$, see Appendix 5.A. Then, as in Proposition 5.A.1 there exists a constant $c > 0$, such that

$$n_\omega(A) l_{n+\delta,\omega}(A)^{n+\delta} = \mathrm{Pers}_{n+\delta}(d_X) \leq c \, \mathrm{Amp}(d_X)^\delta \frac{n + 2\delta}{\delta} \,, \tag{5.43}$$

with $\mathrm{Amp}(d_X) = \max_{x \in \mathrm{Conv}(X)} d_X(x)$. Note that $\mathrm{Amp}(d_X) = d_{\max,\omega}(A)$, so we obtain the desired result for the filtration of Čech complexes. □

## 5.3　Self-similarity

In this section we introduce the notion of self-similar scaling of persistence diagram expectation measures and discuss related phenomena. For this, persistence diagrams are considered depending on an additional parameter $t$, which can be interpreted, for instance, as the time in physics applications, see again [6] and Chapter 4 of this dissertation. Intuitively, self-similar scaling describes geometric quantities blowing up or shrinking as a power-law in time with characteristic scaling exponents. A packing relation between the occurring scaling exponents can be derived from the previous packing lemma.

### 5.3.1　Self-similar scaling

**Definition 5.3.1.** *Let* $(\mathfrak{p}(t))_{t \in (T_0, T_1)}$ *be a family of existing non-zero persistence diagram expectation measures,* $0 < T_0 < T_1$. *For* $t \in (T_0, T_1)$, $A \in \mathcal{B}_b^n$ *we set* $\mathfrak{p}(t, A) := \mathfrak{p}(t)(A)$ *and let* $\{A_k\}$ *be a convex averaging sequence. We say that* $(\mathfrak{p}(t))_{t \in (T_0, T_1)}$ *scales self-similarly between times* $T_0$ *and* $T_1$ *with exponents* $\eta_1, \eta_2 \in \mathbb{R}$, *if for all* $t, t' \in (T_0, T_1)$, $B \in \mathcal{B}(\Delta)$ *and* $k$ *sufficiently large depending on the sequence* $(A_k)$,

$$\mathfrak{p}(t, A_k)(B) = (t/t')^{-\eta_2} \mathfrak{p}(t', A_k)((t/t')^{-\eta_1} B) \,, \tag{5.44}$$

*where* $\kappa B := \{(\kappa b, \kappa d) \,|\, (b, d) \in B\}$ *for* $\kappa \in [0, \infty)$.

Self-similar scaling of persistence diagram expectation measures manifests in the characteristic scaling behavior of corresponding geometric quantities.

**Lemma 5.3.2.** *Let* $(\mathfrak{p}(t))_{t \in (T_0, T_1)}$ *be a family of existing non-zero persistence diagram expectation measures, which scales self-similarly between times* $T_0$ *and* $T_1$ *with exponents* $\eta_1, \eta_2$. *The* $t$-*dependence of any geometric quantity constructed from* $\mathfrak{p}(t)$ *is denoted by an additional* $t$-*argument. Let* $\{A_k\}$ *be a convex averaging sequence. Then for all* $t, t' \in (T_0, T_1)$, $q \geq 1$ *and* $k$ *sufficiently large,*

$$\mathfrak{n}(t, A_k) = (t/t')^{-\eta_2} \mathfrak{n}(t', A_k) \,, \tag{5.45a}$$

$$\mathfrak{l}_q(t, A_k) = (t/t')^{\eta_1} \mathfrak{l}_q(t', A_k) \,, \tag{5.45b}$$

$$\mathfrak{d}_{\max}(t, A_k) = (t/t')^{\eta_1} \mathfrak{d}_{\max}(t', A_k) \,. \tag{5.45c}$$

*Proof.* The derivation of the first two equations follows analogously to the third via push-forward measures and changing integration variables. We let $t, t' \in (T_0, T_1)$, set $f_{t,t'}(x) := (t/t')^{\eta_1} x$ for all $x \in \Delta$ and note that $f_{t,t'}(\Delta) = \Delta$. Let $k$ be sufficiently large. We compute,

$$
\begin{aligned}
\mathfrak{d}_{\max}(t, A_k) &= \lim_{p\to\infty} \left[ \int_\Delta d(x)^p \, \mathfrak{p}(t, A_k)(\mathrm{d}x) \right]^{1/p} \\
&= \lim_{p\to\infty} \left[ (t/t')^{-\eta_2} \int_\Delta d(x)^p \, ((f_{t,t'})_* \mathfrak{p}(t', A_k))(\mathrm{d}x) \right]^{1/p} \\
&= \lim_{p\to\infty} \left[ (t/t')^{-\eta_2} \int_\Delta d(f_{t,t'}(x))^p \, \mathfrak{p}(t', A_k)(\mathrm{d}x) \right]^{1/p} \\
&= \lim_{p\to\infty} (t/t')^{\eta_1 - \eta_2/p} \left[ \int_\Delta d(x)^p \, \mathfrak{p}(t', A_k)(\mathrm{d}x) \right]^{1/p} \\
&= (t/t')^{\eta_1} \mathfrak{d}_{\max}(t', A_k) .
\end{aligned}
\tag{5.46a}
$$

$\square$

In [226] a fractal dimension estimator has been introduced, based on persistent homology. Let $(\mathfrak{p}(t))_{t \in (T_0, T_1)}$ be a family of non-zero persistence diagram expectation measures and let $(\xi(t))_t$ be a family of simple point processes on $\mathbb{R}^n$ having all finite moments, corresponding to the family of persistence diagram expectation measures. For $\alpha > 0$, $A \in \mathcal{B}_b^n$ we define

$$
E^\alpha(\xi(t), A) := \sum_{x \in \bigcup_\ell \mathrm{Dgm}_\ell(X_{\xi(t)}(A))} \mathrm{pers}(x)^\alpha .
\tag{5.47}
$$

Let $\{A_k\}$ be a convex averaging sequence. We set

$$
\vartheta_\alpha(t) := \limsup_{k\to\infty} \frac{\log \mathbb{E}[E^\alpha(\xi(t), A_k)]}{\log \mathbb{E}[\xi(t, A_k)]} .
\tag{5.48}
$$

Then, the persistent homology fractal dimension is defined as

$$
\dim_{\mathrm{PH}}^\alpha(\xi(t)) := \frac{\alpha}{1 - \vartheta_\alpha(t)} .
\tag{5.49}
$$

The following lemma shows that $\dim_{\mathrm{PH}}^\alpha(\xi(t))$ stays constant in the course of time upon self-similar scaling, if the expectation values of $\xi(t, A)$ fulfill a weak assumption on the large-volume behavior.

**Lemma 5.3.3.** *Let $(\mathfrak{p}(t))_{t \in (T_0, T_1)}$ be a family of non-zero persistence diagram expectation measures, which scales self-similarly between times $T_0$ and $T_1$ with exponents $\eta_1, \eta_2$. Let $(\xi(t))_t$ be a family of simple stationary point processes on $\mathbb{R}^n$ having all finite moments and corresponding to the family of persistence diagram expectation measures. Assume that*

$$
\lim_{k\to\infty} \frac{\log \mathbb{E}[\xi(t', A_k)]}{\log \mathbb{E}[\xi(t, A_k)]} = 1 .
\tag{5.50}
$$

*Then, the persistent homology fractal dimension $\dim_{PH}^\alpha(\xi(t))$ stays constant in the course of time for all $\alpha > 0$.*

*Proof.* Let $\rho(t, \cdot)$ be the persistence diagram measure corresponding to $\xi(t)$. Then

$$E_\ell^\alpha(\xi(t), A) = \int_\Delta \text{pers}(x)^\alpha \rho(t, A)(\mathrm{d}x). \tag{5.51}$$

Using Proposition 5.B.3, we obtain

$$\mathbb{E}[E_\ell^\alpha(\xi(t), A)] = \int_\Delta \text{pers}(x)^\alpha \mathfrak{p}(t, A)(\mathrm{d}x). \tag{5.52}$$

Exploiting self-similarity yields for all $t, t' \in (T_0, T_1)$ and $k$ sufficiently large

$$\mathbb{E}[E_\ell^\alpha(\xi(t), A_k)] = (t/t')^{\alpha\eta_1 - \eta_2} \mathbb{E}[E_\ell^\alpha(\xi(t'), A_k)]. \tag{5.53}$$

By means of this equation we find

$$
\begin{aligned}
\vartheta_\alpha(t) &= \limsup_{k\to\infty} \frac{(\alpha\eta_1 - \eta_2)\log(t/t') + \log\mathbb{E}[E_\ell^\alpha(\xi(t'), A_k)]}{\log\mathbb{E}[\xi(t', A_k)]} \frac{\log\mathbb{E}[\xi(t', A_k)]}{\log\mathbb{E}[\xi(t, A_k)]} \\
&= \vartheta_\alpha(t') \lim_{k\to\infty} \frac{\log\mathbb{E}[\xi(t', A_k)]}{\log\mathbb{E}[\xi(t, A_k)]} = \vartheta_\alpha(t').
\end{aligned}
\tag{5.54}
$$

Thus, the persistent homology fractal dimension stays constant in the course of time,

$$\dim_{\text{PH}}^\alpha(\xi(t)) = \frac{\alpha}{1 - \vartheta_\alpha(t)} = \dim_{\text{PH}}^\alpha(\xi(t')). \tag{5.55}$$

$\square$

**Remark 5.3.4.** *The above assumption that $\lim_{k\to\infty} \log\mathbb{E}[\xi(t', A_k)]/\log\mathbb{E}[\xi(t, A_k)] = 1$ is fairly general. A special instance, when it is fulfilled, is when the expectation of $\xi$ satisfies a power-law in time, i.e., if a $\kappa$ exists, such that for all $t, t' \in (T_0, T_1)$, $\mathbb{E}[\xi(t, A)] = (t/t')^\kappa \mathbb{E}[\xi(t', A)]$ for $A \in \mathcal{B}_b^n$.*

**Remark 5.3.5.** *The above results can be generalized to more complicated time-dependences. Let $(\mathfrak{p}(t))_{t\in(T_0,T_1)}$ be a family of existing non-zero persistence diagram expectation measures, $0 < T_0 < T_1$, $\{A_k\}$ a convex averaging sequence and $B \in \mathcal{B}(\Delta)$. Let $f, g : (0, \infty) \to (0, \infty)$ be continuous surjections which strictly increase or decrease, and assume that for all times $t, t' \in (T_0, T_1)$ and $k$ sufficiently large,*

$$\mathfrak{p}(t, A_k)(B) = g(t/t')\mathfrak{p}(t', A_k)(f(t/t')B). \tag{5.56}$$

*Clearly, there exist continuous $F, G : (0, \infty) \to (0, \infty)$, such that*

$$\mathfrak{p}(t, A_k)(B) = (t/t')^{G(t/t')}\mathfrak{p}(t', A_k)((t/t')^{F(t/t')}B). \tag{5.57}$$

*All of the arguments in this section generalize easily to this setting.*

### 5.3.2 The packing relation

In this section we establish a relation between the scaling exponents $\eta_1$ and $\eta_2$ (see Definition 5.3.1). Intuitively, it describes the bounded packing of homology classes of growing

sizes, less of which fit into a given constant volume. The relation can have applications throughout many-body physics whenever self-similar behavior with some parametric dependence occurs for persistent homology quantifiers, e.g. for studies of critical scaling phenomena [78–80] and non-thermal fixed points, see again [6] and Chapter 4 of this dissertation.

**Theorem 5.3.6** (The packing relation). *Let $(\xi(t))_{t\in(T_0,T_1)}$, $0 < T_0 < T_1$, be a family of stationary and ergodic simple point processes on $\mathbb{R}^n$ having all finite moments. Let $(\mathfrak{p}(t))_t$ be the family of persistence diagram expectation measures computed from $(\xi(t))_t$. Assume that all $(\mathfrak{p}(t))_t$ exist, are non-zero and that the family scales self-similarly between times $T_0$ and $T_1$ with exponents $\eta_1, \eta_2 \in \mathbb{R}$. Then, if the interval $(T_0, T_1)$ is sufficiently extended as detailed in the proof, we a.s. find*

$$\eta_2 = n\eta_1 \,. \tag{5.58}$$

*Proof.* The time-dependence of any geometric quantity constructed from $\rho_\omega(t, \cdot)$ and $\mathfrak{p}(t, \cdot)$ is again denoted by an additional $t$-argument. We derive the packing relation from evaluation on a convex averaging sequence $\{A_k\}$. From Lemma 5.2.15 we obtain that for an arbitrary $\delta > 0$,

$$n_\omega(t, A_k) \leq \frac{c\,(n+2\delta)}{\delta} \frac{d_{\max,\omega}(t, A_k)^\delta}{l_{n+\delta,\omega}(t, A_k)^{n+\delta}} \,. \tag{5.59}$$

Using Proposition 5.2.14 we a.s. find for a sample $\omega \in \Omega$, $\epsilon > 0$ and $k$ sufficiently large

$$\epsilon > \left| \mathfrak{d}_{\max}(t, A_k) - \lim_{k'\to\infty} d_{\max,\omega}(t, A_{k'}) \right| \,, \tag{5.60}$$

and a.s. for $q > 0$:

$$\epsilon > \left| \mathfrak{l}_q(t, A_k) - \lim_{k'\to\infty} l_{q,\omega}(t, A_{k'}) \right| \,. \tag{5.61}$$

Exploiting Equation (5.38) from Proposition 5.2.14, Equation (5.59) a.s. yields for sufficiently large $k$ upon taking expectations:

$$\begin{aligned}
\mathfrak{n}(t, A_k) &\leq \lim_{k'\to\infty} \frac{c\,(n+2\delta)}{\delta} \frac{d_{\max,\omega}(t, A_{k'})^\delta}{l_{n+\delta,\omega}(t, A_{k'})^{n+\delta}} + O(\epsilon^\delta) \\
&= \frac{c\,(n+2\delta)}{\delta} \frac{\mathfrak{d}_{\max}(t, A_k)^\delta}{\mathfrak{l}_{n+\delta}(t, A_k)^{n+\delta}} + O(\epsilon^\delta) \,.
\end{aligned} \tag{5.62}$$

Exploiting self-similarity and Lemma 5.3.2, we find for any $t, t' \in (T_0, T_1)$,

$$\frac{\mathfrak{d}_{\max}(t, A_k)^\delta}{\mathfrak{l}_{n+\delta}(t, A_k)^{n+\delta}} = (t/t')^{-n\eta_1} \frac{\mathfrak{d}_{\max}(t', A_k)^\delta}{\mathfrak{l}_{n+\delta}(t', A_k)^{n+\delta}} \,. \tag{5.63}$$

Hence,

$$\mathfrak{n}(t, A_k) = (t/t')^{-\eta_2} \mathfrak{n}(t', A_k) \leq (t/t')^{-n\eta_1} \frac{c\,(n+2\delta)}{\delta} \frac{\mathfrak{d}_{\max}(t', A_k)^\delta}{\mathfrak{l}_{n+\delta}(t', A_k)^{n+\delta}} + O(\epsilon^\delta) \,. \tag{5.64}$$

We assume that $\eta_2 \neq n\eta_1$ and that $t, t' \in (T_0, T_1)$ exist with

$$t/t' > \frac{c(n+2\delta)}{\delta} \max \left\{ \frac{\mathfrak{d}_{\max}(t, A_k)^\delta}{\mathfrak{n}(t, A_k)\mathfrak{l}_{n+\delta}(t, A_k)^{n+\delta}}, \frac{\mathfrak{d}_{\max}(t', A_k)^\delta}{\mathfrak{n}(t', A_k)\mathfrak{l}_{n+\delta}(t', A_k)^{n+\delta}} \right\}^{1/|n\eta_1 - \eta_2|}, \quad (5.65)$$

for any $k$ sufficiently large. Then, either for $n\eta_1 < \eta_2$,

$$(t/t')^{\eta_2 - n\eta_1} = (t'/t)^{n\eta_1 - \eta_2} > \frac{c(n+2\delta)}{\delta} \frac{\mathfrak{d}_{\max}(t, A_k)^\delta}{\mathfrak{n}(t, A_k)\mathfrak{l}_{n+\delta}(t, A_k)^{n+\delta}}, \quad (5.66)$$

or for $n\eta_1 > \eta_2$,

$$(t/t')^{n\eta_1 - \eta_2} > \frac{c(n+2\delta)}{\delta} \frac{\mathfrak{d}_{\max}(t', A_k)^\delta}{\mathfrak{n}(t', A_k)\mathfrak{l}_{n+\delta}(t', A_k)^{n+\delta}}, \quad (5.67)$$

both of them being in contradiction to Equation (5.64) for sufficiently small $\epsilon$. Thus, the desired equality $\eta_2 = n\eta_1$ a.s. follows, provided that the interval $(T_0, T_1)$ is sufficiently extended in the sense of Equation (5.65). $\qquad\square$

## 5.4 Examples

This section is devoted to examples for self-similar scaling. First, we consider a Poisson point process with time-dependent intensity and show self-similar scaling of corresponding persistence diagram measures. The second example considers persistence diagram measures of point clouds sampled uniformly from sublevel sets of smooth functions which themselves scale self-similarly. The third example describes an application of the deduced results in quantum physics [6], which stimulated the present work.

### 5.4.1 Poisson point process with power-law scaling intensity

We consider time-dependent Poisson point processes in the following sense, which generalize usual Poisson point processes [230].

**Definition 5.4.1.** *A family of point processes* $(\xi(t))_{t \in [1, \infty)}$ *on* $\mathbb{R}^n$ *is a* time-dependent Poisson point process *on* $\mathbb{R}^n$*, if there exists an intensity function* $\gamma : [1, \infty) \to (0, \infty)$*, such that for each* $t \in [1, \infty)$*,*

  (i) *the expected number of points in* $A \in \mathcal{B}^n$ *is* $\mathbb{E}[\xi(t, A)] = \gamma(t)\lambda_n(A)$*,*

 (ii) *for every* $A \in \mathcal{B}^n$ *the distribution of* $\xi(t, A)$ *is* $\mathbb{P}[\xi(t, A) = k] = \mathrm{Po}(\gamma(t)\lambda_n(A); k)$ *for all* $k \in \mathbb{N}$*,* $\mathrm{Po}(\lambda; k) = (\lambda^k/k!)\exp(-\lambda)$ *denoting the Poisson distribution,*

(iii) *for every* $m \in \mathbb{N}$ *and all pairwise disjoint Borel sets* $A_1, \dots, A_m \in \mathcal{B}^n$ *the random variables* $\xi(t, A_1), \dots, \xi(t, A_m)$ *are independent.*

A time-dependent Poisson process with properties (i) to (iii) defines a Poisson point process at each time $t$, individually. It is a basic result from the theory of point processes that such a point process $\xi(t)$ is stationary and ergodic, having all finite moments for each $t \in [1, \infty)$ [228–230].

**Proposition 5.4.2.** *Let $(\xi(t))_{t\in[1,\infty)}$ be a time-dependent Poisson point process on $\mathbb{R}^n$ with intensity function*

$$\gamma(t) = \gamma_0 t^{-n\eta_1}, \tag{5.68}$$

*$\gamma_0 > 0$ and $\eta_1 \geq 0$. Let $\{A_k\}$ be a convex averaging sequence. Then the family $(\mathfrak{p}(t, A_k)/\lambda_n(A_k))_t$ of persistence diagram expectation measures computed from $(\xi(t))_t$ normalized to the volume of the convex sets converges vaguely for $k \to \infty$ to a family of Radon measures $(\mathfrak{P}(t))$ which scales self-similarly between $1$ and $\infty$ with exponents $\eta_1$ and $n\eta_1$.*

*Proof.* Let $\tilde{\xi}_0$ be the Poisson point process with intensity $\gamma_0$, such that $\mathbb{E}[\tilde{\xi}_0(A)] = \gamma_0 \lambda_n(A)$ for $A \in \mathcal{B}_b^n$. We draw a sample point cloud $X_{\tilde{\xi}_{0,\omega}}(A)$ of $\tilde{\xi}_0$ and define for all $t \in [1, \infty)$

$$X_{\tilde{\xi}_\omega}(t, A) := \left(t^{\eta_1} X_{\tilde{\xi}_{0,\omega}}(A)\right) \cap A. \tag{5.69}$$

This defines a point process $\tilde{\xi}(t)$ with $\#X_{\tilde{\xi}_\omega}(t, A) = \tilde{\xi}_{0,\omega}(t^{-\eta_1} A)$ for each $t$. Its intensity can be computed,

$$\mathbb{E}[\tilde{\xi}(t, A)] = \mathbb{E}[\#((t^{\eta_1} X_{\tilde{\xi}_{0,\omega}}(A)) \cap A)] = \mathbb{E}[\#X_{\tilde{\xi}_{0,\omega}}(t^{-\eta_1} A)] = \gamma_0 t^{-n\eta_1} \lambda_n(A), \tag{5.70}$$

that is, the intensities of $\xi(t)$ and $\tilde{\xi}(t)$ agree for all $t$. Also, we have

$$\mathbb{P}[\tilde{\xi}(t, A) = k] = \mathbb{P}[\tilde{\xi}_0(t^{-\eta_1} A) = k] = \mathrm{Po}(\gamma_0 \lambda_n(t^{-\eta_1} A); k) = \mathrm{Po}(\gamma(t)\lambda_n(A); k). \tag{5.71}$$

Furthermore, let $A_1, A_2 \subset \mathbb{R}^n$ be disjoint Borel sets. Then, $\tilde{\xi}_0(A_1)$ and $\tilde{\xi}_0(A_2)$ are independent random variables, $\tilde{\xi}_0$ being a Poisson point process. Let $x_i \in A_i$. Then, $|x_1 - x_2| > 0$ and $t^{-\eta_1}|x_1 - x_2| > 0$, i.e., $t^{-\eta_1} A_1$ and $t^{-\eta_1} A_2$ are disjoint, too. Thus, $\tilde{\xi}(t, A_1)$ and $\tilde{\xi}(t, A_2)$ are also independent random variables. The Poisson point process being uniquely characterized by the properties (i) to (iii) of Definition 5.4.1, $\xi(t)$ and $\tilde{\xi}(t)$ can be identified for all $t$.

We employ the strong law of large numbers for persistent Betti numbers, Theorem 5.2.11 and denote the limiting persistent Betti numbers at time $t$ as $\hat{\beta}_\ell^{r,s}(t)$, such that for $k \to \infty$,

$$\frac{\mathbb{E}[\beta_\ell^{r,s}(\mathcal{C}(X_\xi(t, A_k)))]}{\lambda_n(A_k)} \to \hat{\beta}_\ell^{r,s}(t). \tag{5.72}$$

We compute,

$$\begin{aligned}
\frac{\mathbb{E}[\beta_\ell^{r,s}(\mathcal{C}(X_\xi(t, A_k)))]}{\lambda_n(A_k)} &= \frac{\mathbb{E}[\beta_\ell^{r,s}(\mathcal{C}(t^{\eta_1}(X_{\tilde{\xi}_0}(A_k) \cap t^{-\eta_1} A_k)))]}{\lambda_n(A_k)} \\
&= \frac{\mathbb{E}[\beta_\ell^{t^{-\eta_1}r, t^{-\eta_1}s}(\mathcal{C}(X_{\tilde{\xi}_0}(A_k) \cap t^{-\eta_1} A_k))]}{\lambda_n(A_k)} \\
&= \frac{t^{-n\eta_1}\mathbb{E}[\beta_\ell^{t^{-\eta_1}r, t^{-\eta_1}s}(\mathcal{C}(X_{\tilde{\xi}_0}(t^{-\eta_1} A_k)))]}{\lambda_n(t^{-\eta_1} A_k)} \xrightarrow{k\to\infty} t^{-n\eta_1} \hat{\beta}_\ell^{t^{-\eta_1}r, t^{-\eta_1}s}(1).
\end{aligned} \tag{5.73}$$

Both limits need to agree, i.e.,

$$\hat{\beta}_\ell^{r,s}(t) = t^{-n\eta_1} \hat{\beta}_\ell^{t^{-\eta_1} r, t^{-\eta_1} s}(1)\,. \tag{5.74}$$

With $\mathfrak{p}(t, A_k)$ the persistence diagram expectation measure computed from $\xi(t)$ and evaluated on $A_k$, by means of Theorem 5.2.10 we obtain the existence of a unique Radon measure $\mathfrak{P}(t)$ at each time $t$, such that for $k \to \infty$

$$\frac{\mathfrak{p}(t, A_k)}{\lambda_n(A_k)} \xrightarrow{v} \mathfrak{P}(t)\,. \tag{5.75}$$

Starting from Equation (5.74), identical arguments which lead to the proof of Theorem 1.5 in [71] here lead to

$$\mathfrak{P}(t)(B) = t^{-n\eta_1} \mathfrak{P}(1)(t^{-\eta_1} B) \tag{5.76}$$

for any $B \in \mathcal{B}(\Delta)$. $\qquad\square$

### 5.4.2 Scaling from function sublevel sets

The following example establishes a relation between self-similar scaling exponents derived from moments of random variables and those derived from persistence diagram measures, based on single-sample manifestations of an underlying rescaling of the metric.

**Scaling functions.** Let $(T_0, T_1)$ be a time interval. Let $(\Omega, \mathcal{E}, \mathbb{P})$ be a probability space with $\Omega$ a set of smooth functions $Y : (T_0, T_1) \times \mathbb{R}^n \to \mathbb{R}$, $\mathcal{E}$ some event space, such that for arbitrary $t, t' \in (T_0, T_1), x \in \mathbb{R}^n$:

$$\mathbb{P}\left[Y(t, x) = \left(\frac{t}{t'}\right)^\alpha Y(t', (t/t')^\beta x)\right] = 1\,, \tag{5.77}$$

i.e., a.s. all samples reveal self-similar scaling in time. Then, all moments of $\mathbb{P}$ show self-similar behavior, as well:

$$\mathbb{E}\left[\prod_{i=1}^N Y(t, x_i)\right] = \int \prod_{i=1}^N Y(t, x_i) \mathbb{P}(\mathrm{d}Y) = \left(\frac{t}{t'}\right)^{N\alpha} \int \prod_{i=1}^N Y(t', (t/t')^\beta x_i) \mathbb{P}(\mathrm{d}Y)$$
$$= \left(\frac{t}{t'}\right)^{N\alpha} \mathbb{E}\left[\prod_{i=1}^N Y(t', (t/t')^\beta x_i)\right]\,, \tag{5.78}$$

where $x_i \in \mathbb{R}^n$ for $i = 1, \ldots, N$ with $N \in \mathbb{N}$. Let $f : \mathbb{R} \to \mathbb{R}$ be a homogeneous function of degree $\kappa > 0$ with $f(x) \geq 0$ for all $x \in \mathbb{R}$. We define submanifolds of $\mathbb{R}^n$ via

$$X_\nu[Y](t) := \{x \in \mathbb{R}^n \mid f(Y(t, x)) \leq \nu\}\,. \tag{5.79}$$

Then, a.s. we find by Equation (5.77)

$$X_\nu[Y](t) = \left\{x \in \mathbb{R}^n \,\middle|\, f(Y(t', (t/t')^\beta x)) \leq (t/t')^{-\kappa\alpha} \nu\right\} = \left(\frac{t}{t'}\right)^{-\beta} X_{(t/t')^{-\kappa\alpha} \nu}[Y](t')\,. \tag{5.80}$$

**Scaling of the persistence diagram measure.** We demonstrate in the following that this likely implies scaling of persistence diagram measures computed from point clouds appropriately sampled from $X_\nu[Y](t)$.

Let $\{A_k\}$ be a convex averaging sequence in $\mathbb{R}^n$, $\varepsilon > 0$. We choose $q$ points $x_i \in X_\nu[Y](t) \cap A_k$ such that $\bigcup_{i=1}^q B_\varepsilon(x_i)$ is a cover of $X_\nu[Y](t) \cap A_k$. From $X_\nu[Y](t) \cap A_k$ we sample a point cloud $X_{\nu,M}[Y](t, A_k)$ consisting of a number $M$ of i.i.d. uniformly distributed points. Then, there exists $\alpha > 0$ such that $\mathbb{E}[X_{\nu,M}[Y](t, A_k) \cap B_\varepsilon(x_i)] > \alpha$ for all $i$.

With quantifiably high confidence, homology can be inferred from random point samples from manifolds as in [241], which includes a range of probability bounds on point sampling. In particular, by Lemma 5.1 of [241] we then have for $\delta > 0$ that with probability $1 - \delta$

$$X_{\nu,M}[Y](t, A_k) \cap B_\varepsilon(x_i) \neq \emptyset \tag{5.81}$$

for all $i$, given that $M > (\log q - \log \delta)/\alpha$. Thus, with probability $1 - \delta$ we find

$$X_{\nu,M}[Y](t, A_k) \subseteq X_\nu[Y](t) \cap A_k \subseteq \bigcup_{x \in X_{\nu,M}[Y](t,A_k)} B_{2\varepsilon}(x) \subseteq (X_\nu[Y](t) \cap A_k) \oplus B_{2\varepsilon}(0),$$
$$\tag{5.82}$$

$\oplus$ denoting the Minkowski sum among subsets of $\mathbb{R}^n$. To this end, we have shown that with probability $1 - \delta$ a $2\varepsilon$-interleaving between point clouds $X_{\nu,M}[Y](t, A_k)$ and sublevels sets $X_\nu[Y](t) \cap A_k$ exists.

For simplicity we denote the filtration of Čech complexes of $X_{\nu,M}[Y](t, A_k)$ by $\mathcal{C}_t$ and the filtration of growing balls around $X_\nu[Y](t) \cap A_k$, that is, $((X_\nu[Y](t) \cap A_k) \oplus B_r(0))_r$, by $\mathcal{D}_t$. We denote the persistence module computed via simplicial homology from $\mathcal{C}_t$ by $H_*(\mathcal{C}_t)$ and the persistence module computed via singular homology from $\mathcal{D}_t$ by $H_*(\mathcal{D}_t)$. Given the $2\varepsilon$-interleaving, which exists with probability $1 - \delta$, we then find an upper bound for their interleaving distance,

$$d_I(H_*(\mathcal{C}_t), H_*(\mathcal{D}_t)) = \inf\{\epsilon \mid \text{there exists an } \epsilon\text{-interleaving between } H_*(\mathcal{C}_t), H_*(\mathcal{D}_t)\}$$
$$\leq 2\varepsilon. \tag{5.83}$$

Following Theorem 3.5 of [242] we find equality between the bottleneck and the interleaving distance in our case:

$$d_B(H_*(\mathcal{C}_t), H_*(\mathcal{D}_t)) = \inf\{\epsilon \in [0, \infty) \mid \text{there exists an } \epsilon\text{-matching between } H_*(\mathcal{C}_t), H_*(\mathcal{D}_t)\}$$
$$= d_I(H_*(\mathcal{C}_t), H_*(\mathcal{D}_t)) \leq 2\varepsilon, \tag{5.84}$$

with an $\epsilon$-matching defined as in [242]. This implies that if $B \in \mathcal{B}(\Delta)$ fulfills $(b, d) \in B \implies d - b > 4\varepsilon$, then the persistence diagram measures are related as follows:

$$\rho(\mathcal{C}_t)(B) \leq \rho(\mathcal{D}_t)(B \oplus B_{2\varepsilon}(0)) \quad \text{and} \quad \rho(\mathcal{D}_t)(B) \leq \rho(\mathcal{C}_t)(B \oplus B_{2\varepsilon}(0)), \tag{5.85}$$

where the dependence on the sample function $Y$ is implicit here. Thus, we find with probability $1 - \delta$

$$\rho(\mathcal{D}_t)(B) \leq \rho(\mathcal{C}_t)(B \oplus B_{2\varepsilon}(0)) \leq \rho(\mathcal{D}_t)(B \oplus B_{4\varepsilon}(0)) \tag{5.86}$$

and can likely estimate the persistence diagram measure computed from sampled point clouds, $\rho(\mathcal{C}_t)$, from the one of sublevels, directly, $\rho(\mathcal{D}_t)$. Employing Equation (5.80), we find

$$X_\nu[Y](t) \cap A_k = \left(\frac{t}{t'}\right)^{-\beta} \left(X_{(t/t')^{-\kappa\alpha}\nu}[Y](t') \cap (t/t')^\beta A_k\right). \tag{5.87}$$

From this we find the time-dependence of the singular homology groups,

$$H_*((X_\nu[Y](t) \cap A_k) \oplus B_r(0)) = H_*((X_{(t/t')^{-\kappa\alpha}\nu}[Y](t') \cap (t/t')^\beta A_k) \oplus B_{(t/t')^\beta r}(0)). \tag{5.88}$$

Hence, we find for any $B \in \mathcal{B}(\Delta)$:

$$\rho(\mathcal{D}_t)(B) = \rho(\mathcal{D}'_{t,t'})((t/t')^\beta B), \tag{5.89}$$

with $\mathcal{D}'_{t,t'}$ the filtration $((X_{(t/t')^{-\kappa\alpha}\nu}[Y](t') \cap (t/t')^\beta A_k) \oplus B_r(0))_r$ of topological spaces. Insertion into Equation (5.85) leads with probability $1 - \delta$ to

$$\rho(\mathcal{D}'_{t,t'})((t/t')^\beta B) \leq \rho(\mathcal{C}_t)(B \oplus B_{2\varepsilon}(0)) \leq \rho(\mathcal{D}'_{t,t'})((t/t')^\beta B \oplus B_{4(t/t')^\beta\varepsilon}(0)). \tag{5.90}$$

For any given $\varepsilon$ we can always choose the number of sampled points $M$ sufficiently large for the described constructions to apply. To this end, the limit $\varepsilon \to 0$ may be taken in Equations (5.86) and (5.90), leading with probability $1 - \delta$ for any $B \in \mathcal{B}(\Delta)$ to

$$\lim_{\varepsilon \to 0} \rho(\mathcal{C}_t)(B) = \rho(\mathcal{D}'_{t,t'})((t/t')^\beta B) = \lim_{\varepsilon \to 0} \rho(\mathcal{C}'_{t,t'})((t/t')^\beta B). \tag{5.91}$$

Here, $\mathcal{C}'_{t,t'}$ denotes the filtration of Čech complexes of $X_{(t/t')^{-\kappa\alpha}\nu,M}[Y](t, (t/t')^\beta A_k)$.

**Self-similar scaling of the persistence diagram expectation measure.** The scaling of sublevel set homology groups as in Equation (5.88) still encodes temporally varying convex averaging sequences $(t/t')^\beta A_k$. We show that for particular sets of functions $\Omega$ the point clouds sampled make up a stationary point process, then leading via Theorem 5.2.10 to an overall scaling factor of the persistence diagram expectation measure in the infinite-volume limit, resulting in self-similar scaling of the latter in the form of Definition 5.3.1. As a byproduct the packing relation is independently from the proof of Theorem 5.3.6 demonstrated for this particular example.

We assume that the samples $f \circ Y$ resemble stationarity in probability for each time individually, i.e., for all $-\infty \leq a \leq b \leq \infty$, $x, y \in \mathbb{R}^n$ and $t \in (T_0, T_1)$,

$$\mathbb{P}[a \leq f(Y(t,x)) \leq b] = \mathbb{P}[a \leq f(Y(t,y)) \leq b]. \tag{5.92}$$

Then, any point $x \in A_k$ is equally likely included in a point cloud $X_{\nu,M}[Y](t, A_k)$, given

that $X_{\nu,M}[Y](t, A_k)$ consists of i.i.d. uniformly distributed points in $X_\nu[Y](t) \cap A_k$. To this end, under assumption (5.92) $Y(t, \cdot) \mapsto X_{\nu,M}[Y](t, A_k)$ defines a stationary point process on $A_k$ with $Y \in \Omega$. Furthermore, the defined point process has all finite moments, again exploiting that $X_{\nu,M}[Y](t, A_k)$ consists of i.i.d. uniformly distributed points.

Thus, we may apply Theorem 5.2.10 for persistence diagram expectation measures. Let $\mathfrak{p}(\mathcal{C}'_{t,t'}) := \mathbb{E}[\rho(\mathcal{C}'_{t,t'})]$ be the persistence diagram expectation measure computed from the persistence diagram measures of the filtrations of Čech complexes of point clouds sampled from sublevel sets with as special case $\mathfrak{p}(\mathcal{C}_t) := \mathbb{E}[\rho(\mathcal{C}_t)]$. Implicitly, it depends on the parameter $\varepsilon$. By Theorem 5.2.10 we obtain that a limiting Radon measure $\mathfrak{P}_t$ on $\Delta$ exists, such that for any continuous function $g$ on $\Delta$ with compact support,

$$\lim_{k \to \infty} \frac{1}{\lambda_n(A_k)} \lim_{\varepsilon \to 0} \int_\Delta g \, \mathfrak{p}(\mathcal{C}_t) = \int_\Delta g \, \mathfrak{P}_t \,. \tag{5.93}$$

Regard here that $\mathfrak{p}(\mathcal{C}_t)$ implicitly depends on the $A_k$. More generally, we find that a Radon measure $\mathfrak{P}_{t,t'}$ exists, which satisfies the following, again for all continuous functions $g$ on $\Delta$ with compact support:

$$\left(\frac{t}{t'}\right)^{n\beta} \int_\Delta g((t/t')^{-\beta}x) \, \mathfrak{P}_{t,t'}(\mathrm{d}x)$$
$$= \left(\frac{t}{t'}\right)^{n\beta} \lim_{k \to \infty} \frac{1}{\lambda_n((t/t')^\beta A_k)} \lim_{\varepsilon \to 0} \int_\Delta g((t/t')^{-\beta}x) \, \mathfrak{p}(\mathcal{C}'_{t,t'})(\mathrm{d}x)$$
$$= \lim_{k \to \infty} \frac{1}{\lambda_n(A_k)} \lim_{\varepsilon \to 0} \int_\Delta g((t/t')^{-\beta}x) \, \mathfrak{p}(\mathcal{C}'_{t,t'})(\mathrm{d}x) \,. \tag{5.94}$$

We employed here Theorem 5.2.10 together with $((t/t')^\beta A_k)_k$ being a convex averaging sequence. As a limiting case we obtain $\mathfrak{P}_t = \mathfrak{P}_{t,t}$. Using Equation (5.91), we arrive at

$$\lim_{k \to \infty} \frac{1}{\lambda_n(A_k)} \lim_{\varepsilon \to 0} \int_\Delta g(x) \, \mathfrak{p}(\mathcal{C}_t)(\mathrm{d}x) = \lim_{k \to \infty} \frac{1}{\lambda_n(A_k)} \lim_{\varepsilon \to 0} \int_\Delta g((t/t')^{-\beta}x) \, \mathfrak{p}(\mathcal{C}'_{t,t'})(\mathrm{d}x) \,, \tag{5.95}$$

which leads with Equation (5.93) to

$$\int_\Delta g(x) \, \mathfrak{P}_t(\mathrm{d}x) = \left(\frac{t}{t'}\right)^{n\beta} \int_\Delta g((t/t')^{-\beta}x) \, \mathfrak{P}_{t,t'}(\mathrm{d}x) \,. \tag{5.96}$$

If we assume that in a sufficiently large regime of filtration parameters $\nu$ under consideration persistence diagram (expectation) measures are independent from $\nu$, then $\mathfrak{P}_{t,t'}$ is independent from $t'$ up to the power-law denoted in the argument of $g$ on the right-hand side of Equation (5.96). Then, in the limit of large volumes we obtain self-similar scaling of volume-averaged persistence diagram expectation measures, including an independent derivation of the packing relation given in Theorem 5.3.6 for the considered example.

### 5.4.3 Application: Numerical simulations in non-equilibrium quantum physics

Studying quantum physics far from equilibrium, indications for self-similar scaling of persistence diagram expectation measures have been found in numerical simulations of

the non-relativistic Bose gas [6] and of a gluonic plasma, see Chapter 4 of this dissertation. The scaling behavior can be attributed to the existence of a non-thermal fixed point in the dynamics of the system, characterized by such scaling and typically verified by investigating the behavior of correlation functions.

We embed the scenario of [6], where in particular the packing relation first appeared, into the present mathematical framework. The analogous considerations hold for the considerations of Chapter 4 of this dissertation. The simulations of [6] have been carried out in the classical-statistical regime of many particles interacting comparably weakly. In this regime the quantum physics could be accurately mapped to a Gaussian ensemble of complex-valued fields at initial time $t = 0$, $\psi_\omega(0) : \Lambda \to \mathbb{C}$, $\omega \in \Omega$, $\Lambda \subset \mathbb{R}^2$ a uniform finite square lattice with constant lattice spacing, which have then been time-evolved individually according to the Gross-Pitaevskii differential equation in order to obtain $\psi_\omega(t)$ from $\psi_\omega(0)$ for all $t \in [0, \infty)$. This has yielded an ensemble of fields $(\psi_\omega)_{\omega \in \Omega}$, $\psi_\omega : [0, \infty) \times \Lambda \to \mathbb{C}$. Theoretical predictions have been computed as expectation values with respect to this ensemble of fields.

Given a sample $\psi_\omega$, point clouds have been constructed as subsets of the lattice $\Lambda$ at individual times for filtration parameters $\bar{\nu} \in [0, \infty)$,

$$X_{\bar{\nu},\omega}(t) := |\psi_\omega(t)|^{-1}[0, \bar{\nu}] \subset \mathbb{R}^2 \,. \tag{5.97}$$

$\Lambda$ being finite, the $X_{\bar{\nu},\omega}(t)$ have been finite sets, too. Its alpha complexes and their persistence diagrams have been computed. For an impression of the occurring alpha complexes at different radii see Figure 5.4.1. Finally, expectations for functional summaries such as smooth variants of the distribution of birth radii, that is, $\mathfrak{p}(t, \Lambda)([r_1, r_2] \times [0, \infty))$, and $\mathfrak{d}_{\max}(t, \Lambda)$ have been computed.[8]

A scaling-ansatz has been made for the Lebesgue density of the persistence diagram expectation measure,

$$\tilde{\mathfrak{p}}(t, \Lambda)(b, d) = (t/t')^{-\eta_2} \tilde{\mathfrak{p}}(t', \Lambda)((t/t')^{-\eta_1} b, (t/t')^{-\eta_1} d) \,, \tag{5.98}$$

resulting in the self-similar scaling of persistent homology quantities. A possible singular contribution to the persistence diagram expectation measure as it appears in Proposition 5.2.6 has been ignored. Resulting exponents are summarized in Figure 5.4.2. By simple application of the transformation theorem we find

$$\mathfrak{n}(t, A) = (t/t')^{2\eta_1 - \eta_2} \mathfrak{n}(t', A) \,. \tag{5.99}$$

Comparing with a family of persistence diagram expectation measures that scales self-similarly with exponents $\eta_1', \eta_2'$ but yields the same scaling behavior of geometric quantities,

---

[8]Numerically, convolutions with a Gaussian mollifier of arbitrary width, which are necessary to obtain for instance smoothed distributions of death radii, are irrelevant. Simple binning procedures for such distributions and averaging over a sufficiently large number of samples allow for a proper computation of expectation values.
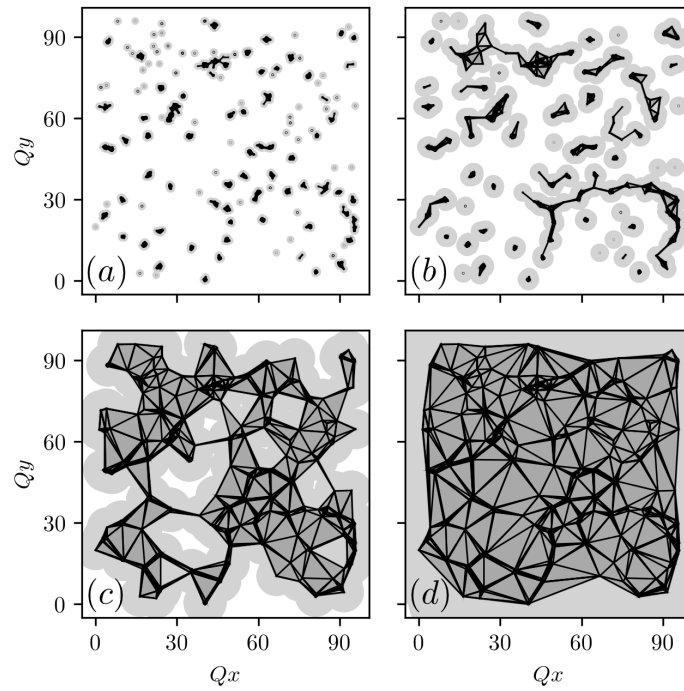
**FIGURE 5.4.1:** Alpha complexes of increasing radii from (a) to (d) in the vicinity of a non-thermal fixed point, reprinted from [6].
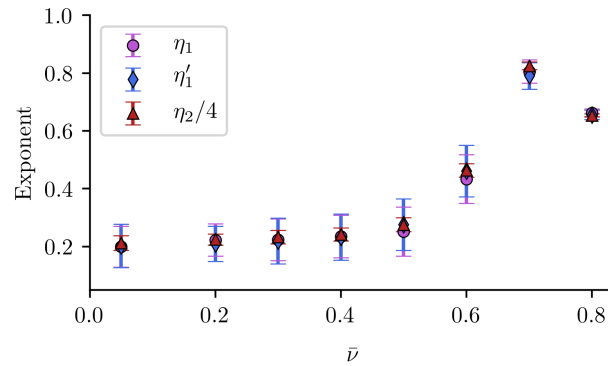


**FIGURE 5.4.2:** Self-similar scaling exponents at a non-thermal fixed point, reprinted from [6]. $\eta_1'$ has been introduced here as an independent scaling exponent for death radii in Equation (5.98).

we obtain $\eta_1 = \eta_1'$ and via Lemma 5.3.2

$$\eta_2 = \eta_2' + 2\eta_1' . \tag{5.100}$$

The packing relation given in Theorem 5.3.6 then translates for the Lebesgue density scaling exponents to $\eta_2 = (2 + n)\eta_1$, in accordance with Figure 5.4.2.

In the simulations the underlying mathematical assumptions of this work could be approximately shown numerically, in particular stationarity and ergodicity of the corresponding point process. First, it has been checked that varying the distance between

neighboring lattice sites does not affect the obtained results, which is theoretically motivated by existing stability theorems for persistent homology [68, 69, 242]. To this end, the specific microscopic lattice geometry can be regarded as unimportant for the displayed results. Furthermore, for the chosen initial ensemble of fields, $\psi_\omega(0)$, physical quantities have numerically revealed (approximate) translation invariance across the lattice, reflecting stationarity. It is easy to verify numerically that classical-statistical simulations are ergodic in the sense of recovering expectation values for intensive quantities from single samples in the limit of large lattices.[9]

## 5.5   Summary and further questions

In this chapter we have studied the persistent homology of point processes, which has provided a mathematically versatile framework to discuss the persistent homology of point clouds in a probabilistic setting. We have constructed measures on the space of persistence diagrams and their expectations, which have facilitated a notion of ergodicity for persistent homology. The strong law of large numbers for persistent Betti numbers has been extended to more general convex averaging sequences.

We have introduced self-similar scaling for time-dependent persistence diagram expectation measures. In the given framework the notion of bounded total persistence has yielded a relation between the occurring scaling exponents, which originated from a bound on the packing of cycles representing persistent homology classes into a time-independent volume. The packing relation has been exemplified for a time-dependent Poisson point process, for certain function sublevel sets, and for numerical simulations in non-equilibrium quantum physics.

From the mathematical viewpoint, a number of further questions can be of interest for later investigations:

1. The self-similar scaling behavior of the persistence diagram expectation measure of a time-dependent Poisson point process and of scaling function sublevel sets has been derived without using the packing relation, though confirming the latter. While the packing relation as derived in this chapter only holds for filtrations of complexes with persistent homology groups isomorphic to those of the Čech complex filtration, the derivation for the Poisson point process holds more generally. This raises the question if the packing relation can be extended to more general situations. A related question is if the ergodicity assumption, which has been crucial at various points for the derivations, can be relaxed.

2. In the application we describe temporally self-similar scaling of persistence diagram expectation measures has been found. In this case, however, also the correlation functions of the point clouds show self-similar scaling [6]. Do there exist other time-dependent point processes, for which persistence diagram expectation measures show self-similar scaling but the correlation functions do not? This would provide further motivation for other applications in the natural sciences.

---

[9]In the field of quantum dynamics this property is better known as self-averaging.

3. With respect to applications an extension of our results to filtrations of weighted simplicial complexes would be of interest.

For a brief discussion of related prospective applications of the results of this chapter in physics we refer to Chapter 8.

# Appendix

## 5.A  Bounded total persistence

In this appendix we discuss the concept of bounded total persistence, as introduced in [69]. With $(M, d)$ a compact, triangulable metric space, let $f : M \to \mathbb{R}$ be a Lipschitz function with $\mathrm{Lip}(f) = \inf\{c \in \mathbb{R} \,|\, |f(x) - f(y)| \leq c\, d(x, y) \,\forall\, x, y \in M\}$ its Lipschitz constant. We denote the $\ell$-th persistence diagram computed via singular homology from the filtration of sublevel sets of a Lipschitz function $f$ by $\mathrm{Dgm}_\ell(f)$ and call $f$ tame, if all its persistence diagrams are finite. Let $K$ be a finite simplicial complex triangulating $M$ via a triangulation homeomorphism $\vartheta$ and set $\mathrm{mesh}(K) := \max_{\sigma \in K} \mathrm{diam}(\sigma)$, $\mathrm{diam}(\sigma) := \max_{x,y \in \sigma} d(\vartheta(x), \vartheta(y))$ the diameter of a simplex $\sigma$. For $r > 0$ we define $N(r) := \min_{\mathrm{mesh}(K) \leq r} \#K$. We consider the total persistence diagram $\cup_\ell \mathrm{Dgm}_\ell(f)$ of a Lipschitz function $f$, and define the degree-$k$ total persistence of $f$ as

$$\mathrm{Pers}_k(f) := \sum_{x \in \cup_\ell \mathrm{Dgm}_\ell(f)} \mathrm{pers}(x)^k. \tag{5.101}$$

**Proposition 5.A.1** (Technical results from [69]). *Assume that the size of the smallest triangulation of a triangulable, compact metric space $M$ grows polynomially with one over the mesh, i.e., there exist $C_0, m$, such that $N(r) \leq C_0/r^m$ for all $r > 0$. Let $\delta > 0$ and $k = m + \delta$. Then,*

$$\mathrm{Pers}_k(f) \leq \frac{m + 2\delta}{\delta} C_0 \,\mathrm{Lip}(f)^m \mathrm{Amp}(f)^\delta, \tag{5.102}$$

*where $\mathrm{Amp}(f) := \max_{x \in M} f(x) - \min_{y \in M} f(y)$ is the amplitude of $f$.*

For $M$ a compact Riemannian $n$-manifold there exist constants $c, C$, such that $c/r^n \leq N(r) \leq C/r^n$ for sufficiently small $r$. A compact metric space $M$ implies bounded degree-$k$ total persistence, if there exists $C_M > 0$, such that $\mathrm{Pers}_k(f) \leq C_M$ for every tame function $f : M \to \mathbb{R}$ with $\mathrm{Lip}(f) \leq 1$.

## 5.B  Functional summaries

Persistence diagrams themselves do not naturally lead to statistical goals [243]. Instead, functional summaries of persistence diagrams such as persistence landscapes [70] have been proposed for their statistical analysis [244]. In recent years, a multitude of different functional summaries have been developed across the literature [244–247].

In this appendix we introduce the notion of functional summaries. Different types of functional summaries accompanied by corresponding limit theorems then lead to proofs of Propositions 5.2.13 and 5.2.14.

## 5.B.1  Additive functional summaries and persistence diagram measures

Let $T$ be a compact metric space and $\mathscr{F}(T)$ a collection of functions, $f : T \to \mathbb{R}$. A functional summary $\mathcal{F}$ is a map $\mathcal{F} : \mathscr{D} \to \mathscr{F}(T)$. We call a functional summary $\mathcal{F}$ additive, if for any two persistence diagrams $D, E \in \mathscr{D}$ with $D + E$ defined as the union of multisets the equation $\mathcal{F}(D + E) = \mathcal{F}(D) + \mathcal{F}(E)$ is fulfilled.[10] We denote the set of additive functional summaries by $\mathscr{A}(T)$.

A functional summary $\mathcal{F}$ is uniformly bounded, if a constant $U < \infty$ exists, such that

$$\sup_{f \in \mathrm{im}(\mathcal{F})} \sup_{s \in T} |f(s)| \leq U \,. \tag{5.103}$$

The following proposition on the pointwise convergence of uniformly bounded functional summaries has been given in the literature [244].

**Proposition 5.B.1** (Pointwise convergence of functional summaries [244])**.** *Let $\mathcal{F}$ be a uniformly bounded functional summary and $D_i \in \mathscr{D}$ for $i \in \mathbb{N}$, sampled i.i.d. from a probability space $(\mathscr{D}, \mathcal{B}(\mathscr{D}), \mathbb{P}_{\mathscr{D}})$. Set $f_i := \mathcal{F}(D_i)$. If $\mathrm{im}(\mathcal{F})$ is equicontinuous, then a.s. for $n \to \infty$*

$$\sup_{s \in T} \left| \frac{1}{m} \sum_{i=1}^{m} f_i(s) - \mathbb{E}[\mathcal{F}(D)(s)] \right| \to 0 \,. \tag{5.104}$$

We restrict to uniformly bounded and equicontinuous functional summaries, such that Proposition 5.B.1 applies.

In the framework of functional summaries persistence diagram (expectation) measures as constructed in Section 5.2.3 naturally show up.

**Proposition 5.B.2.** *Let $\mathcal{A} \in \mathscr{A}(T)$ be an additive functional summary, $s \in T$ and $A \in \mathcal{B}_b^n$. Let $Y_\omega(A) \subset \Delta$ be the multiset of atoms of $\rho_\omega(A)$. In the evaluation of $\mathcal{A}$ the related persistence diagram measure $\rho$ appears,*

$$\mathcal{A}(Y_\omega(A))(s) = \sum_{x \in Y_\omega(A)} \mathcal{A}(\{x\})(s) = \int_\Delta \mathcal{A}(\{x\})(s) \, \rho_\omega(A)(\mathrm{d}x) \,. \tag{5.105}$$

**Proposition 5.B.3.** *Assume that the persistence diagram expectation measure $\mathfrak{p}$ exists. Then, for any functional summary $\mathcal{F} \in \mathscr{F}(T)$, $s \in T$ and $A \in \mathcal{B}_b^n$, we have*

$$\mathbb{E}\left[ \int_\Delta \mathcal{F}(\{x\})(s) \, \rho_\omega(A)(\mathrm{d}x) \right] = \int_\Delta \mathcal{F}(\{x\})(s) \, \mathfrak{p}(A)(\mathrm{d}x) \,. \tag{5.106}$$

*Proof.* This statement is clear from the theory of point processes and their moment measures [229]. Note that for any $A \in \mathcal{B}_b^n$ there exists a bounded $B \subset \overline{\Delta}$, such that

---

[10]In [204, 248] additive functional summaries have been introduced similarly as so-called linear representations of persistence diagrams.

$\text{supp}(\rho_\omega(A)) \subseteq B$ for any $\omega \in \Omega$. Then

$$\int_\Delta \mathcal{F}(\{x\})(s)\, \rho_\omega(A)(\mathrm{d}x) = \int_\Delta \mathcal{F}(\{x\})(s)\chi_B(x)\, \rho_\omega(A)(\mathrm{d}x) \tag{5.107}$$

with indicator function $\chi_B$, and $\mathcal{F}(\cdot)(s)\chi_B$ has bounded support. $\qquad\square$

### 5.B.2 Intensive functional summaries

**Definition 5.B.4.** *Let $\xi$ be a stationary and ergodic simple point process on $\mathbb{R}^n$ and $\mathcal{F} : \mathscr{D} \to \mathscr{F}(T)$ a functional summary. We say that $\mathcal{F}$ is $\xi$-intensive, if for any convex averaging sequence $\{A_k\}$, $\epsilon > 0$ and $k$ sufficiently large we a.s. have*

$$\lim_{l \to \infty} ||\mathcal{F}(D_l) - \mathcal{F}(D_k)||_\infty < \epsilon, \tag{5.108}$$

*where $|| \cdot ||_\infty$ denotes the supremum norm and $D_k := \bigcup_{\ell=0}^{n-1} \mathrm{Dgm}_\ell(X_{\xi_\omega}(A_k))$.*

**Lemma 5.B.5.** *Let $\mathcal{A} \in \mathscr{A}(T)$ be an additive functional summary and $\xi$ a stationary and ergodic simple point process on $\mathbb{R}^n$. Set $D_k := \bigcup_{\ell=0}^{n-1} \mathrm{Dgm}_\ell(X_{\xi_\omega}(A_k))$, where $\{A_k\}$ is a convex averaging sequence. Then $\mathcal{A}(D_k)/\lambda_n(A_k)$ a.s. defines a $\xi$-intensive functional summary.*

*Proof.* Set $X_k := X_{\xi_\omega}(A_k)$. Let $s \in T$ and $k, l \in \mathbb{N}$,

$$\left| \frac{\mathcal{A}(D_l)(s)}{\lambda_n(A_l)} - \frac{\mathcal{A}(D_k)(s)}{\lambda_n(A_k)} \right|$$
$$= \frac{n(X_k)}{\lambda_n(A_k)} \left| \left( \frac{\lambda_n(A_k)}{n(X_k)} \frac{n(X_l)}{\lambda_n(A_l)} - 1 \right) \frac{\mathcal{A}(D_l)(s)}{n(X_l)} - \left( \frac{\mathcal{A}(D_k)(s)}{n(X_k)} - \frac{\mathcal{A}(D_l)(s)}{n(X_l)} \right) \right|$$
$$\leq \frac{n(X_k)}{\lambda_n(A_k)} \left| \frac{\lambda_n(A_k)}{n(X_k)} \frac{n(X_l)}{\lambda_n(A_l)} - 1 \right| \frac{|\mathcal{A}(D_l)(s)|}{n(X_l)} + \frac{n(X_k)}{\lambda_n(A_k)} \left| \frac{\mathcal{A}(D_k)(s)}{n(X_k)} - \frac{\mathcal{A}(D_l)(s)}{n(X_l)} \right|.$$
$$\tag{5.109}$$

By Lemma 5.2.4 we have that $\xi$ is ergodic in persistence. Thus, for $\epsilon > 0$ there exist sufficiently large $k, l$ such that a.s.

$$\left| 1 - \frac{n(X_l)}{n(X_k)} \frac{\lambda_n(A_k)}{\lambda_n(A_l)} \right| < \epsilon. \tag{5.110}$$

Furthermore, by Theorem 5.2.10 a $c^* > 0$ exists, such that for all $k$: $n(X_k)/\lambda_n(A_k) < c^*$. By uniform boundedness of the functional summary there exists a constant $U < \infty$, such that for any persistence diagram $D_k$,

$$\sup_{s \in T} |\mathcal{A}(D_k)(s)| < U. \tag{5.111}$$

By additivity of $\mathcal{A}$ we obtain that $\mathcal{A}(D_k)(s)/n(X_k)$ converges for $k \to \infty$ and every $s$. To this end, for sufficiently large $k, l$ we find

$$\left| \frac{\mathcal{A}(D_k)(s)}{n(X_k)} - \frac{\mathcal{A}(D_l)(s)}{n(X_l)} \right| < \epsilon. \tag{5.112}$$

Estimating Equation (5.109) further, we obtain for sufficiently large $k, l$:

$$\left| \frac{\mathcal{A}(D_l)(s)}{\lambda_n(A_l)} - \frac{\mathcal{A}(D_k)(s)}{\lambda_n(A_k)} \right| < (1 + U)c^* \epsilon . \tag{5.113}$$

Indeed, the $\mathcal{A}(D_k)/\lambda_n(A_k)$ a.s. define a $\xi$-intensive functional summary. $\qquad\square$

**Corollary 5.B.6.** *Given the assumptions of Lemma 5.B.5, $\mathcal{A}(D_k)/n(D_k)$ is a $\xi$-intensive functional summary. This is a direct result of*

$$\frac{\mathcal{A}(D_k)}{n(D_k)} = \frac{\lambda_n(A_k)}{n(D_k)} \frac{\mathcal{A}(D_k)}{\lambda_n(A_k)} , \tag{5.114}$$

*both factors being $\xi$-intensive functional summaries.*

Asymptotically, for $\xi$-intensive functional summaries the ensemble-average can be replaced by the infinite-volume limit.

**Proposition 5.B.7.** *Let $\xi$ be a stationary and ergodic simple point process on $\mathbb{R}^n$. Let $\mathcal{F}$ be a $\xi$-intensive functional summary and $\{A_k\}$ a convex averaging sequence. Choose i.i.d. samples $\omega_i \in \Omega$, $i \in \mathbb{N}$, according to the probability distribution $\mathbb{P}$ and define $D_{k,i} := \bigcup_{\ell=0}^{n-1} \mathrm{Dgm}_\ell(X_{\xi_{\omega_i}}(A_k))$. Then for any $j \in \mathbb{N}$, $\epsilon > 0$ and sufficiently large $k$ we a.s. find*

$$\sup_{s \in T} \left| \lim_{l \to \infty} \mathcal{F}(D_{l,j})(s) - \lim_{m \to \infty} \frac{1}{m} \sum_{i=1}^{m} \mathcal{F}(D_{k,i})(s) \right| < \epsilon . \tag{5.115}$$

*Proof.* Let $s \in T$, $\epsilon > 0$, $j \in \mathbb{N}$, $D_k := \bigcup_{\ell=0}^{n-1} \mathrm{Dgm}_\ell(X_\xi(A_k))$. Since $\mathcal{F}$ is $\xi$-intensive, further exploiting Proposition 5.B.3 and Theorem 5.2.10, we a.s. obtain for sufficiently large $k$

$$\left| \lim_{l \to \infty} \mathcal{F}(D_{l,j})(s) - \mathbb{E}[\mathcal{F}(D_k)(s)] \right| < \frac{\epsilon}{2}. \tag{5.116}$$

Similarly, Proposition 5.B.1 a.s. yields for sufficiently large $k$

$$\left| \mathbb{E}[\mathcal{F}(D_k)(s)] - \lim_{m \to \infty} \frac{1}{m} \sum_{i=1}^{m} \mathcal{F}(D_{k,i})(s) \right| < \frac{\epsilon}{2} . \tag{5.117}$$

Putting things together, we a.s. find

$$\left| \lim_{l \to \infty} \mathcal{F}(D_{l,j})(s) - \lim_{m \to \infty} \frac{1}{m} \sum_{i=1}^{m} \mathcal{F}(D_{k,i})(s) \right|$$

$$\leq \left| \lim_{l \to \infty} \mathcal{F}(D_{l,j})(s) - \mathbb{E}[\mathcal{F}(D_k)(s)] \right| + \left| \mathbb{E}[\mathcal{F}(D_k)(s)] - \lim_{m \to \infty} \frac{1}{m} \sum_{i=1}^{m} \mathcal{F}(D_{k,i})(s) \right| < \epsilon . \tag{5.118}$$

$\qquad\square$

### 5.B.3 Proofs of Proposition 5.2.13 and Proposition 5.2.14

Given the preceding statements on functional summaries, we can now prove Propositions 5.2.13 and 5.2.14.

*Proof of Proposition 5.2.13.* The statement directly follows from Proposition 5.B.3. □

*Proof of Proposition 5.2.14.* The final statement on finiteness of $\mathfrak{d}_{\max}(A)$ and $\mathfrak{l}_q(A)$ is clear for any $A \in \mathcal{B}_b^n$. For $\omega \in \Omega$ and $A \in \mathcal{B}_b^n$ we define

$$L_{q,\omega}(A) := \int_\Delta \mathrm{pers}(x)^q \rho_\omega(A)(\mathrm{d}x). \tag{5.119}$$

Certainly, $L_q$ is an additive functional summary. Under the assumptions of the proposition, Corollary 5.B.6 holds. Therefore $L_{q,\omega}(A)/n_\omega(A)$ constitutes a $\xi$-intensive functional summary. Let $\{A_k\}$ be a convex averaging sequence and for all $i \in \mathbb{N}$ choose i.i.d. $\omega_i \in \Omega$. For any $j \in \mathbb{N}$ we a.s. obtain by means of Proposition 5.B.1, Corollary 5.B.6 and Proposition 5.B.7 for $\epsilon > 0$ and sufficiently large $k$:

$$\left| \mathbb{E}[l_{q,\omega}(A_k)^q] - \lim_{k' \to \infty} l_{q,\omega_j}(A_{k'})^q \right| = \left| \lim_{m \to \infty} \frac{1}{m} \sum_{i=1}^m l_{q,\omega_i}(A_k)^q - \lim_{k' \to \infty} l_{q,\omega_j}(A_{k'})^q \right| < \epsilon. \tag{5.120}$$

Now,

$$l_{q,\omega_j}(A_{k'})^q = \frac{L_{q,\omega_j}(A_{k'})}{n_{\omega_j}(A_{k'})} = \frac{\lambda_n(A_{k'})}{n_{\omega_j}(A_{k'})} \frac{L_{q,\omega_j}(A_{k'})}{\lambda_n(A_{k'})}. \tag{5.121}$$

Each of the two factors on the right-hand side is a $\xi$-intensive functional summary according to Lemma 5.B.5. By the same arguments, we get for sufficiently large $k$

$$\frac{\epsilon}{2} > \left| \mathbb{E}[l_{q,\omega}(A_k)^q]^{1/q} - \left( \lim_{k' \to \infty} \frac{\lambda_n(A_{k'})}{n_{\omega_j}(A_{k'})} \lim_{k' \to \infty} \frac{L_{q,\omega_j}(A_{k'})}{\lambda_n(A_{k'})} \right)^{1/q} \right|. \tag{5.122}$$

Thus we find again for sufficiently large $k$

$$\begin{aligned}
\epsilon &> \left| \mathbb{E}[l_{q,\omega}(A_k)^q]^{1/q} - \left( \frac{\lambda_n(A_k)}{\lim_{m \to \infty} \frac{1}{m} \sum_{i=1}^m n_{\omega_i}(A_k)} \lim_{m \to \infty} \frac{1}{m} \sum_{i=1}^m \frac{L_{q,\omega_i}(A_k)}{\lambda_n(A_k)} \right)^{1/q} \right| + \frac{\epsilon}{2} \\
&> \left| \mathbb{E}[l_{q,\omega}(A_k)^q]^{1/q} - \left( \frac{\lambda_n(A_k)}{\mathbb{E}[n_{\omega_i}(A_k)]} \mathbb{E}\left[ \frac{L_{q,\omega_i}(A_k)}{\lambda_n(A_k)} \right] \right)^{1/q} \right| \\
&= \left| \mathbb{E}[l_{q,\omega}(A_k)^q]^{1/q} - \mathfrak{l}_q(A_k) \right|. \tag{5.123}
\end{aligned}$$

Finally, we find

$$\begin{aligned}
\epsilon &> \left| \mathbb{E}[l_{q,\omega}(A_k)^q]^{1/q} - \left( \lim_{k' \to \infty} l_{q,\omega_j}(A_{k'})^q \right)^{1/q} \right| = \left| \mathbb{E}[l_{q,\omega}(A_k)^q]^{1/q} - \lim_{k' \to \infty} l_{q,\omega_j}(A_{k'}) \right| \\
&= \left| \mathbb{E}[l_{q,\omega}(A_k)^q]^{1/q} - \mathbb{E}[l_{q,\omega}(A_k)] \right|, \tag{5.124}
\end{aligned}$$

completing the proof for $\mathfrak{l}_q(A_k)$. The proof of $|\mathfrak{d}_{\max}(A) - \mathbb{E}[d_{\max,\omega}(A)]| < \epsilon$ proceeds similarly. Defining for all $\mathcal{B}_b^n$ and $q > 0$

$$d_{q,\omega}(A) := \int_\Delta d(x)^q \rho_\omega(A)(\mathrm{d}x)\,, \tag{5.125}$$

we note that via Equation (5.33)

$$\lim_{q \to \infty} \left( \frac{d_{q,\omega}(A)}{n_\omega(A)} \right)^{1/q} = d_{\max,\omega}(A)\,. \tag{5.126}$$

On the other hand, $d_{q,\omega}(A)/n_\omega(A)$ defines a $\xi$-intensive functional summary. Then, arguments analogously to those for $\mathfrak{l}_q(A)$ and monotone convergence lead for sufficiently large $k$ to

$$|\mathfrak{d}_{\max}(A_k) - \mathbb{E}[d_{\max,\omega}(A_k)]| < \epsilon\,. \tag{5.127}$$

Let $p, q \neq 0$. Then, $d_{\max,\omega}(A_k)^p / l_{q,\omega}(A_k)^q$ constitutes a $\xi$-intensive functional summary. As such, Propositions 5.B.1 and 5.B.7 apply and yield Equation (5.38). $\square$

## 5.C  Proofs of limit theorems for convex averaging sequences

In this appendix we provide the proofs for Theorems 5.2.10 and 5.2.11. First, necessary results from convex geometry are revisited.

**Theorem 5.C.1** (Steiner's formula [232]). *Let $C$ be a convex body in $\mathbb{R}^n$. Then for $\delta \geq 0$:*

$$\lambda_n(C \oplus \delta B_1(0)) = \lambda_n(C) + \sum_{i=1}^n \binom{n}{i} W_i(C) \delta^i\,, \tag{5.128}$$

*where $W_i(C)$ are the quermassintegrals, given in Equation (5.6).*

Using Aleksandrov-Fenchel inequalities from convex geometry in terms of the quermassintegrals, an upper bound for the quermassintegrals can be given.

**Theorem 5.C.2** (Theorem 2 in [249] rephrased for quermassintegrals). *Let $K \subset \mathbb{R}^n$ be a convex body. Then, for any $0 \leq j \leq n$*

$$W_{n-j}(K) \leq \frac{n^j \kappa_{n-j}}{j! \binom{n}{j} \kappa_{n-1}^j} W_{n-1}(K)^j\,, \tag{5.129}$$

*with $\kappa_j$ the volume of a $j$-dimensional unit ball.*

*Proof of Theorem 5.2.10.* We largely follow the strategy of [71]. The key step is that we construct a tessellation by cubes for each convex set $A_k$, which allows us to prove a statement on the convergence of persistent Betti numbers of point clouds in the sets $A_k$. The lengthy proof proceeds in three steps. First, we employ Theorem 1.11 in [71] to obtain persistent Betti numbers for large cubic volumes in $\mathbb{R}^n$. Second, we construct a tessellation by cubes for each $A_k$ and use methods from convex geometry to obtain a statement on the convergence of persistent Betti numbers of point clouds in the sets $A_k$. Third, we assemble

the results to obtain the desired statement for measures, similarly to the derivation of Theorem 1.5 in [71].

*First step.* Let $\beta_\ell^{r,s}(\mathcal{C}(X))$ be the $\ell$-th persistent Betti numbers of the Čech complex filtration of a point cloud $X \subset \mathbb{R}^n$. We define for any $A \in \mathcal{B}_b^n$,

$$\psi(A) = \mathbb{E}[\beta_\ell^{r,s}(\mathcal{C}(X_{\xi_\omega}(A)))] \tag{5.130}$$

for some $r \leq s$. For each $L > 0$ let $\Lambda_L := [0, L]^n$ be the cube of side length $L$. For any $A_k$ in the convex averaging sequence there exists a unique $L_k'$, such that $\lambda_n(A_k) = \lambda_n(\Lambda_{L_k'}) = (L_k')^n$. We set

$$L_k := \sup\{L \,|\, \exists\, x \in \mathbb{R}^n : \Lambda_L + x \subseteq A_k\}. \tag{5.131}$$

Note that by construction $L_k \leq L_k'$, and $\{\Lambda_{L_k} \,|\, k\}$ as well as $\{\Lambda_{L_k'} \,|\, k\}$ are convex averaging sequences, too. Given $\epsilon > 0$, by means of Thm. 1.11 in [71] we find for sufficiently large $k, m$

$$\left| \frac{\psi(\Lambda_{L_k'})}{(L_k')^n} - \frac{\psi(\Lambda_{L_m})}{L_m^n} \right| < \epsilon. \tag{5.132}$$

*Second step.* We want to show that for sufficiently large $k, m$:

$$\left| \frac{\psi(A_k)}{\lambda_n(A_k)} - \frac{\psi(\Lambda_{L_m})}{L_m^n} \right| < \epsilon. \tag{5.133}$$

In order to establish this, we investigate the scaling behavior of quermassintegrals $W_i(A_k)$ with the volume of $A_k$. For this purpose, we construct a tessellation made up from cubes. Using the $n$-dimensional lattice

$$L_M \cdot \mathbb{Z}^n = \{(L_M z_1, \dots, L_M z_n) \,|\, z_i \in \mathbb{Z}\} \tag{5.134}$$

with $0 < M \in \mathbb{N}$ arbitrary, we set

$$\Lambda(A_k) := \bigcup_{x \in (L_M \cdot \mathbb{Z}^n) \cap A_k} \left(\Lambda_{L_M} + x\right). \tag{5.135}$$

By boundedness of each $A_k$, $(L_M \cdot \mathbb{Z}^n) \cap A_k$ is finite for all $k$. If we already find $A_k \subseteq \Lambda(A_k)$, we define $C_k := \Lambda(A_k)$. If on the other hand $B_k := A_k \setminus \Lambda(A_k) \neq \emptyset$, we choose $x_1 \in B_k$. For $x_1$ there exist finitely many $x_i' \in L_M \cdot \mathbb{Z}^n$, $i = 1, \dots, N'$, such that $x_1 \in \Lambda_{L_M} + x_i'$ for all $i = 1, \dots, N'$. We define

$$\Lambda_1(A_k) := \Lambda(A_k) \cup \bigcup_{i=1}^{N'} (\Lambda_{L_M} + x_i'), \quad B_{k,1} := A_k \setminus \Lambda_1(A_k). \tag{5.136}$$

By boundedness of $A_k$, we can inductively repeat this construction finitely many times, until $B_{k,N} := A_k \setminus \Lambda_N(A_k) = \emptyset$, i.e., $A_k \subseteq \Lambda_N(A_k)$. Then we set $C_k := \Lambda_N(A_k)$. The $C_k$ give the desired tessellation. Since $A_k \subseteq C_k$, it follows by monotonicity of the quermassintegrals [232] that

$$W_i(A_k) \leq W_i(C_k). \tag{5.137}$$

By construction, we find $C_k \subseteq A_k \oplus \sqrt{n} L_M B_1(0)$. Thus, using Equation (5.137) and Steiner's formula, i.e., Theorem 5.C.1, we obtain

$$\lambda_n(C_k) \leq \lambda_n(A_k \oplus \sqrt{n} L_M B_1(0)) = \lambda_n(A_k) + \sum_{i=1}^{n} \binom{n}{i} (\sqrt{n} L_M)^i W_i(A_k) . \qquad (5.138)$$

By Theorem 5.C.2 constants $\kappa_{n,j} > 0$ exist, such that for $0 \leq j \leq n$: $W_{n-j}(A_k) \leq \kappa_{n,j} W_{n-1}(A_k)^j$. Exploiting that we restrict to sequences $\{A_k\}$ with their $(n-1)$-th quermassintegrals scaling as $W_{n-1}(A_k) = O(\lambda_n(A_k)^{1/n}) = O(L'_k)$ for large $k$, we thus find for $0 \leq j \leq n$ that

$$W_{n-j}(A_k) = O((L'_k)^j) . \qquad (5.139)$$

Using Equations (5.138) and (5.139), we obtain an estimate for the volume difference between $C_k$ and $A_k$,

$$|\lambda_n(C_k) - \lambda_n(A_k)| \leq \left| \sum_{i=1}^{n} \binom{n}{i} W_i(A_k)(\sqrt{n} L_M)^i \right| = O((L'_k)^{n-1} L_M) . \qquad (5.140)$$

Hence,

$$\left| \frac{\lambda_n(C_k)}{\lambda_n(A_k)} - 1 \right| = O(L_M (L'_k)^{-1}) \to 0 \qquad \text{as } k \to \infty . \qquad (5.141)$$

For later use we state the following

$$\left| \frac{\psi(C_k)}{\lambda_n(A_k)} - \frac{\psi(\Lambda_{L_m})}{L_m^n} \right| \leq \left| \left( \frac{\lambda_n(C_k)}{\lambda_n(A_k)} - 1 \right) \frac{\psi(C_k)}{\lambda_n(C_k)} \right| + \left| \frac{\psi(C_k)}{\lambda_n(C_k)} - \frac{\psi(\Lambda_{L_m})}{L_m^n} \right| . \qquad (5.142)$$

There exists $K_1 \in \mathbb{N}$, such that for all $k \geq K_1$ the first term is bounded by $\epsilon/2$ (due to Equation (5.141)). Applying the same argument as in the proof of Theorem 1.11 in [71] for the second term, which is applicable since only cubes appear in it, there exists a $K_2 \in \mathbb{N}$, such that the second term is bounded from above by $\epsilon/2$ for all $k \geq K_2$. Thus, the left-hand side of Equation (5.142) converges to zero for $k, m \to \infty$.

Equation (5.142) provides the necessary inequality to continue with arguments of the proof of Theorem 1.11 in [71]. Starting from

$$|\beta_\ell^{r,s}(\mathcal{C}(X_{\xi_\omega}(C_k))) - \beta_\ell^{r,s}(\mathcal{C}(X_{\xi_\omega}(A_k)))| \leq \sum_{j=\ell}^{\ell+1} F_j(\xi, s; C_k \setminus A_k) , \qquad (5.143)$$

where again $F_j(\xi, r; A)$ is the number of $j$-simplices in $\check{C}_r(X_\xi(\mathbb{R}^n))$ with at least one vertex in $A$ (see the proof of Lemma 5.2.9), we have

$$\mathbb{E}[F_j(\xi, s; C_k \setminus A_k)] = O(\lambda_n(C_k \setminus A_k)) . \qquad (5.144)$$

Again using Equation (5.141), we obtain

$$\left| \frac{\psi(C_k)}{\lambda_n(A_k)} - \frac{\psi(A_k)}{\lambda_n(A_k)} \right| = O(\lambda_n(C_k \setminus A_k) \lambda_n(A_k)^{-1}) \to 0 \qquad \text{as } k \to \infty . \qquad (5.145)$$

Assembling Equations (5.142) and (5.145), we finally get

$$\left| \frac{\psi(A_k)}{\lambda_n(A_k)} - \frac{\psi(\Lambda_{L_m})}{L_m^n} \right| \leq \left| \frac{\psi(C_k)}{\lambda_n(A_k)} - \frac{\psi(\Lambda_{L_m})}{L_m^n} \right| + \left| \frac{\psi(C_k)}{\lambda_n(A_k)} - \frac{\psi(A_k)}{\lambda_n(A_k)} \right| \to 0 \qquad (5.146)$$

for $k, m \to \infty$. Therefore the desired inequality (Equation (5.133)) holds.

*Third step.* Using Equations (5.132) and (5.133), we find for sufficiently large $k, m$

$$\left| \frac{\psi(\Lambda_{L'_k})}{(L'_k)^n} - \frac{\psi(A_k)}{\lambda_n(A_k)} \right| \leq \left| \frac{\psi(\Lambda_{L'_k})}{(L'_k)^n} - \frac{\psi(\Lambda_{L_m})}{L_m^n} \right| + \left| \frac{\psi(\Lambda_{L_m})}{L_m^n} - \frac{\psi(A_k)}{\lambda_n(A_k)} \right| < 2\epsilon . \qquad (5.147)$$

Hence, Theorem 1.11 of [71] holds for any convex averaging sequence $\{A_k\}$ instead of $\{\Lambda_L\}$, that is, there exists a constant $\hat{\beta}_\ell^{r,s}$ such that

$$\frac{\psi(A_k)}{\lambda_n(A_k)} \to \hat{\beta}_\ell^{r,s} \quad \text{for } k \to \infty . \qquad (5.148)$$

The proof of Theorem 1.5 in [71] holds now equally in this more general case. Indeed, on $\Delta$ a unique Radon measure $\mathfrak{P}$ exists with the property

$$\frac{1}{\lambda_n(A_k)} \mathbb{E}[\rho_\omega(A_k)] \xrightarrow{v} \mathfrak{P} \quad \text{for } k \to \infty . \qquad (5.149)$$

$\square$

We now deliver the proof of the strong law of large numbers for persistent Betti numbers using general convex averaging sequences.

*Proof of Theorem 5.2.11.* The first statement follows directly from the proof of Theorem 5.2.10. For the second statement, we construct a tessellation $C_k$ for each of the $A_k$ as in the proof of Theorem 5.2.10. Then we get

$$\left| \frac{\beta_\ell^{r,s}(\mathcal{C}(X_k))}{\lambda_n(A_k)} - \frac{\psi(A_k)}{\lambda_n(A_k)} \right| \leq \left| \frac{\beta_\ell^{r,s}(\mathcal{C}(X_k))}{\lambda_n(A_k)} - \frac{\beta_\ell^{r,s}(\mathcal{C}(X_\xi(C_k)))}{\lambda_n(A_k)} \right|$$
$$+ \left| \frac{\beta_\ell^{r,s}(\mathcal{C}(X_\xi(C_k)))}{\lambda_n(A_k)} - \frac{\psi(C_k)}{\lambda_n(A_k)} \right| + \left| \frac{\psi(C_k)}{\lambda_n(A_k)} - \frac{\psi(A_k)}{\lambda_n(A_k)} \right| . \qquad (5.150)$$

We estimate the first term on the right-hand side via Equation (5.143) as follows,

$$\left| \frac{\beta_\ell^{r,s}(\mathcal{C}(X_k))}{\lambda_n(A_k)} - \frac{\beta_\ell^{r,s}(\mathcal{C}(X_\xi(C_k)))}{\lambda_n(A_k)} \right| \leq \sum_{j=\ell}^{\ell+1} \frac{F_j(\xi, s; C_k \setminus A_k)}{\lambda_n(A_k)} . \qquad (5.151)$$

By means of ergodicity and Equation (5.144) we obtain for sufficiently large $k$

$$F_j(\xi, s; C_k \setminus A_k) \to \mathbb{E}\left[ F_j(\xi, s; C_k \setminus A_k) \right] = O(\lambda_n(C_k \setminus A_k)) . \qquad (5.152)$$

Thus, the first term on the right-hand side of Equation (5.150) converges to zero for $k \to \infty$. The $C_k$ being made up from cubes which intersect only at mutual boundaries, the

subsequent second term converges to zero for $k \to \infty$ by means of ergodicity (see proof of [71, Theorem 1.11]). The third term converges to zero for $k \to \infty$ due to Equation (5.145).

$\square$

# Part II

# Dynamics of non-Abelian gauge theories and geometry
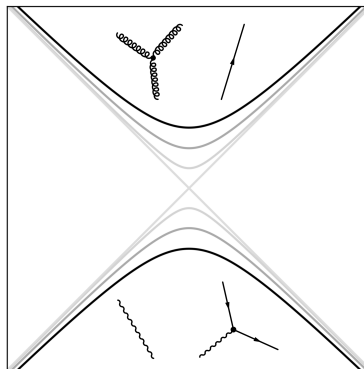
Non-Abelian gauge theories are a cornerstone of the Standard Model of particle physics. They feature confinement, which we explore with topological methods. In fact, one can derive much of the Standard Model structure from quantum fields on projective space-time geometries as we show.

# Chapter 6

# Confinement in non-Abelian lattice gauge theory via persistent homology

This chapter is based on the following article:

- Spitz, D., Urban, J. M., and Pawlowski, J. M., "Confinement in non-Abelian lattice gauge theory via persistent homology", *Phys. Rev. D*, vol. 107, no. 3, p. 034 506, 2023. arXiv: 2208.03955 [hep-lat].

Most of the present chapter is taken from this publication, for which I wrote major parts of the text, extensively contributed to the structure of the study and the interpretation of the results, and carried out the persistent homology and correlation function analyses.

## 6.1   Introduction

Many non-perturbative phenomena are driven by topological configurations or rather their density, or are accompanied by qualitative changes in the latter. This makes topology changes an ideal probe for investigating the mechanisms and signatures of these phenomena, ranging from (topologically driven) phase transitions to non-perturbative scalings as seen in the presence of topological tunneling effects in the anharmonic oscillator. A prominent and important example is QCD, whose confinement-deconfinement phase transition is accompanied by a rapid change in the topological density, and anomalous chiral symmetry breaking is closely related to instantons, which are stable, classical (minimal-action) configurations. Topological confinement mechanisms have been suggested, based on topological defects in QCD such as vortices and monopoles. While not being finite-action configurations in QCD, monopoles and vortices naturally emerge as constituents of instantons. For the discussion of finite temperature instantons (calorons), see e.g. [250–253]. More generically, instanton constituents of different topological types emerge on general compact manifolds [254–257], which may be seen as a simulation with a given topological density.

At finite temperature, instanton-dyons interact with holonomies (Polyakov loops) [251–253], and have been identified in pure lattice gauge theory and lattice QCD [258–262]. Ensembles of instanton-dyons can often readily explain confinement [263–268], even for theories with exceptional gauge groups exhibiting a trivial center such as $G(2)$ [269–271], yet consistently giving rise to center symmetry breaking for theories with non-trivial center. Local correlations exist between topological hotspots and values of the Polyakov

loop trace [272]. Moreover, instantons and instanton-dyons can be linked to spontaneous chiral symmetry breaking in QCD if sufficiently dense [273–275].

Evidently, phase transitions go hand in hand with a topology change in the vacuum manifold, and more generally that of equipotential hypersurfaces [276–279]. Persistent homology has been developed to detect topological structures in finite, noisy data [200], accompanied by profound mathematical works on their stability [68, 69, 242] and benign statistical behavior, see [71] and Chapter 5 of this dissertation. In light of topology changes of equipotential hypersurfaces in the realm of phase transitions, emergent topological structures have been searched for numerically via persistent homology in configuration space [72]. Since the scalability of this approach to larger systems is unclear, studies of a variety of condensed matter and spin systems have since been focusing on persistent homology as sensitive observables in their own right [73–77, 79, 280, 281]. Using a specifically tailored filtration constructed from plaquettes, center vortices have been probed in $SU(2)$ lattice gauge theory [80]. Effective QCD models have also been investigated [192, 193]. Further persistent homology applications in physics include non-thermal fixed points, see [6] and Chapter 4 of this dissertation, quantum entanglement [282], physical chemistry and amorphous materials [283, 284], the cosmic web [285–287], and non-Gaussianities in cosmic microwave background fluctuations [288, 289]. Quantum algorithms for the computation of persistent homology have also been developed [290]. Furthermore, topological neural network layers can be constructed using persistent homology [291, 292].

Typically, the study of classical field configurations in lattice gauge theories requires the application of cooling/smoothing techniques, as well as sophisticated gauge-fixing and -projection procedures [95]. To identify instanton-dyons on the lattice, overlap fermions may be used as probes [293]. In the present chapter we set out to study finite-temperature pure $SU(2)$ gauge theory on a four-dimensional Euclidean lattice via observables constructed from persistent homology. All of the investigated order parameters are gauge-invariant. In addition, our approach is not biased towards particular classical field configurations. The Hybrid/Hamiltonian Monte Carlo (HMC) algorithm [294] is employed to generate samples. To relate structures occurring in the full quantum theory to classical field configurations, a comparison with cooled configurations is provided. Using persistent homology, we investigate sub- and superlevel set cubical complex filtrations of different gauge-invariant local observables such as Polyakov loop traces, topological densities, Polyakov loop algebra element norms, as well as electric and magnetic field strengths. This allows for diverse insights into the (non-)local structures occurring at different couplings: topological densities form spatial lumps instead of string-like structures, approximately invariant under cooling in the confined phase and thus (near-)classical. Probabilistic predictions for the appearance of instantons and instanton-dyons are met by persistent homology quantifiers. Debye screening discriminates between spatial structures of electric and magnetic fields. The identification of the approximate critical coupling is facilitated by the simultaneous appearance of qualitative changes across persistent homology observables.

This chapter is organized as follows. We review relevant aspects of lattice gauge theory calculations as well as the Polyakov loop trace as the common confinement order

parameter in Section 6.2. Section 6.3 deals with the persistent homology of different Polyakov loop descriptors, and begins with a description of (filtered) cubical complexes and persistent homology. Results for the traced Polyakov loop filtration, the Polyakov loop topological density filtration, and the so-called angle-difference filtration of Polyakov loop algebra element norms are discussed. In Section 6.4, we investigate filtrations of traced electric and magnetic field strengths, as well as the topological density. Finally, we summarize in Section 6.5.

## 6.2   Order parameters from lattice calculations

We provide a brief description of our lattice setup in Section 6.2.1. In Section 6.2.2, we discuss standard order parameters for the confinement-deconfinement phase transition, based on the Polyakov loop.

### 6.2.1   Prerequisites

We consider a four-dimensional Euclidean lattice with $N_s^3 \times N_\tau$ sites and periodic boundary conditions in all directions. We denote the set of all lattice sites by $\Lambda$ and the spatial $N_s^3$ lattice given by the coordinates $(n_x, n_y, n_z, 0)$ by $\Lambda_s$. Throughout this work, we fix $N_s = 32$ and $N_\tau = 8$, but aim to investigate different and larger lattice geometries as well as conduct a detailed analysis of the $N_\tau$-dependence in the future.

The gauge degrees of freedom are described in terms of SU(2)-valued links denoted as $U_\mu(x)$. Under a local gauge transformation $V(x)$, links transform as $U_\mu(x) \mapsto V(x)U_\mu(x)V^\dagger(x + \hat{\mu})$. With $\beta$ the inverse coupling squared and the plaquettes $U_{\mu\nu}(x) = U_\mu(x)U_\nu(x + \hat{\mu})U_\mu^\dagger(x + \hat{\nu})U_\nu^\dagger(x)$, the Wilson gauge action reads

$$S[U] = \frac{\beta}{2} \sum_{x \in \Lambda} \sum_{\mu < \nu} \text{Tr}\left[1 - U_{\mu\nu}(x)\right]. \tag{6.1}$$

From lattice renormalization group arguments, close to the critical point a linear relation exists between $\beta$ and the temperature [295]. We evaluate observables at 16 evenly spaced points ranging from $\beta = 1.5$ to $\beta = 3.0$. Throughout this paper, results are given in lattice units. Field configurations $U_\mu(x)$ distributed according to $\exp(-S[U])$ are generated and subsequently further decorrelated using the standard HMC algorithm. Details on the sampling procedure are described in Appendix Section 6.A.1. All expectation values given in this work are computed as averages of 100 samples for each $\beta$. No gauge-fixing is applied during sampling.

In order to understand the occurring structures in relation to ultraviolet fluctuations, we repeatedly compare with results from cooled samples. These are obtained by applying the standard Wilson flow [296], which removes fluctuations by numerically solving a gradient flow equation that minimizes the Wilson action defined in Equation (6.1), thereby smoothing the configurations. Further details of our cooling setup can be found in Appendix Section 6.A.2.

### 6.2.2   Confinement in Polyakov loops and their effective potential

Winding around the periodic time direction, the Polyakov loop

$$\mathcal{P}(\mathbf{x}) = \mathscr{P} \prod_{\tau=1}^{N_\tau} U_4(\mathbf{x}, \tau), \tag{6.2}$$

where $\mathscr{P}$ indicates path ordering, provides a sensitive order parameter for confinement. Related to the free energy of static test quarks interacting via gluons, of particular interest is its trace [297],

$$P(\mathbf{x}) = \frac{1}{2} \text{Tr}\, \mathcal{P}(\mathbf{x}), \tag{6.3}$$

as well as the expectation value of its absolute volume average,

$$L = \frac{1}{N_s^3} \langle | \sum_{\mathbf{x} \in \Lambda_s} P(\mathbf{x}) | \rangle. \tag{6.4}$$

In order to account for the restoration of center symmetry for Polyakov loop observables in the statistical limit, for their evaluation we augment our Monte Carlo ensembles by adding duplicate samples with $P(\mathbf{x}) \mapsto -P(\mathbf{x})$.

In Figure 6.2.1(a) we display two-dimensional single-sample slices of $P(\mathbf{x})$ for three different values of $\beta$, of configurations with and without cooling applied. Throughout $\beta$-values, uncooled samples show many fluctuations on small length scales. For $\beta = 2.5$ and $\beta = 3.0$, a bias towards non-zero $P(\mathbf{x})$-values can be recognized. A comparison with cooled variants shows that for $\beta = 1.5$, barely any structural changes can be observed. For $\beta = 2.5$ and $\beta = 3.0$, large domains of like-signed $P(\mathbf{x})$-values are visible after cooling.

Under a center transformation, $z \in Z(\text{SU}(2)) = \{\pm 1\}$, the traced Polyakov loop transforms non-trivially as $P(\mathbf{x}) \mapsto z P(\mathbf{x})$. Unbroken center symmetry requires $L = 0$. If center symmetry is spontaneously broken, $L > 0$ is possible. This effect shows up in $L(\beta)$, see Figure 6.2.1(b): $L(\beta) \approx 0$ below $\beta \simeq 2.3$ in our calculations, while for $\beta \gtrsim 2.3$ we find $L(\beta) > 0$. This signals spontaneously broken center symmetry above $\beta \simeq 2.3$. We identify $\beta_c \simeq 2.3$ as the (approximate) critical inverse coupling squared,[1] similar to previous works on critical properties of $\text{SU}(2)$ lattice gauge theory on lattices of comparable size to ours [295, 298]. This explains the structures visible in Figure 6.2.1(a): above $\beta_c$ spontaneous symmetry breaking is responsible for the formation of like-signed $P(\mathbf{x})$-domains, which in particular show up in cooled configurations.

All this can be attributed to a second-order phase transition manifesting in the effective Polyakov loop potential $V(L)$. We schematically display $V(L)$ in Figure 6.2.1(c), where contributions from a leading-order large-coupling expansion and contributions from the $\text{SU}(2)$ Haar measure (Vandermonde determinant) are taken into account [297]. Linearly mapping inverse couplings squared to temperatures, $V(L)$ has a global minimum at $L = 0$ below $\beta_c$. $L = 0$ corresponds to an infinite energy cost to excite a single static test quark. It thus becomes impossible to excite states which transform non-trivially under

---

[1]Note that the value of $\beta_c$ reported in the literature based on the computation of the Binder cumulant is slightly larger. A precise determination of $\beta_c$ is not the aim of this work, and we merely use the point where $L(\beta)$ becomes non-zero as a rough approximation.
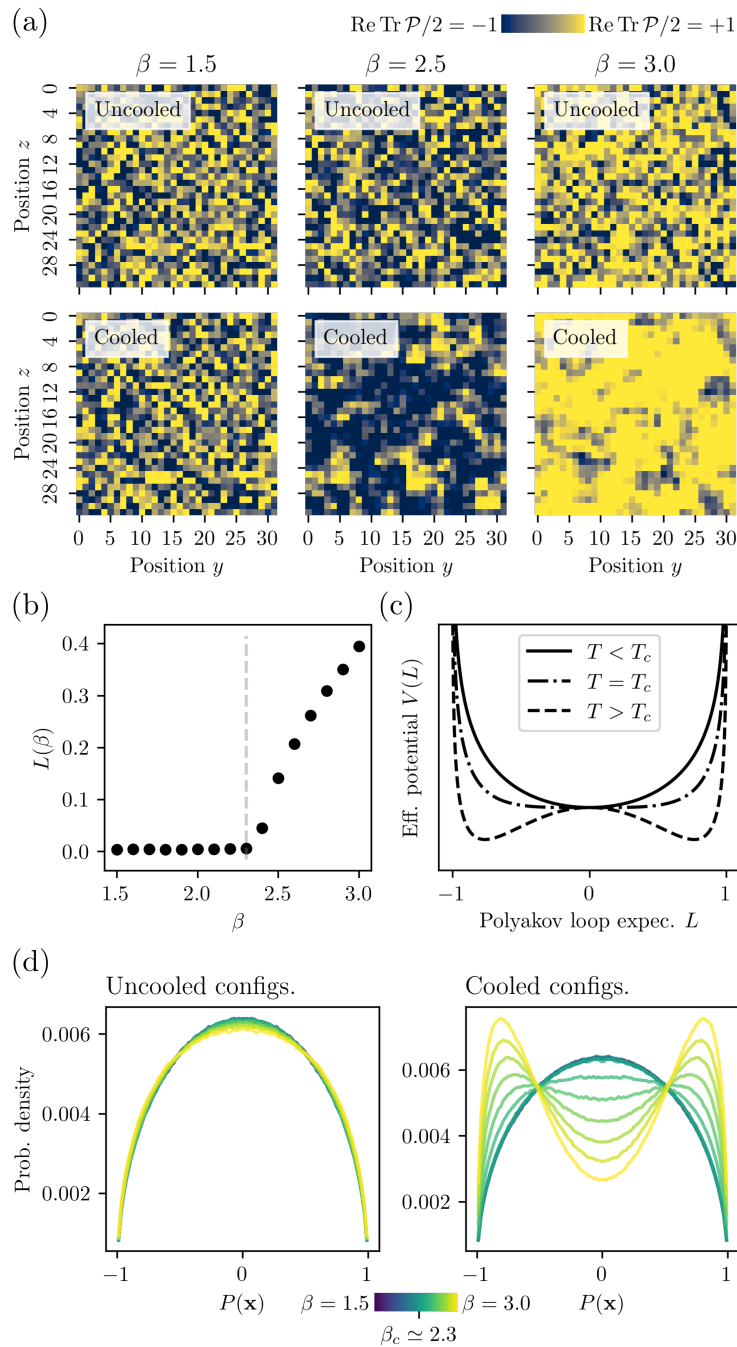
**FIGURE 6.2.1:** (a): Slices at constant $\mathbf{x}^1$ of the Polyakov loop $P(\mathbf{x})$ without cooling applied (top row) and with cooling applied (bottom row), at different $\beta$. (b): Absolute value of the volume-averaged Polyakov loop expectation value versus $\beta$ with $\beta_c \simeq 2.3$ indicated (grey, dashed line). Errors are smaller than marker size. (c): Schematic, effective Polyakov loop potential in the confined phase (solid line), at the phase transition (dashed-dotted line) and in the deconfined phase (dashed line), derived from leading-order contributions of a strong coupling expansion and Haar measure (Vandermonde determinant) contributions [297]. (d): Probability densities of local Polyakov loop $P(\mathbf{x})$ values, for uncooled (left) and cooled configurations (right). Data is given in lattice units.

gauge transformations, indicating confinement. At $\beta_c$ the minimum becomes degenerate, leading for $\beta > \beta_c$ to two global minima at $L \neq 0$. Spatially, this is reflected by domain formation [299]. For uncooled and cooled configurations, the probability densities for local $P(\mathbf{x})$-values displayed in Figure 6.2.1(d) agree with this phenomenology. Including quarks, similar probability densities have been computed in [300]; the phase transition smears out to a crossover at finite baryon densities.

Correlations of multiple traced Polyakov loops are related to the free energy of static multi-quark configurations and similarly make up interpretable confinement order parameters [297]. In Section 6.B.1, we discuss two-point function results for Polyakov loop correlations computed from the lattice data.

Non-trivial topology is related to non-trivial holonomies in the Polyakov loop. For $|\mathbf{x}| \to \infty$ the Polyakov loop is diagonalizable with

$$\lim_{|\mathbf{x}|\to\infty} \mathcal{P}(\mathbf{x}) = \begin{pmatrix} \exp(2\pi i \mu_1) & 0 \\ 0 & \exp(2\pi i \mu_2) \end{pmatrix}, \tag{6.5}$$

with $\mu_1 \leq \mu_2$ and $\mu_1 + \mu_2 = 0$. The holonomies $\mu_1, \mu_2$ are related to the masses $8\pi^2(\mu_2 - \mu_1)$ and $8\pi^2(1 + \mu_1 - \mu_2)$ of SU(2) instanton-dyons, two of which form a Kraan-van Baal-Lee-Lu (KvBLL) caloron [251–253]. Instanton-dyons as well as calorons are (anti-)self-dual solutions to the classical Yang-Mills equations: $F_{\mu\nu}(x) = \pm \tilde{F}_{\mu\nu}(x)$, i.e., $\mathbf{E}(x) = \pm \mathbf{B}(x)$. Holonomy potentials computed from instanton-dyon ensembles can approximately account for the Polyakov loop effective potential $V(L)$ [268, 270].

Without cooling, calorons and instanton-dyons are specific field configurations difficult to detect in lattice data. However, the cooling process also unavoidably removes relevant physical information. This prompts the question whether persistent homology is able to detect meaningful signatures of the underlying topology in the raw data.

## 6.3   Geometric structures in Polyakov loops from persistent homology

Persistent homology provides a means to algorithmically deduce topological structures from potentially noisy numerical data, including with persistence a measure of their dominance. In this section, we utilize the persistent homology of different types of filtrations constructed from Polyakov loops and related algebra fields in order to unravel relevant (de-)confinement features. The latter include the formation of spatial lumps of topological density instead of extended, string-like configurations, accompanied by probabilistic evidence for the occurance of calorons and instanton-dyons. We stress that all of the involved constructions are gauge-invariant without a priori assumptions on the type of excitations under study.

We begin in Section 6.3.1 with an intuitive introduction to cubical complexes and persistent homology. In Section 6.3.2 we discuss persistent homology results of the sublevel set filtration of topological densities computed from Polyakov loops, first introducing

the latter. Section 6.3.3 is devoted to signals of the confinement phase transition in the so-called angle difference filtration applied to Polyakov loop algebra element norms.

### 6.3.1 A primer on persistent homology via sublevel sets of the traced Polyakov loop

We introduce concepts of persistent homology with the example of the traced Polyakov loop field $P(\mathbf{x}) = (1/2)\mathrm{Tr}\,\mathcal{P}(\mathbf{x})$ and its sublevel set filtration of cubical complexes.[2] Technical details of mathematical constructions have been given in Appendix 4.A.

The *sublevel sets* $M_P(\nu)$ of $P(\mathbf{x})$ displayed in Figure 6.2.1(a) are subsets of the spatial lattice,

$$M_P(\nu) := P^{-1}(-\infty, \nu] = \{\mathbf{x} \in \Lambda_s \,|\, P(\mathbf{x}) \leq \nu\}. \tag{6.6}$$

Superlevel sets are defined as

$$N_P(\nu) := P^{-1}[\nu, \infty) = \{\mathbf{x} \in \Lambda_s \,|\, P(\mathbf{x}) \geq \nu\}. \tag{6.7}$$

The lattice Polyakov loop $P(\mathbf{x})$ approximates the continuum Polyakov loop in a cube[3] $\mathbf{x} + [-1/2, 1/2]^3$. The (point set) topology of $M_P(\nu)$ and $N_P(\nu)$ merely amounting to point counting, we seek to construct spaces reflecting the cubical structures while still corresponding to $M_P(\nu)$, $N_P(\nu)$.

#### Filtered cubical complexes

Particularly suitable for the algorithmic computation of topological descriptors of pixelized data are cubical complexes. Let $\mathfrak{C}$ be the full cubical complex, consisting of one cube $\mathbf{x} + [-1/2, 1/2]^3$ of top dimension (here, three) for each spatial lattice point $\mathbf{x}$. Every 3-cube comes with all its faces, edges and vertices. In fact, it is a defining property of cubical complexes to be closed under taking boundaries of any of its top- and lower-dimensional cubes. The boundary of a 3-cube is the union of all its six faces, the boundary of a 2-cube (face) is the union of its four boundary edges, the boundary of a 1-cube (edge) consists of its two endpoints, and the boundary of a 0-cube (point) is empty. The boundary operator $\partial$ provides the map from a cube to its boundary.

How can we equip the full cubical complex $\mathfrak{C}$ with the information contained in $P$? We inductively construct a suitable map $\tilde{P} : \mathfrak{C} \to \mathbb{R}$. While in principle we constructed $\tilde{P}$ already in Appendix 4.D, we repeat the construction here for the Polyakov loop traces at hand, also for better readability. Any 3-cube $C \in \mathfrak{C}$ has a unique lattice point $\mathbf{x}$ at its center. We set $\tilde{P}(C) := P(\mathbf{x})$. Any 2-cube $D \in \mathfrak{C}$ is contained in the boundary of two 3-cubes. For all 2-cubes $D \in \mathfrak{C}$ we set

$$\tilde{P}(D) := \min\{\tilde{P}(C) \,|\, D \in \partial C, C \in \mathfrak{C}\,\text{3-cube}\}. \tag{6.8}$$

---

[2]The values of $P(\mathbf{x})$ scattering evenly around zero, we expect similar results for superlevel instead of sublevel sets.

[3]To clarify notations: $\mathbf{x} + [-1/2, 1/2]^3 = \{\mathbf{y} \in \mathbb{R}^3 \,|\, \mathbf{y} - \mathbf{x} \in [-1/2, 1/2]^3\}$.

Similarly, any 1-cube is contained in the boundaries of four 2-cubes, any 0-cube is contained in the boundaries of six 1-cubes. Equation (6.8) is applied to all 1-cubes instead of 2-cubes with values induced from 2-cubes, and finally to all 0-cubes with values induced from 1-cubes, until $\tilde{P}$ is defined on all cubes of all dimensions in $\mathfrak{C}$. Sublevel sets of $\tilde{P}$,

$$\mathfrak{C}_P(\nu) := \tilde{P}^{-1}(-\infty, \nu] = \{C \in \mathfrak{C} \,|\, \tilde{P}(C) \leq \nu\}, \tag{6.9}$$

are closed under taking boundaries, constituting cubical complexes which correspond to pixelizations of the lattice sublevel sets $M_P(\nu)$. We define superlevel set cubical complexes as

$$\mathfrak{D}_P(\nu) := \mathfrak{C}_{-P}(-\nu), \tag{6.10}$$

corresponding to the lattice superlevel sets $N_P(\nu)$. All these constructions work analogously in higher dimensions.

The sublevel set cubical complexes $\mathfrak{C}_P(\nu)$ form a filtration of cubical complexes,

$$\mathfrak{C}_P(\nu) \subseteq \mathfrak{C}_P(\mu), \text{ whenever } \nu \leq \mu. \tag{6.11}$$

With its construction, this filtration is called the lower-star filtration. Analogously, a filtration of superlevel set cubical complexes occurs,

$$\mathfrak{D}_P(\nu) \supseteq \mathfrak{D}_P(\mu), \text{ whenever } \nu \leq \mu. \tag{6.12}$$

The lattice $\Lambda_s$ consisting of finitely many points, these filtrations consist of only finitely many distinct complexes.

**Persistent homology: holes in complexes**

Generically, the cubical complexes $\mathfrak{C}_P(\nu)$ do not contain a cube for every spatial lattice point. Holes appear, described by homology groups. Their elements, homology classes, are constructed comparably to homotopy classes and capture similar topological information [201], but are algebraically much better accessible. In particular, homology classes are also homotopy-invariant, i.e., continuous deformations of holes leave homology classes invariant. For an impression of low-dimensional homology classes, we refer to Figure 6.3.1(a). Connected components are described by dimension zero homology classes. Planar-like holes, circumscribed by a circle which cannot be continuously deformed into a point within the cubical complex, belong to the dimension one homology group. The dimension two homology group captures enclosed volumes, described by a 2-sphere. Higher-dimensional homology classes correspond to analogous higher-dimensional holes.

As in cubical complex filtrations the filtration parameter $\nu$ is swept through, homology classes may be born and die again. Persistent homology captures this. In Figure 6.3.1(b) we indicate two scenarios for superlevel sets of exemplary functions on a surface. The left function shows three distinct peaks. For $\nu$ larger than the maximum value of the highest peak the cubical complex is empty with trivial homology. As $\nu$ is lowered to exactly the latter value (indicated in Figure 6.3.1(b), left panel, by the green plane), a zero-dimensional
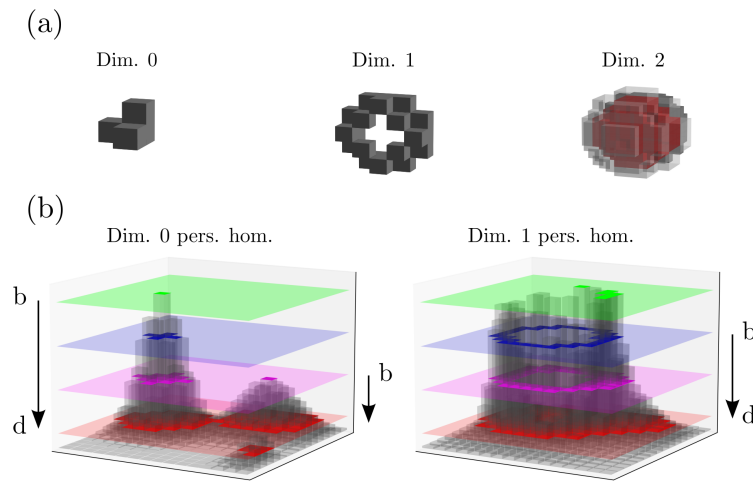
**FIGURE 6.3.1:** (a): Cubical complexes giving rise to homology classes of dimensions zero to two from left to right. The enclosed volume in dimension two is indicated in red. (b): Schematically, dimension zero and dimension one persistent homology classes of superlevel sets of a function with two-dimensional domain. Exemplary superlevel set cubical complexes are indicated by different colors; birth and death of corresponding persistent homology classes are indicated by $b$ and $d$, respectively.

homology class is born, with birth $b = \nu$. Lowering $\nu$ further (blue plane), the single 2-cube turns into an accumulation of 2-cubes, nothing changing in homology. At the $\nu$-value indicated by the pink plane, a second zero-dimensional homology class is born with the second peak showing up in the complex. Again, for the first homology class nothing changes. At the $\nu$-value indicated by the red plane, the two accumulations of 2-cubes merge into one. The first homology class dies with $d = \nu$ its death. We call $p = d - b$ its persistence. The second homology class dies later upon merging with the third peak (not indicated). Turning to the right function in Figure 6.3.1(b), for $\nu$-values larger than the one indicated by the blue plane, different dimension-zero homology classes are born and die upon merging with each other. For $\nu$ corresponding to the blue plane, a circular structure surrounding a hole appears in the corresponding complex: a one-dimensional homology class is born. For $\nu$ between the pink and red planes, the hole disappears, getting fully filled by 2-cubes. The homology class dies.

In higher dimensions, dimension zero homology classes can still be imagined as independent connected components. Dimension one homology classes correspond to structures such as approximate circles or empty tori surrounded by cubes. Dimension two homology classes are empty 3-volumes.

The $\ell$-th persistence diagram $\mathrm{Dgm}_\ell(\mathfrak{C}_P)$ consists of birth-death pairs $(b, d)$, one for each independent homology class of dimension $\ell$ in a given filtration such as $\mathfrak{C}_P$. Betti numbers $\beta_\ell(\nu)$ specify the number of independent $\ell$-dimensional homology classes in $\mathfrak{C}_P(\nu)$. They can be obtained from $\mathrm{Dgm}_\ell(\mathfrak{C}_P)$ as

$$\beta_\ell(\nu) = \#\{(b, d) \in \mathrm{Dgm}_\ell(\mathfrak{C}_P) \,|\, b \leq \nu < d\}. \tag{6.13}$$
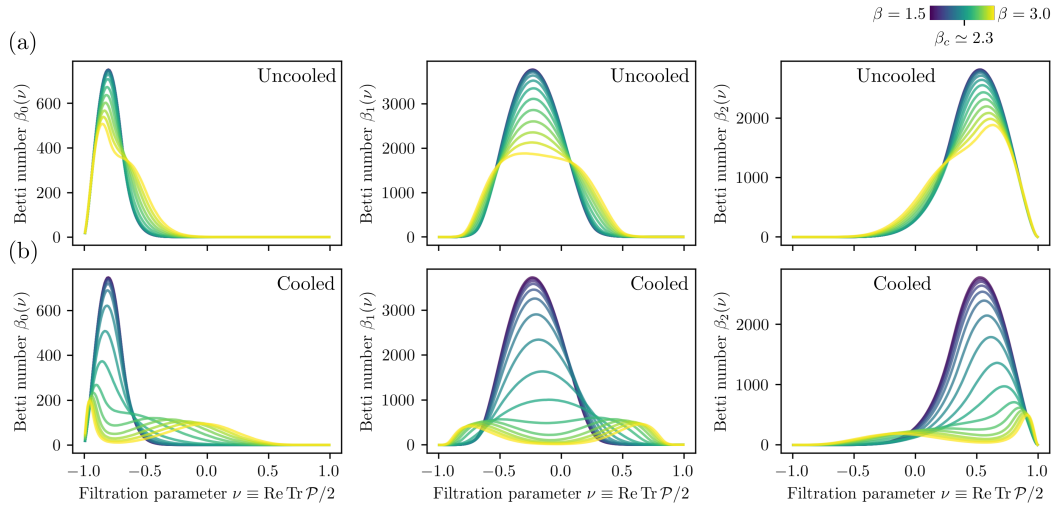
**FIGURE 6.3.2:** Betti number distributions of dimensions zero to two for the sublevel set filtration of $P(\mathbf{x}) = \operatorname{Tr} \mathcal{P}(\mathbf{x})/2$ for (a) uncooled and (b) cooled configurations.

From $\operatorname{Dgm}_\ell(\mathfrak{C}_P)$ we may also obtain statistics such as the number of independent homology classes with a given birth $b$, $\mathcal{B}_\ell(b)$, or the number of independent homology classes with a given persistence $p$, $\mathcal{P}_\ell(p)$. Note that homology classes can have infinite persistence. For instance, the full cubical complex $\mathfrak{C}$ is one connected component. Also, periodic boundaries turn the full complex $\mathfrak{C}$ into a 3-torus which has three independent dimension one and three independent dimension two homology classes, and even a one-dimensional homology group in dimension three.

Statistically evaluating expectation values, throughout this work persistent homology quantifiers are computed from individual samples and subsequently averaged. The investigated persistent homology descriptors can be consistently defined in a statistical setting with limit theorems for large-volume asymptotics existing, see [71] and Chapter 5 of this dissertation. Well-defined thermodynamic limits actually require the latter.

Importantly, persistence diagrams are stable against small perturbations of the input function $P$ [68, 69, 242], which facilitates the numerics. We again compute persistent homology of cubical complexes with periodic boundary conditions using the Python and C++ interfaces of the versatile computational topology library GUDHI [203].

**Traced Polyakov loop results**

Numerical Betti number distributions of different dimensions of the sublevel set filtration $\mathfrak{C}_P(\nu)$ are displayed in Figure 6.3.2 for configurations without and with cooling applied, for all inverse couplings squared from $\beta = 1.5$ to $\beta = 3.0$. All Betti number distributions show a distinct peak, whose position consistently shifts to larger filtration parameters $\nu$ with increasing homology class dimensions. This is characteristic to sublevel set filtrations: lowest in the filtration, connected components form in order to merge into extended circular structures at larger filtration parameters, similar to Figure 6.3.1(b). Typically, enclosed voids form out of pitted, hollow networks of cubes with many dimension one

homology classes dying in order to form a dimension two homology class. This behavior usually continues to higher dimensions.

Without cooling, we observe from Figure 6.3.2(a) that Betti number distributions approximately lay on top of each other for $\beta \lesssim \beta_c \simeq 2.3$. For $\beta \gtrsim \beta_c$ and throughout dimensions, peaks diminish in height with $\beta$ and broaden. In particular, in dimensions zero and two, an additional bump occurs on the peak side pointing towards filtration parameter zero. As seen in Figure 6.3.2(b), cooling enhances these effects. The peaks already decrease in height for $\beta > 1.8$, with moderately constant peak positions up to $\beta \simeq 2.2$. For $\beta \gtrsim 2.3$, the peak splits up in two. Qualitatively, dimension zero and two Betti number distributions seem to be mirrored at $\nu = 0$.

These observations can be understood from the effective Polyakov loop potential $V(L)$, see Figure 6.2.1(c). Below $\beta_c \simeq 2.3$, the $\mathbb{Z}_2$ center symmetry of $L$ is unbroken: the distribution of local $P(\mathbf{x})$-values is symmetric around zero and approximately constant, see Figure 6.2.1(d). The constancy of uncooled $\beta_\ell(\nu)$ for $\beta \lesssim \beta_c$ is a manifestation of this. Also, the qualitative mirroring between dimensions zero and two reflects this: in sublevel set filtrations, a minimum shows up as a dimension zero homology class. A maximum shows up as a dimension two homology class. Both are expected to occur comparably likely if the $\mathbb{Z}_2$ symmetry is unbroken.

Above $\beta_c$ the center symmetry is spontaneously broken, see Figure 6.2.1(a): individual samples acquire non-zero volume averages $L$. Center symmetry is restored only in the statistical limit. In Betti number distributions, the appearance of additional bumps without cooling or two peaks with cooling resembles the spontaneous symmetry breaking behavior and statistical restoration of center symmetry. The decrease in the peak's heights can be understood from a homogenization of $P(\mathbf{x})$ above $\beta_c$: structures become fewer. For cooled configurations, effects are enhanced due to less ultraviolet fluctuations.

Domains of like-signed Polyakov loops forming, the behavior is consistent with a percolation interpretation of deconfinement [299]. Beyond that, can we identify topological excitations?

### 6.3.2 Sublevel sets of topological densities from Polyakov loops

Topological excitations such as calorons are characterized by non-trivial topological densities. However, in typical Monte Carlo samples, topological densities contain strong signatures of ultraviolet fluctuations and of the lattice discretization. Effectively averaging temporal fluctuations, Polyakov loops reveal less such fluctuations. We consider in this section the sublevel set filtration of the Polyakov loop topological density on the lattice,

$$q_{\mathcal{P}}(\mathbf{x}) := \frac{1}{24\pi^2}\varepsilon_{ijk}\mathrm{Tr}\left[(\mathcal{P}^{-1}(\mathbf{x})\partial_i\mathcal{P}(\mathbf{x}))(\mathcal{P}^{-1}(\mathbf{x})\partial_j\mathcal{P}(\mathbf{x}))(\mathcal{P}^{-1}(\mathbf{x})\partial_k\mathcal{P}(\mathbf{x}))\right]. \qquad (6.14)$$

For comparison, we discuss the superlevel set filtration of the usual topological density $q \sim \mathrm{Tr}\,\mathbf{E}\cdot\mathbf{B}$ in Section 6.4.2.

Indeed, the nomenclature is justified. In a theory with continuous Euclidean space-time and periodic boundary conditions, i.e., with space-time the 4-torus $T^4$, we can rewrite

the winding number

$$Q_{\text{top}} = \frac{1}{32\pi^2} \int_{T^4} \varepsilon_{\alpha\beta\mu\nu} \text{Tr}\, F_{\alpha\beta} F_{\mu\nu} \tag{6.15}$$

in terms of the Polyakov loop $\mathcal{P} : T^3 \to \text{SU}(2)$, based on [301]. We take the 4-torus $T^4$ to have extents $N_x, N_y, N_z, N_\tau$, analogously to the lattice of interest. Starting from gauge potentials $A_\mu$ on the 4-torus $T^4$, transition functions defined on the entire $\mathbb{R}^4$ are defined via the periodicity properties of $T^4$, which manifests for all $x \in T^4$ and $\mu = 1, \ldots, 4$ in

$$A_\mu(x + N_\nu) = U_\nu^{-1}(x) A_\mu(x) U_\nu(x) + \mathrm{i} U_\nu^{-1}(x) \partial_\mu U_\nu(x) . \tag{6.16}$$

The transition functions fulfil the cocycle condition

$$U_\mu(x) U_\nu(x + N_\mu) = U_\nu(x) U_\mu(x + N_\nu) \tag{6.17}$$

and transform under a gauge transformation $V(x)$ as

$$U_\mu^V(x) = V^{-1}(x) U_\mu(x) V(x + N_\mu) . \tag{6.18}$$

Suppose the transition functions satisfy $U_i(\mathbf{x}, \tau = 0) = 1$ for all $i = 1, 2, 3$ and $U_4 = 1$. Then, skipping derivation steps detailed in [301], we find

$$Q_{\text{top}} = \frac{1}{24\pi^2} \int_{B_4} \varepsilon_{0ijk} \text{Tr}\left[ (\mathcal{P}^{-1}\partial_i\mathcal{P})(\mathcal{P}^{-1}\partial_j\mathcal{P})(\mathcal{P}^{-1}\partial_k\mathcal{P}) \right] = \int_{B_4} q_{\mathcal{P}} , \tag{6.19}$$

where $B_4 = \{(\mathbf{x}, \tau) \in T^4 \,|\, \tau = 0\}$. This establishes $q_{\mathcal{P}}(\mathbf{x})$ as a topological density variant.

In Figure 6.3.3 we display birth and persistence distributions of the sublevel set filtration of $q_{\mathcal{P}}$ for uncooled configurations. Cooling barely has any effect on the shown homological descriptors below $\beta_c$ and enhances the occurring trends above $\beta_c$, see Section 6.C.1. We deduce that topologically non-trivial excitations are mostly due to (near-)classical configurations. Similar to the traced Polyakov loop, the birth distributions in Figure 6.3.3 reveal a single distinct peak for each $\beta$. Birth distributions are constant for $\beta \lesssim \beta_c$. Above $\beta_c$ distributions broaden for increasing $\beta$. Dimension zero birth distributions have support below birth $b = 0$, dimension one around birth $b \approx 0$, and dimension two with a bias towards birth $b > 0$.

The dimension zero and dimension two persistence distributions of Figure 6.3.3(b) are almost identical in shape. For most $\beta$-values, these distributions follow nearly exponential behavior, approximately constant for $\beta \lesssim \beta_c$. An exponential fit of the $\beta = 1.5$ dimension two persistence distribution reveals $\mathcal{P}_2(p) \sim \exp(-sp)$ with $s = 26.51 \pm 0.04$. The dimension one persistence distribution does not show comparable behavior for persistences $p \gtrsim 0.02$ and quickly declines. Up to $p \approx 0.02$ it looks similar to dimensions zero and two.

We may interpret the similarity of persistence distributions in dimensions zero and two analogously to the qualitative similarity of Betti numbers of traced Polyakov loops in Figure 6.3.2(b): $q_{\mathcal{P}}$ being statistically symmetric around zero, minima and maxima occur comparably likely. While the former show up as dimension zero homology classes in the $q_{\mathcal{P}}$-sublevel set filtration, the latter give rise to dimension two homology classes.
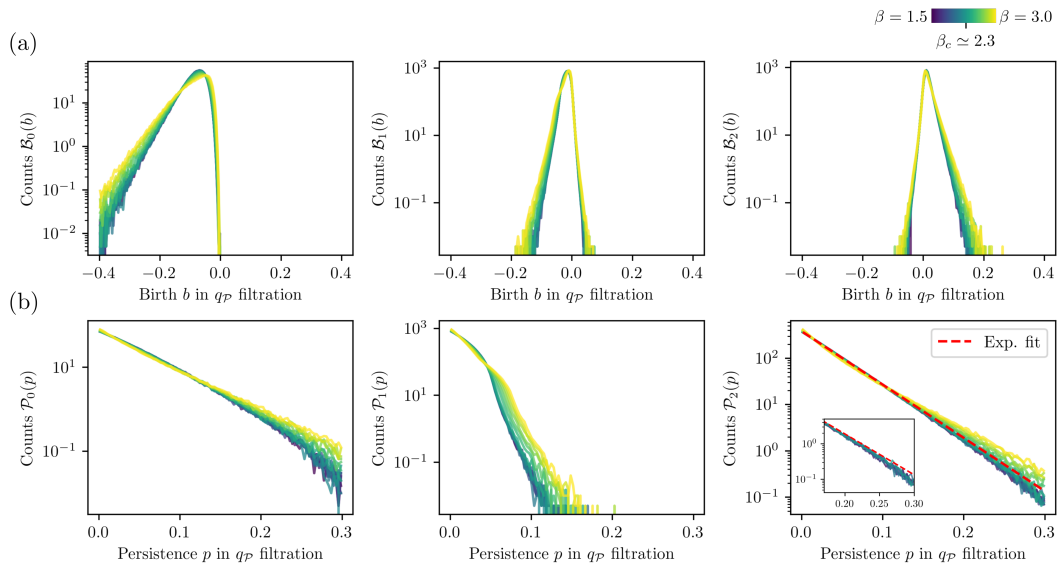
**FIGURE 6.3.3:** Homological quantifiers of the sublevel set filtration of the Polyakov loop topological density $q_{\mathcal{P}}(\mathbf{x})$. (a): Birth distributions for dimensions zero to two. (b): Persistence distributions for dimensions zero to two. The exponential fit of the $\beta = 1.5$ persistence distribution reveals $\mathcal{P}_2(p) \sim \exp(-sp)$ with $s = 26.51 \pm 0.04$. Inset shows large-persistence, dimension two persistence distributions for inverse couplings up to $\beta_c$. No cooling has been applied in all data shown in this Figure, though cooling leaves the data shown approximately invariant for $\beta \lesssim \beta_c \simeq 2.3$. Results are given in lattice units.

$q_{\mathcal{P}}(\mathbf{x})$ is governed by local accumulations of non-zero topological density. Dimension one homology classes originate primarily from (thermal) noise, explaining the small-persistence support of $\mathcal{P}_1(p)$.

For well-separated peaks, the persistence $p$ of dimension zero and dimension two homology classes provides a quantifier of their dominance. In [302] it has been argued that for an instanton dyon-antidyon pair [of type $M\bar{M}$ or $L\bar{L}$ in SU(2)] at large separation $r$, the due to time-independence effectively three-dimensional action $S_3$,

$$ S = \frac{1}{g^2} \int_0^{1/T} d\tau \, S_3 \,, \tag{6.20} $$

behaves as

$$ S_3 = 8\pi v + (m_1 m_2 - e_1 e_2) \frac{4\pi}{r} \,, \tag{6.21} $$

with dyon magnetic charges $m_1$, $m_2$ and electric charges $e_1$, $e_2$. The holonomy parameter $v$ originates from $A_4^a(x \to \infty) \to v\hat{r}_a$ for a given $\mathfrak{su}(2)$ direction vector $\hat{r}_a$ in the instanton-dyon parametrization used [302]. If we take $T = 1/g^2$, then for time-independent configurations $S_3 = S$. For self-dual excitations, $S$ further equates to $Q_{\text{top}} = \int_{\mathbf{x}} q_{\mathcal{P}}(\mathbf{x})$. One is tempted to observe that, at leading order in $1/r$, $S_3/v \simeq 8\pi \simeq 25.1$ is close to the fitted value of $s \simeq 26.5$ for the dimension two persistence distribution in the confining phase. Effects of the lattice discretization, thermal noise, contributions from configurations with more than two dyons,[4] and in general $g^2 T \neq 1$ are expected. Nonetheless, we find that

---

[4]For in total $n$ instanton-(anti-)dyons it is expected that the $8\pi v$ contribution is to be replaced by $4\pi n v$ [270].
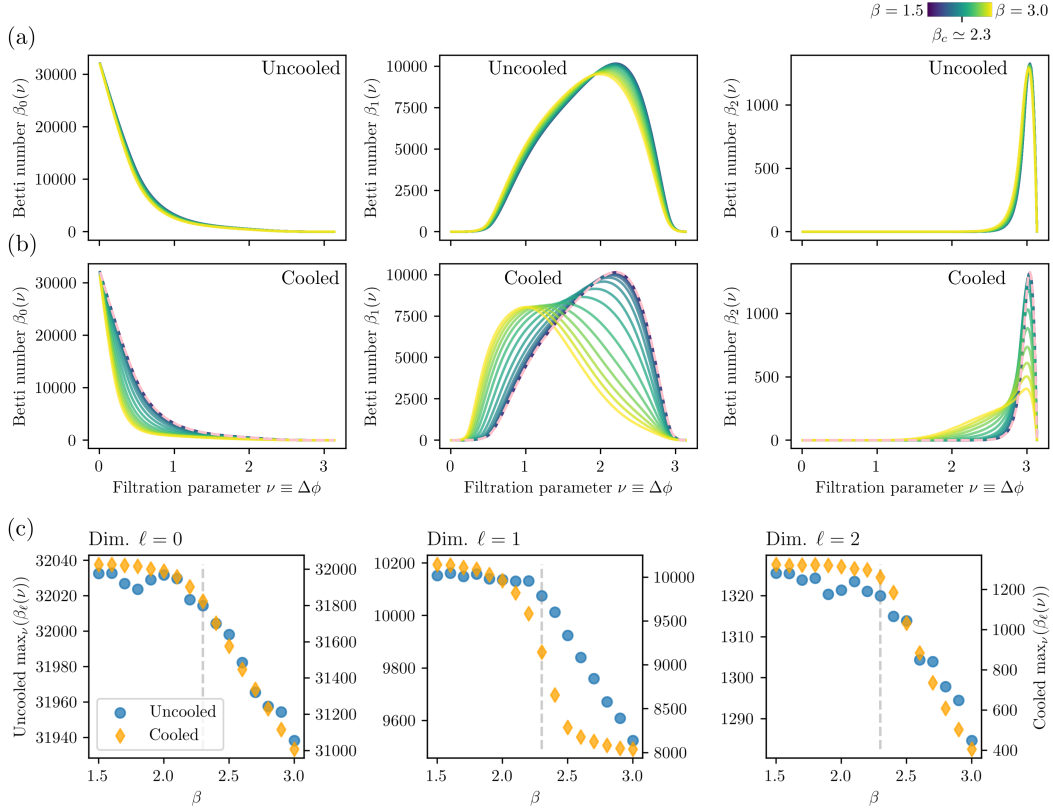
**FIGURE 6.3.4:** Homological quantifiers of the angle difference filtration constructed from $\phi(\mathbf{x}) = \arg(\operatorname{Tr}\mathcal{P}(\mathbf{x})/2)$. (a): Betti number distributions of uncooled configurations for dimensions zero to two. (b): Betti number distributions of cooled configurations for dimensions zero to two, the pink dashed line indicating the uncooled Betti number distribution for $\beta = 1.5$. (c) Maxima of Betti number distributions of dimensions zero to two versus $\beta$ for uncooled (left axes) and cooled configurations (right axes).

in the confining phase persistence distributions of $q_\mathcal{P}$ resemble the exponential behavior of the (semi-)classical instanton-dyon occurrence probability $\sim \exp(-S)$. The behavior of $\mathcal{P}_\ell(p)$ above $\beta_c$ shows growing deviations from this. Other topological excitations such as domain walls can show up in $q_\mathcal{P}$ configurations above $\beta_c$ due to spontaneous center symmetry breaking. It is suggestive that growing persistences above $\beta_c$ are at least partially triggered by these topological structures.

### 6.3.3 Angle-difference filtration of local Polyakov holonomies

The $SU(2)$-valued Polyakov loop can be written in terms of an algebra field as

$$\mathcal{P}(\mathbf{x}) = \exp(\mathrm{i}\phi^a(\mathbf{x})T^a) , \tag{6.22}$$

with $T^a = \sigma^a/2$ the Hermitian $\mathfrak{su}(2)$ generators given in terms of the Pauli matrices $\sigma^a$. A $2\pi$-periodic scalar field can be defined as half the norm of the Polyakov loop Lie algebra components,

$$\phi(\mathbf{x}) = \frac{1}{2}\sqrt{(\phi^1(\mathbf{x}))^2 + (\phi^2(\mathbf{x}))^2 + (\phi^3(\mathbf{x}))^2} . \tag{6.23}$$
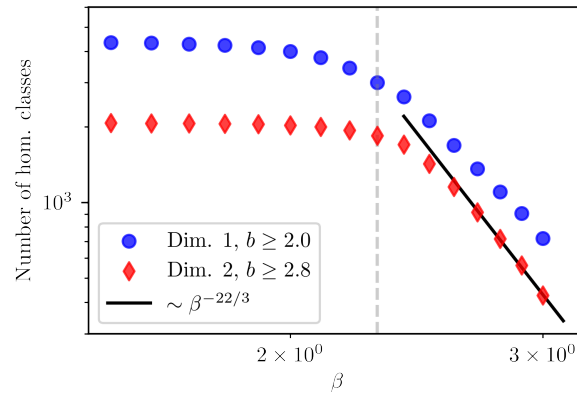
**FIGURE 6.3.5:** Number of homology classes in the angle difference filtration constructed from $\phi(\mathbf{x}) = \arg(\operatorname{Tr} \mathcal{P}(\mathbf{x})/2)$ with birth $b \geq 2.0$ for dimension one and $b \geq 2.8$ for dimension two, compared to the semi-classical one-loop instanton appearance probability scaling behavior $\sim \beta^{-22/3}$.

Then, $P(\mathbf{x}) = \operatorname{Tr} \mathcal{P}(\mathbf{x})/2 = \cos \phi(\mathbf{x})$. If the traced Polyakov loop $P(\mathbf{x})$ locally changes, this can give rise to non-trivial spatial structures occurring in $\phi(\mathbf{x})$.

In [79] a filtration has been constructed, that is only sensitive to local differences of periodic fields. The filtration differs from the lower-star filtration discussed so far in that function values are assigned to edges instead of top-dimensional cubes. Specifically, with $\mathfrak{C}$ again the full 3-dimensional cubical complex as in Section 6.3.1, we construct from $\phi(\mathbf{x})$ a map $\tilde{\phi} : \mathfrak{C} \to [0, \pi]$, whose sublevel sets then form cubical subcomplexes of $\mathfrak{C}$. Lattice points $\mathbf{x} \in \Lambda_s$ are mapped to vertices of the full complex $\mathfrak{C}$, defining[5] $\tilde{\phi}(\{\mathbf{x}\}) := 0$. With $\mathbf{x}$ and $\mathbf{y}$ nearest neighbors in $\Lambda_s$, we set

$$\Delta\phi(\mathbf{x}, \mathbf{y}) := \min\{|\phi(\mathbf{x}) - \phi(\mathbf{y})|, 2\pi - |\phi(\mathbf{x}) - \phi(\mathbf{y})|\}, \tag{6.24}$$

and define $\tilde{\phi}(\{\mathbf{x}, \mathbf{y}\}) := \Delta\phi(\mathbf{x}, \mathbf{y})$ with $\{\mathbf{x}, \mathbf{y}\}$ the edge connecting $\mathbf{x}$ with $\mathbf{y}$. We extend to higher-dimensional cubes via the upper-star filtration, i.e., we induce values from lower-dimensional cubes,

$$\tilde{\phi}(C) := \max\{\tilde{\phi}(D) \,|\, D \in \partial C\}, \tag{6.25}$$

and apply this construction inductively until $\tilde{\phi}$ is defined on all $\mathcal{C}$. Sublevel sets of $\tilde{\phi}$ yield the angle-difference filtration,

$$\tilde{\phi}^{-1}[0, \nu] \subseteq \tilde{\phi}^{-1}[0, \mu], \text{ whenever } \nu \leq \mu, \tag{6.26}$$

whose persistent homology we shall investigate.

By construction, the angle-difference filtration of $\phi(\mathbf{x})$ does not contain information on the volume-averaged traced Polyakov loop expectation value $L$. Indeed, we expand $L$ in

---

[5]Strictly speaking, we here choose the 3-cubes of $\mathfrak{C}$ to be $\mathbf{x} + [0, 1]^3$ for lattice points $\mathbf{x} \in \Lambda_s$.

terms of $\phi(\mathbf{x})$:

$$L = \frac{1}{N_s^3}\langle|\sum_{\mathbf{x}\in\Lambda_s}\cos(\phi(\mathbf{x}))|\rangle = \frac{1}{N_s^3}\langle|\sum_{n=0}^{\infty}\frac{(-1)^n}{(2n)!}\sum_{\mathbf{x}\in\Lambda_s}\phi^{2n}(\mathbf{x})|\rangle\,, \tag{6.27}$$

i.e., only volume-averages of even powers of $\phi$ enter $L$. The spatial average $\sum_{\mathbf{x}\in\Lambda_s}\phi(\mathbf{x})/N_s^3$ does not enter the angle-difference filtration of the holonomy Lie algebra field $\phi$ directly. In addition, the angle-difference filtration of $\phi$ is by construction center symmetric ($\phi\mapsto\phi+\pi$).

Betti number distributions of the angle-difference filtration for uncooled and cooled configurations are displayed in Figure 6.3.4(a) and (b), respectively. Points entering as independent connected components at filtration parameter $\nu = 0$ and merging at $\nu = \Delta\phi(\mathbf{x},\mathbf{y})$ into edges, by construction dimension zero Betti numbers monotonously decrease with growing filtration parameters and contain information on the statistics of nearest-neighbor $\Delta\phi(\mathbf{x},\mathbf{y})$-values. Throughout dimensions, Betti number distributions of uncooled configurations are constant for $\beta \lesssim \beta_c$. For $\beta$ near 1.5, cooling leaves the Betti number distributions invariant (see the pink, dashed line in Figure 6.3.4(b)). Dimension one Betti numbers show a distinct peak around $\nu \equiv \Delta\phi \simeq 2.2$ for $\beta \lesssim \beta_c$, slightly wandering towards smaller filtration parameters with increasing $\beta$. This behavior is pronounced for cooled configurations and starts off at smaller $\beta$ already. Dimension two Betti numbers of uncooled configurations show a prominent peak around $\nu \simeq 3.0$. After cooling, it decreases vastly in height for increasing $\beta$. A population of dimension two homology classes emerges at smaller $\nu$ for larger $\beta$.

The above observations can be understood as follows: below $\beta_c$ Polyakov loop samples are dominated by vast fluctuations between $\approx -1$ and $\approx +1$ on tiny length scales, see Figure 6.2.1(a). The formation of dimension two persistent homology classes in the angle-difference filtration thus requires large phase jumps of order $\pi$ to occur everywhere around local minima or maxima, thus occurring in the angle-difference filtration below $\beta_c$ primarily for $\nu \approx \pi$. As discussed in Section 6.3.1 above $\beta_c$, extended domains of like-signed $P(\mathbf{x})$-values form, however without cooling strongly overlaid by thermal fluctuations. Fewer dimension two homology classes corresponding to extended domains fit into the given lattice volume compared to those originating from single-pixel fluctuations, explaining the peak decline in $\beta_2(\nu)$ in particular for cooled configurations. On top of the like-signed domains forming above $\beta_c$, fluctuations occur. The population of dimension two homology classes emerging for $\beta \gtrsim \beta_c$ below the $\nu \simeq 3.0$-peak may be understood as a signal of these.

Dimension one Betti numbers show the strongest $\beta$-dependence. In [79] the angle-difference filtration has been employed to uncover the behavior of vortices in two spatial dimensions. In three dimensions, these would show up as closed vortex lines, which would manifest as signals in dimension one Polyakov topological densities. It has been a key finding of Section 6.3.2 that $q_{\mathcal{P}}$-sublevel sets barely show such signatures, but instead predominantly give rise to local lumps of topological density. We thus expect that the strong $\beta$-dependence of dimension one Betti numbers originates from locally

large phase gradients spreading through space around like-signed Polyakov loop regions with fluctuations on top. Then, the angle-difference filtration yields at intermediate filtration parameters randomized scaffold-like cubical complexes with a variety of one-dimensional homology classes occurring. This is qualitatively in accordance with space-filling instanton-dyon positions in models of instanton-dyon ensembles [266, 270].

Displayed in Figure 6.3.4(c), maxima of Betti numbers of uncooled configurations show a clear kink around $\beta_c$, thus providing an order parameter for the confinement-deconfinement phase transition.

In Figure 6.3.5, we display the number of homology classes with high birth values in cooled configurations, in dimension one with birth $b \geq 2.0$, in dimension two with birth $b \geq 2.8$. We explicitly checked that the displayed results are approximately independent in shape from the choice of threshold values of comparable sizes. For $\beta \gtrsim 2.6$ the number of dimension two homology classes is compatible with a power-law with exponent $\simeq -22/3$. Linearly mapping inverse couplings squared to temperatures, the latter describes a dilute gas of instantons with semi-classical instanton appearance probability

$$\exp(-S) = \exp\left(-\frac{8\pi^2}{g^2(T)}\right) \sim \left(\frac{\Lambda_{\mathrm{UV}}}{T}\right)^b, \qquad (6.28)$$

where $\Lambda_{\mathrm{UV}}$ is a UV-cutoff scale and $b = 11N_c/3$ from the one-loop beta function for $\mathrm{SU}(N_c)$ gauge theory [266], $N_c = 2$ in our case. The behavior of the semi-classical instanton-dyon exponentiated action shows the same scaling behavior with $T$ [266, 302]. One-dimensional homology classes with large birth show similar behavior, though with larger deviations from the $T^{-22/3}$ behavior. Likely, they are more affected by thermal fluctuations.

In Section 6.C.2 we display and discuss birth and persistence distributions of the angle-difference filtration.

## 6.4 Electric and magnetic fields in persistent homology

We search for signatures of electric and magnetic screening effects as well as self-duality in superlevel set filtrations of the three gauge-invariant, rotationally invariant quadratic forms constructible from $\mathbf{E}(x)$ and $\mathbf{B}(x)$: $\mathrm{Tr}\,\mathbf{E}^2(x)$, $\mathrm{Tr}\,\mathbf{B}^2(x)$, and the topological density $q(x) \sim \mathrm{Tr}\,(\mathbf{E}(x) \cdot \mathbf{B}(x))$.

On the lattice $\mathrm{SU}(2)$-valued electric and magnetic fields, denoted $\mathbf{E}(x)$ and $\mathbf{B}(x)$, can be defined via antisymmetric averaging of four neighboring plaquettes, analogous to Section 4.2. For these clover-leaf variants the topological density reads

$$q(x) = -\frac{1}{16\pi^2}\mathrm{Tr}\,(\mathbf{E}(x) \cdot \mathbf{B}(x)) \qquad (6.29)$$

and has well-defined parity, see Section 6.A.3. For an impression of $\mathrm{Tr}\,\mathbf{E}^2(x)$, $\mathrm{Tr}\,\mathbf{B}^2(x)$, and $\mathrm{Tr}\,(\mathbf{E}(x) \cdot \mathbf{B}(x)) = -16\pi^2 q(x)$ we display two-dimensional slices in Figure 6.4.1 for $\beta = 1.5$ in the confined and $\beta = 3.0$ in the deconfined phase for cooled configurations. Throughout observables, fewer structures are present for $\beta = 3.0$ compared to $\beta = 1.5$ variants, also smaller by values. This effect is pronounced for $\mathrm{Tr}\,\mathbf{B}^2$ compared to both
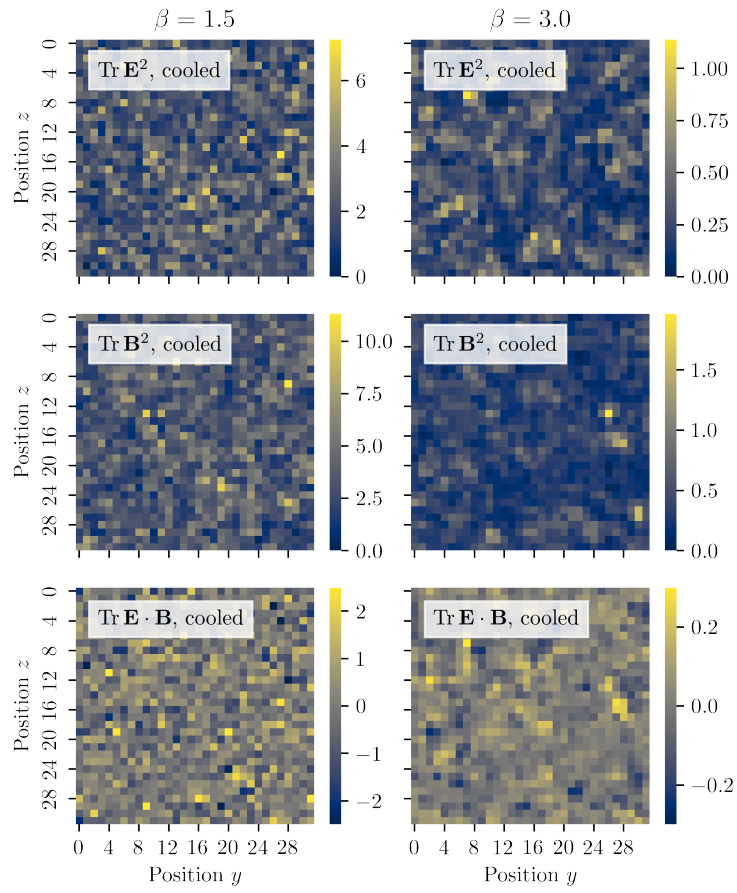
**FIGURE 6.4.1:** Slices of $\mathrm{Tr}\,\mathbf{E}^2(x)$, $\mathrm{Tr}\,\mathbf{B}^2(x)$ and $q(x)$ for constant $\mathbf{x}^1$ and $\tau$ for a single cooled configuration. Data is given in lattice units.

$\mathrm{Tr}\,\mathbf{E}^2$ and $\mathrm{Tr}\,\mathbf{E}\cdot\mathbf{B}$. Barely any structural changes with $\beta$ are visible without cooling (not shown).

So far, persistent homology quantifiers have been constructed via cubical complexes in three dimensions. Constructions work the same in higher dimensions. For instance, the sublevel set filtration $\mathfrak{C}_{\mathrm{Tr}\,\mathbf{E}^2}$ is constructed by assigning to the 4-cube corresponding to each $x \in \Lambda$ the value $\mathrm{Tr}\,\mathbf{E}^2(x)$, inductively expanding to lower-dimensional cubes via the lower-star filtration, Equation (6.8). We define the corresponding superlevel set filtration as

$$\mathfrak{D}_{\mathrm{Tr}\,\mathbf{E}^2}(\nu) := \mathfrak{C}_{-\mathrm{Tr}\,\mathbf{E}^2}(-\nu)\,. \tag{6.30}$$

$\mathrm{Tr}(\mathbf{E}^2(x))$ and $\mathrm{Tr}(\mathbf{B}^2(x))$ are restricted to positive values. For better comparability of low-dimensional persistent homology with unbounded filtrations such as $q(x)$ we investigate their superlevel set filtrations in this section. For unbounded filtrations sub- and superlevel set filtrations are expected to yield similar results. Subsequently, we study topological density superlevel sets.

### 6.4.1 Superlevel sets of $\mathrm{Tr}\,\mathrm{E}^2$ and $\mathrm{Tr}\,\mathrm{B}^2$

We display Betti number distributions of dimension zero homology classes for the superlevel set filtrations of $\mathrm{Tr}\,\mathbf{E}^2$ and $\mathrm{Tr}\,\mathbf{B}^2$ in Figure 6.4.2(a). Higher-dimensional Betti number
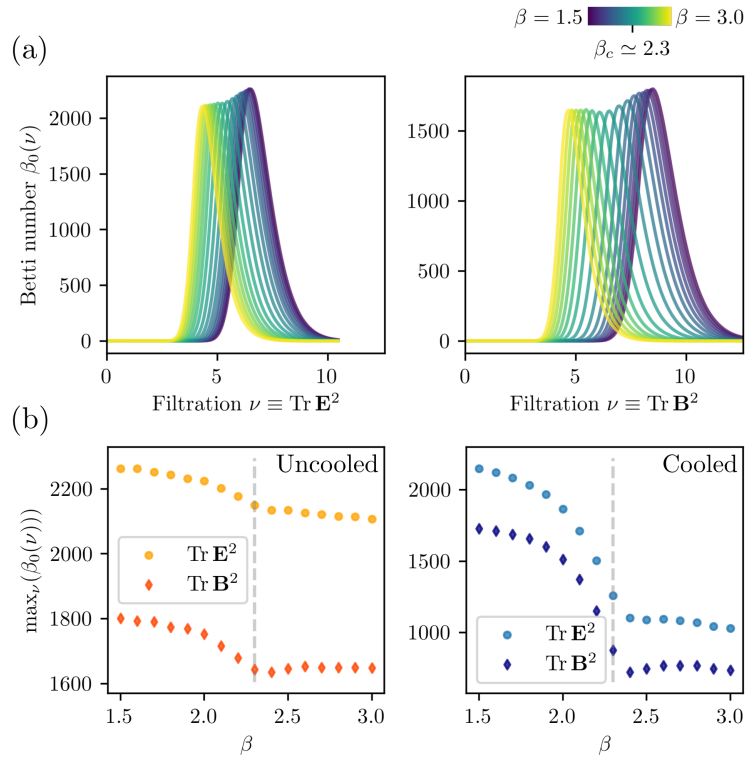
**FIGURE 6.4.2:** (a): Dimension zero Betti number distributions of $\mathrm{Tr}\,\mathbf{E}^2(x)$ (left) and $\mathrm{Tr}\,\mathbf{B}^2(x)$ (right) superlevel set filtrations. No cooling has been applied. Data is given in lattice units. (b): Maxima of dimension zero Betti number distributions for uncooled (left) and cooled (right) configurations.

distributions look similar, see Appendix Section 6.C.3. For cooled Betti number distributions of $\mathrm{Tr}\,\mathbf{E}^2$ and $\mathrm{Tr}\,\mathbf{B}^2$, we also refer to Appendix Section 6.C.3. For every $\beta$ we observe a distinct peak in both filtrations with positions shifting to lower $\nu$ for increasing $\beta$. This is due to $\langle \mathrm{Tr}\,\mathbf{E}^2(x) \rangle$ and $\langle \mathrm{Tr}\,\mathbf{B}^2(x) \rangle$ decreasing in the calculations. Starting slowly, shifts are enhanced at intermediate $\beta$, slowing down again for $\beta \gtrsim 2.7$. This is particularly visible in $\mathrm{Tr}\,\mathbf{B}^2$. Dimension zero homology classes, which are in the superlevel set filtration made up by local maxima, occur in the $\mathrm{Tr}\,\mathbf{B}^2$ filtration mostly at larger filtration parameters compared to $\mathrm{Tr}\,\mathbf{E}^2$. For both $\mathrm{Tr}\,\mathbf{E}^2$ and $\mathrm{Tr}\,\mathbf{B}^2$ peaks are broadened for low $\beta$.

In Figure 6.4.2(b) we compare $\beta$-dependencies of maximal dimension zero Betti numbers of $\mathrm{Tr}\,\mathbf{E}^2$ and $\mathrm{Tr}\,\mathbf{B}^2$ filtrations, i.e., the maximal number of connected components occurring as the filtration parameter is swept through. Both uncooled and cooled configurations give rise to kink-like behavior at $\beta_c$, indicative of the confinement phase transition. Throughout, we observe a concave decline below $\beta_c$. For $\mathrm{Tr}\,\mathbf{E}^2$ the decline continues above $\beta_c$ with a smaller slope; cooling enhances these effects without qualitative changes. For $\mathrm{Tr}\,\mathbf{B}^2$ above $\beta_c$ we observe less of a further decline compared to $\mathrm{Tr}\,\mathbf{E}^2$, both uncooled and cooled.

Inferred from correlations of $\mathrm{Tr}\,\mathbf{E}^2$ and $\mathrm{Tr}\,\mathbf{B}^2$ as detailed in Appendix Section 6.B.2, masses of $\mathrm{Tr}\,\mathbf{E}^2$ excitations are larger than for $\mathrm{Tr}\,\mathbf{B}^2$ due to electric Debye screening outpacing magnetic screening. Similarly, the mass of electric excitations is expected to be larger than the magnetic mass, resulting in $\langle \mathrm{Tr}\,\mathbf{E}^2 \rangle < \langle \mathrm{Tr}\,\mathbf{B}^2 \rangle$ and explaining why
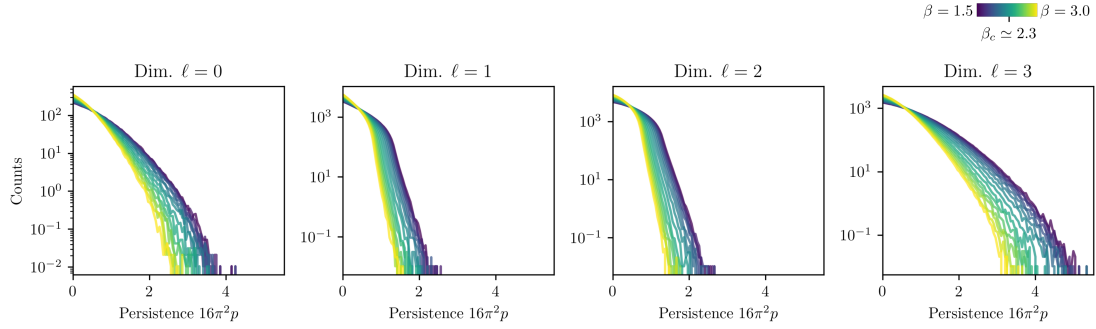
**FIGURE 6.4.3:** Persistence distributions of the topological density superlevel set filtration from dimensions zero to three. No cooling has been applied; cooled configurations look similar. Results are given in lattice units.

magnetic field homology classes persist to larger filtration parameters compared to electric ones. $\text{Tr}\,\mathbf{E}^2$ Betti number maxima in Figure 6.4.2(b) laying above $\text{Tr}\,\mathbf{B}^2$ maxima indicates that $\text{Tr}\,\mathbf{E}^2$ sublevel sets contain finer structures, irrespectively of on average higher $\text{Tr}\,\mathbf{B}^2$ values. This can already be seen for a single sample in Figure 6.4.1. The slow approach of maximal $\text{Tr}\,\mathbf{E}^2$ and $\text{Tr}\,\mathbf{B}^2$ Betti numbers for growing $\beta \gtrsim \beta_c$ suggests that screening effects discriminate less between electric and magnetic fields at larger inverse couplings. This is again consistent with the approaching masses of $\text{Tr}\,\mathbf{E}^2$ and $\text{Tr}\,\mathbf{B}^2$ excitations.

Signatures of a higher dominance of self-dual excitations in cooled configurations would manifest in maxima of $\text{Tr}\,\mathbf{E}^2$ and $\text{Tr}\,\mathbf{B}^2$ which are closer to each other. This is at least not significantly the case and barely visible in the single-sample observables shown in Figure 6.4.1.

### 6.4.2 Superlevel sets of topological densities

In Section 6.3.2 we have studied the persistent homology of topological densities computed from Polyakov loops, $q_{\mathcal{P}}$. In this section we discuss the topological density $q(x) \sim \text{Tr}\,\mathbf{E}(x) \cdot \mathbf{B}(x)$, with domain the full four-dimensional lattice $\Lambda$. We show persistence distributions of topological density superlevel sets in Figure 6.4.3 for uncooled configurations. The distributions monotonously decrease for all dimensions and inverse couplings $\beta$. However, their support is reduced to $16\pi^2 p \lesssim 2.5$ for dimensions one and two, while ranging for dimension zero up to $\approx 4.0$ and for dimension three up to $\approx 5.0$. The extended persistence of dimension zero and dimension three homology classes holds for all $\beta$ and indicates that the topological density forms peaks well-separated in space-time, similar to $q_{\mathcal{P}}$ as discussed in Section 6.3.2. Cooling barely affects persistence distributions (not displayed). We conclude that lumps of topological density are primarily due to (near-)classical field configurations.

It has been a key finding of Section 6.3.2 that top-dimensional persistence distributions of $q_{\mathcal{P}}$ follow an exponential distribution which is compatible with instanton-dyon predictions. Such exponential behavior is not visible for $q \sim \text{Tr}\,\mathbf{E} \cdot \mathbf{B}$ as displayed in Figure 6.4.3. This hints at $q_{\mathcal{P}}$ providing a more suitable lattice approximation to continuous space-time topological densities than $q \sim \text{Tr}\,\mathbf{E} \cdot \mathbf{B}$, less sensitive to temporal fluctuations affected by lattice artifacts. Based on the exact equality of $\int q_{\mathcal{P}}$ and $\int q$ in the continuum,

as briefly discussed in Appendix Section 6.C.1, we expect that the information content of both topological density variants becomes more similar for larger and finer lattices.

## 6.5    Summary

We have shown that persistent homology can be used for unraveling topological structures in the confinement-deconfinement phase transition of finite-temperature Yang-Mills theory with gauge group $\mathrm{SU}(2)$. With persistent homology analyses relying on a hierarchical, combinatorial description of the input data, a multitude of different cubical complex filtrations constructed from sampled lattice field configurations has allowed for the extraction of the multifaceted picture of confinement. All filtrations constructed in this chapter have been gauge-invariant and without an a priori bias towards particular classical configurations. While information about the confinement-deconfinement phase transition may be extracted from a persistent homology analysis of various observables such as the topological density, the traces of electric and magnetic field strengths, and the traced Polyakov loop, we have found that amongst these observables the traced Polyakov loop and in particular the related algebra field (6.22) is best-suited for an application of persistent homology.

The analysis has revealed that lumps of the topological density formulated in terms of the Polyakov loop have dominated the configurations, with persistence statistics indicative of the instanton-dyon occurrence probability. Persistent homology has proven crucial for this observation. Filtering by the Polyakov loop algebra field has given access to topological scaling as present in an instanton gas approximation above $T_c$: we have shown that homology follows the semi-classical scaling arising from the exponential of the instanton action with a (one-loop) running coupling, see Figure 6.3.5. Unlike [80] we have not specifically aimed for particular field configurations such as center vortices. The main results have been barely affected by the cooling procedure.

For prospective related research questions we refer to Chapter 8.

## Appendix

## 6.A    Details on the lattice setup

In this appendix, we first discuss the HMC setup for our lattice gauge theory calculations. Subsequently, we summarize important aspects of the Wilson flow used for cooling, and provide further details about clover-leaf fields.

### 6.A.1    HMC details

We employ the standard HMC algorithm to sample field configurations, using 10 leapfrog steps per trajectory with a step size of 0.2. This results in acceptance rates between 60% and 80%. First, for each of the considered values of $\beta$, a single Markov chain is initialized with a hot start and then thermalized. Sufficient equilibration is confirmed by observing

convergence of the average plaquette and Polyakov loop. 100 samples separated by 10 HMC steps are recorded for each $\beta$ and then further decorrelated in individual Markov chains with 1000 steps each, in order to ensure statistical independence of the data.

### 6.A.2 Wilson flow details

A variety of heuristic algorithms for the smoothing of ultraviolet fluctuations in lattice gauge field configurations has been proposed in the literature, commonly called cooling algorithms. The Wilson or gradient flow was introduced as a more rigorous theoretical ansatz to achieve the same goal. The central idea is similar in all approaches, namely minimizing the Wilson gauge action locally in a series of small steps.

For the Wilson flow in particular, this is achieved by numerically solving the gradient flow equation [303]

$$\partial_t U_\mu(x,t) = -g^2 (\partial_{x,\mu} S[U(t)]) U_\mu(x,t) \tag{6.31}$$

with a finite step size approximation. Here, $g$ is the bare gauge coupling, $t$ denotes the flow time, and the initial condition $U_\mu(x,0)$ is given by a field configuration obtained through sampling from $\exp(-S[U])$ as described above. The link derivatives are defined in the usual way,

$$\partial_{x,\mu} f(U) = \mathrm{i} \sum_a T^a \frac{\mathrm{d}}{\mathrm{d}s} f(e^{\mathrm{i}sX^a} U)\Big|_{s=0} \equiv \mathrm{i} \sum_a T^a \partial_{x,\mu}^{(a)} f(U) \,, \tag{6.32}$$

where the $T^a$ are the Hermitian generators of the associated $\mathfrak{su}(N_c)$ algebra (i.e., the Pauli spin matrices for $N_c = 2$), and

$$X^a(y,\nu) = \begin{cases} T^a & \text{if } (y,\nu) = (x,\mu), \\ 0 & \text{else.} \end{cases} \tag{6.33}$$

This is equivalent to the computation of the forces in HMC. Throughout this work, the cooled configurations used to compute various results are obtained after 200 flow steps, using a comparably small step size of $\delta t = 0.001$ to avoid discretization errors.

### 6.A.3 Clover-leaf electric and magnetic fields

Similar to Equations (4.9) and (4.11), clover-leaf electric fields are the $\mathrm{SU}(2)$ elements

$$\begin{aligned} E_i(x) := \frac{1}{4}\mathrm{Im}\Big[ & U_{4i}(x) + U_i^\dagger(x-\hat{i})U_{4i}(x-\hat{i})U_i(x-\hat{i}) \\ & + U_4^\dagger(x-\hat{4})U_{4i}(x-\hat{4})U_4(x-\hat{4}) \\ & + U_4^\dagger(x-\hat{4})U_i^\dagger(x-\hat{i}-\hat{4})U_{4i}(x-\hat{i}-\hat{4})U_i(x-\hat{i}-\hat{4})U_4(x-\hat{4})\Big], \end{aligned} \tag{6.34}$$

which transform under a local gauge transformation $V(x)$ as $E_i(x) \mapsto V(x)E_i(x)V^\dagger(x)$, and clover-leaf magnetic fields are the $\mathrm{SU}(2)$ elements

$$
\begin{aligned}
B_i(x) = \frac{1}{8}\varepsilon^{ijk}\mathrm{Im}\Big[ & U_{jk}(x) + U_j^\dagger(x-\hat{j})U_{jk}(x-\hat{j})U_j(x-\hat{j}) \\
& + U_k^\dagger(x-\hat{k})U_{jk}(x-\hat{k})U_k(x-\hat{k}) \\
& + U_k^\dagger(x-\hat{k})U_j^\dagger(x-\hat{j}-\hat{k})U_{jk}(x-\hat{j}-\hat{k})U_j(x-\hat{j}-\hat{k})U_k(x-\hat{k})\Big],
\end{aligned}
\tag{6.35}
$$

transforming as $B_i(x) \mapsto V(x)B_i(x)V^\dagger(x)$.

By spatial antisymmetrization the clover-leaf topological density,

$$
q(x) = -\frac{1}{2^9\pi^2}\sum_{\mu\nu\rho\sigma=\pm1}^{\pm4}\tilde{\varepsilon}^{\mu\nu\rho\sigma}\mathrm{Tr}\left(U_{\mu\nu}(x)U_{\rho\sigma}(x)\right),
\tag{6.36}
$$

has a well-defined parity [95, 304]. The fully antisymmetric $\tilde{\varepsilon}^{\mu\nu\rho\sigma} = \tilde{\varepsilon}_{\mu\nu\rho\sigma}$ is defined through $1 = \tilde{\varepsilon}_{1234} = -\tilde{\varepsilon}_{2134} = -\tilde{\varepsilon}_{(-1)234}$. Plaquettes for negative directions equate to

$$
U_{(-\mu)\nu}(x) = U_\mu^\dagger(x-\hat{\mu})U_{\mu\nu}^\dagger(x-\hat{\mu})U_\mu(x-\hat{\mu}),
\tag{6.37a}
$$

$$
U_{\mu(-\nu)}(x) = U_\nu^\dagger(x-\hat{\nu})U_{\mu\nu}^\dagger(x-\hat{\nu})U_\nu(x-\hat{\nu}),
\tag{6.37b}
$$

$$
\begin{aligned}
U_{(-\mu)(-\nu)}(x) = & U_\nu^\dagger(x-\hat{\nu})U_\mu^\dagger(x-\hat{\mu}-\hat{\nu}) \\
& \times U_{\mu\nu}(x-\hat{\mu}-\hat{\nu})U_\mu(x-\hat{\mu}-\hat{\nu})U_\nu(x-\hat{\nu}).
\end{aligned}
\tag{6.37c}
$$

A straight-forward lattice computation confirms Equation (6.29) for $q(x)$ in terms of $E_i(x)$ and $B_i(x)$.

## 6.B   Correlation functions

In this appendix we discuss two-point correlation functions of traced Polyakov loops $P(\mathbf{x})$ and electric and magnetic fields squared. This will provide insights into emergent screening masses and infrared behavior related to confinement.

We focus on connected correlation functions and their $y$-, $z$- and $\tau$-direction zero-modes. We define

$$
\bar{E}^2(n_x) := \frac{1}{N_s^2 N_\tau}\sum_{n_y,n_z,n_\tau}\left[\mathrm{Tr}\,\mathbf{E}^2(n_x,n_y,n_z,n_\tau) - \langle\mathrm{Tr}\,\mathbf{E}^2(n_x,n_y,n_z,n_\tau)\rangle\right],
\tag{6.38}
$$

maintaining fluctuations depending on $n_x$. Then, correlations are computed as

$$
\langle|\mathrm{Tr}\,\mathbf{E}^2(p_x)|^2\rangle_c = \sum_x \bar{E}^2(n_x)\bar{E}^2(0)e^{-\mathrm{i}p_x n_x}
\tag{6.39}
$$
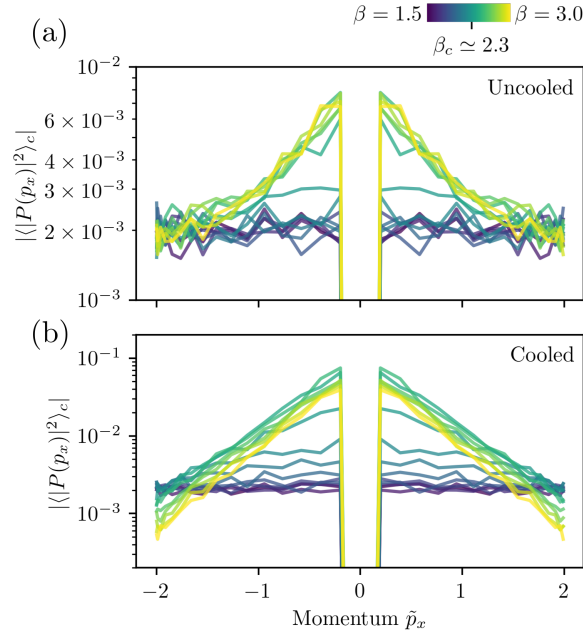
**FIGURE 6.B.1:** Connected Polyakov loop two-point correlation function $|\langle |P(p_x)|^2 \rangle_c|$ for (a) uncooled and (b) cooled configurations. Data is given in lattice units.

for $n_x \in \{0, \ldots, N_s - 1\}$ and

$$p_x \in \left\{ -\pi, -\frac{(N_s - 2)\pi}{N_s}, \ldots, \frac{(N_s - 2)\pi}{N_s} \right\} , \tag{6.40}$$

and analogously for $\text{Tr } \mathbf{B}^2(x)$ and $q(x)$. For $P(\mathbf{x})$ correlations, temporal averaging is trivial. Correlations are displayed depending on physical momenta on the lattice,

$$\tilde{p}_x = 2 \sin\left(\frac{p_x}{2}\right) . \tag{6.41}$$

Due to the connectedness of the shown correlators, values at $p_x = 0$ are largely suppressed. Zero modes of the correlators including disconnected contributions would give rise to susceptibilies.

## 6.B.1   Polyakov loop correlations

In Figure 6.B.1 we display Polyakov loop correlations for (a) uncooled and (b) cooled configurations for the entire $\beta$-range. A qualitative change can be observed around $\beta_c$ for uncooled configurations. Below $\beta_c$ the correlator is constant in $\beta$ and in $\tilde{p}_x$ up to fluctuations, indicative of free quasi-particles dominating $P(\mathbf{x})$ [264]. Above $\beta_c$ a peak emerges around the $\tilde{p}_x = 0$ mode, indicative of $P(\mathbf{x})$ excitations acquiring a screening mass due to spontaneous center symmetry breaking. Above an intermediate regime up to $\beta \simeq 2.5$ correlations stay approximately constant. They level off for large momenta to baseline fluctuations.

Below $\beta_c$ cooling smoothens the baseline fluctuations, leaving their height unaltered. Thus, they are due to (near-)classical configurations. With cooling, for smaller $\beta$ than
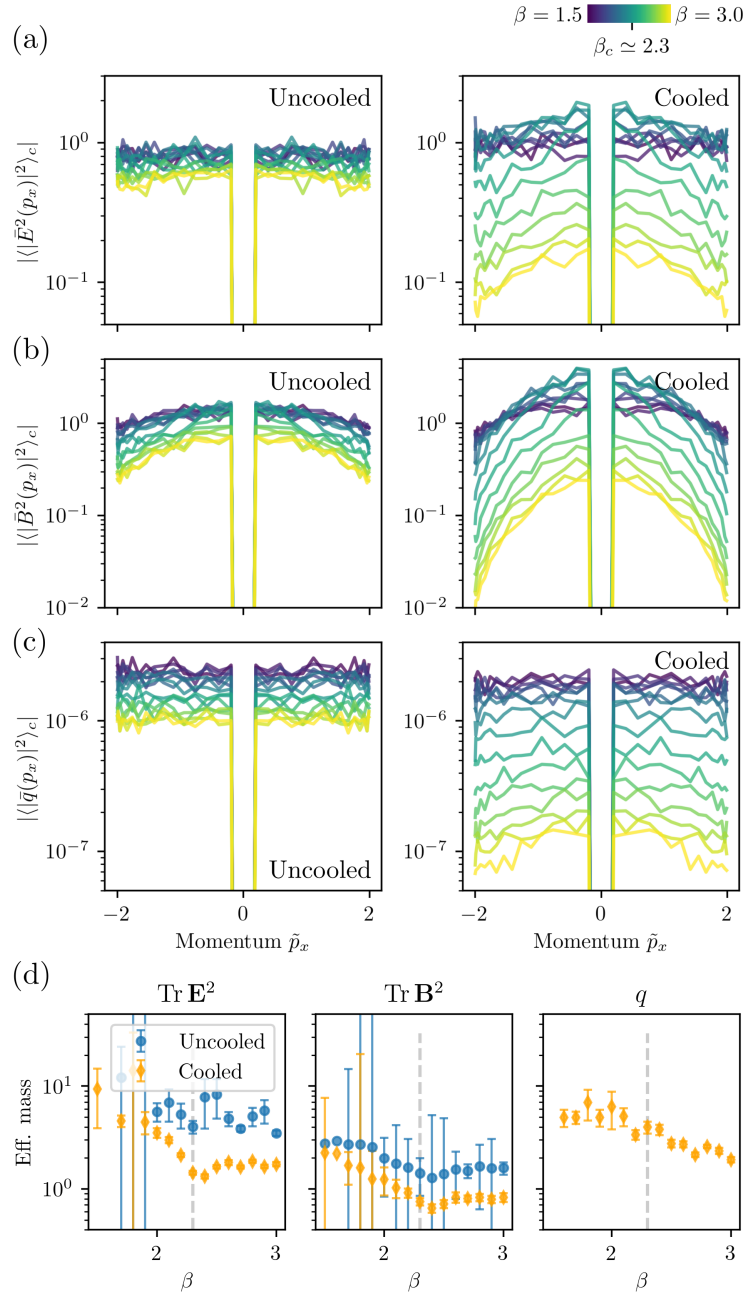
**FIGURE 6.B.2:** Connected two-point correlations of (a) electric and (b) magnetic field strengths, as well as (c) topological densities for uncooled (left) and cooled (right) configurations. The dip at $\tilde{p}_x = 0$ is due to (approximately homogeneous) disconnected contributions removed. (d): Effective masses of $\mathrm{Tr}\,\mathbf{E}^2$ (left), $\mathrm{Tr}\,\mathbf{B}^2$ (center) and $q$ (right) excitations, deduced from a least-squares fit to a Lorentz curve $\sim m/(\tilde{p}_x^2 + m^2)$. Zero modes are excluded from fits; errorbars are extracted from the least-squares fit covariance matrix. Fits did not converge for uncooled $q$. Data is given in lattice units.

before a peak emerges in the deep infrared, until it fully developed for $\beta \simeq 2.6$. For such couplings, the momentum-dependence of the peak-tails is approximately exponential. The peak decreases in overall height for large $\beta$ above 2.7, potentially indicative of the reduction of instantons with increasing temperatures as observed already in Section 6.3.3.

### 6.B.2    Correlations of electric and magnetic excitations

In Figure 6.B.2(a) to (c) we display connected two-point correlation functions of electric and magnetic fields squared, $\mathrm{Tr}\,\mathbf{E}^2$ and $\mathrm{Tr}\,\mathbf{B}^2$, as well as of the topological density $q \sim \mathrm{Tr}\,\mathbf{E}\cdot\mathbf{B}$. First discussing configurations without cooling, barely any $\beta$-dependence is visible at low $\beta$ near 1.5. For intermediate values of $\beta$ correlations decrease in value, slowing down again for $\beta$-values near 3.0. Electric fields give rise to a slightly enhanced infrared peak at larger inverse couplings squared. For magnetic fields this effect is visible more clearly. Topological density correlations are nearly flat for the entire $\beta$-range.

The consequences of cooling are similar to the Polyakov loop correlator. Deviations from the constant behavior for $\beta$ near 1.5 start to occur for $\beta \gtrsim 1.8$. Any behavior present for larger inverse couplings is pronounced by cooling. This is due to more dominant (near-)classical field configurations after cooling.

All this can be understood from effective masses of the excitations. We extract masses from correlators using a least-squares fit to a Lorentz curve $\sim m/(\tilde{p}_x^2 + m^2)$. In Figure 6.B.2(d) we display correspondingly fitted masses, comparing cooled and uncooled ones. Cooling reduces masses, since less ultraviolet fluctuations enter self-energies and effectively generate the masses. Masses of $\mathrm{Tr}\,\mathbf{E}^2$ excitations are observed to be consistently larger than masses of $\mathrm{Tr}\,\mathbf{B}^2$ excitations — a direct consequence of Debye screening. In addition, a kink is visible in effective masses near $\beta_c$, suggesting that the relevant structures for confinement enter self-energies, too. Fits of $q$-masses did not converge for uncooled configurations. Masses of $q$ excitations after cooling lay somewhat between those of $\mathrm{Tr}\,\mathbf{E}^2$ and $\mathrm{Tr}\,\mathbf{B}^2$ excitations. Their comparable height can be regarded as a signature of self-dual configurations playing a role.

## 6.C    Further persistent homology results

This appendix is devoted to further persistent homology results not shown in the main text of this chapter. In Section 6.C.1 we discuss the persistent homology of Polyakov loop topological densities after cooling, in Section 6.C.2 we give birth and persistence distributions for the angle difference filtration. In Section 6.C.3 we discuss Betti number distributions of electric and magnetic fields, as well as topological densities, followed by their cooled variants.

### 6.C.1    Polyakov loop topological densities

In Figure 6.C.1 we display birth and persistence distributions of the Polyakov loop topological density sublevel set filtration for cooled configurations. Comparing to Figure 6.3.3, where uncooled variants have been shown, we note that below $\beta_c$ cooled distributions are similar to uncooled ones though persistence distributions have larger support. Above $\beta_c$ major deviations occur. The broadening of uncooled birth distributions transforms after cooling into an additional peak in dimension zero and a novel shoulder in dimension one after cooling. Dimension two birth distributions above $\beta_c$ reveal larger broadening

towards positive $q_\mathcal{P}$-values. This goes along with persistence distributions after cooling spreading more towards larger persistences compared to uncooled data.

While the similarity of cooled and uncooled $q_\mathcal{P}$-structures below $\beta_c$ indicates that topological densities are dominated by (near-)classical configurations, above $\beta_c$ ultraviolet fluctuations show up more often. Cooling reveals additional topological structures above $\beta_c$.

### 6.C.2 Angle difference filtration

In Figure 6.C.2(a) we display birth distributions of the angle difference filtration of the holonomy Lie algebra field $\phi(\mathbf{x}) = \arccos(P(\mathbf{x}))$ for cooled configurations. Zero-dimensional birth distributions are not displayed, since they are by construction trivial: all dimension zero homology classes are born at filtration parameter zero. Dimension one birth distributions at $\beta \approx 1.5$ have two peaks: one near $b \approx 0.9$ and a second near $b \approx 2.1$. The latter strongly diminishes above $\beta_c$, while the former gets enhanced. The lower-$\Delta\phi$ peak emerges in dimension two homology classes only above $\beta_c$. Below, a single large peak near $\Delta\phi \approx 3.0$ is present, which strongly decreases in height for $\beta \gtrsim \beta_c$.

Persistence distributions are shown in Figure 6.C.2(b) for cooled configurations. Persistences of dimension zero homology classes in the angle difference filtration monotonously decrease, though with smaller $\beta$-dependence for lower $\beta \approx 1.5$. In dimension one we see a second peak near $\Delta\phi \approx 2.0$ at low $\beta$, which vanishes above $\beta_c$ and gives rise to a persistence peak near $\Delta\phi \approx 1.2$. Noise results again in a large number of homology classes with very low persistences. Persistences of dimension two homology classes are mostly very low, which follows from comparably large birth parameters and the phase difference bound $\Delta\phi \leq \pi$.

### 6.C.3 Persistent homology of $\mathrm{Tr}\,\mathbf{E}^2$, $\mathrm{Tr}\,\mathbf{B}^2$ and $q$ superlevel sets

We first discuss the persistent homology for all dimensions zero to three of gauge-invariant electric and magnetic field quadratic forms, as well as topological densities. A comparison with cooled configurations follows.

We display dimension zero to dimension three Betti number distributions of the superlevel set filtrations of $\mathrm{Tr}\,\mathbf{E}^2$ and $\mathrm{Tr}\,\mathbf{B}^2$ for uncooled configurations in Figure 6.C.3(a) and (b). The topological density Betti number distributions shown in Figure 6.C.3(c) are discussed below. For every $\beta$ we observe a single peak, shifting to lower filtration parameters with increasing dimension. This is due to the superlevel set filtration. Decreasing the filtration parameter $\nu$, at first maxima appear as dimension zero homology classes. A multitude of these with saddle points in between is required to form dimension one homology classes; they get born at lower $\nu$. This trend continues to higher dimensions. Finally, dimension three homology classes (enclosed 3-volumes) die if $\nu$ reaches corresponding minimum values.

For both $\mathrm{Tr}\,\mathbf{E}^2$ and $\mathrm{Tr}\,\mathbf{B}^2$ peak positions shift to lower $\nu$ with increasing $\beta$ due to $\langle\mathrm{Tr}\,\mathbf{E}^2(x)\rangle$ and $\langle\mathrm{Tr}\,\mathbf{B}^2(x)\rangle$ decreasing in simulations. Topological structures of any dimension occur in the $\mathrm{Tr}\,\mathbf{B}^2$ filtration mostly at larger filtration parameters compared to $\mathrm{Tr}\,\mathbf{E}^2$.
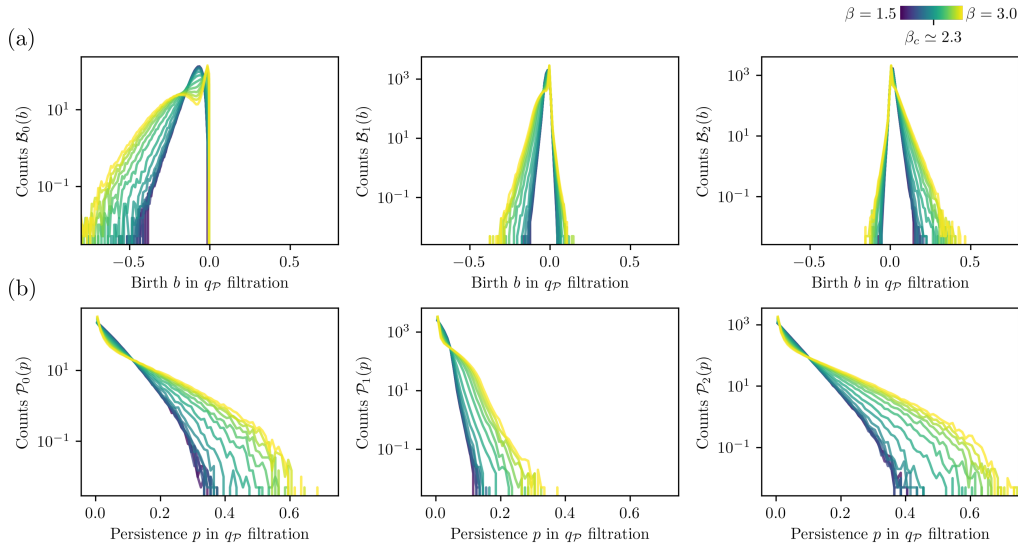
**FIGURE 6.C.1:** Homological quantifiers of Polyakov loop topological density $q_{\mathcal{P}}$ sublevel sets. (a): Birth distributions for dimensions zero to two. (b): Persistence distributions for dimensions zero to two. Data is given in lattice units for cooled configurations.
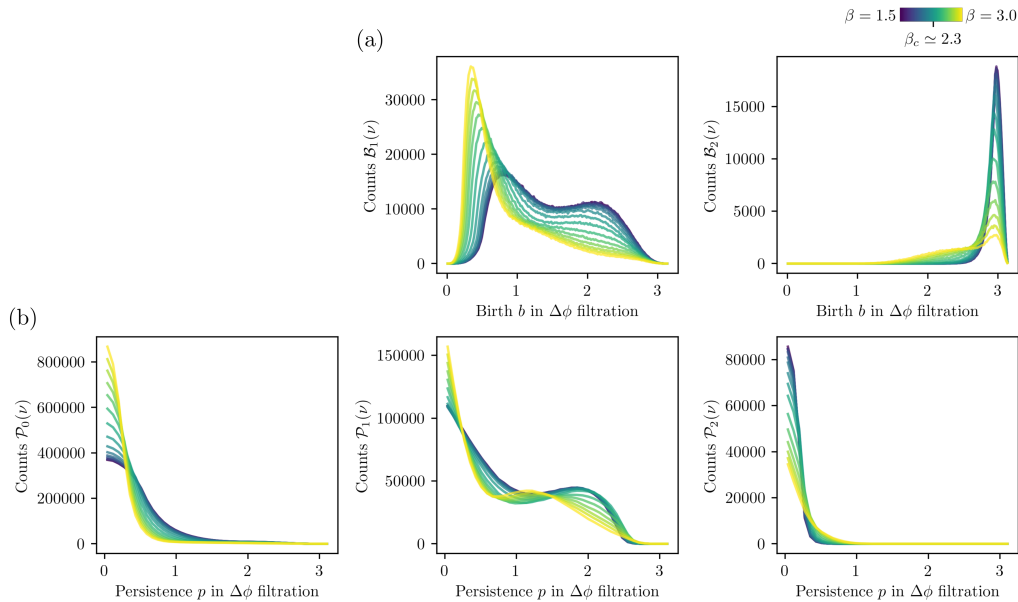


**FIGURE 6.C.2:** Homological quantifiers of the angle difference filtration. (a): Birth distributions for dimensions one and two. All connected components are born at zero in the angle difference filtration, thus dimension zero birth distributions are not displayed. (b): Persistence distributions for dimensions zero to two. Data is shown for cooled configurations.

Across dimensions and for both $\mathrm{Tr}\,\mathbf{E}^2$ and $\mathrm{Tr}\,\mathbf{B}^2$, peaks are broadened for low $\beta$. All this is qualitatively similar to the dimension zero Betti numbers discussed in Section 6.4 and consistent with electric and magnetic screening masses as deduced in Appendix Section 6.B.2.

Topological densities not bounded from below as electric and magnetic fields squared, their Betti number distributions in Figure 6.C.3(c) are not limited to positive filtration parameters. Instead, dimension two distributions have support around zero filtration parameters, dimension three distributions mostly at negative filtrations parameters. This is indicative of local topological density values scattering symmetrically around zero. Maximal values reveal kink-like behavior around $\beta \approx \beta_c$ and in overall numbers are comparable to the $\mathrm{Tr}\,\mathbf{E}^2$ filtration.

For cooled configurations we show Betti number distributions of all dimensions for $\mathrm{Tr}\,\mathbf{E}^2$ and $\mathrm{Tr}\,\mathbf{B}^2$ superlevel set filtrations in Figure 6.C.4. Similar plots have been shown in Figure 6.C.3(a) and (b) for configurations without cooling. Upon comparison, we see that cooling has barely any effect for low $\beta \approx 1.5$. However, after cooling and for larger $\beta$ the number of homology classes is reduced compared to uncooled configurations. Qualitative changes across all dimensions occur near $\beta_c$. For $\beta \gtrsim \beta_c$ maxima of Betti number distributions saturate in height as indicated already in Figure 6.4.2(b). Cooled structures move to very small filtration parameters compared to uncooled ones.
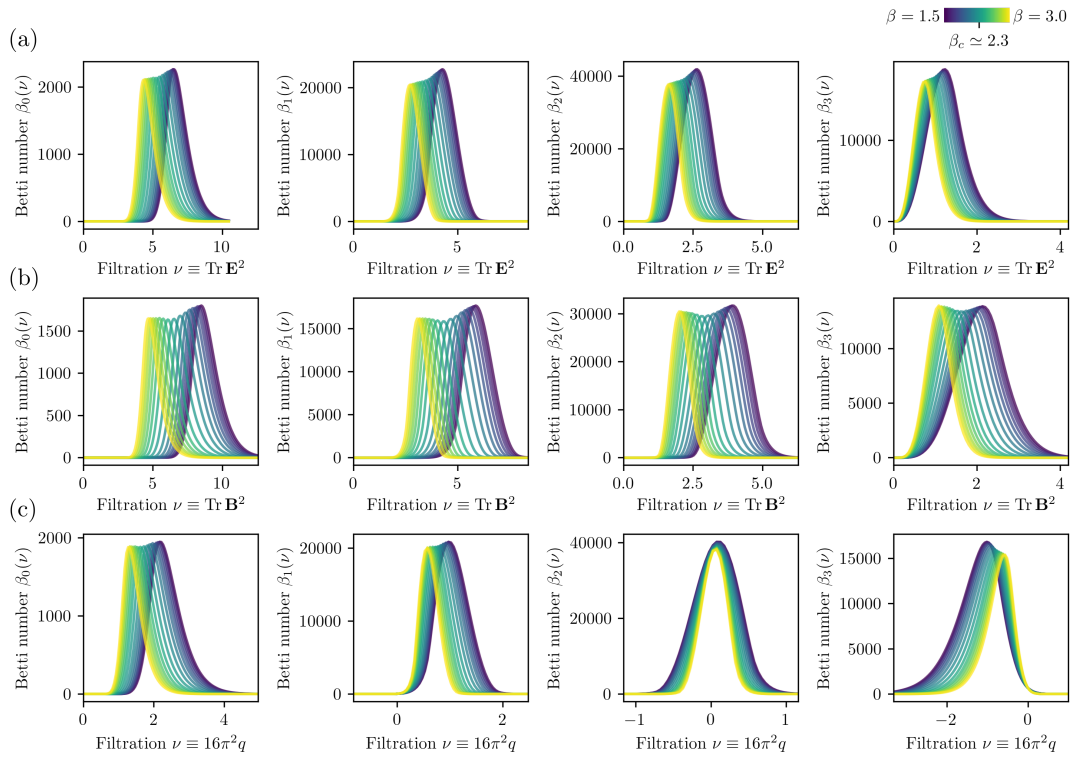
**FIGURE 6.C.3:** Betti number distributions in dimensions zero to three of (a) $\mathrm{Tr}\,\mathbf{E}^2$, (b) $\mathrm{Tr}\,\mathbf{B}^2$, (c) $q$ superlevel set filtrations for uncooled configurations. Data is given in lattice units.
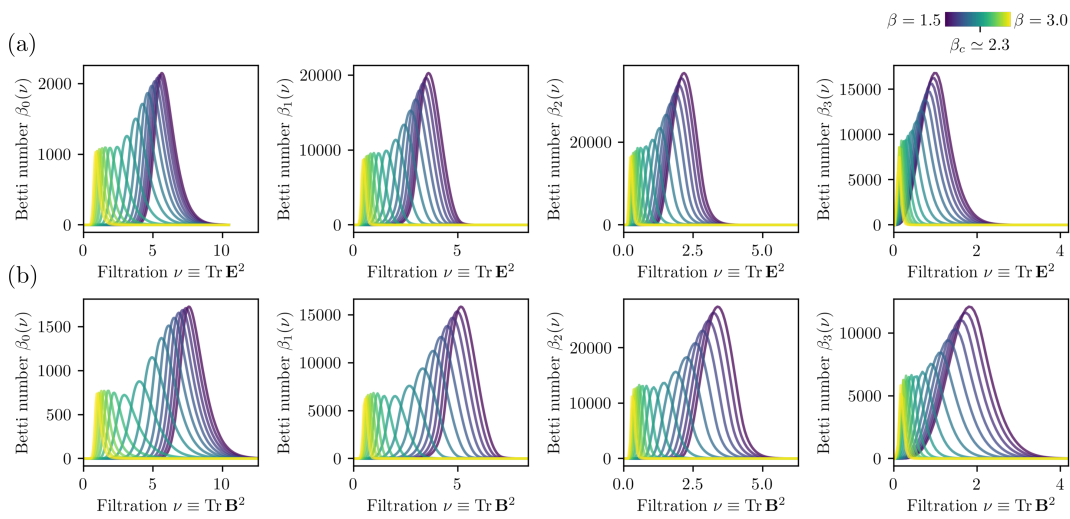


**FIGURE 6.C.4:** Betti number distributions in dimensions zero to three of (a) $\mathrm{Tr}\,\mathbf{E}^2$ and (b) $\mathrm{Tr}\,\mathbf{B}^2$ superlevel set filtrations for cooled configurations. Data is given in lattice units.

# Chapter 7

# Standard Model gauge theory from projective geometries

This chapter represents unpublished work not reported about anywhere else yet. It is devoted to quantum fields on projective geometries, and their relation to known Standard Model structures. The derivations are restricted to representation-theoretic aspects of quantum fields. These are suitably and in this chapter described with mathematical rigor.

## 7.1 Introduction

The Standard Model of particle physics [14–16] has seen a tremendous amount of experimental validation in the past decades, notably at the LHC, Fermilab and other collider facilities. It is centered around a gauge theory with gauge group $G_{\mathrm{SM}} = (\mathrm{U}(1) \times \mathrm{SU}(2) \times \mathrm{SU}(3))/\mathbb{Z}_6$, the cyclic $\mathbb{Z}_6$ subgroup generated by $(\exp(\pi\mathrm{i}/3), -1_{2\times2}, \exp(2\pi\mathrm{i}/3) \cdot 1_{3\times3})$ [91]. Three generations of Dirac fermions with particular $G_{\mathrm{SM}}$ representation (charge) patterns interact with the gauge bosons. Oscillations among the generations occur, and the fermions acquire effective masses due to the Higgs mechanism, which also provides masses to the $W^\pm$ and $Z$ gauge bosons.

A unified framework to understand the peculiar structure of the Standard Model, optimally based on widely accepted physical entities, is lacking. The exterior algebra $\bigwedge \mathbb{C}^5$ provided an early, remarkably simple finding in this regard. As first demonstrated in [305], with the non-trivial identification $\mathrm{S}(\mathrm{U}(2) \times \mathrm{U}(3)) \cong G_{\mathrm{SM}}$ it yields the Standard Model gauge group representation of the fermions augmented by two trivial representations, described in detail in [91]. This stimulated far-reaching research on grand unified theories extending the Standard Model gauge group [18]. Despite significant experimental efforts, evidence for the related proton decays remains absent [306]. Not aiming for grand unification, a number of mathematical constructions, which in part appear more exotic from the physical viewpoint, give rise to $G_{\mathrm{SM}}$ gauge theory and further Standard Model structures. They are based on e.g. non-commutative geometry [25, 26], the octonions [27–30], or Twistor theory [31]. In contrast, we derive the particle content of one generation of the Standard Model with regard to their gauge and Poincaré transformation behavior in this chapter, based on projective models of established space-time geometries, causality and the spin-statistics relation. Unlike the Standard Model, gauge and Poincaré transformations do not act independently from each other in our approach.

Space-time geometries set the stage for physical models, and can themselves take part in their dynamics. We consider four-dimensional homogeneous (Klein) geometries $(X, O)$, which consist of a space-time manifold $X$ and a structure group $O$ acting transitively on $X$. Physically relevant examples include Poincaré, de Sitter and anti-de Sitter, non-relativistic Galilei and ultra-relativistic Carroll geometries [307]. Deformed through the presence of gravitational matter, more general non-homogeneous space-times give rise to *locally* homogeneous geometries as we show.

Limits of (locally) deformed geometries can appear naturally for general-relativistic space-times, e.g. degenerate near-horizon limits around black holes, or steadily diluted matter for which curved geometries transform towards flat Poincaré geometry. In physics such limits are conventionally taken by contracting the Lie algebras of structure groups, i.e., by *ad hoc* sending individual commutators to zero [307, 308]. Commutators of contracted Lie algebras are in general not matrix commutators anymore, and space-time manifolds remain inconsistently unaltered. Instead, many four-dimensional geometries $(X, O)$ can be considered within the real projective geometry $(\mathbb{RP}^4, \mathrm{PGL}_5\mathbb{R})$. Then a canonical framework exists to discuss their deformations and limits [309], based on matrix products. In the projective setting geometries remain well-defined in limits and merely degenerate; no infinite blow-ups occur for structure groups and projective frames. Physical examples of limits include infinite dilatations in specific directions [310–313] and infinite scale transformations in renormalization group studies.

Quantum field theories can be formulated on curved space-time geometries both in the more usual non-rigorous approaches [314] and in algebraic approaches [315–317]. Much of the algebraic formalism is not necessary for our derivations. We consider quantum fields on the ambient geometry $(\mathbb{RP}^4, \mathrm{PGL}_5\mathbb{R})$, focussing on the involved representation-theoretic structures, which link the quantum fields to the space-time geometry. Let $\mathcal{H}$ be the Hilbert space of the quantum field theory.

**Definition 7.1.1.** *A quantum field* $\hat{\mathcal{O}} = (U, \rho, \{\hat{\mathcal{O}}_\alpha([x]) \,|\, [x] \in \mathbb{RP}^4, \alpha = 1, \ldots, \dim \rho\})$ *consists of a projective unitary* $\mathrm{PGL}_5\mathbb{R}$ *representation* $U$ *on* $\mathcal{H}$ *with adjoint* $^\dagger$, *a finite-dimensional complex* $\mathrm{PGL}_5\mathbb{R}$ *representation* $\rho$, *and a family of linear operators* $\hat{\mathcal{O}}_\alpha([x]) : \mathcal{H} \to \mathcal{H}$, *such that for all* $[x] \in \mathbb{RP}^4$, $[g] \in \mathrm{PGL}_5\mathbb{R}$, $\alpha = 1, \ldots, \dim \rho$:

$$U([g])\hat{\mathcal{O}}_\alpha([x])U^\dagger([g]) = \sum_{\beta=1}^{\dim \rho} \rho_{\alpha\beta}([g^{-1}]) \, \hat{\mathcal{O}}_\beta([g \cdot x]) \,. \tag{7.1}$$

*On the (space-time) geometry* $(X, O) < (\mathbb{RP}^4, \mathrm{PGL}_5\mathbb{R})$ *the quantum field is given by restriction,*

$$\hat{\mathcal{O}}|_{(X,O)} := (U|_O, \rho, \{\hat{\mathcal{O}}_\alpha([x]) \,|\, [x] \in X, \alpha = 1, \ldots, \dim \rho\}) \,. \tag{7.2}$$

This definition canonically generalizes representation-theoretic aspects of the Wightman axioms for quantum fields [318]. We show that such quantum fields transform naturally under deformations and limits of geometries. Fermionic and bosonic super-selection sectors can be extended to quantum fields on the entire ambient geometry

$(\mathbb{RP}^4, \mathrm{PGL}_5\mathbb{R})$. We construct composite quantum fields, discuss their irreducibility as well as the implementation of the spin-statistics relation.

The geometries $(\mathsf{X}, \mathrm{O})$ naturally admit local projective frames which form the related projective frame bundle with structure group $\mathrm{PGL}_5\mathbb{R}$. Connections of this bundle thus correspond to gauge fields with gauge group $\mathrm{PGL}_5\mathbb{R}$. The $\mathrm{PGL}_5\mathbb{R}$ gauge fields can naturally interact with the field operators $\hat{\mathcal{O}}([x])$ via the representation $\rho$. For Poincaré and homogeneous Lorentzian geometries we prove that causality, i.e., space-like separated field operators commute, effectively reduces the $\mathrm{PGL}_5\mathbb{R}$ gauge group to $\mathrm{P}(\mathrm{GL}_2\mathbb{R} \times \mathrm{GL}_3\mathbb{R})$. We further show that for the subgroup $\mathrm{P}(\mathrm{GL}_2\mathbb{R} \times 1) \cong \mathbb{R}_{\neq 0} \times \mathrm{PGL}_2\mathbb{R}$ physical scale invariance breaking appears, which is reminiscent of a Higgs-like mechanism to generate masses for the quantum fields.

Quantum fields can be characterized according to irreducibility of the representation $\rho$. For fermionic statistics all finite-dimensional irreducible representations $\rho$ are given by exterior powers of the fundamental representation $\mathbb{CP}^4_{\mathrm{PGL}_5\mathbb{R}}$. Considered for the reduced gauge group $\mathrm{P}(\mathrm{GL}_2\mathbb{R} \times \mathrm{GL}_3\mathbb{R})$, this is analogous to $\bigwedge \mathbb{C}^5$ as a $\mathrm{S}(\mathrm{U}(2) \times \mathrm{U}(3)) \cong G_{\mathrm{SM}}$ representation and reminiscent of the gauge group representations of the Standard Model fermions. For bosonic statistics Higgs-like scalar fields occur, which carry symmetrized tensor product representations of the $\mathrm{P}(\mathrm{GL}_2\mathbb{R} \times 1) \cong \mathbb{R}_{\neq 0} \times \mathrm{PGL}_2\mathbb{R}$ gauge subgroup. No spontaneous symmetry breaking of larger gauge groups, and no sophisticated mathematical constructions are required for this.

In projective geometry all fields are taken modulo scalar functions on space-time. We conjecture that this implies the possibility to renormalize the theory.

This chapter is organized as follows. In Section 7.2 we motivate and discuss (homogeneous) geometries and their deformations as well as their local appearance in gravity. Section 7.3 is devoted to quantum fields on the ambient real projective geometry $(\mathbb{RP}^4, \mathrm{PGL}_5\mathbb{R})$ through the lens of representations. Superselection sectors, composite quantum fields, their spin-statistics behavior as well as their irreducibility, and the dependence on the ambient geometry are explored. In Section 7.4 we introduce $\mathrm{PGL}_5\mathbb{R}$ gauge fields corresponding to connections of the projective frame bundle. We deduce the causality-based gauge group reduction to $\mathrm{P}(\mathrm{GL}_2\mathbb{R} \times \mathrm{GL}_3\mathbb{R})$ and the physical scale invariance breaking by $\mathrm{P}(\mathrm{GL}_2\mathbb{R} \times 1)$ gauge bosons. We study irreducible fermionic quantum fields and implications for particle physics models. Section 7.5 provides a summary.

## 7.2 Geometries and limits

Mathematically, a (Klein) geometry is defined as a pair $(\mathsf{X}, \mathrm{O})$ of a manifold $\mathsf{X}$ (the model space) and a Lie group $\mathrm{O}$ (the structure group) acting transitively on it, i.e., for any pair of points $x, y \in \mathsf{X}$ there exists $g \in \mathrm{O}$, such that $y = g \cdot x$. Transitivity identifies the model space $\mathsf{X}$ with the homogeneous space $\mathrm{O}/\mathrm{O}_x$, where $\mathrm{O}_x$ denotes the stabilizer of an arbitrary point $x \in \mathsf{X}$.

Similarly, the geometry of a homogeneous physical space-time includes both a space-time manifold and a Lie group of space-time symmetry transformations. Space-time symmetry groups often contain the indefinite orthogonal groups $\mathrm{O}(p, q)$, i.e., the groups

of isometries of the metric tensor

$$- (\mathrm{d}x^{\,1})^2 - \cdots - (\mathrm{d}x^{\,p})^2 + (\mathrm{d}x^{\,p+1})^2 + \cdots + (\mathrm{d}x^{\,p+q})^2 \,, \qquad (7.3)$$

with examples the Lorentz group $O(3,1)$ or the de Sitter group $O(4,1)$. Here, $\mathrm{d}x^{\,1}, \ldots, \mathrm{d}x^{\,p+q}$ denote the canonical 1-forms on $\mathbb{R}^{p+q}$, and $(\mathrm{d}x^{\,j})^2 = \mathrm{d}x^{\,j} \odot \mathrm{d}x^{\,j}$ with $\odot$ the symmetrized tensor product. More generally, the groups

$$\mathrm{O}((p_0, q_0), \ldots, (p_k, q_k)) := \begin{pmatrix} \mathrm{O}(p_0, q_0) & 0 & \cdots & 0 \\ \mathbb{R}^{p_1+q_1} & \mathrm{O}(p_1, q_1) & & 0 \\ \vdots & \vdots & \ddots & \vdots \\ \mathbb{R}^{p_k+q_k} & \mathbb{R}^{p_k+q_k} & \cdots & \mathrm{O}(p_k, q_k) \end{pmatrix} \qquad (7.4)$$

can appear. For reasons which become clear later, we consider projective geometries with projective structure groups $\mathrm{PO}((p_0, q_0), \ldots, (p_k, q_k))$ instead of $\mathrm{O}((p_0, q_0), \ldots, (p_k, q_k))$, defined modulo multiplication by constants. For instance, $\mathrm{PO}((1), (3, 1))$ is isomorphic to the Poincaré group in 3+1 space-time dimensions, the latter isomorphically embedded in $\mathrm{PGL}_5\mathbb{R}$. The elements of $\mathbb{R}^4$, which appear in the lower-left corner of the $\mathrm{PO}((1), (3, 1))$ matrices (cf. Equation (7.4) for $k = 1$, $p_0 + q_0 = 1$, $p_1 = 3$, $q_1 = 1$), then correspond to the usual space-time translations. For an introduction to projective geometry we refer e.g. to [319, 320].

The group $\mathrm{PO}((p_0, q_0), \ldots, (p_k, q_k))$ with $p_0 + q_0 + \cdots + p_k + q_k = m$ acts transitively on the model space

$$\begin{aligned}
&\mathsf{X}((p_0, q_0), \ldots, (p_k, q_k)) \\
&\quad := \{[x_0, \ldots, x_{m-1}] \in \mathbb{RP}^{m-1} \mid -x_0^2 - \cdots - x_{p_0-1}^2 + x_{p_0}^2 + \cdots + x_{p_0+q_0-1}^2 < 0\}. \quad (7.5)
\end{aligned}$$

The pairs

$$\mathsf{G}((p_0, q_0), \ldots) := (\mathsf{X}((p_0, q_0), \ldots), \mathrm{PO}((p_0, q_0), \ldots)) \qquad (7.6)$$

are geometries.[1] We restrict to four-dimensional space-time geometries in this chapter ($m = 5$). For instance, $\mathsf{G}(4, 1)$ with model space $\mathsf{X}(4, 1)$ is the projective model of four-dimensional de Sitter geometry, while $\mathsf{G}((1), (3, 1))$ with

$$\mathsf{X}((1), (3, 1)) = \{[x_0, \ldots, x_4] \mid x_0 \neq 0\} = \mathbb{A}^{3,1} \,, \qquad (7.7)$$

is the projective model of Poincaré geometry, which can be identified with Poincaré geometry itself. $\mathbb{A}^{p,q}$ denotes the $(p+q)$-dimensional affine space with the $(p,q)$-signature metric tensor (7.3), and the identification in Equation (7.7) is via

$$[x_0, \ldots, x_4] = [1, x_1/x_0, \ldots, x_4/x_0] \mapsto (x_1/x_0, \ldots, x_4/x_0) \,. \qquad (7.8)$$

Poincaré geometry comes with the metric tensor $-(\mathrm{d}y^{\,1})^2 - (\mathrm{d}y^{\,2})^2 - (\mathrm{d}y^{\,3})^2 + (\mathrm{d}y^{\,4})^2$, $y_\mu = x_\mu/x_0$ for $\mu = 1, \ldots, 4$, which is the usual Minkowski metric tensor. Galilei geometry

---

[1]Moreover, the geometries $\mathsf{G}((p_0, q_0), \ldots)$ actually come with affine bundle structures as detailed in [309].

$\mathsf{G}((1),(1),(3))$ has the model space $\mathsf{X}((1),(1),(3)) = \mathbb{A}^1 \times \mathbb{A}^3$ and comes with degenerate Galilean structures, ultra-relativistic Carroll geometry $\mathsf{G}((1),(3),(1))$ has the model space $\mathsf{X}((1),(3),(1)) = \mathbb{A}^3 \times \mathbb{A}^1$ and comes with degenerate Carroll structures [307, 321].

### 7.2.1 Deformations and limits

Geometric deformations such as the flattening of $\mathrm{dS}^4$ to $\mathbb{A}^{3,1}$, i.e., the Poincaré limit of de Sitter space-time, or the non-relativistic (Galilei) limit of Poincaré geometry can be described in terms of projective geometries. For this consider a four-dimensional geometry $\mathsf{G} = (\mathsf{X}, \mathrm{O})$ which is a subgeometry of the ambient geometry $(\mathbb{RP}^4, \mathrm{PGL}_5\mathbb{R})$, i.e., $\mathsf{X}$ is an open submanifold of $\mathbb{RP}^4$ and $\mathrm{O}$ is a subgroup of $\mathrm{PGL}_5\mathbb{R}$. All $\mathsf{G}((p_0,q_0),\ldots,(p_k,q_k))$ for $p_0 + q_0 + \cdots + p_k + q_k = 5$ are of this type, for instance.

**Remark 7.2.1.** *While the choice of $(\mathbb{RP}^4, \mathrm{PGL}_5\mathbb{R})$ as the ambient geometry is not unique, the results of this chapter are to some extent independent from the choice of ambient geometries of type $(\mathbb{RP}^{m-1}, \mathrm{PGL}_m\mathbb{R})$ for $m \geq 5$, see Section 7.3.4. Setting $m = 5$ can be seen as a minimal choice.*

Let $[b_n] \in \mathrm{PGL}_5\mathbb{R}$ be a sequence of group elements. On points $[x] \in \mathsf{X}$ the $[b_n]$ act via (projective) matrix multiplication, $[x] \mapsto [b_n \cdot x]$. Group elements $[g] \in \mathrm{O}$ are conjugated by the $[b_n]$, $[g] \mapsto \mathrm{Ad}_{[b_n]}[g] = [b_n \cdot g \cdot b_n^{-1}]$, analogously to a change of basis acting on matrices. On the geometry $\mathsf{G}$ the sequence $[b_n]$ thus acts as

$$\mathsf{G} = (\mathsf{X}, \mathrm{O}) \to ([b_n] \cdot \mathsf{X}, \mathrm{Ad}_{[b_n]}\mathrm{O}) =: [b_n]_*\mathsf{G}, \tag{7.9}$$

with $\mathrm{Ad}_{[b_n]}\mathrm{O} := [b_n] \cdot \mathrm{O} \cdot [b_n^{-1}]$.

The sequence $\mathrm{Ad}_{[b_n]}\mathrm{O}$ converges geometrically to a subgroup $\mathrm{O}' < \mathrm{PGL}_5\mathbb{R}$ for $n \to \infty$, if every $g \in \mathrm{O}'$ is the limit of some sequence $h_n \in \mathrm{Ad}_{[b_n]}\mathrm{O}$, and if every accumulation point of every sequence $h_n \in \mathrm{Ad}_{[b_n]}\mathrm{O}$ lies in $\mathrm{O}'$. Then, $\mathrm{O}'$ is called a conjugacy limit of $\mathrm{O}$. Conjugacy limits are identical to limits on the space of closed subgroups of $\mathrm{PGL}_5\mathbb{R}$ with respect to the Chabauty topology; for details see e.g. [309, 322–324]. The sequence $[b_n]_*\mathsf{G} \subset (\mathbb{RP}^4, \mathrm{PGL}_5\mathbb{R})$ converges to the geometry $\mathsf{G}' = (\mathsf{X}', \mathrm{O}')$, if $\mathrm{Ad}_{[b_n]}\mathrm{O}$ converges geometrically to $\mathrm{O}'$ and there exists[2] $z \in \mathsf{X}' \subset \mathbb{RP}^4$ such that for all $n$ sufficiently large $z \in [b_n] \cdot \mathsf{X}$. All such limits of $\mathsf{G}((p_0,q_0),\ldots,(p_k,q_k)) \subset (\mathbb{RP}^4, \mathrm{PGL}_5\mathbb{R})$ have been classified and are up to conjugacy[3] within $(\mathbb{RP}^4, \mathrm{PGL}_5\mathbb{R})$ of the form $\mathsf{G}((p_0',q_0'),\ldots,(p_l',q_l'))$ for $l \geq k$, $p_0 + \cdots + p_k = p_0' + \cdots + p_l'$ and $q_0 + \cdots + q_k = q_0' + \cdots + q_l'$, potentially after exchanging some $(p_i,q_i)$ with $(q_i,p_i)$ [309]. Such a limit geometry is called a refinement of $\mathsf{G}((p_0,q_0),\ldots,(p_k,q_k))$.

On Lie algebra level the $[b_n]$ act analogously. They map $X \in \mathfrak{o}$ to $\mathrm{Ad}_{[b_n]}X$, $\mathfrak{o}$ the Lie algebra of $\mathrm{O}$. With $\mathrm{O} \to \mathrm{O}'$ a conjugacy limit via $[b_n] \in \mathrm{PGL}_5\mathbb{R}$ and $\mathfrak{o}' = \mathrm{Lie}(\mathrm{O}')$, in Appendix 7.A and [325] it is shown that

$$\mathfrak{o}' = \lim_{n\to\infty} [b_n] \cdot \mathfrak{o} \cdot [b_n^{-1}], \tag{7.10}$$

convergence defined as for the geometric convergence of Lie groups.

---

[2]This condition exemplifies the *hit-and-miss* character of the Chabauty topology [325].
[3]For the model space actually up to multiplication of points by a $\mathrm{PGL}_5\mathbb{R}$ element.

**Example 7.2.2.** *(i) To explore the deformation of Poincaré geometry* $\mathsf{G}((1), (3, 1))$ *by*

$$[b_n] = \mathrm{P} \begin{pmatrix} e^{-n} & & \\ & 1_{3\times 3} & \\ & & e^{-n} \end{pmatrix}, \tag{7.11}$$

*focus on a boost generator of the Poincaré Lie algebra such as[4]*

$$[K] = \mathrm{P} \begin{pmatrix} 0 & & & & \\ & 0 & & & \\ & & 0 & & \\ & & & 0 & -\mathrm{i} \\ & & & -\mathrm{i} & 0 \end{pmatrix}. \tag{7.12}$$

*The element* $[b_n]$ *acts via conjugation on* $[K]$, *with the non-trivial submatrix mapped as*

$$\begin{pmatrix} 0 & -\mathrm{i} \\ -\mathrm{i} & 0 \end{pmatrix} \mapsto \begin{pmatrix} 0 & -\mathrm{i}\, e^{n} \\ -\mathrm{i}\, e^{-n} & 0 \end{pmatrix}. \tag{7.13}$$

*Multiplication by* $\exp(-n)$ *yields the well-defined* $n \to \infty$ *limit*

$$\begin{pmatrix} 0 & -\mathrm{i} \\ 0 & 0 \end{pmatrix}. \tag{7.14}$$

*The multiplication by* $\exp(-n)$ *is an identity map in the employed projective setting. In the non-projective setting the limit matrix would contain diverging elements. After application of the coordinate index permutation* $\tau = (0)\,(1\,2\,3\,4)$ *in cycle notation, in the* $n \to \infty$ *limit the structure group* $\mathrm{Ad}_{[b_n]}\mathrm{PO}((1), (3, 1))$ *becomes*

$$\tau_* \lim_{n\to\infty} \mathrm{Ad}_{[b_n]}\mathrm{PO}((1), (3, 1)) = \mathrm{PO}((1), (1), (3)), \tag{7.15}$$

*which can be identified with the Galilei group. In particular, the limit process turns Lorentz boosts with generators such as (7.12) into Galilean velocity additions as generated by the projective matrix corresponding to (7.14). The model space* $\mathsf{X}((1), (3, 1))$ *is invariant under* $[b_n]$, *such that for* $n \to \infty$ *Galilei geometry is retrieved:*

$$[b_n]_* \mathsf{G}((1), (3, 1)) \to \tau_*^{-1} \mathsf{G}((1), (1), (3)). \tag{7.16}$$

*(ii) Consider*

$$[b_n] = \mathrm{P} \begin{pmatrix} e^{-4n} & \\ & e^{n} \cdot 1_{4\times 4} \end{pmatrix} \tag{7.17}$$

*acting on projective de Sitter geometry* $\mathsf{G}(4, 1)$. *Let* $[x_0, \dots, x_4] \in [b_n] \cdot \mathsf{X}(4, 1)$, *i.e.,*

$$-\,e^{8n} x_0^2 - e^{-2n} x_1^2 - e^{-2n} x_2^2 - e^{-2n} x_3^2 + e^{-2n} x_4^2 < 0. \tag{7.18}$$

---

[4]As everywhere in this dissertation, we employ physics conventions for Lie algebras, such that a simply connected Lie group $G$ has Lie algebra $\mathfrak{g}$ and $G = \exp(\mathrm{i}\mathfrak{g})$.

*In the projective setting, the left-hand side is identical to*

$$- x_0^2 - e^{-10n} x_1^2 - e^{-10n} x_2^2 - e^{-10n} x_3^2 + e^{-10n} x_4^2 \,, \tag{7.19}$$

*yielding the well-defined limit constraint $x_0 \neq 0$ for $n \to \infty$. Thus, the model space $\mathsf{X}(4,1)$ changes in the $n \to \infty$ limit to $\mathsf{X}((1),(3,1)) = \mathbb{A}^{3,1}$. In the non-projective setting the $n \to \infty$ limit of Equation (7.18) would have led again to an infinite blow-up. The projective formulation generally prevents singular behavior for limit processes. Explicit computation shows that for $n \to \infty \,\mathrm{Ad}_{[b_n]}\mathrm{PO}(4,1)$ converges geometrically to the Poincaré group. The limit process flattens the de Sitter model space, and the structure group changes accordingly. The limit geometry of projective de Sitter geometry deformed by the $[b_n]$ of (7.17) is Poincaré geometry $\mathsf{G}((1),(3,1))$.*

Given a conjugacy limit $\mathrm{O} \to \mathrm{O}'$ with Lie algebras $\mathfrak{o} \to \mathfrak{o}'$, we show in Appendix 7.A that $\mathfrak{o}'$ is isomorphic to a contraction[5] of $\mathfrak{o}$. Yet, contractions and conjugacy limits of Lie algebras are not equivalent. While contractions can render any (here 10-dimensional) Lie algebra *Abelian* by trivializing all commutators, conjugacy limits of any $\mathfrak{o}((p_0, q_0), \dots, (p_k, q_k))$ terminate up to conjugacy at the final limit $\mathfrak{o}((1),(1),\dots,(1))$, which for $p_0 + q_0 + \cdots + p_k + q_k = 5$ is a 3-step *non-Abelian* nilpotent Lie algebra. No further limit refinement of the latter is possible by any sequence $[b_n] \in \mathrm{PGL}_5\mathbb{R}$. Arguing in favor of conjugacy limits, they appear naturally from canonical constructions in the framework of geometries, which is in contrast to contractions.

### 7.2.2 Projective frames and limits

Let us consider projective vector fields and related projective frames. We define projective vector fields on a geometry model space $\mathsf{X}$ as equivalence classes $[W]$ of vector fields on $\mathsf{X}$, which are locally defined up to the equivalence relation $W \sim \tilde{W}$ if there exists $\lambda \in C^\infty(\mathsf{X}, \mathbb{R}_{\neq 0})$ such that for all $[x] \in \mathsf{X}$: $\tilde{W}([x]) = \lambda([x]) W([x])$, in short $\tilde{W} = \lambda W$.

**Remark 7.2.3.** *This definition of projective vector fields is consistent with the more common definition of projectively related torsion-free connections on a Riemannian manifold. According to [327–329] two torsion-free connections $\nabla, \tilde{\nabla}$ on $\mathsf{X}$ are projectively related if they have the same geodesics as point sets, i.e., up to parametrization. Let $\lambda \in C^\infty(\mathsf{X}, \mathbb{R}_{\neq 0})$, $W \in \mathfrak{X}(\mathsf{X})$ and $\tilde{W} = \lambda W$. Given the connection $\nabla$, for every $[x] \in \mathsf{X}$ there is a unique geodesic $\gamma : (-\epsilon, \epsilon) \to \mathsf{X}$, $\epsilon > 0$, with $\gamma(0) = [x]$ and $\mathrm{d}\gamma(s)/\mathrm{d}s |_{s=0} = W([x])$. Similarly, $\tilde{W}$ induces a geodesic $\tilde{\gamma} : (-\tilde{\epsilon}, \tilde{\epsilon}) \to \mathsf{X}$, $\tilde{\epsilon} > 0$, with $\tilde{\gamma}(0) = [x]$ and*

$$\left.\frac{\mathrm{d}}{\mathrm{d}s}\right|_{s=0} \tilde{\gamma}(s) = \tilde{W}([x]) = \lambda([x])W([x]) = \lambda([x])\left.\frac{\mathrm{d}}{\mathrm{d}s}\right|_{s=0} \gamma(s) \,. \tag{7.20}$$

*The geodesics $\gamma$ and $\tilde{\gamma}$ are the same as sets. Then there exists a torsion-free connection $\tilde{\nabla}$ with geodesic $\tilde{\gamma}$, such that $\nabla, \tilde{\nabla}$ are projectively related [329]. Thus, projectively equivalent vector fields give rise to projectively related connections.*

---

[5]A contraction of a Lie algebra $\mathfrak{g} = (\mathcal{V}, [\cdot, \cdot])$ is defined by sending commutators $[X, Y] \to 0$ for some $X, Y \in \mathcal{V}$, such that $\mathcal{V}$ together with the limiting commutators consistently defines a Lie algebra [308, 326].

Locally, projective vector fields are linear combinations of projective frame vectors. A projective frame on the four-dimensional space $\mathsf{X}$ is defined from a frame $\{e_1, \ldots, e_4\}$ on $\mathsf{X}$ as

$$\{([x], \{[e_1([x])], \ldots, [e_4([x])], [e_1([x]) + \cdots + e_4([x])]\}) \mid [x] \in \mathsf{X}\}. \tag{7.21}$$

In the projective setting, any set $\{[e_A] \mid A = 1, \ldots, 5\}$ is of this form, if $(e_A)_{A \neq B}$ defines a frame on $\mathsf{X}$ for every $B = 1, \ldots, 5$, since $[e_A] = [\lambda_A e_A]$ for all $\lambda_A \in C^\infty(\mathsf{X}, \mathbb{R}_{\neq 0})$, $A = 1, \ldots, 5$, such that $[e_1 + \cdots + e_4]$ is a general linear combination of $[e_1], \ldots, [e_4]$.

**Remark 7.2.4.** *Five projective vector fields are required to uniquely specify a projective frame on the four-dimensional model space $\mathsf{X}$ by the following argument [320]. Assume that $[e_\mu] = [f_\mu]$ for all $\mu = 1, \ldots, 4$. Then, $e_\mu = \lambda_\mu f_\mu$ for $\lambda_\mu \in C^\infty(\mathsf{X}, \mathbb{R}_{\neq 0})$. With the fifth projective vector field $[e_1 + \cdots + e_4] = [f_1 + \cdots + f_4]$ we have $e_1 + \cdots + e_4 = \lambda(f_1 + \cdots + f_4)$. Together this yields $0 = (\lambda_1 - \lambda)f_1 + \cdots + (\lambda_4 - \lambda)f_4$, such that by linear independence of the $f_\mu$: $\lambda_\mu = \lambda$ for all $\mu = 1, \ldots, 4$. In the projective setting the two frames agree.*

Projective vector fields are generally different from non-projective vector fields on $\mathsf{X}$, as the following example demonstrates.

**Example 7.2.5.** *Consider Poincaré geometry $\mathsf{G}((1), (3, 1))$. The map $[1, x_1/x_0, \ldots, x_4/x_0] \mapsto (x_1/x_0, \ldots, x_4/x_0)$ identifies $\mathsf{X}((1), (3, 1))$ with $\mathbb{A}^{3,1}$. With $y_\mu := x_\mu/x_0$, $\mu = 1, \ldots, 4$, the corresponding standard vector fields on $\mathbb{A}^{3,1}$ are given by $\partial/\partial y_\mu = x_0 \, \partial/\partial x_\mu$. A projective vector field $[W]$ on $\mathsf{X}((1), (3, 1))$ is given by the linear combination*

$$[W([x])] = \sum_{\mu=1}^{4} W_\mu([x]) \left[\frac{\partial}{\partial y_\mu}\right] + W_5([x]) \left[\sum_{\mu=1}^{4} \frac{\partial}{\partial y_\mu}\right]. \tag{7.22}$$

*Generally, $W_5([x])$ can be non-zero, such that five independent functions on $\mathsf{X}((1), (3, 1))$ appear, taken modulo the projective equivalence relation $\sim$.*

*This is in contrast to non-projective vector fields. A non-projective vector field $Z$ on $\mathsf{X}((1), (3, 1))$ can be thought of as a vector field on the tangent space of the four-dimensional submanifold $\{(1, y_1, \ldots, y_4) \in \mathbb{R}^5\}$, for which only four independent components appear.*

We denote the set of projective frames on $\mathsf{X}$ by $\mathcal{P}(\mathsf{X})$, which can be given a smooth structure. With the projection map

$$\pi : ([x], \{[e_1([x])], \ldots, [e_4([x])], [e_1([x]) + \cdots + e_4([x])]\}) \mapsto [x], \tag{7.23}$$

the fiber bundle $\mathcal{P}(\mathsf{X}) \to \mathsf{X}$ is obtained.

Matrices $c \in \mathrm{GL}_4\mathbb{R}$ act on local frame vectors $e_1([x]), \ldots, e_4([x])$, $[x] \in \mathsf{X}$, via matrix multiplication, $e_\mu([x]) \mapsto c \cdot e_\mu([x])$ for $\mu = 1, \ldots, 4$. This action is transitive: any two local frames on $\mathsf{X}$ are connected by a general linear transformation. Similarly, the group $\mathrm{PGL}_5\mathbb{R}$ acts on fibers of the bundle $\mathcal{P}(\mathsf{X}) \to \mathsf{X}$. For the action let $\{[\partial_A] \mid A = 1, \ldots, 5\}$ denote the standard projective frame on $\mathsf{X}$, e.g. $\{[\partial/\partial y_1], \ldots, [\partial/\partial y_4], [\partial/\partial y_1 + \cdots + \partial/\partial y_4]\}$ for the case of $\mathsf{X} = \mathsf{X}((1), (3, 1))$. Locally, any frame $\{[e_1], \ldots, [e_4], [e_5]\}$ is a linear combination of the $[\partial_A]$, $A = 1, \ldots, 5$, defined up to prefactor. This yields a projective invertible $5 \times 5$

matrix, on which elements of $\mathrm{PGL}_5\mathbb{R}$ act via matrix multiplication. The action is transitive, giving the projective frame bundle over X, i.e., the principal $\mathrm{PGL}_5\mathbb{R}$-bundle

$$\mathrm{PGL}_5\mathbb{R} \to \mathcal{P}(\mathsf{X}) \to \mathsf{X}. \tag{7.24}$$

To study the behavior of frames under deformations of geometries, let $[b_n] \in \mathrm{PGL}_5\mathbb{R}$ and $\{[e_1], \dots\}$ be a projective frame on X. The frame vector fields transform for all $A = 1, \dots, 5$ as

$$([x], [e_A([x])]) \mapsto ([b_n \cdot x], [b_n] \cdot [e_A([x])]), \tag{7.25}$$

with $[b_n] \cdot [e_A([x])]$ the described matrix multiplication for projective frame vectors. Neglecting infinite oscillatory behavior, $n \to \infty$ limits of vector fields $[b_n] \cdot [e_A([x])]$ are well-defined, since infinite blow-ups of components with respect to the standard frame on $\mathbb{RP}^4$ are automatically cured in the projective setting. Yet, the limit matrices $\lim_{n\to\infty}[b_n]$ can decrease in rank, cf. the $n \to \infty$ limit of the matrix (7.11), whose rank decreases from 5 to 3. Projective frames can thus degenerate in limits, then spanning up strict subspaces of the projective tangent spaces of X.

We define projective tensor fields on X analogously to projective vector fields modulo multiplication by $C^\infty(\mathsf{X}, \mathbb{R}_{\neq 0})$ elements. On projective tensor fields such as projective metrics or projective differential forms deformations of geometries act as tensor contractions with the $[b_n]$ or $[b_n^{-1}]$, depending on the projective tensor field under consideration. Analogously to projective vector fields, projective tensor fields can degenerate in limit processes, but remain well-defined in the absence of infinite oscillations of the $[b_n]$. For instance, no singularities appear for metrics in the projective formulation. This is in contrast to standard general relativity, where singularities can render the theory inconsistent in their surrounding neighborhoods.

### 7.2.3 Locally homogeneous geometries from gravity

General-relativistic space-time manifolds are rarely homogeneous spaces. We argue that homogeneous geometries are realized locally in the presence of gravitational matter, based on the projective analogue of Einstein-Cartan gravity. To this end, we expect that many of the following derivations for homogeneous geometries actually hold in more generality.

In standard Einstein-Cartan gravity for four-dimensional manifolds $M$ [89] the frame fields, i.e., $\mathrm{GL}_4\mathbb{R}$-valued sections of the frame bundle, and the Cartan connections appear as the independent degrees of freedom. The related projective formulation can be based on projective frames and connections of the projective frame bundle $\mathrm{PGL}_5\mathbb{R} \to \mathcal{P}(M) \to M$. The physically realized projective frames and connections are expected to solve certain equations of motion, whose specific form is irrelevant for the present argument and will be discussed elsewhere.

Assume that $M \subset \mathbb{RP}^4$, which applies to all four-dimensional geometries considered in this chapter as well as their (local) deformations and limits. Intuitively speaking, infinitesimal space-time deformations can be considered irrelevant for any physical measurement. It is thus physically reasonable to assume that in an *arbitrarily small* open subset $N \subset M$ a

non-degenerate geometry $\mathsf{G}(p,q)$ for $p+q = 5$ is realized,[6] i.e., there exists an embedding $N \hookrightarrow \mathsf{X}(p,q)$, such that $\mathsf{G}(p,q)$ induces an action of a Lie subgroup $H < \mathrm{PO}(p,q)$ on $N$ which includes the local isotropy groups $\mathrm{PO}(p,q)_{[x]} < H$ for all $[x] \in N$. Otherwise an infinitesimal modification of $M$ is necessary, which is physically irrelevant. The symmetry group $\mathrm{PO}(p,q)$ appears as the set of fixed points of the involution $\tau = \sigma \circ \theta$, with $\theta([h]) = [(h^{-1})^T]$ the Cartan involution and $\sigma([h]) = [JhJ^{-1}]$ with

$$ J = \begin{pmatrix} -1_{p \times p} & \\ & 1_{q \times q} \end{pmatrix}, \tag{7.26} $$

for all $[h] \in \mathrm{PGL}_5\mathbb{R}$.

Choose an extended neighborhood $N'$ of $N$, not required to be open or closed, such that we can consider a projective frame on $N'$, which can be identified with a section $N' \ni ([x] \mapsto [g([x])])$ of the projective frame bundle $\mathrm{PGL}_5\mathbb{R} \to \mathcal{P}(N') \to N'$. $N$ locally realizing the geometry $\mathsf{G}(p,q)$, we can choose $[g([x])]$ so that $[g([x])] = 1$ for all $[x] \in N$. For such a section $[g]$ the deformed local involution $([g]_*\sigma)_{[x]}$ at $[x] \in N'$ is defined for all $[h] \in \mathrm{PGL}_5\mathbb{R}$ as

$$ ([g]_*\sigma)_{[x]}([h]) = (\mathrm{Ad}_{[g([x])]}[J])[h](\mathrm{Ad}_{[g([x])]}[J^{-1}]). \tag{7.27} $$

The Cartan involution $\theta$ deforms locally to $([g]_*\theta)_{[x]}([h]) = \mathrm{Ad}_{[g([x])]}[(h^{-1})^T]$. We set $[g]_*\tau = ([g]_*\sigma) \circ ([g]_*\theta)$. Its fixed point set at $[x]$ is $\mathrm{Ad}_{[g([x])]}\mathrm{PO}(p,q)$, i.e., the local conjugation of $\mathrm{PO}(p,q)$ by $[g([x])]$, which we encountered before but globally. The local geometry at $[x] \in N'$ is $[g([x])]_*\mathsf{G}(p,q)$.

**Remark 7.2.6.** *While on $N$ we are able to choose a metric with isometry group $\mathrm{PO}(p,q)$, on the larger $N'$ it may not be possible to choose a metric with isometry group $\mathrm{Ad}_{[g([x])]}\mathrm{PO}(p,q)$ at all $[x] \in N'$. In principle, the local isometry groups need not even include the local isotropy groups.*

If $M$ is parallelizable, we can extend $N'$ to the full $M$, since $[g]$ can be defined globally. For manifolds $M$ with non-trivial topology (yielding space-time horizons) we need multiple such extended neighborhoods $N'$, related to the minimal atlas of $M$ and potentially modified infinitesimally in order to locally realize some of the semi-simple symmetry groups $\mathrm{PO}(p,q)$. Towards boundaries of $N'$ limits of geometries might be required, which can readily be taken in the given framework.

## 7.3   Quantum fields on deformed geometries

Quantum fields are tied to space-time geometries by means of their behavior under space-time symmetry transformations, which involves projective unitary representations of the space-time symmetry groups acting on the Hilbert space [8]. Irreducibility of the representations characterizes fundamental quantum particles, and the Hilbert space of the theory is constructed from these. Geometries thus dictate the types of particles that can occur, and the structure of the Hilbert space. For instance, in Poincaré geometry particles

---

[6]For instance, it is expected that the universe is asymptotically de Sitter at late cosmological times [330].

are described by the well-known massive spin and massless helicity representations of the Poincaré group.

We introduce quantum fields on four-dimensional subgeometries of $(\mathbb{RP}^4, \mathrm{PGL}_5\mathbb{R})$ in Section 7.3.1. These as well as related field operator correlators transform naturally under deformations and limits. Topological superselection sectors appear for the related representations of $\mathrm{PGL}_5\mathbb{R}$, described in Section 7.3.2. We introduce composite and irreducible quantum fields in Section 7.3.3. In Section 7.3.4 we discuss the dependence on the ambient geometry.

### 7.3.1 Quantum fields and their correlators

We focus on representation-theoretic properties of quantum fields related to space-time geometries and do not aim for their complete mathematical characterization. Let $\mathcal{H}$ be a fixed, given Hilbert space, on which the quantum field theory can be consistently formulated. We omit the discussion of its specific form in this chapter. $\mathcal{U}(\mathcal{H})$ denotes the set of unitary linear operators on $\mathcal{H}$.

**Definition 7.3.1.** *A quantum field $\hat{\mathcal{O}} = (U, \rho, \{\hat{\mathcal{O}}_\alpha([x]) \,|\, [x] \in \mathbb{RP}^4, \alpha = 1, \ldots, \dim\rho\})$ consists of a projective unitary $\mathrm{PGL}_5\mathbb{R}$ representation $U : \mathrm{PGL}_5\mathbb{R} \to \mathcal{U}(\mathcal{H})$ with adjoint $^\dagger$, a finite-dimensional complex $\mathrm{PGL}_5\mathbb{R}$ representation $\rho$, and a family of linear operators $\hat{\mathcal{O}}([x]) = (\hat{\mathcal{O}}_1([x]), \ldots, \hat{\mathcal{O}}_{\dim\rho}([x]))$ with $\hat{\mathcal{O}}_\alpha([x]) : \mathcal{H} \to \mathcal{H}$, such that for all $[x] \in \mathbb{RP}^4$, $[g] \in \mathrm{PGL}_5\mathbb{R}$, $\alpha = 1, \ldots, \dim\rho$:*

$$U([g])\hat{\mathcal{O}}_\alpha([x])U^\dagger([g]) = \sum_{\beta=1}^{\dim\rho} \rho_{\alpha\beta}([g^{-1}])\hat{\mathcal{O}}_\beta([g \cdot x]). \tag{7.28}$$

*Often we omit the component indices $\alpha, \beta$ from notations. When denoted as $\hat{\mathcal{O}}$, $\hat{\mathcal{O}} = (U, \rho, \{\hat{\mathcal{O}}([x])\})$ is understood. The $\hat{\mathcal{O}}_\alpha([x])$ and $\hat{\mathcal{O}}([x])$ are synonymously called* field operators. *All adjoint field operators $\hat{\mathcal{O}}_\alpha^\dagger([x])$ are assumed to exist. On the geometry $(\mathsf{X}, \mathsf{O}) < (\mathbb{RP}^4, \mathrm{PGL}_5\mathbb{R})$ the quantum field is given by restriction,*

$$\hat{\mathcal{O}}|_{(\mathsf{X}, \mathsf{O})} := (U|_\mathsf{O}, \rho, \{\hat{\mathcal{O}}_\alpha([x]) \,|\, [x] \in \mathsf{X}\}). \tag{7.29}$$

Upon restriction to the geometry $(\mathsf{X}, \mathsf{O})$, no restriction of the representation $\rho$ to $\rho|_\mathsf{O}$ is included in order to be able to consistently include $\mathrm{PGL}_5\mathbb{R}$ gauge transformations later.

**Remark 7.3.2.** *While in Definition 7.3.1 $U$ is a projective unitary representation, $\rho$ is non-projective. This is sensible, since if $\rho$ was projective, its multiplier would be equivalent to the trivial one, see Proposition 7.3.7. The finite dimensionality of $\rho$ is part of established formal approaches [318].*

To restrict to the formal minimum, in Definition 7.3.1 no assumptions are made on the smoothness of field operator expectation values smeared by suitable test functions as for Wightman field operators. No equal-time commutation relations are discussed, whose formulation for curved geometries would rest on an observer-specific, distinguished time direction as available for globally hyperbolic space-times [331]. Implications of causality

for Lorentzian geometries will be discussed in Section 7.4. As part of a complete algebraic characterization of quantum fields, Definition 7.3.1 can be naturally incorporated in Haag-Kastler conditions for nets of von Neumann operator algebras, extended to the ambient geometry $(\mathbb{RP}^4, \mathrm{PGL}_5\mathbb{R})$ [84, 318, 332].

Definition 7.3.1 extends the standard behavior of quantum fields under Poincaré transformations, as the following example demonstrates.

**Example 7.3.3.** *Let* $V : \mathrm{PO}((1),(3,1)) \to \mathcal{U}(\mathcal{H}')$ *be a projective unitary irreducible representation of the Poincaré group acting on some Hilbert space* $\mathcal{H}'$. *These are induced from finite-dimensional irreducible representations of the little group* $\mathrm{O}(3,1)$ *[8, 333]. Lorentz transformations act on the representation space of the little group and translations act on the induced function space. In the projective picture, a Poincaré transformation*

$$[(\Lambda, t)] := \mathrm{P}\begin{pmatrix} 1 & 0 \\ t & \Lambda \end{pmatrix} \in \mathrm{PO}((1),(3,1)) \tag{7.30}$$

*acts for the unitary vector representation* $V$ *of the Poincaré group on field operators* $[\hat{A}([x])]$ *(defined for all* $[x] \in \mathbb{RP}^4$*) corresponding to a projective vector field as*

$$V([(\Lambda, t)])[\hat{A}([x])]V^\dagger([(\Lambda, t)]) = [(\Lambda, t)]^{-1} \cdot [\hat{A}([\Lambda \cdot x + t])]. \tag{7.31}$$

*Here, the action of* $[(\Lambda, t)]^{-1} = [(\Lambda^{-1}, -\Lambda^{-1} \cdot t)]$ *on* $[\hat{A}([\Lambda \cdot x + t])]$ *is via the fundamental representation* $\mathbb{CP}^4_{\mathrm{PGL}_5\mathbb{R}}|_{\mathrm{PO}((1),(3,1))}$ *of* $\mathrm{PO}((1),(3,1))$ *acting on* $\mathbb{CP}^4$ *via (projective) matrix multiplication.*

*Following Example 7.2.5,* $[\hat{A}]$ *has five independent components* $\hat{A}_B$, $B = 1,\dots,5$, *as a projective vector field. Equation* (7.31) *yields for* $\mu = 1,\dots,4$:

$$V([(\Lambda, t)])\hat{A}_{\mu+1}(y)V^\dagger([(\Lambda, t)]) = \sum_{\nu=1}^4 (\Lambda^{-1})_\mu{}^\nu \hat{A}_{\nu+1}(\Lambda \cdot y + t), \tag{7.32}$$

$(\Lambda^{-1})_\mu{}^\nu$ *denotes the* $\mu\nu$ *matrix element of* $\Lambda^{-1}$. *This is the usual transformation behavior of a vector field on Minkowski space-time.*

$V$ *induces a unitary representation* $U : \mathrm{PGL}_5\mathbb{R} \to \mathcal{U}(\mathcal{H})$, $\mathcal{H}$ *the induced Hilbert space. The tuple* $(U, \mathbb{CP}^4_{\mathrm{PGL}_5\mathbb{R}}, \{[\hat{A}([x])] \,|\, [x] \in \mathbb{RP}^4\})$ *is a quantum field in the sense of Definition 7.3.1. Restricted to Poincaré geometry, the transformation behavior* (7.28) *implies Equation* (7.31).

Quantum fields transform naturally under geometry deformations, specified by the following lemma.

**Lemma 7.3.4.** *Consider a quantum field* $\hat{\mathcal{O}}$ *on the geometry* $\mathsf{G} = (\mathsf{X}, \mathsf{O})$, *and let* $[b_n] \in \mathrm{PGL}_5\mathbb{R}$. *The quantum field on* $[b_n]_*\mathsf{G}$ *is given by restriction to* $[b_n]_*\mathsf{G} = ([b_n] \cdot \mathsf{X}, \mathrm{Ad}_{[b_n]}\mathsf{O})$. *In particular,* $\hat{\mathcal{O}}|_{[b_n]_*\mathsf{G}}$ *comes with the projective* $\mathrm{Ad}_{[b_n]}\mathsf{O}$ *representation* $U|_{\mathrm{Ad}_{[b_n]}\mathsf{O}}$. *On the limit geometry* $(\mathsf{X}', \mathsf{O}') = \lim_{n\to\infty}([b_n]_*\mathsf{G})$, *the geometry-restricted quantum fields become* $\hat{\mathcal{O}}|_{(\mathsf{X}',\mathsf{O}')}$ *with the projective* $\mathsf{O}'$ *representation* $U|_{\mathsf{O}'}$.

*Proof.* Let $\omega$ be the (Schur) multiplier of the projective representation $U$. A geometry deformation via $[b_n] \in \mathrm{PGL}_5\mathbb{R}$ acts on a field operator $\hat{\mathcal{O}}([x])$, transformed via $[g] \in$

PGL$_5\mathbb{R}$, as

$$U([g])\hat{\mathcal{O}}([x])U^\dagger([g]) \mapsto U([b_n])U([g])\hat{\mathcal{O}}([x])U^\dagger([g])U^\dagger([b_n])$$
$$= \omega([b_n], [g])\omega([b_n g], [b_n^{-1}])U([b_n g b_n^{-1}])U([b_n])\hat{\mathcal{O}}([x])U^\dagger([b_n])$$
$$\times \omega([b_n], [g^{-1}])\omega([b_n g^{-1}], [b_n^{-1}])U^\dagger([b_n g b_n^{-1}])$$
$$= U([b_n g b_n^{-1}])U([b_n])\hat{\mathcal{O}}([x])U^\dagger([b_n])U^\dagger([b_n g b_n^{-1}]) , \tag{7.33}$$

where we used multiplier cyclicity, i.e.,

$$\omega([b_n], [g])\omega([b_n g], [b_n^{-1}]) = \omega([b_n], [g b_n^{-1}])\omega([g], [b_n^{-1}]) , \tag{7.34}$$

and

$$\omega([b_n], [g^{-1}])U([b_n g^{-1}]) = U([b_n])U([g^{-1}])$$
$$= (U([g])U([b_n^{-1}]))^{-1} = \frac{1}{\omega([g], [b_n^{-1}])}U([b_n g^{-1}]) , \tag{7.35}$$

analogously for $\omega([b_n g^{-1}], [b_n^{-1}])$. The field operator $\hat{\mathcal{O}}([x])$ is thus changed to

$$U([b_n])\hat{\mathcal{O}}([x])U^\dagger([b_n]) = \rho([b_n^{-1}])\hat{\mathcal{O}}([b_n \cdot x]) , \tag{7.36}$$

and the symmetry group O is conjugated by $[b_n]$.

We prove in Appendix 7.B that the conjugacy limit of $U|_\mathrm{O}$ via $U([b_n])$ inside of $U$ is the same as $U|_{\mathrm{O}'}$ up to multiplier, i.e., the diagram

$$
\begin{array}{ccc}
\lim_{n\to\infty} \mathrm{Ad}_{[b_n]} : & \mathrm{O} \longrightarrow \mathrm{O}' & \\
& \left\downarrow{\scriptstyle U|_\mathrm{O}} \qquad \left\downarrow{\scriptstyle U|_{\mathrm{O}'}} & \\
\lim_{n\to\infty} \mathrm{Ad}_{U([b_n])} : & U(\mathrm{O}) \longrightarrow [U(\mathrm{O}')] &
\end{array}
\tag{7.37}
$$

commutes. $[U(\mathrm{O}')]$ denotes $U(\mathrm{O}')$ modulo U(1) prefactors. In fact, by the considerations of Appendix 7.B multipliers of $U|_{\mathrm{O}'}$ are limits of multipliers of $U$, which can become trivial. The analogous diagram for $\rho$ commutes without modulo U(1) multipliers. No faithfulness of $U$ or $\rho$ is necessary for this. The quantum fields thus change in the geometry limit from $\hat{\mathcal{O}}|_{(\mathrm{X},\mathrm{O})}$ to $\hat{\mathcal{O}}|_{(\mathrm{X}',\mathrm{O}')}$. $\qquad\square$

An algebra $\mathfrak{A}(\mathsf{X})$ of field operator correlators can formally be defined as

$$\mathfrak{A}(\mathsf{X}) := \left\{ \sum_{\ell=1}^{L} \int_{\mathsf{X}^\ell} a_\ell([x_{j_1}^{(\ell)}], \ldots, [x_{j_\ell}^{(\ell)}])\rho_{\alpha_1\beta_1}^{(\dagger)}([g_1^{(\ell)}])\hat{\mathcal{O}}_{\beta_1}^{(\dagger)}([x_{j_1}^{(\ell)}]) \circ \cdots \right.$$

$$\circ \rho_{\alpha_\ell\beta_\ell}^{(\dagger)}([g_\ell^{(\ell)}])\hat{\mathcal{O}}_{\beta_\ell}^{(\dagger)}([x_{j_\ell}^{(\ell)}]) \, \mathrm{d}^4[x_{j_1}^{(\ell)}]\cdots\mathrm{d}^4[x_{j_\ell}^{(\ell)}] \,\middle|\, \forall\ell : [g_\ell^{(\ell)}] \in \mathrm{PGL}_5\mathbb{R},$$

$$\left. \int_{\mathsf{X}^\ell} a_\ell([x_{j_1}^{(\ell)}], \ldots, [x_{j_\ell}^{(\ell)}]) \, \mathrm{d}^4[x_{j_1}^{(\ell)}]\cdots\mathrm{d}^4[x_{j_\ell}^{(\ell)}] < \infty, L \in \mathbb{N}_{>0} \right\}, \tag{7.38}$$

where we imply the summation over repeated indices $\beta_j$, and the superscript (†) denotes taking the adjoint or not, which must be taken consistently for $\rho$ and the corresponding field operator $\hat{\mathcal{O}}([x])$ involved in the matrix product. By construction $a_\ell([x_{j_1}^{(\ell)}], \ldots, [x_{j_\ell}^{(\ell)}])$ can be a distribution on $\mathsf{X}^\ell$, in particular also a product of $\ell$ Dirac $\delta$-functions. This can recover usual field operator correlators such as $\hat{\mathcal{O}}_{\alpha_1}^{(\dagger)}([x_{j_1}^{(\ell)}]) \cdots \hat{\mathcal{O}}_{\alpha_\ell}^{(\dagger)}([x_{j_\ell}^{(\ell)}])$.

**Proposition 7.3.5.** *Let $[b_n] \in \mathrm{PGL}_5\mathbb{R}$, $(\mathsf{X}, \mathrm{O}) < (\mathbb{RP}^4, \mathrm{PGL}_5\mathbb{R})$ be a geometry. Deformations of $(\mathsf{X}, \mathrm{O})$ via $[b_n]$ give the commutative diagram*

$$
\begin{array}{ccc}
\mathrm{Ad}_{[b_n]}: & \mathrm{O} \xrightarrow{\;\sim\;} \mathrm{Ad}_{[b_n]}\mathrm{O} \\[2pt]
& \downarrow{\scriptstyle \mathrm{Ad}_U} \qquad\qquad \downarrow{\scriptstyle \mathrm{Ad}_U} \\[4pt]
\mathrm{Ad}_{U([b_n])}: & \mathfrak{A}(\mathsf{X}) \xrightarrow{\;\sim\;} \mathfrak{A}([b_n] \cdot \mathsf{X}),
\end{array}
\tag{7.39}
$$

*where the horizontal maps are bijections. A correlator $\hat{C} \in \mathfrak{A}(\mathsf{X})$ transforms as*

$$
\hat{C} \mapsto U([b_n])\hat{C}U^\dagger([b_n]) \in \mathfrak{A}([b_n] \cdot \mathsf{X}). \tag{7.40}
$$

*Proof.* The claim follows from

$$
\hat{\mathcal{O}}_{\beta_1}^{(\dagger)}([x_{j_1}^{(\ell)}]) \cdots \hat{\mathcal{O}}_{\beta_\ell}^{(\dagger)}([x_{j_\ell}^{(\ell)}]) \mapsto U([b_n])\hat{\mathcal{O}}_{\beta_1}([x_{j_1}^{(\ell)}]) \cdots \hat{\mathcal{O}}_{\beta_\ell}([x_\ell^{(\ell)}])U^\dagger([b_n]), \tag{7.41}
$$

together with

$$
\begin{aligned}
&\int_{\mathsf{X}^\ell} a_\ell([x_{j_1}^{(\ell)}], \ldots, [x_{j_\ell}^{(\ell)}]) U([b_n])\hat{\mathcal{O}}_{\beta_1}^{(\dagger)}([x_{j_1}^{(\ell)}]) \cdots \hat{\mathcal{O}}_{\beta_\ell}^{(\dagger)}([x_{j_\ell}^{(\ell)}])U^\dagger([b_n])\, \mathrm{d}^4[x_{j_1}^{(\ell)}] \cdots \mathrm{d}^4[x_{j_\ell}^{(\ell)}] \\
&= \int_{\mathsf{X}^\ell} a_\ell([x_{j_1}^{(\ell)}], \ldots, [x_{j_\ell}^{(\ell)}]) \rho_{\beta_1\gamma_1}^{(\dagger)}([b_n^{-1}])\hat{\mathcal{O}}_{\gamma_1}^{(\dagger)}([b_n \cdot x_{j_1}^{(\ell)}]) \circ \cdots \\
&\qquad\qquad\qquad \circ \rho_{\beta_\ell\gamma_\ell}^{(\dagger)}([b_n^{-1}])\hat{\mathcal{O}}_{\gamma_\ell}^{(\dagger)}([b_n \cdot x_{j_\ell}^{(\ell)}])\, \mathrm{d}^4[x_{j_1}^{(\ell)}] \cdots \mathrm{d}^4[x_{j_\ell}^{(\ell)}] \\
&= \int_{([b_n]\cdot\mathsf{X})^\ell} a_\ell([b_n^{-1} \cdot y_{j_1}^{(\ell)}], \ldots, [b_n^{-1} \cdot y_{j_\ell}^{(\ell)}]) \rho_{\beta_1\gamma_1}^{(\dagger)}([b_n^{-1}])\hat{\mathcal{O}}_{\gamma_1}^{(\dagger)}([y_{j_1}^{(\ell)}]) \circ \cdots \\
&\qquad\qquad\qquad \circ \rho_{\beta_\ell\gamma_\ell}^{(\dagger)}([b_n^{-1}])\hat{\mathcal{O}}_{\gamma_\ell}^{(\dagger)}([y_{j_\ell}^{(\ell)}])\, \mathrm{d}^4[y_{j_1}^{(\ell)}] \cdots \mathrm{d}^4[y_{j_\ell}^{(\ell)}]. \tag{7.42}
\end{aligned}
$$

This provides a bijective map into $\mathfrak{A}([b_n] \cdot X)$. $\qquad\square$

Proposition 7.3.5 is similar to a related statement for universal enveloping algebras of Lie algebras and their conjugacy limits, given in Appendix Section 7.A.3. It can be generalized to the closure of smeared variants of correlators in $\mathfrak{A}(\mathsf{X})$ with respect to suitable operator topologies, as shown in Appendix 7.C. In particular, this can include correlators of infinite order in field operators.

### 7.3.2 Superselection sectors

Inequivalent multipliers of the projective representation $U$ yield different superselection sectors for the quantum field $\hat{\mathcal{O}}$. On Poincaré geometry this gives bosonic and fermionic representations, which we extend to the ambient geometry $(\mathbb{RP}^4, \mathrm{PGL}_5\mathbb{R})$.

Let $\omega$ be the multiplier of the projective representation $U$. $\mathrm{PGL}_5\mathbb{R}$ is connected, so for $[g], [h] \in \mathrm{PGL}_5\mathbb{R}$ we can define the path $\gamma([g], [h])$ from $[1] \in \mathrm{PGL}_5\mathbb{R}$ to $[g]$ to $[gh]$ and then back to $[1]$ via the exponential map.

**Proposition 7.3.6.** *$H^2(\mathrm{PGL}_5\mathbb{R}, \mathrm{U}(1)) \cong \mathbb{Z}_2$, generated by the two inequivalent cocycles*

$$\omega_+([g], [h]) = +1 \tag{7.43}$$

*and*

$$\omega_-([g], [h]) = \begin{cases} +1\,, & \text{if } \gamma([g], [h]) \text{ is contractible}\,, \\ -1\,, & \text{if } \gamma([g], [h]) \text{ is not contractible}\,, \end{cases} \tag{7.44}$$

*for all $[g], [h] \in \mathrm{PGL}_5\mathbb{R}$.*

*Proof.* $\mathrm{PGL}_5\mathbb{R} \cong \mathrm{SL}_5\mathbb{R}$ since $-1_{5\times 5} \notin \mathrm{SL}_5\mathbb{R}$. Since $\mathrm{SL}_5\mathbb{R}$ is perfect, the universal central extension yields the short exact sequence of groups [334, 335]

$$1 \to H_2(\mathrm{PGL}_5\mathbb{R}, \mathbb{Z}) \cong \pi_1(\mathrm{PGL}_5\mathbb{R}) \to \overline{\mathrm{PGL}_5\mathbb{R}} \to \mathrm{PGL}_5\mathbb{R} \to 1\,, \tag{7.45}$$

with $\overline{\mathrm{PGL}_5\mathbb{R}}$ the universal cover of $\mathrm{PGL}_5\mathbb{R}$. The fundamental group is $\pi_1(\mathrm{PGL}_5\mathbb{R}) \cong \pi_1(\mathrm{SL}_5\mathbb{R}) \cong \mathbb{Z}_2$. With $H_1(\mathrm{SL}_5\mathbb{R}, \mathbb{Z}) \cong 0$ since $\mathrm{SL}_5\mathbb{R}$ is perfect, we have by the universal coefficient theorem

$$H^2(\mathrm{PGL}_5\mathbb{R}, \mathrm{U}(1)) \cong \mathrm{Hom}_{\mathbb{Z}}(H_2(\mathrm{PGL}_5\mathbb{R}, \mathbb{Z}), \mathrm{U}(1)) \cong \mathrm{Hom}_{\mathbb{Z}}(\mathbb{Z}_2, \mathrm{U}(1)) \cong \mathbb{Z}_2\,. \tag{7.46}$$

Generators can be chosen of the claimed topological type [8]. $\square$

The following proposition shows that requiring $\rho$ non-projective for quantum fields as in Definition 7.3.1 is no restriction.

**Proposition 7.3.7.** *Assume that for a quantum field $(U, \rho, \{\hat{\mathcal{O}}([x])\})$ the representation $\rho$ is projective instead of non-projective. It can be chosen with trivial multiplier independent from the multiplier of $U$, if not all field operators are zero.*

*Proof.* Assume $U$ and $\rho$ have multipliers $\omega_i$ and $\omega_j$ for $i, j \in \{+, -\}$, respectively. The transformation behavior of the field operators $\hat{\mathcal{O}}([x])$, $[x] \in \mathbb{RP}^4$, implies for $[g], [h] \in \mathrm{PGL}_5\mathbb{R}$:

$$\begin{aligned} \rho_{\alpha\beta}([h^{-1}])\rho_{\beta\gamma}([g^{-1}])\hat{\mathcal{O}}_\gamma([gh \cdot x]) &= \rho_{\alpha\beta}([h^{-1}])U([g])\hat{\mathcal{O}}_\beta([h \cdot x])U^\dagger([g]) \\ &= U([g])U([h])\hat{\mathcal{O}}_\alpha([x])U^\dagger([h])U^\dagger([g]) \\ &= \omega_i([g], [h])^2 U([gh])\hat{\mathcal{O}}_\alpha([x])U^\dagger([gh]) \\ &= U([gh])\hat{\mathcal{O}}_\alpha([x])U^\dagger([gh]) \\ &= \rho_{\alpha\beta}([h^{-1}g^{-1}])\hat{\mathcal{O}}_\beta([gh \cdot x])\,, \end{aligned} \tag{7.47}$$

where the summation over repeated indices is understood. By Equation (7.47):

$$\hat{\mathcal{O}}([gh \cdot x]) = \rho([g])\rho([h])\rho([h^{-1}g^{-1}])\hat{\mathcal{O}}([gh \cdot x]) = \omega_j([g], [h])\hat{\mathcal{O}}([gh \cdot x])\,, \tag{7.48}$$

i.e., $\omega_j([g], [h]) = +1$. $\square$

Multipliers of projective unitary representations do not discriminate between homogeneous Lorentzian geometry structure groups, the Poincaré group, $\mathrm{PGL}_5\mathbb{R}$ isotropy subgroups, or the full $\mathrm{PGL}_5\mathbb{R}$, as the following lemma shows. By a homogeneous Lorentzian geometry we mean a geometry of the form $[g]_*\mathsf{G}(4,1)$ for $[g] \in \mathrm{PGL}_5\mathbb{R}$.

**Lemma 7.3.8.** *Let* $\mathrm{O} < \mathrm{PGL}_5\mathbb{R}$ *be of type* $\mathrm{O} = \mathrm{Ad}_{[g]}\mathrm{PO}(4,1)$, $\mathrm{O} = \mathrm{PO}((1),(3,1))$, *or* $\mathrm{O} = \mathrm{PGL}_5\mathbb{R}_{[x]}$ *for some* $[x] \in \mathbb{RP}^4$. *Its cohomology group* $H^2(\mathrm{O}, \mathrm{U}(1))$ *is generated by* $\omega_\pm$ *as in Proposition 7.3.6. If a projective unitary* $\mathrm{PGL}_5\mathbb{R}$ *representation* $U$ *has multiplier* $\omega_i$ *upon restriction to* $\mathrm{O}$, $i \in \{+,-\}$, *then* $U$ *has the same multiplier* $\omega_i$ *on the full* $\mathrm{PGL}_5\mathbb{R}$, *and vice versa.*

*Proof.* The Lie algebra cohomology groups corresponding to the Lie groups $\mathrm{Ad}_{[g]}\mathrm{PO}(4,1)$ and $\mathrm{PO}((1),(3,1))$ are trivial,

$$H^2(\mathrm{Ad}_{[g]}\mathfrak{po}(4,1),\mathbb{R}) \cong H^2(\mathfrak{po}(4,1),\mathbb{R}) \cong H^2(\mathfrak{po}((1),(3,1)),\mathbb{R}) \cong 0\,, \qquad (7.49)$$

such that

$$H^2(\mathrm{Ad}_{[g]}\mathrm{PO}(4,1),\mathrm{U}(1)) \cong H^2(\mathrm{PO}(4,1),\mathrm{U}(1)) \cong H^2(\mathrm{PO}((1),(3,1)),\mathrm{U}(1))$$
$$\cong \pi_1(\mathrm{Ad}_{[g]}\mathrm{PO}(4,1)) \cong \pi_1(\mathrm{PO}(4,1)) \cong \pi_1(\mathrm{PO}((1),(3,1))) \cong \mathbb{Z}_2 \qquad (7.50)$$

by the same arguments as for the proof of Proposition 7.3.6. For the isotropy subgroup $\mathrm{PGL}_5\mathbb{R}_{[x]}$ assume without loss of generality $x_0 \neq 0$, and write $[x] = [x_0,\ldots,x_4] = [1,y_1,\ldots,y_4]$ with $y_\mu = x_\mu/x_0$ for $\mu = 1,\ldots,4$, else permute coordinates. Then $\mathrm{PGL}_5\mathbb{R}_{[x]}$ is given by

$$\mathrm{PGL}_5\mathbb{R}_{[x]} = \mathrm{P}\begin{pmatrix} 1 & & & \\ y_1 & 1 & & \\ \vdots & & \ddots & \\ y_4 & & & 1 \end{pmatrix} \mathrm{P}\begin{pmatrix} 1 & \mathbb{R}^4 \\ & \mathrm{GL}_4\mathbb{R} \end{pmatrix} \mathrm{P}\begin{pmatrix} 1 & & & \\ -y_1 & 1 & & \\ \vdots & & \ddots & \\ -y_4 & & & 1 \end{pmatrix}\,. \qquad (7.51)$$

Together with $H^2(\mathfrak{pgl}_4\mathbb{R},\mathbb{R}) \cong 0$ this gives $H^2(\mathrm{PGL}_5\mathbb{R}_{[x]},\mathrm{U}(1)) \cong H^2(\mathrm{PGL}_4\mathbb{R},\mathrm{U}(1)) \cong \pi_1(\mathrm{PGL}_4\mathbb{R}) \cong \mathbb{Z}_2$. In particular, the 2-cycles $\omega_\pm$ generate all the cohomology groups $H^2(\mathrm{Ad}_{[g]}\mathrm{PO}(4,1),\mathrm{U}(1))$, $H^2(\mathrm{PO}((1),(3,1)),\mathrm{U}(1))$, $H^2(\mathrm{PGL}_5\mathbb{R},\mathrm{U}(1))$, $H^2(\mathrm{PGL}_5\mathbb{R}_{[x]},\mathrm{U}(1))$, since all of these cohomology groups are entirely due to non-trivial fundamental groups.

Assume a projective unitary representation $V$ of $\mathrm{O}$ of any type as in the claim acts on the Hilbert space $\mathcal{H}$ with multiplier $\omega_-$, and $U$ has multiplier $\omega_+$. There exist $[g],[h] \in \mathrm{O}$ such that $\gamma([g],[h]) \subset \mathrm{O}$ is not contractible, i.e., for these $[g],[h]$ we have $\omega_-([g],[h]) = -1$. On the other hand, $\omega_+([g],[h]) = +1$. Thus, $V$ cannot be the restriction of $U$ to $\mathrm{O}$; the multipliers need to agree. The same holds if $V$ has multiplier $\omega_+$ and $U$ has multiplier $\omega_-$, showing the claim. The converse holds trivially. $\qquad\square$

This allows for the consistent extension of the classification of quantum fields into bosons and fermions, usually done for Poincaré geometry, to the ambient projective geometry.

**Definition 7.3.9.** *A quantum field* $\hat{\mathcal{O}}$ *is* bosonic *if* $U$ *has a multiplier equivalent to the trivial multiplier* $\omega_+$, *and* fermionic *if* $U$ *has a multiplier equivalent to* $\omega_-$.

The following proposition shows that no non-trivial superpositions of bosonic and fermionic quantum states are possible.

**Proposition 7.3.10.** *Let $U$ be a projective unitary $\mathrm{PGL}_5\mathbb{R}$ representation acting on a Hilbert space $\mathcal{H}$. Then no non-trivial splitting $\mathcal{H} = \mathcal{H}^+ \oplus \mathcal{H}^-$ together with $U = U^+ \oplus U^-$ and $U^\pm$ acting trivially on $\mathcal{H}^\mp$ exists, such that $U^+ \oplus 1_{\mathcal{H}^-}$ has multiplier $\omega_+$ and $1_{\mathcal{H}^+} \oplus U^-$ has multiplier $\omega_-$. This also holds for the restriction of quantum fields to general four-dimensional geometries $(\mathsf{X}, \mathsf{O})$ independent from the inequivalent multipliers of $U|_{\mathsf{O}}$, which may only be the trivial one.*

*Proof.* Assume $\mathcal{H} = \mathcal{H}^+ \oplus \mathcal{H}^-$, and $U|_{\mathcal{H}^\pm}$ has multiplier $\omega_\pm$. Let $0 \neq v_\pm \in \mathcal{H}^\pm$. Choose $[g], [h] \in \mathrm{PGL}_5\mathbb{R}$, such that the loop $\gamma([g], [h])$ is not contractible. Then, $U([g])U([h])v_\pm = \pm U([gh])v_\pm$. On the other hand, multipliers only depend on the representation $U$, such that $U([g])U([h])v_\mp = \pm U([gh])v_\mp$. This yields $\pm U([gh])v_\pm = \mp U([gh])v_\pm$, such that $U([gh])v_\pm = 0$, i.e., $v_\pm = 0$, which is a contradiction.

The same reasoning applies to the restriction to any geometry $(\mathsf{X}, \mathsf{O})$. The claim holds trivially, if $\omega_-$ is not a multiplier of $U|_{\mathsf{O}}$, e.g. for the final nilpotent limit group $\mathsf{O}((1), (1), (1), (1), (1))$, which has trivial fundamental group, since it can be continuously deformed to a point. $\qquad\square$

In the setting of quantum fields the multipliers $\omega_\pm$ of $\mathrm{PGL}_5\mathbb{R}$ indeed label different superselection sectors, justifying the previous definition.

### 7.3.3 Composite quantum fields and irreducibility

We construct composite and irreducible quantum fields from a quantum field $\hat{\mathcal{O}} = (U, \rho, \{\hat{\mathcal{O}}([x])\})$. Together with the spin-statistics relation and causality requirements, irreducible fermionic quantum fields carry the known Standard Model gauge group representations, as we show later in Section 7.4.3.

**Composite quantum fields**

Let $\hat{\mathcal{O}}^*([x]) : \mathcal{H}^* \to \mathcal{H}^*$ be the dual field operator to $\hat{\mathcal{O}}([x]) : \mathcal{H} \to \mathcal{H}$. The field operators of certain composite quantum fields can then be defined from the $\hat{\mathcal{O}}_\alpha([x])$ as

$$
\begin{aligned}
(\hat{\mathcal{O}}&(p, q; [x]))_{\alpha_1 \dots \alpha_p, \beta_1 \dots \beta_q} \\
&:= (\underbrace{\hat{\mathcal{O}}([x]) \otimes_\rho \cdots \otimes_\rho \hat{\mathcal{O}}([x])}_{p} \otimes_\rho \underbrace{\hat{\mathcal{O}}^*([x]) \otimes_\rho \cdots \otimes_\rho \hat{\mathcal{O}}^*([x])}_{q})_{\alpha_1 \dots \alpha_p, \beta_1 \dots \beta_q} \\
&:= \hat{\mathcal{O}}_{\alpha_1}([x]) \cdots \hat{\mathcal{O}}_{\alpha_p}([x]) \hat{\mathcal{O}}^*_{\beta_1}([x]) \cdots \hat{\mathcal{O}}^*_{\beta_q}([x]),
\end{aligned}
\tag{7.52}
$$

for $\alpha_1, \dots, \alpha_p, \beta_1, \dots, \beta_q \in \{1, \dots, \dim \rho\}$. The individual components provide linear operators $\mathcal{H} \to \mathcal{H}$, i.e., the Hilbert space remains the Hilbert space of the original quantum field $\hat{\mathcal{O}}$, and the tensor products only encompass the index structure corresponding to the finite-dimensional representation involved in the construction of quantum fields, and not the Hilbert space itself. The field operators $\hat{\mathcal{O}}(p, q; [x])$ are equipped with the

finite-dimensional $\mathrm{PGL}_5\mathbb{R}$ representation $\rho^{\otimes p} \otimes (\rho^*)^{\otimes q}$, with $\rho^* = (\rho^{-1})^T$ the dual (contragredient) representation of $\rho$, which the $\hat{\mathcal{O}}^*([x])$ carry. We write

$$\hat{\mathcal{O}}(p,q) := \hat{\mathcal{O}}^{\otimes_\rho p} \otimes_\rho \hat{\mathcal{O}}^{*,\otimes_\rho q} = (U, \rho^{\otimes p} \otimes (\rho^*)^{\otimes q}, \hat{\mathcal{O}}(p,q;[x])) \,. \tag{7.53}$$

**Proposition 7.3.11.** *The tuple $\hat{\mathcal{O}}(p,q)$ is a quantum field for any $p, q \in \mathbb{N}$. As $(\dim \rho)^{p+q}$-vectors of (partly dual) Hilbert space operators, the field operators $\hat{\mathcal{O}}(p,q;[x])$ can be identified with linear operators acting on*

$$\mathcal{H}^{(\dim \rho)^p} \otimes (\mathcal{H}^*)^{(\dim \rho)^q} \cong \mathcal{H} \otimes \underbrace{\mathbb{C}^{\dim \rho} \otimes \cdots \otimes \mathbb{C}^{\dim \rho}}_{p} \otimes \underbrace{(\mathbb{C}^*)^{\dim \rho} \otimes \cdots \otimes (\mathbb{C}^*)^{\dim \rho}}_{q} \,. \tag{7.54}$$

*Proof.* The statement is clear from the definition of quantum fields together with basic properties of the tensor products. $\qquad\square$

**Definition 7.3.12.** *We call $(\mathcal{H}', \hat{\mathcal{O}}(p,q))$ for $\mathcal{H}' \subset \mathcal{H}^{(\dim \rho)^p} \otimes (\mathcal{H}^*)^{(\dim \rho)^q}$ Hilbert subspace and all $\hat{\mathcal{O}}(p,q;[x])$ endomorphisms on $\mathcal{H}'$ a* composite quantum field.

Under additional assumptions such as energy positivity, the spin-statistics theorem has been proven for quantum field theories on Poincaré geometry [336]. Translated into the present framework, it connects quantum state statistics with causality and multipliers of the projective representation $U|_{\mathrm{PO}((1),(3,1))}$. Only completely symmetric (anti-symmetric) quantum states appear in the physical Hilbert space for bosonic (fermionic) quantum fields with integer spin (half-odd integer spin) Poincaré group representations, which obey the spin-statistics relation. Based on algebraic quantum field theory, the spin-statistics theorem can be extended to globally hyperbolic space-times [337], which include the homogeneous Lorentzian geometries of type $[g]_*\mathsf{G}(4,1)$. Without proof, in this chapter we assume the spin-statistics relation for composite quantum fields.

**Definition 7.3.13.** *A composite quantum field $(\mathcal{H}', \hat{\mathcal{O}}(p,q))$ obeys spin-statistics, if*

(i) *for $\hat{\mathcal{O}}(p,q)$ bosonic: under the identification (7.54) $\mathcal{H}'$ only contains states which are completely symmetric under permutations of the first $p$ factors of $\mathbb{C}^{\dim \rho}$ and, independently, under permutations of the last $q$ factors of $(\mathbb{C}^*)^{\dim \rho}$,*

(ii) *for $\hat{\mathcal{O}}(p,q)$ fermionic: under the identification (7.54) $\mathcal{H}'$ only contains states which are completely anti-symmetric under permutations of the first $p$ factors of $\mathbb{C}^{\dim \rho}$ and, independently, under permutations of the last $q$ factors of $(\mathbb{C}^*)^{\dim \rho}$,*

While spin is a property of the restricted projective representation $U|_{\mathrm{PO}((1),(3,1))}$, the multipliers $\omega_\pm$ appear for both the full $\mathrm{PGL}_5\mathbb{R}$ and $\mathrm{PO}((1),(3,1))$ and need to agree by Lemma 7.3.8. Definition 7.3.13 thus provides a consistent formulation of the spin-statistics relation for composite quantum fields on the entire ambient geometry $(\mathbb{RP}^4, \mathrm{PGL}_5\mathbb{R})$. It can be naturally extended to quantum fields acting on multi-particle Hilbert spaces, which is beyond the present work.

## Irreducible quantum fields

Quantum fields can be characterized according to irreducibility of the $\mathfrak{pgl}_5\mathbb{R}$ representation $\tilde{\rho}$ corresponding to the $\mathrm{PGL}_5\mathbb{R}$ representation $\rho$. Elements of $\mathfrak{pgl}_5\mathbb{R}$ are defined modulo the addition of multiples of the $5 \times 5$ identity matrix.

**Definition 7.3.14.** *A quantum field $\hat{\mathcal{O}}$ is* irreducible, *if $\tilde{\rho}$ is irreducible as a $\mathfrak{pgl}_5\mathbb{R}$ representation.*

We consider here Lie algebra instead of Lie group representations, since all projective unitary representations $U$ correspond to non-projective unitary $\overline{\mathrm{PGL}_5\mathbb{R}}$ representations coming from associated $\mathfrak{pgl}_5\mathbb{R}$ representations. On the Lie algebra level, Definition 7.3.14 coincides with the standard definition of irreducibility for Hilbert space operators [338].

By the construction of quantum fields, $\tilde{\rho}$ is finite-dimensional. All finite-dimensional irreducible representations of $\mathfrak{pgl}_5\mathbb{R} \cong \mathfrak{sl}_5\mathbb{R}$ are given by Schur modules for a pair of Young tableaux. For this we require $\tilde{\rho}$ to be the fundamental representation $\mathbb{CP}^4_{\mathfrak{pgl}_5\mathbb{R}}$ of $\mathfrak{pgl}_5\mathbb{R}$ acting on $\mathbb{CP}^4$ via (projective) matrix multiplication. We describe the related construction of partly symmetrized, partly anti-symmetrized composite quantum fields. The treatment closely follows the standard construction of Schur modules [338–340].

A Young tableau is an assignment of the numbers $1, \ldots, p$ to a Young diagram $\lambda = \{\lambda_1, \ldots, \lambda_r\}$ with $\#\lambda = p$ boxes. Let $(\lambda, \lambda')$ be a pair of Young tableaux, $\lambda = \{\lambda_1, \ldots, \lambda_r\}$, $\lambda' = \{\lambda'_1, \ldots, \lambda'_{r'}\}$ with $\#\lambda = p$, $\#\lambda' = q$, and $\bigcup_i \lambda_i = \{1, \ldots, p\}$, $\bigcup_j \lambda'_j = \{1, \ldots, q\}$. Such a pair can act on tensors in $\mathcal{H} \otimes \mathbb{CP}^4(p, q) := \mathcal{H} \otimes \mathbb{CP}^{4p} \otimes ((\mathbb{CP}^4)^*)^{4q}$, which we call $(p, q)$ tensors. For the Young tableau $\lambda$ we define subgroups of the degree-$p$ symmetric group $S_p$:

$$P_\lambda = \{\pi \in S_p \,|\, \pi \text{ preserves each row}\} \,, \tag{7.55}$$

$$Q_\lambda = \{\pi \in S_p \,|\, \pi \text{ preserves each column}\} \,, \tag{7.56}$$

analogously for $\lambda'$ and $S_q$. Elements $\pi \in S_p$, $\pi' \in S_q$ can act on $(p, q)$ tensors as

$$\sum \phi \otimes v_1 \otimes \cdots \otimes v_p \otimes \varphi_1 \otimes \cdots \otimes \varphi_q \mapsto \sum \phi \otimes v_{\pi(1)} \otimes \cdots \otimes v_{\pi(p)} \otimes \varphi_{\pi'(1)} \otimes \cdots \otimes \varphi_{\pi'(q)} \,, \tag{7.57}$$

where the left-hand side is a general $(p, q)$ tensor, with $v_i \in \mathbb{CP}^4$, $\varphi_j \in (\mathbb{CP}^4)^*$ for all $i, j$. Denote this action of $(\pi, \pi')$ on $(p, q)$ tensors by $e_\pi \otimes e_{\pi'}^*$. Then set

$$a_{(\lambda, \lambda')} := \sum_{(\pi, \pi') \in P_\lambda \times P_{\lambda'}} e_\pi \otimes e_{\pi'}^* \,, \qquad b_{(\lambda, \lambda')} := \sum_{(\pi, \pi') \in Q_\lambda \times Q_{\lambda'}} \mathrm{sgn}(\pi)\, \mathrm{sgn}(\pi') \cdot e_\pi \otimes e_{\pi'}^* \,. \tag{7.58}$$

The Young symmetrizer is defined as $c_{(\lambda, \lambda')} = a_{(\lambda, \lambda')} \circ b_{(\lambda, \lambda')}$. It corresponds to symmetrizing elements of $\mathcal{H} \otimes \mathbb{CP}^4(p, q)$ along rows of the Young tableaux $(\lambda, \lambda')$, and anti-symmetrizing them along columns of $(\lambda, \lambda')$, both with regard to $\mathbb{CP}^4(p, q)$.

Finally, we define the *Schur-Hilbert space*

$$\mathcal{H}'_{(\lambda, \lambda')} := \mathrm{im}(c_{(\lambda, \lambda')}) \,, \tag{7.59}$$

which is a subspace of $\mathcal{H} \otimes \mathbb{CP}^4(p, q)$.

It comes with the $\mathrm{PGL}_5\mathbb{R}$ representation $1_\mathcal{H} \otimes \rho_{(\lambda, \lambda')}$, where $\rho_{(\lambda, \lambda')}$ is the usual Schur module construction applied to $\rho$ for the pair $(\lambda, \lambda')$. The $\mathfrak{pgl}_5\mathbb{R}$ Lie algebra representation

corresponding to $\rho_{(\lambda,\lambda')}$ is $\tilde{\rho}_{(\lambda,\lambda')} = \mathbb{CP}^4_{(\lambda,\lambda')}$, which is the usual complex $\mathfrak{pgl}_5\mathbb{R}$ Schur module. Analogous to the construction of $\mathcal{H}'_{(\lambda,\lambda')}$, the Schur field operators $\hat{\mathcal{O}}^{\text{Schur}}_{(\lambda,\lambda')}([x])$ are constructed by partly symmetrizing, partly anti-symmetrizing the composite field operators $\hat{\mathcal{O}}(p,q;[x])$.

We define the composite Schur quantum field as

$$\hat{\mathcal{O}}^{\text{comp}}_{(\lambda,\lambda')} = \left(\mathcal{H}'_{(\lambda,\lambda')}, (U, \rho_{(\lambda,\lambda')}, \{\hat{\mathcal{O}}_{(\lambda,\lambda')}([x])\})\right). \tag{7.60}$$

**Example 7.3.15.** *Consider $(2,0)$ tensors and $\tilde{\rho} = \mathbb{CP}^4_{\mathfrak{pgl}_5\mathbb{R}}$, such that the maximal composite Hilbert space is $\mathcal{H} \otimes \mathbb{CP}^4 \otimes \mathbb{CP}^4$. Consider the Young tableaux*

$$\lambda = \boxed{\begin{array}{|c|c|} \hline 1 & 2 \\ \hline \end{array}}, \tag{7.61}$$

*$\lambda'$ empty. The Schur-Hilbert space is the symmetrization, $\mathcal{H}'_{(\lambda,\emptyset)} = \mathcal{H} \otimes \text{Sym}^2\mathbb{CP}^4$, and $\tilde{\rho}_{(\lambda,\emptyset)} = \mathbb{CP}^4_{\mathfrak{pgl}_5\mathbb{R}} \tilde{\odot} \mathbb{CP}^4_{\mathfrak{pgl}_5\mathbb{R}} := \mathbb{CP}^4_{\mathfrak{pgl}_5\mathbb{R}} \odot 1 + 1 \odot \mathbb{CP}^4_{\mathfrak{pgl}_5\mathbb{R}}$. If*

$$\lambda = \boxed{\begin{array}{|c|} \hline 1 \\ \hline 2 \\ \hline \end{array}}, \tag{7.62}$$

*the Schur-Hilbert space is the anti-symmetrization, $\mathcal{H}'_{(\lambda,\emptyset)} = \mathcal{H} \otimes \bigwedge^2\mathbb{CP}^4$, which comes with $\tilde{\rho}_{(\lambda,\emptyset)} = \mathbb{CP}^4_{\mathfrak{pgl}_5\mathbb{R}} \tilde{\wedge} \mathbb{CP}^4_{\mathfrak{pgl}_5\mathbb{R}} := \mathbb{CP}^4_{\mathfrak{pgl}_5\mathbb{R}} \wedge 1 + 1 \wedge \mathbb{CP}^4_{\mathfrak{pgl}_5\mathbb{R}}$. The representations $\tilde{\rho}_{i_1} \tilde{\odot} \tilde{\rho}_{i_2}$ and $\tilde{\rho}_{i_1} \tilde{\wedge} \tilde{\rho}_{i_2}$ are the tensor product representation $\tilde{\rho}_{i_1} \tilde{\otimes} \tilde{\rho}_{i_2}$ acting on $\mathbb{CP}^4 \odot \mathbb{CP}^4$ and $\mathbb{CP}^4 \wedge \mathbb{CP}^4$, respectively.*

The following proposition shows that irreducible quantum fields are similar to Schur quantum fields with regard to the involved finite-dimensional representation.

**Proposition 7.3.16.** *A quantum field $\hat{\mathcal{O}} = (U, \rho', \{\hat{\mathcal{O}}([x])\})$ is irreducible, if and only if for a pair of Young tableaux $(\lambda, \lambda')$ there is a complex finite-dimensional $\text{PGL}_5\mathbb{R}$ representation $\rho$ such that $\rho' = \rho_{(\lambda,\lambda')}$ with $\tilde{\rho} = \mathbb{CP}^4_{\mathfrak{pgl}_5\mathbb{R}}$. If $|\lambda|, |\lambda'| = 5$, $\tilde{\rho}_{(\lambda,\lambda')}$ is the trivial representation of $\mathfrak{pgl}_5\mathbb{R}$, and if $|\lambda| \geq 6$ or $|\lambda'| \geq 6$, $\tilde{\rho}_{(\lambda,\lambda')} = 0$.*

*Proof.* $\hat{\mathcal{O}}$ is irreducible if and only if $\tilde{\rho}'$ is irreducible. The statements follow with $\mathfrak{pgl}_5\mathbb{R} \cong \mathfrak{sl}_5\mathbb{R}$ from the standard classification of finite-dimensional irreducible representations of $\mathfrak{sl}_5\mathbb{R}$ [338, 339]. $\square$

Proposition 7.3.16 implies that with regard to the finite-dimensional representation $\rho$ all irreducible quantum fields are of the form of composite Schur quantum fields. If Proposition 7.3.16 applies, we write the quantum field $\hat{\mathcal{O}}$ as $\hat{\mathcal{O}}_{(\lambda,\lambda')}$. Obeying spin-statistics manifests for irreducible quantum fields as follows.

**Lemma 7.3.17.** *Let $\hat{\mathcal{O}}_{(\lambda,\lambda')}$ be an irreducible quantum field, which obeys spin-statistics. Then*

  *(i) for $\hat{\mathcal{O}}_{(\lambda,\lambda')}$ bosonic both $\lambda$ and $\lambda'$ consist of single rows, or*

  *(ii) for $\hat{\mathcal{O}}_{(\lambda,\lambda')}$ fermionic both $\lambda$ and $\lambda'$ consist of single columns.*

*Proof.* The statement is a direct consequence of Proposition 7.3.16 together with Definition 7.3.13. $\square$

Thus, bosonic (fermionic) irreducible quantum fields obeying spin-statistics are similar to composite Schur quantum fields but contain only completely symmetrized (anti-symmetrized) finite-dimensional representations. Based on the existing spin-statistics theorems the corresponding field operators are expected to generate the entire physical Hilbert space.

### 7.3.4 Dependence on the ambient geometry

The construction of quantum fields depends on the non-unique choice of the ambient projective geometry $(\mathbb{RP}^4, \mathrm{PGL}_5\mathbb{R})$. We show that this is at least partly without loss of generality.

**Proposition 7.3.18.** *Let* $\mathsf{G} = (\mathsf{X}, \mathrm{O}) < (\mathbb{RP}^4, \mathrm{PGL}_5\mathbb{R})$ *be a four-dimensional geometry. If* $\mathsf{G}$ *is viewed as a subgeometry of* $(\mathbb{RP}^{m-1}, \mathrm{PGL}_m)$, $m \geq 5$, *all deformations and limits preserving the subgeometry* $(\mathbb{RP}^4, \mathrm{PGL}_5\mathbb{R}) < (\mathbb{RP}^{m-1}, \mathrm{PGL}_m)$ *containing* $\mathsf{G}$ *arise up to conjugation within* $(\mathbb{RP}^{m-1}, \mathrm{PGL}_m)$ *from deformations and limits of* $\mathsf{G}$ *in* $(\mathbb{RP}^4, \mathrm{PGL}_5\mathbb{R})$.

*Proof.* With $\mathrm{O} \hookrightarrow \mathrm{PGL}_m\mathbb{R}$ subgroup, it is conjugate within $\mathrm{PGL}_m\mathbb{R}$ to the canonical form

$$\mathrm{P}((\mathrm{P}^{-1}\mathrm{O}) \times 1) := \mathrm{P}\begin{pmatrix} \mathrm{P}^{-1}\mathrm{O} & \\ & 1_{(m-5)\times(m-5)} \end{pmatrix}. \tag{7.63}$$

Let $[c_n] \in \mathrm{PGL}_m\mathbb{R}$. We write

$$[c_n] = \mathrm{P}\begin{pmatrix} A_n & B_n \\ C_n & D_n \end{pmatrix}, \tag{7.64}$$

with $[A_n] \in \mathrm{GL}_5\mathbb{R}$ and all other submatrices of matching sizes. Preservation of $(\mathbb{RP}^4, \mathrm{PGL}_5\mathbb{R}) < (\mathbb{RP}_{m-1}, \mathrm{PGL}_m)$, where $\mathsf{G} < (\mathbb{RP}^4, \mathrm{PGL}_5\mathbb{R}) < (\mathbb{RP}_{m-1}, \mathrm{PGL}_m)$, yields $B_n = 0$ and $C_n = 0$. Then,

$$[c_n]\mathrm{P}((\mathrm{P}^{-1}\mathrm{O}) \times 1)[c_n^{-1}] = \mathrm{P}(A_n(\mathrm{P}^{-1}\mathrm{O})A_n^{-1} \times 1). \tag{7.65}$$

Deformations and limits of $\mathrm{O} < \mathrm{PGL}_m\mathbb{R}$ are up to conjugation within $\mathrm{PGL}_m\mathbb{R}$ the same as within $\mathrm{PGL}_5\mathbb{R}$, if the subgroup $\mathrm{PGL}_5\mathbb{R} < \mathrm{PGL}_m\mathbb{R}$ containing $\mathrm{O}$ is preserved. The claim for the related model spaces follows analogously. $\qquad\square$

**Lemma 7.3.19.** *Consider a quantum field* $\hat{\mathcal{O}} = (U, \rho, \{\hat{\mathcal{O}}([x]) \mid [x] \in \mathbb{RP}^{m-1}\})$ *for ambient geometry* $(\mathbb{RP}^{m-1}, \mathrm{PGL}_m\mathbb{R})$, *i.e.,* $U : \mathrm{PGL}_m\mathbb{R} \to \mathcal{U}(\mathcal{H})$ *is a projective unitary representation and* $\rho$ *is a finite-dimensional* $\mathrm{PGL}_m\mathbb{R}$ *representation. Restricted to the four-dimensional geometry* $\mathsf{G} = (\mathsf{X}, \mathrm{O}) < (\mathbb{RP}^{m-1}, \mathrm{PGL}_m\mathbb{R})$, *deformations and limits of* $\hat{\mathcal{O}}|_{(\mathsf{X}, \mathrm{O})}$ *which preserve the second embedding of* $(\mathsf{X}, \mathrm{O}) < (\mathbb{RP}^4, \mathrm{PGL}_5\mathbb{R}) < (\mathbb{RP}^{m-1}, \mathrm{PGL}_m\mathbb{R})$ *agree up to* $\mathrm{PGL}_m\mathbb{R}$ *conjugation with those of* $\hat{\mathcal{O}}$ *for the ambient geometry* $(\mathbb{RP}^4, \mathrm{PGL}_5\mathbb{R})$.

*Proof.* The claim is a direct consequence of Proposition 7.3.18 together with quantum field properties. $\qquad\square$

This does not include ambient geometries which are not real projective geometries. Yet, one can heuristically argue in favor of the projective geometry setting in three dimensions.

As for Thurston's geometrization program, all eight Thurston geometries (almost) admit a representation in real projective geometry [341, 342].

In the next section we formulate $\mathrm{PGL}_5\mathbb{R}$ gauge theory based on local projective frame transformations, which are sections of the projective frame bundle (7.24). Since projective frames only depend on the model space $\mathsf{X}$ of the geometry $(\mathsf{X}, \mathsf{O}) < (\mathbb{RP}^{m-1}, \mathrm{PGL}_m\mathbb{R})$, the gauge group $\mathrm{PGL}_5\mathbb{R}$ is independent from the ambient geometry, so are the related results.

## 7.4 $\mathrm{PGL}_5\mathbb{R}$ **gauge theory on Lorentzian geometries**

Connections of the projective frame bundle (7.24) provide the gauge fields for $\mathrm{PGL}_5\mathbb{R}$ gauge theory, as described in Section 7.4.1. On Poincaré and homogeneous Lorentzian geometries causality preservation reduces the gauge group involved in non-trivial interactions with other quantum fields to $\mathrm{P}(\mathrm{GL}_2\mathbb{R} \times \mathrm{GL}_3\mathbb{R})$. The reduction is not due to spontaneous symmetry breaking, but is expected also on the classical level. Physical scale invariance is broken by the $\mathrm{P}(\mathrm{GL}_2\mathbb{R} \times 1) \cong \mathbb{R}_{\neq 0} \times \mathrm{PGL}_2\mathbb{R}$ gauge bosons, reminiscent of a Higgs-like mechanism. This and the gauge group reduction are shown in Section 7.4.2. Fermionic irreducible quantum fields come with a Standard Model-like representation of $\mathrm{P}(\mathrm{GL}_2\mathbb{R} \times \mathrm{GL}_3\mathbb{R})$, derived in Section 7.4.3. In Section 7.4.4 implications for particle physics models are discussed.

Throughout this section, let $\mathcal{H}$ be a given Hilbert space, which admits all of the following constructions but whose structure we again do not further discuss here.

### 7.4.1 **Projective frame transformations as** $\mathrm{PGL}_5\mathbb{R}$ **gauge theory**

We review the construction of $\mathrm{PGL}_5\mathbb{R}$ gauge fields. More details on the mathematics of gauge theories can be found e.g. in [89].

Consider a four-dimensional geometry $(\mathsf{X}, \mathsf{O}) < (\mathbb{RP}^4, \mathrm{PGL}_5\mathbb{R})$. The right action $R_{[g]} : \mathcal{P}(\mathsf{X}) \to \mathcal{P}(\mathsf{X})$ locally acts as

$$[x] \mapsto [x], \qquad [e_A([x])] \mapsto \sum_{B=1,\ldots,5} [g_A{}^B([x])] \cdot [e_B([x])], \qquad (7.66)$$

where $[e] = \{[e]([x]) \mid [x] \in \mathsf{X}\} = \{([x], [e_1([x])], \ldots, [e_5([x])])\} \in \mathcal{P}(\mathsf{X})$, $[e_5([x])] = [e_1([x]) + \cdots + e_4([x])]$ and $[(g_A{}^B)] \in \mathrm{PGL}_5\mathbb{R}$. Let $a : \mathfrak{pgl}_5\mathbb{R} \to \mathfrak{X}(\mathcal{P}(\mathsf{X}))$ be the fundamental vector field on $\mathcal{P}(\mathsf{X})$, i.e., for all projective frames $[e] \in \mathcal{P}(\mathsf{X})$, $[Y] \in \mathfrak{pgl}_5\mathbb{R}$:

$$a([Y])_{[e]} := \left.\frac{\mathrm{d}}{\mathrm{d}t}\right|_{t=0} R_{\exp(it[Y])}[e]. \qquad (7.67)$$

A connection 1-form of the projective frame bundle

$$\mathrm{PGL}_5\mathbb{R} \to \mathcal{P}(\mathsf{X}) \to \mathsf{X} \qquad (7.68)$$

is a $\mathfrak{pgl}_5\mathbb{R}$-valued differential form $\omega \in \Omega^1(\mathsf{X}, \mathfrak{pgl}_5\mathbb{R})$, such that for all $[g] \in \mathrm{PGL}_5\mathbb{R}$ the pull-back via $R_{[g]}$ fulfils $R_{[g]}^*\omega = \mathrm{Ad}_{[g^{-1}]}\omega$ and $\omega(a([Y])) = [Y]$ for all $[Y] \in \mathfrak{pgl}_5\mathbb{R}$.

The projective frame bundle comes with a local trivialization $\{(U_\alpha, [\psi_\alpha])\}$, such that diffeomorphically $\pi^{-1}(U_\alpha) \to U_\alpha \times \mathrm{PGL}_5\mathbb{R}$, $[e]([x]) \mapsto (\pi([e]([x])) = [x], [\psi_\alpha([e]([x]))])$, the projection $\pi$ given by (7.23). Define the local sections $\sigma_\alpha : U_\alpha \to \pi^{-1}(U_\alpha)$, $\sigma_\alpha([x]) := ([x], [\psi_\alpha^{-1}([1])])$. On the $U_\alpha$ there are the pull-backs

$$[\mathscr{A}_\alpha] = \sigma_\alpha^* \omega \in \Omega^1(U_\alpha, \mathfrak{pgl}_5\mathbb{R}), \tag{7.69}$$

which locally define the gauge 1-form $[\mathscr{A}]$. Vice versa, all $[\mathscr{A}_\alpha]$ together uniquely fix the connection 1-form $\omega$. To $[\mathscr{A}]$ corresponds a unique projective (gauge) vector field $[A]$, which can be written as

$$[A([x])] = \sum_{B=1}^{5} [A_B([x])] [\partial_B([x])], \tag{7.70}$$

where $[A_B([x])] \in \mathfrak{pgl}_5\mathbb{R}$ and $\{[\partial_1], \dots, [\partial_5]\}$ is the standard projective frame on $\mathsf{X}$.

The transition functions $[g_{\alpha\beta}([x])] = [\psi_\alpha([x]) \cdot \psi_\beta^{-1}([x])]$ are defined on the intersection $U_\alpha \cap U_\beta$:

$$[A_{\alpha,B}] = \sum_\beta [g_{\beta\alpha}^{-1} \cdot A_{\beta,B} \cdot g_{\beta\alpha}] + \mathrm{i}\,[g_{\beta\alpha}^{-1} \cdot \partial_B g_{\beta\alpha}]. \tag{7.71}$$

Let $[\Psi] : \mathcal{P}(\mathsf{X}) \to \mathcal{P}(\mathsf{X})$ be a gauge transformation, i.e., a $\mathrm{PGL}_5\mathbb{R}$-equivariant diffeomorphism, such that $\pi \circ [\Psi] = \pi$. Let $\omega' = [\Psi^{-1}]^* \omega$ be the gauge-transformed connection 1-form, and $[A_\alpha]$, $[A'_\alpha]$ the gauge fields corresponding to $\omega, \omega'$, respectively. Then,

$$[A'_{\alpha,B}] = [\Psi_\alpha \cdot A_{\alpha,B} \cdot \Psi_\alpha^{-1}] + \mathrm{i}\,[\Psi_\alpha \cdot \partial_B \Psi_\alpha^{-1}]. \tag{7.72}$$

So far we described classical gauge fields. A rigorous non-perturbative treatment of gauge *quantum* fields has not been established yet [316]. We follow the approach of Section 7.3.1 and focus on representation-theoretic properties, which provide the link to geometries.

**Definition 7.4.1.** *A $\mathrm{PGL}_5\mathbb{R}$ gauge quantum field $[\hat{A}] = (U_A, \rho_A, \{[\hat{A}([x])]\})$ is a quantum field with Hilbert space $\mathcal{H}$, transforming under a $\mathrm{PGL}_5\mathbb{R}$ gauge transformation $[\Psi]$ for all $[x] \in \mathbb{RP}^4$ as*

$$[\hat{A}_B([x])] \mapsto [\Psi([x]) \cdot \hat{A}_B([x]) \cdot \Psi([x])^{-1}] + \mathrm{i}\,[\Psi([x]) \cdot \partial_B \Psi^{-1}([x])], \tag{7.73}$$

*with chart indices suppressed. Upon restriction to the geometry $(\mathsf{X}, \mathrm{O}) < (\mathbb{RP}^4, \mathrm{PGL}_5\mathbb{R})$, gauge transformations and their action (7.73) on $[\hat{A}]$ are restricted to $\mathsf{X}$. When denoted as $[\hat{A}]$, $[\hat{A}] = (U_A, \rho_A, \{[\hat{A}([x])]\})$ is understood.*

Deformations and limits of geometries act naturally on gauge quantum fields and their correlators, since they are quantum fields in the sense of Definition 7.3.1. We assume the gauge transformation $[\Psi]$ acts on a quantum field $\hat{\mathcal{O}}$ as

$$\hat{\mathcal{O}}([x]) \mapsto \rho([\Psi([x])])\hat{\mathcal{O}}([x]). \tag{7.74}$$

This action preserves locality in X. A corresponding covariant derivative acting on $\hat{\mathcal{O}}([x])$ is defined similar to spin connections [343, 344] as

$$\hat{\nabla}_B([x]) = [\partial_B] - \mathrm{i}\rho([\hat{A}_B([x])]) \,. \tag{7.75}$$

The algebra $\mathfrak{A}_{\hat{\mathcal{O}},\hat{A}}(\mathsf{X})$ of field operator correlators for both quantum fields $\hat{\mathcal{O}}$ and $[\hat{A}]$ is defined from the $\hat{\mathcal{O}}^{(\dagger)}([x])$ and the $[\hat{A}^{(\dagger)}]$ together with $\rho, \rho_A$ analogously to $\mathfrak{A}(\mathsf{X})$ as in Equation (7.38). In particular, $\mathfrak{A}_{\hat{\mathcal{O}},\hat{A}}(\mathsf{X})$ includes mixed correlators for which both the field operators $\hat{\mathcal{O}}^{(\dagger)}([x])$ and the $[\hat{A}^{(\dagger)}([x])]$ act consecutively on each other.

### 7.4.2 Causality and gauge group reduction

**Gauge group reduction on Poincaré geometry**

We consider Poincaré geometry $\mathsf{G}((1),(3,1))$ and focus on geometry deformations by

$$[c(\kappa)] = \mathrm{P}\begin{pmatrix} \kappa & & \\ & 1_{3\times3} & \\ & & \kappa \end{pmatrix} \quad \text{for} \quad \kappa > 0 \,. \tag{7.76}$$

Similar derivations for homogeneous Lorentzian geometries are given later. In Example 7.2.2(i) we derived that $\lim_{\kappa\to0}[c(\kappa)]_*\mathsf{G}((1),(3,1))$ is Galilei geometry $\mathsf{G}((1),(1),(3))$ up to the coordinate index permutation $\tau = (0)(1\,2\,3\,4)$. In the limit $\kappa \to \infty$ the geometry becomes the ultra-relativistic (Carroll) geometry $\mathsf{G}((1),(3),(1))$. Physically, the deformation by $[c(\kappa)]$ corresponds to a change in the (coordinate) speed of light.

The action of $[c(\kappa)]$ thus deforms causal cones. Let $[x], [x'] \in \mathsf{X}((1),(3,1))$ be time-like separated, i.e., with

$$\begin{aligned} [x] &= [x_0,\ldots,x_4] = [1, x_1/x_0, \ldots, x_4/x_0] \,, \\ [x'] &= [x'_0,\ldots,x'_4] = [1, x'_1/x'_0, \ldots, x'_4/x'_0] \,, \end{aligned} \tag{7.77}$$

and $\Delta y_\mu := x'_\mu/x'_0 - x_\mu/x_0$ for $\mu = 1,\ldots,4$:

$$\Delta y^2 := \sum_{\mu,\nu=1}^{4} \eta^{\mu\nu}\Delta y_\mu\Delta y_\nu = -\Delta y_1^2 - \Delta y_2^2 - \Delta y_3^2 + \Delta y_4^2 > 0 \,, \tag{7.78}$$

where $(\eta^{\mu\nu}) = \mathrm{diag}(-1,-1,-1,+1)$ is the (Minkowski) metric tensor on $\mathbb{A}^{3,1}$. The action of $[c(\kappa)]$ maps the left-hand side to

$$[c(\kappa)]_*\Delta y^2 = -\frac{1}{\kappa^2}(\Delta y_1^2 + \Delta y_2^2 + \Delta y_3^2) + \Delta y_4^2 \,. \tag{7.79}$$

By the time-like separation $\Delta y_4 \neq 0$. Assume $[x]$ and $[x']$ have non-zero spatial distance, i.e., at least one $\Delta y_a \neq 0$, $a = 1,2,3$. Then $0 < \kappa < 1$ exists, so that $[c(\kappa)]_*\Delta y^2 < 0$; $[c(\kappa)]_*\Delta y^2$ becomes space-like. Analogously, space-like separated space-time regions can become time-like separated via $[c(\kappa)]$ for some $\kappa > 1$. Light-like separated space-time regions can become both time-like and space-like separated via $[c(\kappa)]$.

For quantum fields on Poincaré geometry the following definition of causality preservation is commonly employed [84, 318, 332].

**Definition 7.4.2.** *On Poincaré geometry a quantum field $\hat{\mathcal{O}}$ preserves causality, if for all space-like separated $[x], [x'] \in \mathsf{X}((1),(3,1))$:*

$$[\hat{\mathcal{O}}([x]), \hat{\mathcal{O}}([x'])]_{\mp} := \hat{\mathcal{O}}([x])\hat{\mathcal{O}}([x']) \mp \hat{\mathcal{O}}([x'])\hat{\mathcal{O}}([x]) = 0, \quad [\hat{\mathcal{O}}([x]), \hat{\mathcal{O}}^{\dagger}([x'])]_{\mp} = 0, \quad (7.80)$$

*with '$-$' for $\hat{\mathcal{O}}$ bosonic and '$+$' for $\hat{\mathcal{O}}$ fermionic. On Poincaré geometry the quantum field $\hat{\mathcal{O}}$ is* non-trivial, *if light-like or time-like separated $[x], [x'] \in \mathsf{X}((1),(3,1))$ with non-zero spatial distance exist, such that*

$$[\hat{\mathcal{O}}([x]), \hat{\mathcal{O}}([x'])]_{\mp} \neq 0 \quad and \quad [\hat{\mathcal{O}}([x]), \hat{\mathcal{O}}^{\dagger}([x'])]_{\mp} \neq 0 \quad (7.81)$$

*with '$-$' for $\hat{\mathcal{O}}$ bosonic and '$+$' for $\hat{\mathcal{O}}$ fermionic.*

An algebra-related definition is required for the treatment of operator algebras.

**Definition 7.4.3.** *An algebra $\mathcal{A}$ with commutator $[\cdot, \cdot]$ is* commutator-generated, *if for all $a' \in \mathcal{A}$ there exist $a(a'), b(a'), c(a') \in \mathcal{A}$: $a' = a(a')[b(a'), c(a')]$. If the algebra $\mathcal{A}$ comes with multiple commutators $[\cdot, \cdot]_1, [\cdot, \cdot]_2, \ldots$, it is* simultaneously commutator-generated *with respect to the commutators $[\cdot, \cdot]_1, [\cdot, \cdot]_2, \ldots$, if for all $a' \in \mathcal{A}$ and all $i$ there exist $a_i(a'), b_i(a'), c_i(a') \in \mathcal{A}$: $a' = a_i(a')[b_i(a'), c_i(a')]_i$.*

The ordering choice in this definition is without loss of generality, since $a[b, c] = [ab, c] - [a, c]b$.

**Example 7.4.4.** *Commutator-generated algebras naturally appear for causality-preserving quantum fields on Poincaré geometry which obey canonical equal-time commutation relations:*

$$[\hat{\mathcal{O}}([x_0, \ldots, x_3, x_4]), \hat{\mathcal{O}}^{\dagger}([x'_0, \ldots, x'_3, x_4])]_{\mp} = \delta^{(3)}([x_0, \ldots, x_3] - [x'_0, \ldots, x'_3]) \cdot 1_{\mathcal{H}}, \quad (7.82)$$

*where $\delta^{(3)}([x_0, \ldots, x_3] - [x'_0, \ldots, x'_3])$ denotes the Dirac $\delta$-function in 3 dimensions. Indeed, then*

$$
\begin{aligned}
\hat{\mathcal{O}}([x]) &= \int_{\{[x'] \in \mathsf{X}((1),(3,1)) \,|\, x'_4 = x_4\}} \mathrm{d}^3[x'] \, \hat{\mathcal{O}}([x]) \, \delta^{(3)}([x_0, \ldots, x_3] - [x'_0, \ldots, x'_3]) \\
&= \int_{\{[x'] \in \mathsf{X}((1),(3,1)) \,|\, x'_4 = x_4\}} \mathrm{d}^3[x'] \, \hat{\mathcal{O}}([x]) \, [\hat{\mathcal{O}}([x_0, \ldots, x_3, x_4]), \hat{\mathcal{O}}^{\dagger}([x'_0, \ldots, x'_3, x_4])]_{\mp},
\end{aligned}
$$
$$(7.83)$$

*which includes a commutator.*

We can now state the gauge group reduction theorem central to this chapter. Intuitively, commutativity with $[c(\kappa)]$ probes causality preservation.

**Theorem 7.4.5** (Gauge group reduction). *Let $\hat{\mathcal{O}}$ be a quantum field, $[\hat{A}]$ a $\text{PGL}_5\mathbb{R}$ gauge quantum field, both defined for the same Hilbert space $\mathcal{H}$, and $\text{PGL}_5\mathbb{R}$ gauge transformations act on $\hat{\mathcal{O}}([x])$ as in Equation (7.74). Consider Poincaré geometry $\mathsf{G}((1),(3,1))$ and assume:*

*(i)* $\hat{\mathcal{O}}$ *and* $[\hat{A}]$ *are causality-preserving on Poincaré geometry with commutators* $[\cdot,\cdot]_{\hat{\mathcal{O}},\mp}$ *and* $[\cdot,\cdot]_{[\hat{A}],\mp}$,

*(ii)* $\mathfrak{A}_{\hat{\mathcal{O}},\hat{A}}(\mathsf{X}((1),(3,1)))$ *is simultaneously commutator-generated with respect to* $[\cdot,\cdot]_{\hat{\mathcal{O}},\mp}$ *and* $[\cdot,\cdot]_{[\hat{A}],\mp}$, *and*

*(iii) the quantum fields* $\hat{\mathcal{O}}$ *and* $[\hat{A}]$ *are non-trivial on Poincaré geometry.*

*Then,* $U([c(\kappa)])$ *and* $U_A([c(\kappa)])$ *commute with all field operators, i.e., maximally the representations* $\rho_A$ *and* $\rho$ *of the gauge subgroup*

$$\tau_*^{-1}\mathrm{P}\begin{pmatrix}\mathrm{GL}_2\mathbb{R} & \\ & \mathrm{GL}_3\mathbb{R}\end{pmatrix} < \mathrm{PGL}_5\mathbb{R}\,, \tag{7.84}$$

*which is isomorphic to* $\mathrm{P}(\mathrm{GL}_2\mathbb{R}\times\mathrm{GL}_3\mathbb{R})$, *do not act trivially on* $\mathfrak{A}_{\hat{\mathcal{O}},\hat{A}}(\mathsf{X}((1),(3,1)))$.

*Proof.* By non-triviality light-like or time-like separated $[x],[x']\in\mathsf{X}((1),(3,1))$ with

$$[\hat{\mathcal{O}}([x]),\hat{\mathcal{O}}^{(\dagger)}([x'])]_{\hat{\mathcal{O}},\mp}\neq 0 \tag{7.85}$$

exist. This gives

$$\begin{aligned}
U([c(\kappa)])\,&[\hat{\mathcal{O}}([x]),\hat{\mathcal{O}}^{(\dagger)}([x'])]_{\hat{\mathcal{O}},\mp}\,U^{\dagger}([c(\kappa)]) \\
&= [U([c(\kappa)])\hat{\mathcal{O}}([x])U^{\dagger}([c(\kappa)]),U([c(\kappa)])\hat{\mathcal{O}}^{(\dagger)}([x'])U^{\dagger}([c(\kappa)])]_{\hat{\mathcal{O}},\mp}\neq 0\,. \tag{7.86}
\end{aligned}$$

The transformation behavior (7.28) implies that

$$\mathrm{Ad}_{U([c(\kappa)])}:\hat{\mathcal{O}}([x])\mapsto\hat{\mathcal{O}}([c(\kappa)\cdot x])\,,\qquad\hat{\mathcal{O}}^{(\dagger)}([x'])\mapsto\hat{\mathcal{O}}^{(\dagger)}([c(\kappa)\cdot x'])\,. \tag{7.87}$$

By the above there exists $\kappa$, such that $[c(\kappa)\cdot x]$ and $[c(\kappa)\cdot x']$ are space-like separated. Then Equation (7.86) is a contradiction to causality preservation.

$U([c(\kappa)])$ thus needs to commute with the commutator (7.85). The same argument applies to $U_A([c(\kappa)])$, which needs to commute with commutators of light-like or time-like separated gauge field operators $[\hat{A}([x])]$. By causality preservation $U([c(\kappa)])$ and $U_A([c(\kappa)])$ trivially commute with all commutators of space-like separated field operators. $\mathfrak{A}_{\hat{\mathcal{O}},\hat{A}}(\mathsf{X}((1),(3,1)))$ is commutator-generated, which implies that $U([c(\kappa)])$ and $U_A([c(\kappa)])$ commute with all $\mathfrak{A}_{\hat{\mathcal{O}},\hat{A}}(\mathsf{X}((1),(3,1)))$, in particular with $\hat{\mathcal{O}}([x])$ and $[\hat{A}([x])]$ themselves.

By Equation (7.28) the related $\rho([c(\kappa)])$ acts on $\hat{\mathcal{O}}([x])$ as

$$\hat{\mathcal{O}}([x]) = \rho([c(\kappa)^{-1}])\hat{\mathcal{O}}([c(\kappa)\cdot x])\,. \tag{7.88}$$

This yields upon acting on it with a gauge transformation $[\Psi]$:

$$\begin{aligned}
\rho([\Psi([x])])\hat{\mathcal{O}}([x]) &= \rho([c(\kappa)^{-1}])\rho([\Psi([c(\kappa)\cdot x])])\hat{\mathcal{O}}([c(\kappa)\cdot x]) \\
&= \rho([c(\kappa)^{-1}\cdot\Psi([c(\kappa)\cdot x])\cdot c(\kappa)])\hat{\mathcal{O}}([x])\,. \tag{7.89}
\end{aligned}$$

Assume that $[\Psi([x])] = [\Psi([c(\kappa) \cdot x])]$, then upon their action on the field operators $\hat{\mathcal{O}}([x])$, $\rho([c(\kappa)])$ and $\rho([\Psi([x])])$ need to commute. For the field operators $[\hat{A}([x])]$ and the representation $\rho_A$ the analogous statements hold. Maximally gauge transformations with values in $\tau_*^{-1}P(\mathrm{GL}_2\mathbb{R} \times \mathrm{GL}_3\mathbb{R})$ can interact non-trivially with the field operators (again $\tau = (0)\,(1\,2\,3\,4)$). Indeed, with

$$\tau_*([c(\kappa)]) = P\begin{pmatrix} \kappa \cdot 1_{2\times 2} & \\ & 1_{3\times 3} \end{pmatrix} \tag{7.90}$$

and $A, B, C, D$ corresponding matrix blocks:

$$\tau_*([c(\kappa)])\,P\begin{pmatrix} A & B \\ C & D \end{pmatrix}\tau_*(c(\kappa))^{-1} = P\begin{pmatrix} A & \kappa B \\ \kappa^{-1}C & D \end{pmatrix}, \tag{7.91}$$

which is invariant if and only if $B, C = 0$. $\qquad\square$

Theorem 7.4.5 implies that maximally a principal $\tau_*^{-1}P(\mathrm{GL}_2\mathbb{R} \times \mathrm{GL}_3\mathbb{R})$-subbundle of the projective frame bundle on $\mathsf{X}((1), (3, 1))$ is implemented faithfully on operator level:

$$\tau_*^{-1}P(\mathrm{GL}_2\mathbb{R} \times \mathrm{GL}_3\mathbb{R}) \to \mathcal{P}(\mathsf{X}((1), (3, 1)))^{[c(\kappa)]} \to \mathsf{X}((1), (1, 3)), \tag{7.92}$$

where $\mathcal{P}(\mathsf{X}((1), (3, 1)))^{[c(\kappa)]}$ denotes the space of projective frames invariant under the action of $[c(\kappa)]$. It consists of all projective frames on $\mathsf{X}((1), (3, 1))$ which preserve the splitting into space, and time together with the additional projective coordinate, i.e., two of the projective frame vector fields locally generate $\mathrm{Span}([\partial_0], [\partial_4])$, the remaining three generate $\mathrm{Span}([\partial_1], [\partial_2], [\partial_3])$, and the $\tau_*^{-1}P(\mathrm{GL}_2\mathbb{R} \times \mathrm{GL}_3\mathbb{R})$ action preserves this splitting.

To construct quantum field theories from classical action functionals, the classical limit is of interest. Various related methods exist, e.g. contractions of commutation relation Lie algebras ($\hbar \to 0$), Moyal bracket truncations, or considering highly occupied potentially coherent quantum states [112, 345]. The gauge group reduction is expected to be preserved in classical limits of suitable near-classical quantum states, since Theorem 7.4.5 holds on operator level without reference to quantum states.

**Conjecture 7.4.6.** *In the setting of Theorem 7.4.5 the reduction of the* $\mathrm{PGL}_5\mathbb{R}$ *gauge group to* $\tau_*^{-1}P(\mathrm{GL}_2\mathbb{R} \times \mathrm{GL}_3\mathbb{R})$ *is preserved in the classical limit and thus appears in corresponding classical action functionals.*

It is necessary to include quantum states and their classical limits into the given framework in order to make this conjecture precise and prove it.

**Physical scale dependence**

The identification $\mathsf{X}((1), (3, 1)) = \mathbb{A}^{3,1}$ is via the diffeomorphism

$$\xi([x_0, x_1, \ldots, x_4]) := (x_1/x_0, \ldots, x_4/x_0). \tag{7.93}$$

The metric tensor (7.78) on $\mathsf{X}((1),(3,1))$ depends only on the image of $\xi$. A physical scale transformation acts as $\xi([x]) \mapsto s\xi([x])$ for $s > 0$. Via $\xi^{-1}$ this is equivalent to

$$[x_0, x_1, \ldots, x_4] \mapsto [x_0, sx_1, \ldots, sx_4]. \tag{7.94}$$

The $\mathrm{PGL}_5\mathbb{R}$ element implementing the scale transformation is

$$[d(s)] = \mathrm{P}\begin{pmatrix} 1 & \\ & s \cdot 1_{4\times4} \end{pmatrix}. \tag{7.95}$$

Poincaré geometry remains invariant under $[d(s)]$.

Commutativity with $U([d(s)])$ probes physical scale invariance on operator level and yields the following lemma.

**Lemma 7.4.7** (Scale invariance breaking). *Assume the setting of Theorem 7.4.5 and $\rho$ and $\rho_A$ are non-trivial as representations of $\tau_*^{-1}\mathrm{P}(\mathrm{GL}_2\mathbb{R} \times 1)$. Then for $s \neq 1$:*

$$\rho([d(s)^{-1}])\rho([k^{-1}])\rho([d(s)])\rho([k]) \neq 1\,, \qquad \rho_A([d(s)^{-1}])\rho_A([k^{-1}])\rho_A([d(s)])\rho_A([k]) \neq 1 \tag{7.96}$$

*for some $[k] \in \tau_*^{-1}\mathrm{P}(\mathrm{GL}_2\mathbb{R} \times 1)$, while the group commutators equate to one for $[k] \in \tau_*^{-1}\mathrm{P}(1 \times \mathrm{GL}_3)$.*

*Proof.* The claim follows by comparing $[d(s) \cdot k]$ with $[k \cdot d(s)]$ for $[k] \in \tau_*^{-1}\mathrm{P}(\mathrm{GL}_2\mathbb{R} \times 1)$ and $[k] \in \tau_*^{-1}\mathrm{P}(1 \times \mathrm{GL}_3\mathbb{R})$, together with basic representation properties. $\square$

This lemma shows that $\tau_*^{-1}\mathrm{P}(\mathrm{GL}_2\mathbb{R} \times 1) \cong \mathrm{P}(\mathrm{GL}_2\mathbb{R} \times 1) \cong \mathbb{R}_{\neq 0} \times \mathrm{PGL}_2\mathbb{R}$ gauge bosons break physical scale invariance and must be massive in related particle physics models. It is tempting to associate these with the $W^{\pm}, Z$ gauge bosons of the Standard Model, and to deduce from Lemma 7.4.7 the necessity for a Higgs-like mechanism to generate their masses via an additional quantum field. If masses of $\mathrm{P}(\mathrm{GL}_2\mathbb{R} \times 1)$ gauge bosons are effectively due to a non-zero Poincaré-invariant vacuum expectation value of an additional quantum field, it must be a scalar quantum field upon restriction to Poincaré geometry, i.e., $\rho|_{\mathrm{PO}((1),(3,1))}$ must be trivial.

**Example 7.4.8.** *The projective vector quantum field $[\hat{W}]$ comes with (Hilbert space operator-valued) components $\hat{W}_B$, $B = 1, \ldots, 5$, defined up to a common $C^\infty(\mathsf{X}((1),(3,1)), \mathbb{R}_{\neq 0})$ multiple; choose an arbitrary one. Consider Poincaré geometry $\mathsf{G}((1),(3,1))$. Under a Poincaré transformation $(\Lambda, t)$ the tuple $(\hat{W}_\mu)_{\mu=2,\ldots,5}$ transforms as a 4-vector, i.e., for all $\mu = 1, \ldots, 4$:*

$$\hat{W}_{\mu+1}([x]) \mapsto \sum_{\nu=1}^{4} \Lambda_\mu{}^\nu \hat{W}_{\nu+1}([x]), \tag{7.97}$$

*as noted already in Example 7.3.3. With the projection $\mathrm{pr}_1 : (\hat{W}_1([x]), \ldots, \hat{W}_5([x])) \mapsto \hat{W}_1([x])$, $\mathrm{pr}_1(\hat{W}([x])) = \hat{W}_1([x])$ transforms as a Poincaré scalar:*

$$(\hat{W}_1([x]), 0, \ldots, 0) \overset{(\Lambda,t)\cdot}{\mapsto} (\hat{W}_1([x]), t_1\hat{W}_1([x]), \ldots, t_4\hat{W}_1([x])) \overset{\mathrm{pr}_1}{\mapsto} \hat{W}_1([x]). \tag{7.98}$$

*An element $k \in \tau_*^{-1}(\mathrm{GL}_2\mathbb{R} \times 1)$ acts on $(\hat{W}_1([x]), 0, \ldots, 0)$ in general non-trivially:*

$$(\hat{W}_1([x]), 0, \ldots, 0) \mapsto (k_{11}\hat{W}_1([x]), 0, 0, 0, k_{51}\hat{W}_1([x])). \tag{7.99}$$

*The gauge subgroup $\tau_*^{-1}\mathrm{P}(1 \times \mathrm{GL}_3\mathbb{R})$ acts trivially on $(\hat{W}_1([x]), 0, \ldots, 0)$. The gauge transformation behavior of the field operator $(\hat{W}_1([x]), 0, \ldots, 0)$ is thus similar to the Standard Model Higgs field.*

**Generalization to homogeneous Lorentzian geometries**

Theorem 7.4.5 and Lemma 7.4.7 have been formulated for Poincaré geometry. We turn to the analogous derivations for homogeneous Lorentzian geometries of the form

$$[g]_*\mathsf{G}(4,1) = ([g] \cdot \mathsf{X}(4,1), \mathrm{Ad}_{[g]}\mathrm{PO}(4,1)) \tag{7.100}$$

for some $[g] \in \mathrm{PGL}_5\mathbb{R}$. Poincaré geometry $\mathsf{G}((1),(3,1))$ is a limit of this, see Example 7.2.2(ii).

We introduce causal structures on $[g]_*\mathsf{X}(4,1)$. $\mathrm{P}^{-1}\mathsf{X}(4,1)$ comes with the metric tensor $h = -(\mathrm{d}x^0)^2 - \cdots - (\mathrm{d}x^3)^2 + (\mathrm{d}x^4)^2$. On $\mathrm{P}^{-1}([g] \cdot \mathsf{X}(4,1)) = g \cdot \mathrm{P}^{-1}\mathsf{X}(4,1)$ it induces the metric tensor

$$\tilde{h} := g_*h = \sum_{A,B=0}^{4} \overline{h}_{AB} \, \mathrm{d}x^A \odot \mathrm{d}x^B, \qquad \overline{h} = (g^{-1})^T \begin{pmatrix} -1_{4 \times 4} & \\ & 1 \end{pmatrix} g^{-1}. \tag{7.101}$$

On the charts $V_A := \{[x] \in [g] \cdot \mathsf{X}(4,1) \mid x_A \neq 0\}$, $A = 0, \ldots, 4$, individual metric tensors can be defined as follows. Let $[x], [x'] \in V_A$, i.e., $[x] = [x_0/x_A, \ldots, 1, \ldots, x_4/x_A]$ and $[x'] = [x_0'/x_A', \ldots, 1, \ldots, x_4'/x_A']$. This identifies the projective $V_A$ with a non-projective subset of $\mathbb{R}^4$ via $[x] \mapsto (x_0/x_A, \ldots, x_{A-1}/x_A, x_{A+1}/x_A, \ldots, x_4/x_A)$. With the coordinate differences $\Delta y_B = x_B'/x_A' - x_B/x_A$, $B = 0, \ldots, 4$: $\Delta y_A = 0$. Metric tensors $h_A'$ on the $V_A$ are defined by evaluating $\tilde{h}$ for the $\Delta y_B$ instead of the $\mathrm{d}x^B$ for all $B = 0, \ldots, 4$. The $h_A'$ can be glued together by multiplication with a partition of unity subordinate to the atlas $\{V_A\}$ and summation, to form a metric tensor defined on the full $[g] \cdot \mathsf{X}(4,1)$, denoted $h'$.

Two points $[x], [x'] \in [g] \cdot \mathsf{X}(4,1)$ are called time-like separated, if $h'([x], [x']) > 0$, null if $h'([x], [x']) = 0$, and space-like separated if $h'([x], [x']) < 0$. Their spatial distance is defined as $h'|_{\Delta y_4 \to 0}([x], [x'])$.

To probe causality preservation we consider

$$[c(\kappa)] = [g] \cdot \mathrm{P}\begin{pmatrix} \kappa & & \\ & 1_{3 \times 3} & \\ & & \kappa \end{pmatrix} \cdot [g^{-1}] \quad \text{for} \quad \kappa > 0. \tag{7.102}$$

**Lemma 7.4.9.** *Let $[x] \in [g] \cdot \mathsf{X}(4,1)$, and define the causal cone*

$$\mathscr{C}([x]) := \{[x'] \in [g] \cdot \mathsf{X}(4,1) \mid h'([x] - [x']) \geq 0\}. \tag{7.103}$$

*Then, $[c(\kappa)]$ deforms the causal cone $\mathscr{C}([x])$ for $\kappa \neq 1$: $[c(\kappa)] \cdot \mathscr{C}([x]) \neq \mathscr{C}([x])$.*

*Proof.* Let $[x'] \in \mathscr{C}([x])$ with $[x'] \neq [x]$, i.e., $h'([x] - [x']) \geq 0$. Assume without loss of generality $x_3, x'_3 \neq 0$, such that this is equivalent to

$$-\sum_{A=0}^{3}(g^{-1}(x/x_3 - x'/x'_3))_A^2 + (g^{-1}(x/x_3 - x'/x'_3))_4^2 \geq 0. \tag{7.104}$$

Choose without loss of generality $[x]$ and $[x']$ such that $(g^{-1}(x/x_3 - x'/x'_3))_1 \neq 0$. The element $[c(\kappa)]$ transforms the left-hand side to

$$-\kappa^2(g^{-1}(x/x_3 - x'/x'_3))_0^2 - \sum_{A=1}^{3}(g^{-1}(x/x_3 - x'/x'_3))_A^2 + \kappa^2(g^{-1}(x/x_3 - x'/x'_3))_4^2. \tag{7.105}$$

There exists $\kappa > 0$ such that this is strictly smaller than zero, i.e., $[x'] \notin [c(\kappa)] \cdot \mathscr{C}([x])$. $\square$

The following definition is analogous to Definition 7.4.2 for Poincaré geometry.

**Definition 7.4.10.** *On the geometry $[g]_*\mathsf{G}(4,1)$ a quantum field $\hat{\mathcal{O}}$ preserves causality, if for all space-like separated $[x], [x'] \in [g] \cdot \mathsf{X}(4,1)$, i.e., $[x'] \notin \mathscr{C}([x])$:*

$$[\hat{\mathcal{O}}([x]), \hat{\mathcal{O}}([x'])]_\mp = 0, \quad [\hat{\mathcal{O}}([x]), \hat{\mathcal{O}}^\dagger([x'])]_\mp = 0, \tag{7.106}$$

*with '$-$' for $\hat{\mathcal{O}}$ bosonic and '$+$' for $\hat{\mathcal{O}}$ fermionic. On the geometry $[g]_*\mathsf{G}(4,1)$ the quantum field $\hat{\mathcal{O}}$ is non-trivial, if light-like or time-like separated $[x], [x'] \in [g] \cdot \mathsf{X}(4,1)$ with non-zero spatial distance exist, such that $[\hat{\mathcal{O}}([x]), \hat{\mathcal{O}}([x'])]_\mp \neq 0$ and $[\hat{\mathcal{O}}([x]), \hat{\mathcal{O}}^\dagger([x'])]_\mp \neq 0$, again with '$-$' for $\hat{\mathcal{O}}$ bosonic and '$+$' for $\hat{\mathcal{O}}$ fermionic.*

**Theorem 7.4.11.** *Let $\hat{\mathcal{O}}$ be a quantum field, $[\hat{A}]$ a $\mathrm{PGL}_5\mathbb{R}$ gauge quantum field, both defined for the same Hilbert space $\mathcal{H}$, and $\mathrm{PGL}_5\mathbb{R}$ gauge transformations act on $\hat{\mathcal{O}}([x])$ as in Equation (7.74). Consider the geometry $[g]_*\mathsf{G}(4,1)$ and assume:*

*(i) $\hat{\mathcal{O}}$ and $[\hat{A}]$ are causality-preserving on the geometry $[g]_*\mathsf{G}(4,1)$ with commutators $[\cdot,\cdot]_{\hat{\mathcal{O}},\mp}$ and $[\cdot,\cdot]_{[\hat{A}],\mp}$,*

*(ii) $\mathfrak{A}_{\hat{\mathcal{O}},\hat{A}}([g] \cdot \mathsf{X}(4,1))$ is simultaneously commutator-generated with respect to $[\cdot,\cdot]_{\hat{\mathcal{O}},\mp}$ and $[\cdot,\cdot]_{[\hat{A}],\mp}$, and*

*(iii) the quantum fields $\hat{\mathcal{O}}$ and $[\hat{A}]$ are non-trivial on the geometry $[g]_*\mathsf{G}(4,1)$ .*

*Then, $U([g\,c(\kappa)\,g^{-1}])$ and $U_A([g\,c(\kappa)\,g^{-1}])$ commute with all field operators, i.e., maximally the representations $\rho_A$ and $\rho$ of the gauge subgroup*

$$[g] \cdot \tau_*^{-1}\mathrm{P}\begin{pmatrix} \mathrm{GL}_2\mathbb{R} & \\ & \mathrm{GL}_3\mathbb{R} \end{pmatrix} \cdot [g^{-1}] < \mathrm{PGL}_5\mathbb{R}, \tag{7.107}$$

*which is again isomorphic to $\mathrm{P}(\mathrm{GL}_2\mathbb{R} \times \mathrm{GL}_3\mathbb{R})$, do not act trivially on $\mathfrak{A}_{\hat{\mathcal{O}},\hat{A}}([g] \cdot \mathsf{X}(4,1))$.*

*Proof.* The proof is analogous to the proof of Theorem 7.4.5 by replacing Poincaré geometry with $[g]_*\mathsf{G}(4,1)$ and $[c(\kappa)]$ with $[g\,c(\kappa)\,g^{-1}]$. $\square$

Deformations and limits of geometries thus conjugate the reduced gauge group within PGL$_5\mathbb{R}$. Still, they can leave the reduced gauge group invariant as the following example demonstrates.

**Example 7.4.12.** *Consider the Poincaré limit of de Sitter geometry, i.e., the limit via*

$$[b_n] = \mathrm{P}\begin{pmatrix} e^{-4n} & \\ & e^n \cdot 1_{4\times 4} \end{pmatrix}, \tag{7.108}$$

*as discussed in Example 7.2.2(ii). The reduced gauge group on de Sitter geometry deforms for* $n \to \infty$ *to*

$$\lim_{n\to\infty} \mathrm{Ad}_{[b_n]}\tau_*^{-1}\mathrm{P}(\mathrm{GL}_2\mathbb{R} \times \mathrm{GL}_3\mathbb{R}) = \lim_{n\to\infty} \mathrm{Ad}_{[b_n]}\mathrm{P}\begin{pmatrix} * & 0 & * \\ 0 & \mathrm{GL}_3\mathbb{R} & 0 \\ * & 0 & * \end{pmatrix}$$

$$= \mathrm{P}\begin{pmatrix} * & 0 & * \\ 0 & \mathrm{GL}_3\mathbb{R} & 0 \\ * & 0 & * \end{pmatrix} \tag{7.109}$$

*with the* $2 \times 2$ *matrix defined from the four corner elements having non-zero determinant. This is the same* $\tau_*^{-1}\mathrm{P}(\mathrm{GL}_2\mathbb{R} \times \mathrm{GL}_3\mathbb{R})$ *as for Poincaré geometry by Theorem 7.4.5.*

We expect Conjecture 7.4.6 on classical limits to equally apply to the geometry $[g]_*\mathsf{G}(4,1)$. On the geometry $[g]_*\mathsf{G}(4,1)$ a variant of physical scale invariance can be probed with

$$[d'(s)] = [g] \cdot \mathrm{P}\begin{pmatrix} 1 & \\ & s \cdot 1_{4\times 4} \end{pmatrix} \cdot [g^{-1}] \quad \text{for} \quad s > 0, \tag{7.110}$$

which for $[g] = [b_n]$ with the $[b_n]$ of Equation (7.17) yields $[d(s)]$ as for Poincaré geometry. The following lemma is analogous to Lemma 7.4.7.

**Lemma 7.4.13.** *Assume the setting of Theorem 7.4.11. Let $\rho$ and $\rho_A$ be non-trivial as representations of* $\mathrm{Ad}_{[g]}\tau_*^{-1}\mathrm{P}(\mathrm{GL}_2\mathbb{R} \times 1)$. *Then for* $s \neq 1$:

$$\rho([d'(s)^{-1}])\rho([k^{-1}])\rho([d'(s)])\rho([k]) \neq 1, \quad \rho_A([d'(s)^{-1}])\rho_A([k^{-1}])\rho_A([d'(s)])\rho_A([k]) \neq 1 \tag{7.111}$$

*for some* $[k] \in \mathrm{Ad}_{[g]}\tau_*^{-1}\mathrm{P}(\mathrm{GL}_2\mathbb{R} \times 1)$, *while the group commutators equate to one for* $[k] \in \mathrm{Ad}_{[g]}\tau_*^{-1}\mathrm{P}(1 \times \mathrm{GL}_3\mathbb{R})$.

*Proof.* The proof is analogous to the proof of Lemma 7.4.7 using $[d'(s)]$ given by Equation (7.110) instead of $[d(s)]$. $\square$

**Remark 7.4.14.** *There are geometries such as Galilei geometry* $\mathsf{G}((1),(1),(3))$ *or spherical geometry* $\mathsf{G}(5)$, *which do not canonically possess a non-trivial causal structure. For these the gauge group reduction of Theorem 7.4.11 does not apply. Still, there is a gauge subgroup of* PGL$_5\mathbb{R}$, *for which the related gauge bosons break scale invariance along the lines of Lemmas 7.4.7 and 7.4.13.*

### 7.4.3   Gauge group representations for fermions

We show that irreducible fermionic quantum fields give rise to gauge transformation behavior similar to the Standard Model fermions. We implicitly consider the geometries $\mathsf{G}((1),(3,1))$ and $[g]_*\mathsf{G}(4,1)$ here, such that the gauge group reduction of Theorems 7.4.5 and 7.4.11 applies.

By Lemma 7.3.17, the irreducible quantum fields all have the form $\hat{\mathcal{O}}_{(\lambda,\lambda')}$ for a pair of Young tableaux $(\lambda,\lambda')$, where $\tilde{\rho}_{(\lambda,\lambda')} = \mathbb{CP}^4_{(\lambda,\lambda')}$. Specifically, considered for the full gauge group $\mathrm{PGL}_5\mathbb{R}$ we find the following gauge transformation behavior, if $\hat{\mathcal{O}}_{(\lambda,\lambda')}$ is fermionic and obeys spin-statistics.

**Proposition 7.4.15.** *For a pair of Young tableaux $(\lambda,\lambda')$ let $\hat{\mathcal{O}}_{(\lambda,\lambda')}$ be a fermionic irreducible quantum field with finite-dimensional representation $\rho' = \rho_{(\lambda,\lambda')}$ as in Proposition 7.3.16, which obeys spin-statistics. Let*

$$\hat{\mathcal{O}}([x]) \mapsto \rho_{(\lambda,\lambda')}([\Psi([x])])\,\hat{\mathcal{O}}([x]) \tag{7.112}$$

*under a gauge transformation $[\Psi]$ on $\mathbb{RP}^4$. Then the quantum field $\hat{\mathcal{O}}_{(\lambda,\lambda')}$ gauge-transforms via a gauge group representation with corresponding Lie algebra representation*

$$\tilde{\bigwedge}^{\#\lambda}\,\mathbb{CP}^4_{\mathfrak{pgl}_5\mathbb{R}} \,\tilde{\otimes}\, \tilde{\bigwedge}^{\#\lambda'}\,\mathbb{CP}^{4*}_{\mathfrak{pgl}_5\mathbb{R}}\,, \tag{7.113}$$

*which is trivial if both $\#\lambda, \#\lambda' \in \{0,5\}$, and zero if $\#\lambda \geq 6$ or $\#\lambda' \geq 6$.*

*Proof.* Lemma 7.3.17 implies that for the fermionic quantum fields under consideration $\lambda$ and $\lambda'$ must consist of single columns only. This implies the representation of the form (7.113). The isomorphism $\mathrm{PGL}_5\mathbb{R} \cong \mathrm{SL}_5\mathbb{R}$ implies triviality of $\tilde{\bigwedge}^r\,\mathbb{CP}^4_{\mathfrak{pgl}_5\mathbb{R}}$ and $\tilde{\bigwedge}^r\,\mathbb{CP}^{4*}_{\mathfrak{pgl}_5\mathbb{R}}$ for $r = 0, 5, 6, \ldots$ in the two forms specified.   $\square$

Based on Theorem 7.4.5, representations restricted to the reduced gauge group *conjugate* in $\mathrm{PGL}_5\mathbb{R}$ to $\mathrm{P}(\mathrm{GL}_2\mathbb{R} \times \mathrm{GL}_3\mathbb{R})$ need to be considered. Conjugation of the reduced gauge group results in equivalent representations. We thus focus on $\mathrm{P}(\mathrm{GL}_2\mathbb{R} \times \mathrm{GL}_3\mathbb{R})$ itself. The following group isomorphisms can be established.

**Proposition 7.4.16.** *The map $\eta : \mathbb{R}_{\neq 0} \times \mathrm{PGL}_2\mathbb{R} \times \mathrm{PGL}_3\mathbb{R} \to \mathrm{P}(\mathrm{GL}_2\mathbb{R} \times \mathrm{GL}_3\mathbb{R})$,*

$$\eta(\alpha, g, h) = \mathrm{P}\begin{pmatrix} \alpha^3 g & \\ & \alpha^{-2} h \end{pmatrix}, \tag{7.114}$$

*is a group isomorphism. Similarly, the map $\eta' : \mathbb{R}_{>0} \times \mathrm{SL}_2\mathbb{R} \times \mathrm{SL}_3\mathbb{R} \to \mathrm{S}(\mathrm{GL}_2\mathbb{R} \times \mathrm{GL}_3\mathbb{R})$,*

$$\eta'(\alpha, g, h) = \begin{pmatrix} \alpha^3 g & \\ & \alpha^{-2} h \end{pmatrix}, \tag{7.115}$$

*is a group isomorphism.*

*Proof.* Clearly, $\eta$ is a Lie group homomorphism. A general element of $\mathrm{P}(\mathrm{GL}_2\mathbb{R} \times \mathrm{GL}_3\mathbb{R})$ can be written as

$$\mathrm{P}\begin{pmatrix} \tilde{\alpha}^5 g & \\ & \tilde{\beta} h \end{pmatrix} = \mathrm{P}\begin{pmatrix} \tilde{\alpha}^5 \tilde{\beta}^{-1} g & \\ & h \end{pmatrix} \tag{7.116}$$

for $\tilde{\alpha}, \tilde{\beta} \in (0, \infty)$ and $g \in \mathrm{SL}_2\mathbb{R}$, $h \in \mathrm{SL}_3\mathbb{R}$, noting that $-1_{2\times 2} \in \mathrm{SL}_2\mathbb{R}$. Setting $\alpha := \tilde{\alpha}\tilde{\beta}^{-1/5}$, the matrix (7.116) equals

$$\mathrm{P}\begin{pmatrix} \alpha^5 g & \\ & h \end{pmatrix} = \mathrm{P}\begin{pmatrix} \alpha^3 g & \\ & \alpha^{-2}h \end{pmatrix}, \tag{7.117}$$

which is in the image of $\eta$; the map $\eta$ is surjective. In particular, this parametrization of $\mathrm{P}(\mathrm{GL}_2\mathbb{R} \times \mathrm{GL}_3\mathbb{R})$ elements via $\alpha \in (0, \infty)$, $g \in \mathrm{SL}_2\mathbb{R}$, $h \in \mathrm{SL}_3\mathbb{R}$ is the same as the parametrization by $\alpha \in \mathbb{R}_{\neq 0}$, $g \in \mathrm{SL}_2\mathbb{R}/\mathbb{Z}_2$, $h \in \mathrm{SL}_3\mathbb{R}$, and $\mathrm{PGL}_2\mathbb{R} \cong \mathrm{SL}_2\mathbb{R}/\mathbb{Z}_2$, $\mathrm{PGL}_3\mathbb{R} \cong \mathrm{SL}_3\mathbb{R}$. To show injectivity, we compute the kernel and set

$$[1] = \eta(\alpha, g, h) = \mathrm{P}\begin{pmatrix} \alpha^3 g & \\ & \alpha^{-2}h \end{pmatrix}, \tag{7.118}$$

for some $\alpha \in (0, \infty)$ and $g \in \mathrm{SL}_2\mathbb{R}$, $h \in \mathrm{SL}_3\mathbb{R}$. Equation (7.118) yields $\alpha^3 g = \alpha^{-2}h = \beta \cdot 1_{5\times 5}$ for some $\beta \neq 0$. The only $g \in \mathrm{SL}_2\mathbb{R}$ proportional to $1_{2\times 2}$ are $\pm 1_{2\times 2}$, the only $h \in \mathrm{SL}_3\mathbb{R}$ proportional to $1_{3\times 3}$ is $1_{3\times 3}$. Hence, $\beta = \alpha^{-2}$ and $\beta = \pm\alpha^{-3}$, such that $\alpha = \pm 1$. But $\alpha \in (0, \infty)$, such that $\alpha = 1$ and $\beta = 1$, which implies $g = 1_{2\times 2}$. The kernel of $\eta$ is indeed trivial.

The statement for $\eta'$ has been proven implicitly. $\qquad\square$

The isomorphisms of Proposition 7.4.16 are analogous to $\mathrm{S}(\mathrm{U}(2) \times \mathrm{U}(3)) \cong G_{\mathrm{SM}} = (\mathrm{U}(1) \times \mathrm{SU}(2) \times \mathrm{SU}(3))/\mathbb{Z}_6$. No quotient by $\mathbb{Z}_6$ appears for the real groups, since the only roots of unity in $\mathrm{SL}_2\mathbb{R}$ are $\pm 1_{2\times 2}$, which are taken care of by restricting the Abelian subgroup to $\mathbb{R}_{>0}$, and $\mathrm{SL}_3\mathbb{R}$ has trivial center.

We note that the powers $\alpha^3, \alpha^{-2}$ in the definition of $\eta'$ in Proposition 7.4.16 are fixed up to common multiples by the unit determinant requirement. As for $\eta'$, any combination of powers of $\alpha$ other than common multiples of $\alpha^3, \alpha^{-2}$ would break commutativity of the diagram

$$\begin{array}{ccc} \mathbb{R}_{\neq 0} \times \mathrm{PGL}_2\mathbb{R} \times \mathrm{PGL}_3\mathbb{R} & \xrightarrow{\sim} & \mathbb{R}_{>0} \times \mathrm{SL}_2\mathbb{R} \times \mathrm{SL}_3\mathbb{R} \\ \downarrow{\eta} & & \downarrow{\eta'} \\ \mathrm{P}(\mathrm{GL}_2\mathbb{R} \times \mathrm{GL}_3\mathbb{R}) & \xrightarrow{\Xi} & \mathrm{S}(\mathrm{GL}_2\mathbb{R} \times \mathrm{GL}_3\mathbb{R}), \end{array} \tag{7.119}$$

where all maps are group isomorphisms and $\Xi$ maps $[g \times h] \in \mathrm{P}(\mathrm{GL}_2\mathbb{R} \times \mathrm{GL}_3\mathbb{R})$ to the unique unit-determinant representative of the equivalence class.

The fundamental complex representation of $\mathfrak{pgl}_m\mathbb{R}$ is denoted by $\mathbb{CP}^{m-1}_{\mathfrak{pgl}_m\mathbb{R}}$ and its dual representation by $\mathbb{CP}^{m-1,*}_{\mathfrak{pgl}_m\mathbb{R}}$; its trivial representation is $1_{\mathfrak{pgl}_m\mathbb{R}}$. The Abelian representation $\mathbb{R} \ni a \mapsto [\kappa a \cdot 1_{m\times m}] \in \mathfrak{pgl}_m\mathbb{R}$ is denoted $\mathbb{C}_{\kappa/3}$ for $\kappa \in \mathbb{R}$, $\kappa/3$ is called the weak hypercharge. As $\mathbb{R} \times \mathfrak{pgl}_2\mathbb{R} \times \mathfrak{pgl}_3\mathbb{R}$ representations, we find the following behavior of irreducible fermionic quantum fields upon restriction of the gauge group to $\mathrm{P}(\mathrm{GL}_2\mathbb{R} \times \mathrm{GL}_3\mathbb{R})$, which is based on Theorems 7.4.5 and 7.4.11.

**Lemma 7.4.17.** *Consider the irreducible fermionic quantum fields $\hat{\mathcal{O}}_{(\lambda,\lambda')}$ for the setting of Proposition 7.4.15. Upon restriction of the gauge group $\mathrm{PGL}_5\mathbb{R}$ to $\mathrm{P}(\mathrm{GL}_2\mathbb{R} \times \mathrm{GL}_3\mathbb{R})$ the field operators $\hat{\mathcal{O}}_{(\lambda,\lambda')}([x])$ gauge-transform via a representation which has as the Lie algebra*

*representation the tensor product of the #$\lambda$-th and the dual representation corresponding to the #$\lambda'$-th of the following representations:*

$$\tilde{\bigwedge}^1 \mathbb{CP}^4|_{\mathfrak{p}(\mathfrak{gl}_2\mathbb{R}\times\mathfrak{gl}_3\mathbb{R})} \cong (\mathbb{C}_{+1} \tilde{\otimes} \mathbb{CP}^1 \tilde{\otimes} 1) \oplus (\mathbb{C}_{-2/3} \tilde{\otimes} 1 \tilde{\otimes} \mathbb{CP}^2), \tag{7.120a}$$

$$\tilde{\bigwedge}^2 \mathbb{CP}^4|_{\mathfrak{p}(\mathfrak{gl}_2\mathbb{R}\times\mathfrak{gl}_3\mathbb{R})} \cong (\mathbb{C}_{+2} \tilde{\otimes} 1 \tilde{\otimes} 1) \oplus (\mathbb{C}_{+1/3} \tilde{\otimes} \mathbb{CP}^1 \tilde{\otimes} \mathbb{CP}^2) \oplus (\mathbb{C}_{-4/3} \tilde{\otimes} 1 \tilde{\otimes} \mathbb{CP}^{2*}), \tag{7.120b}$$

$$\tilde{\bigwedge}^3 \mathbb{CP}^4|_{\mathfrak{p}(\mathfrak{gl}_2\mathbb{R}\times\mathfrak{gl}_3\mathbb{R})} \cong (\mathbb{C}_{-2} \tilde{\otimes} 1 \tilde{\otimes} 1) \oplus (\mathbb{C}_{-1/3} \tilde{\otimes} \mathbb{CP}^{1*} \tilde{\otimes} \mathbb{CP}^{2*}) \oplus (\mathbb{C}_{+4/3} \tilde{\otimes} 1 \tilde{\otimes} \mathbb{CP}^2), \tag{7.120c}$$

$$\tilde{\bigwedge}^4 \mathbb{CP}^4|_{\mathfrak{p}(\mathfrak{gl}_2\mathbb{R}\times\mathfrak{gl}_3\mathbb{R})} \cong (\mathbb{C}_{-1} \tilde{\otimes} \mathbb{CP}^{1*} \tilde{\otimes} 1) \oplus (\mathbb{C}_{+2/3} \tilde{\otimes} 1 \tilde{\otimes} \mathbb{CP}^{2*}) \tag{7.120d}$$

*The decompositions are into irreducible representations of $\mathbb{R} \times \mathfrak{pgl}_2\mathbb{R} \times \mathfrak{pgl}_3\mathbb{R}$ (omitting most group subscripts), and the weak hypercharges of Equations (7.120a) to (7.120d) are unique up to two linear maps on the different exterior powers. Further,*

$$\tilde{\bigwedge}^r \mathbb{CP}^4_{\mathfrak{pgl}_5\mathbb{R}}\Big|_{\mathfrak{p}(\mathfrak{gl}_2\mathbb{R}\times\mathfrak{gl}_3\mathbb{R})} \tag{7.121}$$

*is the trivial representation for $r = 0$ and $r = 5$, and equates to zero for $r > 5$.*

*Proof.* Decomposition (7.120a) is clear with $\mathbb{CP}^4 \cong \mathrm{P}(\mathbb{C}^2 \oplus \mathbb{C}^3)$ via the isomorphism of Proposition 7.4.16. Equation (7.120b) follows with the Künneth formula for exterior powers of direct sums of Lie algebra representations:

$$\tilde{\bigwedge}^2 [(\mathbb{C}_{+1} \tilde{\otimes} \mathbb{CP}^1 \tilde{\otimes} 1) \oplus (\mathbb{C}_{-2/3} \tilde{\otimes} 1 \tilde{\otimes} \mathbb{CP}^2)]$$
$$\cong \tilde{\bigwedge}^2 (\mathbb{C}_{+1} \tilde{\otimes} \mathbb{CP}^1 \tilde{\otimes} 1) \oplus [(\mathbb{C}_{+1} \tilde{\otimes} \mathbb{CP}^1 \tilde{\otimes} 1) \tilde{\otimes} (\mathbb{C}_{-2/3} \tilde{\otimes} 1 \tilde{\otimes} \mathbb{CP}^2)]$$
$$\oplus \tilde{\bigwedge}^2 (\mathbb{C}_{-2/3} \tilde{\otimes} 1 \tilde{\otimes} \mathbb{CP}^2)$$
$$\cong (\mathbb{C}_{+2} \tilde{\otimes} 1 \tilde{\otimes} 1) \oplus (\mathbb{C}_{+1/3} \tilde{\otimes} \mathbb{CP}^1 \tilde{\otimes} \mathbb{CP}^2) \oplus (\mathbb{C}_{-4/3} \tilde{\otimes} 1 \tilde{\otimes} \mathbb{CP}^{2*}), \tag{7.122}$$

where for the last isomorphism we employed that Hodge duality yields $\tilde{\bigwedge}^2 \mathbb{CP}^1_{\mathfrak{pgl}_2\mathbb{R}} \cong 1_{\mathfrak{pgl}_2\mathbb{R}}$, $\tilde{\bigwedge}^2 \mathbb{CP}^2_{\mathfrak{pgl}_3\mathbb{R}} \cong \mathbb{CP}^{2*}_{\mathfrak{pgl}_3\mathbb{R}}$. The decompositions (7.120c) and (7.120d) follow with the Hodge duality

$$\tilde{\bigwedge}^r \mathbb{CP}^4|_{\mathfrak{p}(\mathfrak{gl}_2\mathbb{R}\times\mathfrak{gl}_3\mathbb{R})} \cong \left(\tilde{\bigwedge}^{5-r} \mathbb{CP}^4|_{\mathfrak{p}(\mathfrak{gl}_2\mathbb{R}\times\mathfrak{gl}_3\mathbb{R})}\right)^*. \tag{7.123}$$

The weak hypercharges of the decompositions (7.120a) to (7.120d) are by the projective construction only fixed up to linear maps $\xi_r(\kappa/3) := C_r\kappa/3 + D_r$ for arbitrary $C_r, D_r \in \mathbb{R}$. The Hodge duality (7.123) yields $\xi_1 = \xi_4$ and $\xi_2 = \xi_3$. Two of the linear maps $\xi_r$ remain unfixed. $\qquad\square$

The requirement of a commutative diagram such as (7.119) would fix the weak hypercharges up to one common multiple.

**Remark 7.4.18.** *The gauge group reduction to $\mathrm{P}(\mathrm{GL}_2\mathbb{R} \times \mathrm{GL}_3\mathbb{R})$ has been proven for the geometries $[g]_*\mathsf{G}(4, 1)$ and $\mathsf{G}((1), (3, 1))$ in Theorems 7.4.5 and 7.4.11. Lemma 7.4.17 is thus sensible for these.*

### 7.4.4 Implications for particle physics models

The results of this work suggest that particle physics models based on four-dimensional subgeometries of real projective geometry include a $\mathrm{PGL}_5\mathbb{R}$ gauge quantum field $[\hat{A}]$ and the bosonic or fermionic irreducible quantum fields $\hat{\mathcal{O}}_{(\lambda,\lambda')}$. We restrict to the case that the $\hat{\mathcal{O}}_{(\lambda,\lambda')}$ are composite Schur quantum fields of the quantum field $\hat{\mathcal{O}}_{(\square,\emptyset)}$, which is barely a restriction with regard to the specified transformation behavior as we discuss. We consider Poincaré geometry $\mathsf{G}((1),(3,1))$ in this subsection. Regarding the physical content, a few of the results of this subsection are somewhat more speculative and necessitate further investigations.

Particle physics models are regularly given in the functional integral formalism. There, an action functional is constructed from the quantum fields, which is gauge and Poincaré invariant. Corresponding kinetic terms allow for the propagation of quantum field excitations in space-time. Potential terms can give rise to (effective) masses as well as self-interactions, and the inclusion of gauge covariant derivatives implements interactions among the gauge bosons and the matter fields. The following thus includes a discussion of implications of our framework for physical action functionals.

#### Gauge fields

Though corresponding to a projective vector field, on $\mathbb{A}^{3,1} = \mathsf{X}((1),(3,1))$ the gauge quantum field $[\hat{A}]$ *looks like* a usual non-projective vector field. Indeed, based on Example 7.2.5, for $[x] \in \mathsf{X}((1),(3,1))$ the projective vector field $[\hat{A}([x_0,\ldots,x_4])]$ can be identified with a non-projective vector field $\hat{A}_\mu(y)$, which has the components

$$\hat{A}_\mu(y_1,\ldots,y_4) + \hat{A}_5(y_1,\ldots,y_4)\,, \tag{7.124}$$

$y_\mu := x_\mu/x_0$ for $\mu = 1,\ldots,4$. A conjectured implication of the actual projective formulation, related to renormalizability, is provided below.

The gauge field operators $[\hat{A}(y)]$ do not readily lead to negative-definite kinetic (Yang-Mills-like) terms for the gauge bosons to include in an action functional, since the reduced gauge group $\mathrm{P}(\mathrm{GL}_2\mathbb{R} \times \mathrm{GL}_3\mathbb{R})$ is non-compact. As a quantum field, $[\hat{A}(y)]$ comes with a finite-dimensional *complex* representation of $\mathfrak{pgl}_5\mathbb{R}$, which is the same as a representation of its complexification $\mathfrak{pgl}_5\mathbb{C}$. For the reduced gauge group $\mathrm{P}(\mathrm{GL}_2\mathbb{R} \times \mathrm{GL}_3\mathbb{R})$ with Lie algebra $\mathfrak{p}(\mathfrak{gl}_2\mathbb{R} \oplus \mathfrak{gl}_3\mathbb{R})$ this implies that it is on Lie algebra level the same as a representation of $\mathfrak{p}(\mathfrak{gl}_2\mathbb{C} \oplus \mathfrak{gl}_3\mathbb{C})$. Only representations of the compact real form of $\mathfrak{p}(\mathfrak{gl}_2\mathbb{C} \oplus \mathfrak{gl}_3\mathbb{C})$ can have positive-definite trace forms in finite dimensions, which provide negative-definite kinetic terms for action functionals [90]. The compact real form of $\mathfrak{p}(\mathfrak{gl}_2\mathbb{C} \oplus \mathfrak{gl}_3\mathbb{C})$ is

$$\mathfrak{p}(\mathfrak{u}(2) \oplus \mathfrak{u}(3)) \cong \mathfrak{s}(\mathfrak{u}(2) \oplus \mathfrak{u}(3))\,, \tag{7.125}$$

with corresponding compact Lie group $\mathrm{S}(\mathrm{U}(2) \times \mathrm{U}(3)) \cong G_{\mathrm{SM}}$ [91]. This suggests that the gauge quantum field $[\hat{A}]$ is in the action functional indistinguishable from the Standard Model gauge fields.

**Matter fields**

The irreducible quantum fields have with regard to the involved finite-dimensional representation the building blocks $\hat{\mathcal{O}}_{(\square,\emptyset)}$ and $\hat{\mathcal{O}}_{(\emptyset,\square)}$, one being the dual of the other. The quantum field $\hat{\mathcal{O}}_{(\square,\emptyset)}$ splits into a scalar field and a Dirac fermion.

**Lemma 7.4.19.** *The field operator $\hat{\mathcal{O}}([x])$, $[x] \in \mathsf{X}((1),(3,1))$, of an irreducible quantum field of type $\hat{\mathcal{O}} = \hat{\mathcal{O}}_{(\square,\emptyset)}$ splits into a sum of a field operator $\hat{H}([x])$ on which $\rho(\mathrm{P}(1 \times \mathrm{O}(3,1)))$ acts trivially, and a field operator $\hat{\Psi}([x])$ on which $\rho(\mathrm{P}(1 \times \mathrm{O}(3,1)))$ acts as for Dirac fermions. If $\hat{\mathcal{O}}$ is bosonic, $\hat{\mathcal{O}}$ with $\hat{\mathcal{O}}([x]) \neq 0$ for some $[x] \in \mathsf{X}((1),(3,1))$ cannot exist as a quantum field.*

*Proof.* Considered as a $\mathfrak{pgl}_5\mathbb{C}$ representation, $\tilde{\rho}$ is $\mathbb{CP}^4_{\mathfrak{pgl}_5\mathbb{C}}$. Write $\hat{\mathcal{O}}([x]) = \hat{H}([x]) + \hat{\Psi}([x])$, where

$$\hat{H}([x]) = [\hat{\mathcal{O}}_1([x]), 0, 0, 0, 0], \qquad \hat{\Psi}([x]) = [0, \hat{\mathcal{O}}_2([x]), \dots, \hat{\mathcal{O}}_5([x])]. \tag{7.126}$$

By Example 7.4.8, $\hat{H}([x])$ transforms trivially under $\mathrm{P}(1 \times \mathrm{O}(3,1))$ transformations. The Lie algebra complexification $\mathrm{Lie}(1 \times \mathrm{O}(3,1))_\mathbb{C} = (0 \oplus \mathfrak{o}(3,1))_\mathbb{C} \cong 0 \oplus \mathfrak{su}(2)_\mathbb{C} \oplus \overline{\mathfrak{su}(2)}_\mathbb{C}$ acts on $\hat{\Psi}([x])$ by matrix multiplication as for a Dirac fermion, which has spin $(1/2,0) \oplus (0,1/2)$.

Let $\omega$ be the multiplier of $U$. If the projective representation $U|_{\mathrm{P}(1 \times \mathrm{O}(3,1))}$ has integer (half-odd integer) spin, it comes with multiplier $\omega_+$ ($\omega_-$). This comes about, since $\mathrm{P}(1 \times \mathrm{O}(3,1)) \cong \mathrm{O}(3,1)$ has $\mathrm{SO}^+(3,1)$ as connected component of the identity, and $\mathrm{Spin}(3,1) \cong \mathrm{SL}_2\mathbb{C}$ is the (universal) double cover of $\mathrm{SO}^+(3,1)$. The irreducible $(1/2,0) \oplus (0,1/2)$ representation of the Poincaré group thus comes with multiplier equivalent to $\omega_-$, and the irreducible higher spin Poincaré group representations, which are partly symmetrized tensor product representations of the $(1/2,0) \oplus (0,1/2)$ representation, come with multipliers equivalent to powers of $\omega_-$. Further, $U$ being a projective unitary representation, it decomposes into a direct sum or direct integral of irreducible projective unitary $\mathrm{PGL}_5\mathbb{R}$ representations [85], such that the multipliers only depend on the spin also without irreducibility. For instance, for $U|_{\mathrm{P}(1 \times \mathrm{O}(3,1))}$ having spin $(1/2,0) \oplus (0,1/2)$, it must be a direct sum or direct integral of *one* spin $(1/2,0) \oplus (0,1/2)$ irreducible Poincaré group representation with potentially many trivial Poincaré group representations, such that its multiplier is in full generality equivalent to $\omega_-$. $\hat{\mathcal{O}}$ violates this for $\omega$ equivalent to $\omega_+$, which yields the non-existence statement. Indeed, the transformation property (7.28) for all $\mathrm{PGL}_5\mathbb{R}$ implies that all field operator components of $\hat{\mathcal{O}}([x])$ are non-zero, such that the (projective) Lorentz transformations $\mathrm{P}(1 \times \mathrm{O}(3,1))$ act non-trivially on $\hat{\mathcal{O}}([x])$. $\qquad \square$

From $\hat{\mathcal{O}}_{(\square,\emptyset)}$ we can construct the composite Schur quantum field $\hat{\mathcal{O}}_{(\lambda,\lambda')} := \hat{\mathcal{O}}_{(\lambda,\lambda')}^{\mathrm{comp}}$, which comes with the irreducible representation $\rho_{(\lambda,\lambda')}$. We can carry out the same construction using the field operators $\hat{\Psi}([x])$ instead, yielding $\hat{\Psi}_{(\lambda,\lambda')}$. $\hat{\Psi}_{(\lambda,\lambda')}$ constitutes a quantum field if restricted to Poincaré geometry. Indeed, on Poincaré geometry the set of field operators $\{\hat{\Psi}_{(\lambda,\lambda'),\alpha}([x])\}$ consistently fulfils the transformation property (7.28), and in Definition 7.3.1 no requirement of it being closed under the action of $\rho$ as for gauge transformations (7.112) is contained. Taking into account the involved zero field operators, the $\hat{\Psi}_{(\lambda,\lambda')}$ effectively transform under Poincaré transformations as specified by the following proposition.

**Proposition 7.4.20.** *Assume both $\lambda, \lambda'$ consist of a single column, as required by Lemma 7.3.17 for irreducible fermionic quantum fields which obey spin-statistics. A Poincaré transformation $[(\Lambda, t)] \in \mathrm{PO}((1), (3, 1))$ acts on the fermionic $\hat{\Psi}_{(\lambda, \lambda')}$ as follows:*

*(i) for $\hat{\Psi}_{(\lambda, \emptyset)}$ and $\hat{\Psi}_{(\emptyset, \lambda)}$ via the $(0, 0)$ (scalar) representation if $\#\lambda = 0, 4$, via the $(1/2, 0) \oplus (0, 1/2)$ (Dirac fermion) representation if $\#\lambda = 1, 3$, and via the $(1/2, 1/2)$ (vector) representation if $\#\lambda = 2$,*

*(ii) for $\hat{\Psi}_{(\lambda, \lambda')} = \hat{\Psi}_{(\lambda, \emptyset)} \otimes \hat{\Psi}_{(\emptyset, \lambda')}$ via the tensor product of the $\mathrm{PO}((1), (3, 1))$ representations of the two factors.*

*If any $\#\lambda, \#\lambda' \geq 5$, the corresponding field operators are all zero.*

*Proof.* We note that $\tilde{\bigwedge}^n (0 \oplus \mathbb{C}^2 \oplus \overline{\mathbb{C}}^2)_{0 \oplus \mathfrak{su}(2) \oplus \mathfrak{su}(2)} \cong \tilde{\bigwedge}^n (\mathbb{C}^2 \oplus \overline{\mathbb{C}}^2)_{\mathfrak{su}(2) \oplus \mathfrak{su}(2)}$. This can be viewed as a special case of the Künneth formula for general exterior powers of direct sums of Lie algebra representations,

$$\tilde{\bigwedge}^n (V \oplus W) \cong \bigoplus_{p=0}^n \tilde{\bigwedge}^p V \tilde{\otimes} \tilde{\bigwedge}^{n-p} W \,, \tag{7.127}$$

where $V, W$ are two Lie algebra representations. With this we compute:

$$\tilde{\bigwedge}^n (\mathbb{C}^2_{\mathfrak{su}(2)} \oplus \overline{\mathbb{C}}^2_{\mathfrak{su}(2)}) \cong \bigoplus_{p=0}^n \tilde{\bigwedge}^p \mathbb{C}^2_{\mathfrak{su}(2)} \tilde{\otimes} \tilde{\bigwedge}^{n-p} \overline{\mathbb{C}}^2_{\mathfrak{su}(2)} \,, \tag{7.128}$$

where $\overline{\mathbb{C}}^2_{\mathfrak{su}(2)}$ denotes the complex conjugate representation of $\mathbb{C}^2_{\mathfrak{su}(2)}$. Noting that $\bigwedge^2 \mathbb{C}^2_{\mathfrak{su}(2)} \cong \mathbb{C}$ is trivial as a group representation, and $\bigwedge^p \mathbb{C}^2_{\mathfrak{su}(2)} \cong 0$ for $p \geq 3$ is trivial as a vector space yields the claim. $\qquad\square$

**Remark 7.4.21.** *If instead of the restricted $\hat{\Psi}_{(\lambda, \lambda')}|_{\mathsf{G}((1),(3,1))}$ we consider the general irreducible fermionic quantum fields $\hat{\mathcal{O}}_{(\lambda, \lambda')}$ with all involved field operators $\hat{\mathcal{O}}_{(\lambda, \lambda'), \alpha}([x])$ non-zero, then translations $[(1_{4\times 4}, t)] \in \mathrm{PO}((1), (3, 1))$ can act non-trivially on the field operators $\hat{\mathcal{O}}_{(\lambda, \lambda')}([x])$ via the finite-dimensional representation $\rho_{(\lambda, \lambda')}$. Yet, if $\hat{\mathcal{O}}_{(\lambda, \lambda')}$ transforms as an irreducible Poincaré group representation under $\mathrm{PO}((1), (3, 1))$ elements, which is induced from the Lorentz group $\mathrm{O}(3, 1)$, then $\rho_{(\lambda, \lambda')}([(1_{4\times 4}, t)])$ is required to act trivially on all $\hat{\mathcal{O}}_{(\lambda, \lambda')}([x])$. This suggests a behavior under Poincaré transformations similar to Proposition 7.4.20, since analogous to Example 7.3.3 some of the field operator components $\hat{\mathcal{O}}_{(\lambda, \lambda'), \alpha}([x])$ need to be zero. Details are left to be worked out.*

Lemma 7.4.17 describes how the fermions $\hat{\Psi}_{(\lambda, \lambda')}$ transform with respect to the real projective gauge group $\mathrm{P}(\mathrm{GL}_2\mathbb{R} \times \mathrm{GL}_3\mathbb{R})$. As a representation of the compact group $\mathrm{S}(\mathrm{U}(2) \times \mathrm{U}(3))$, the Abelian Lie algebra representation $\mathbb{C}_{\kappa/3}$ of $\mathbb{R}$ becomes the $\mathrm{U}(1)$ Lie group representation $\mathrm{U}(1) \ni \exp(\mathrm{i}\varphi) \mapsto \exp(\mathrm{i}\kappa\varphi/3) \cdot 1_{m\times m} \in \mathrm{U}(m)$, synonymously denoted $\mathbb{C}_{\kappa/3}$, with weak hypercharge $\kappa/3$. The Lie algebra representation $\mathbb{CP}^{m-1}_{\mathfrak{pgl}_m\mathbb{R}}$ is mapped to $\mathbb{C}^m_{\mathrm{SU}(m)}$, and $\mathbb{CP}^{m-1,*}_{\mathfrak{pgl}_m\mathbb{R}}$ to $\mathbb{C}^{m*}_{\mathrm{SU}(m)} = \overline{\mathbb{C}}^m_{\mathrm{SU}(m)}$. The trivial representation $1_{\mathfrak{pgl}_m\mathbb{R}}$ is mapped to $\mathbb{C}_{\mathrm{SU}(m)}$. Tensor products of $\mathrm{U}(1)$, $\mathrm{SU}(2)$ and $\mathrm{SU}(3)$ representations then need

| $(\#\lambda, \#\lambda')$ | $G_{\mathrm{SM}}$ rep. | Poincaré rep. | SM fermion |
|---|---|---|---|
| $(0,0)$ | $0 \otimes 1 \otimes 1$ | $(0,0)$ | ♭ |
| $(1,0)$ | $(+1 \otimes 2 \otimes 1) \oplus (-\frac{2}{3} \otimes 1 \otimes 3)$ | $(\frac{1}{2},0) \oplus (0,\frac{1}{2})$ | $(e_R^+, \overline{\nu}_R) \oplus (d_R)$ |
| $(0,1)$ | $(-1 \otimes \overline{2} \otimes 1) \oplus (+\frac{2}{3} \otimes 1 \otimes \overline{3})$ | $(\frac{1}{2},0) \oplus (0,\frac{1}{2})$ | $(e_L^-, \nu_L) \oplus (\overline{d}_L)$ |
| $(2,0)$ | $(+2 \otimes 1 \otimes 1) \oplus (+\frac{1}{3} \otimes 2 \otimes 3)$ $\oplus (-\frac{4}{3} \otimes 1 \otimes \overline{3})$ | $(\frac{1}{2},\frac{1}{2})$ | ♭ |
| $(0,2)$ | $(-2 \otimes 1 \otimes 1) \oplus (-\frac{1}{3} \otimes \overline{2} \otimes \overline{3})$ $\oplus (+\frac{4}{3} \otimes 1 \otimes 3)$ | $(\frac{1}{2},\frac{1}{2})$ | ♭ |
| $(3,0)$ | $(-2 \otimes 1 \otimes 1) \oplus (-\frac{1}{3} \otimes \overline{2} \otimes \overline{3})$ $\oplus (+\frac{4}{3} \otimes 1 \otimes 3)$ | $(\frac{1}{2},0) \oplus (0,\frac{1}{2})$ | $(e_R^-) \oplus (\overline{u}_R, \overline{d}_R) \oplus (u_R)$ |
| $(0,3)$ | $(+2 \otimes 1 \otimes 1) \oplus (+\frac{1}{3} \otimes 2 \otimes 3)$ $\oplus (-\frac{4}{3} \otimes 1 \otimes \overline{3})$ | $(\frac{1}{2},0) \oplus (0,\frac{1}{2})$ | $(e_L^+) \oplus (u_L, d_L) \oplus (\overline{u}_L)$ |
| $(4,0)$ | $(-1 \otimes \overline{2} \otimes 1) \oplus (+\frac{2}{3} \otimes 1 \otimes \overline{3})$ | $(0,0)$ | ♭ |
| $(0,4)$ | $(+1 \otimes 2 \otimes 1) \oplus (-\frac{2}{3} \otimes 1 \otimes 3)$ | $(0,0)$ | ♭ |

**TABLE 7.4.1:** Summary of gauge and Poincaré transformation behavior of the irreducible fermionic restricted quantum fields $\hat{\Psi}_{(\lambda,\emptyset)}|_{\mathsf{G}((1),(3,1))}$ and $\hat{\Psi}_{(\emptyset,\lambda)}|_{\mathsf{G}((1),(3,1))}$ obeying spin-statistics. Column 1: Number of rows of the Young tableaux pair. Column 2: $G_{\mathrm{SM}}$ gauge group representation, for the U(1) factor denoted by the weak hypercharge, for SU(2) and SU(3) factors denoted by dimension and complex conjugation. Column 3: Behavior under Poincaré transformations, denoted by the spins of the two Weyl spinor components of the Poincaré irreducible representation. Column 4: A suggestive identification with Standard Model fermions, taking both the behavior under gauge and Poincaré transformations into account. SU(3) (color) indices have been suppressed. The symbol ♭ denotes that the field operators come with integer spin and multiplier of $U$ equivalent to $\omega_-$, which is inconsistent, such that they cannot exist. The field operators $\hat{\Psi}_{(\lambda,\emptyset)}([x])$ and $\hat{\Psi}_{(\emptyset,\lambda)}([x])$ are zero for $\#\lambda \geq 5$.

to be taken modulo $\mathbb{Z}_6$ due to the isomorphism $(\mathrm{U}(1) \times \mathrm{SU}(2) \times \mathrm{SU}(3))/\mathbb{Z}_6 = G_{\mathrm{SM}} \cong \mathrm{S}(\mathrm{U}(2) \times \mathrm{U}(3))$.

As part of a physical action functional, which includes only the compact real form of the gauge quantum fields, the irreducible fermionic quantum fields $\hat{\Psi}_{(\lambda,\lambda')}$ transform as in Lemma 7.4.17 but with the described representation mapping. This leads to the identification with one generation of the Standard Model fermions. Taking into account both gauge and Poincaré group representations, a summary of the behavior of the $\hat{\Psi}_{(\lambda,\emptyset)}|_{\mathsf{G}((1),(3,1))}$ and $\hat{\Psi}_{(\emptyset,\lambda')}|_{\mathsf{G}((1),(3,1))}$ is given in Table 7.4.1.

The field operators $\hat{H}_{(\lambda,\lambda')}([x]) := \hat{H}_{(\lambda,\lambda')}^{\mathrm{comp}}([x])$ together with $U$ and $\rho_{(\lambda,\lambda')}$ do not form a quantum field, even if restricted to Poincaré geometry, since they generally violate the transformation property (7.28). They can interact non-trivially with $\mathrm{S}(\mathrm{U}(2) \times 1) \cong \mathrm{SU}(2)$ gauge bosons and must come with bosonic statistics if obeying spin-statistics, since the (projective) Lorentz group $\mathrm{P}(1 \times \mathrm{O}(3,1))$ acts trivially on them. The field operators $\hat{H}_{(\lambda,\lambda')}([x])$ thus gauge-transform via the symmetrized tensor product representation

$$\mathrm{Sym}^{\#\lambda} \mathbb{C}^5_{\mathrm{S}(\mathrm{U}(2)\times 1)} \otimes \mathrm{Sym}^{\#\lambda'} \overline{\mathbb{C}}^5_{\mathrm{S}(\mathrm{U}(2)\times 1)}. \tag{7.129}$$

This is similar to the Higgs boson in the Standard Model.

**Remark 7.4.22.** *The derivations in this section are for Poincaré geometry $\mathsf{G}((1),(3,1))$. All involved quantum fields and their correlators transform naturally under deformations of geometries, see Lemma 7.3.4 and Proposition 7.3.5. This suggests that the results of this section hold in a certain sense approximately for more general Lorentzian space-time geometries of type $[g]_*\mathsf{G}(4,1)$, if they are sufficiently close to Poincaré geometry. The metrics involved in this statement are to be specified.*

**A conjecture on renormalizability**

In the projective setting of this work, all quantum fields are defined up to local prefactors $\lambda \in C^\infty(\mathsf{X}((1),(3,1)) = \mathbb{A}^{3,1}, \mathbb{R}_{\neq 0})$. We can thus equivalently choose any such $\lambda$, so that expressions are well-defined. We noted already that the projective formulation facilitates well-defined limits of geometries such as the non-relativistic limit of Poincaré geometry, see Example 7.2.2(i). As the infrared limit, this is of considerable relevance to renormalization group studies for quantum field theories with a mass gap.

Restricting to constant prefactors $\lambda(y) = \mathrm{const.}$, the prefactor choice invariance may be interpreted as the possibility to perform wave function renormalization for all involved quantum fields. Potential non-trivial space-time dependences of $\lambda$ suggest the possibility to renormalize any involved mass scale and higher-order correlation functions.

**Example 7.4.23.** *Consider as an example the quantum field $\hat{\Psi} := \hat{\Psi}_{(\lambda,\lambda')}|_{\mathsf{G}((1),(3,1))}$ for some pair $(\lambda, \lambda')$ of Young tableaux, chosen such that $\hat{\Psi}$ behaves as a Dirac fermion under Poincaré transformations. In the projective setting, the field operator map $\hat{\Psi}(y) \mapsto Z\hat{\Psi}(y)$, $Z \in \mathbb{R}_{\neq 0}$, is an identity map, which is analogous to the possibility of wave function renormalization for the field operators $\hat{\Psi}(y) \equiv \hat{\Psi}([x])$. Let $\lambda(y) = \exp(Z^\sigma y_\sigma)$ with summation convention, $Z^\sigma \in \mathbb{R}$ for $\sigma = 1, \dots, 4$. A kinetic term for the action functional of the related particle physics model comes with the operator[7]*

$$\mathrm{i} \int_{\mathsf{X}((1),(3,1))} \mathrm{d}^4 y\, \hat{\Psi}^\dagger(y)\tilde{\gamma}^0\tilde{\gamma}^\mu\nabla_\mu\hat{\Psi}(y)\,, \qquad \tilde{\gamma}_\mu := \begin{pmatrix} 1 & \\ & \gamma^\mu \end{pmatrix} \qquad (7.130)$$

*with $\gamma^\mu$ the standard Dirac $\gamma$-matrices, but considering our index ordering, where the index 4 specifies the temporal direction of $\mathsf{X}((1),(3,1)) = \mathbb{A}^{3,1}$. Under the map $\hat{\Psi}(y) \mapsto \exp(Z^\nu y_\nu)\hat{\Psi}(y)$, which is an identity map in the projective setting, this equates to*

$$\mathrm{i} \int_{\mathsf{X}((1),(3,1))} \mathrm{d}^4 y\, \hat{\Psi}^\dagger(y)\tilde{\gamma}^0\tilde{\gamma}^\mu e^{2Z^\sigma y_\sigma}(Z_\mu + \nabla_\mu)\hat{\Psi}(y)\,. \qquad (7.131)$$

*The factor $\exp(2Z^\sigma y_\sigma)$ can again be ignored in the projective setting. A mass term for the quantum field $\hat{\Psi}$ is provided by*

$$-\int_{\mathsf{X}((1),(3,1))} \mathrm{d}^4 y\, M(\hat{\Psi}, \dots)\hat{\Psi}^\dagger(y)\tilde{\gamma}^0\hat{\Psi}(y)\,, \qquad (7.132)$$

---

[7]We again ignore the discussion of boundedness and continuity of the operator.

*for $M(\hat{\Psi}, \dots)$ an effective mass, which can in particular include effective contributions from interactions among all involved quantum fields such as $\hat{\Psi}$. Equation (7.131) provides with the term proportional to $Z^\sigma$ a counterterm for a potentially diverging effective mass $M(\hat{\Psi}, \dots)$ by means of choosing $Z^\sigma$ to match the corresponding divergent contribution. A counterterm for e.g. a four-point correlation function, which may diverge due to contact interactions, can presumably be derived from a local peak in $\lambda(y)$.*

This leads to the conjecture, that renormalization of the constructed quantum field theory is made possible by the projective geometry setting. More specifically, the conjecture can be phrased as follows.

**Conjecture 7.4.24** (Renormalizability). *In the given framework every counterterm necessary to renormalize occurring divergences in expectation values of field operator correlators can be reinterpreted as coming from multiplication of the field operators with suitable prefactors with non-trivial space-time dependences, which is an identity map in the projective setting.*

A proof of this conjecture requires methods beyond the present approach and is deferred to future work. Especially, full invariance under multiplication with prefactors in $C^\infty(\mathsf{X}((1), (3,1)), \mathbb{R}_{\neq 0})$ can provide an uncountable number of counterterms for occurring divergences.

## 7.5 Summary

In this chapter we have considered homogeneous space-time geometries within real projective geometry. This has provided a framework in which deformations and limits of geometries can be canonically considered. We have viewed quantum fields through the lens of representation theory, and have shown that they behave naturally under such geometry deformations and limits. Connections on the corresponding projective frame bundle have yielded $\mathrm{PGL}_5\mathbb{R}$ gauge fields.

The requirement of causality for the quantum fields has led to an effective gauge group reduction to $\mathrm{P}(\mathrm{GL}_2\mathbb{R} \times \mathrm{GL}_3\mathbb{R})$, which has manifested in corresponding physical action functionals as $\mathrm{S}(\mathrm{U}(2) \times \mathrm{U}(3)) \cong G_{\mathrm{SM}}$ gauge fields. These have been indistinguishable from the Standard Model gauge fields in the action functional. We have found that $\mathrm{P}(\mathrm{GL}_2\mathbb{R} \times 1)$ gauge bosons break physical scale invariance, based on the identification $\mathsf{X}((1), (3,1)) \cong \mathbb{A}^{3,1}$. This is reminiscent of the Higgs mechanism, since the $\mathrm{P}(\mathrm{GL}_2\mathbb{R} \times 1)$ gauge bosons appear in the action as $\mathrm{S}(\mathrm{U}(2) \times 1) \cong \mathrm{SU}(2)$ gauge bosons. Irreducible fermionic quantum fields have given Dirac fermions transforming under $\mathrm{P}(\mathrm{GL}_2\mathbb{R} \times \mathrm{GL}_3\mathbb{R})$ or $\mathrm{S}(\mathrm{U}(2) \times \mathrm{U}(3))$ analogous to the Standard Model fermions. We have concluded with a conjecture on that the projective geometry setting actually facilitates renormalization of field operator correlator expectation values in the quantum field theory.

The work described in this chapter suggests a number of further questions, which we give in Chapter 8. In particular, this includes a brief discussion of our framework compared to models in which representations of space-time and internal symmetry groups form tensor products in line with the Coleman-Mandula theorem [346].

# Appendix

## 7.A  Conjugacy limits on Lie algebra level

In this section we prove that conjugacy limits of Lie groups correspond to contractions on the level of Lie algebras. The converse is not true: a general contraction does not correspond to a conjugacy limit. Similar results for conjugacy limits of Lie algebras have been obtained in [325].

Much of what follows is based on the $KBH$ decomposition of $\mathrm{PGL}_m\mathbb{R}$. For $H$ an indefinite orthogonal group or a deformation or limit of such, $B < \mathrm{PGL}_m\mathbb{R}$ is the subgroup of diagonal invertible projective matrices. We omit the explicit notation of projective equivalence classes in this appendix.

### 7.A.1  Conjugating Lie algebras

**Proposition 7.A.1.** *Let $L$ be a conjugacy limit of a symmetric subgroup $H < \mathrm{PGL}_m\mathbb{R}$, obtained by conjugation with a sequence $b_n \in B$ and taking $n \to \infty$. Then, its Lie algebra $\mathfrak{l} = \mathrm{Lie}(L)$ arises from $\mathfrak{h} = \mathrm{Lie}(H)$ via conjugation,*

$$\mathfrak{l} = \lim_{n\to\infty} \mathrm{Ad}_{b_n}\mathfrak{h}\,, \tag{7.133}$$

$\lim_{n\to\infty} \mathrm{Ad}_{b_n}\mathfrak{h}$ *the set of all existing limits* $\lim_{n\to\infty} \mathrm{Ad}_{b_n} X_n \in \mathfrak{pgl}_m\mathbb{R}$ *for sequences $X_n \in \mathfrak{h}$.*

*Proof.* Let $X_n \in \mathfrak{h}$ be a sequence and assume $Y = \lim_{n\to\infty} \mathrm{Ad}_{b_n} X_n$ exists for $b_n \in B$. Define for $t \in [0, \epsilon)$ with $\epsilon > 0$ sufficiently small $g(t) := \lim_{n\to\infty} \mathrm{Ad}_{b_n} \exp(\mathrm{i}tX_n)$, which exists and defines a path $g : [0, \epsilon) \to L$. It is differentiable at zero, since with the matrix exponential of $\mathfrak{pgl}_m\mathbb{R}$:

$$\left.\frac{\mathrm{d}g(t)}{\mathrm{d}t}\right|_{t=0} = \left.\frac{\mathrm{d}}{\mathrm{d}t}\right|_{t=0} \lim_{n\to\infty} \mathrm{Ad}_{b_n}(1 + \mathrm{i}tX_n + O(t^2)) = \mathrm{i}Y\,. \tag{7.134}$$

Thus, $Y \in \mathfrak{l}$, and $\lim_{n\to\infty} \mathrm{Ad}_{b_n}\mathfrak{h} \subseteq \mathfrak{l}$ is a subalgebra. Further, $\mathrm{PGL}_m\mathbb{R}$ and symmetric subgroups of $\mathrm{PGL}_m\mathbb{R}$ are algebraic, such that by Prop. 3.1 of [309] conjugacy limits of $H$ preserve the group dimension. Thus, $\dim\mathfrak{h} = \dim\mathfrak{l}$.

Since we have already shown $\dim\lim_{n\to\infty} \mathrm{Ad}_{b_n}\mathfrak{h} \leq \dim\mathfrak{l} = \dim\mathfrak{h}$, it remains to show that $\dim\lim_{n\to\infty} \mathrm{Ad}_{b_n}\mathfrak{h} \geq \dim\mathfrak{h}$. We construct explicit generators. We define the $m \times m$ matrix $E_{ij}$ via $(E_{ij})_{kl} := \delta_{ik}\delta_{jl}$ and decompose the generators $T^a$ of $\mathfrak{h}$,

$$T^a = \sum_{i,j} t^a_{ij} E_{ij}\,. \tag{7.135}$$

With $b_n = \mathrm{diag}(b_{n,1}, \ldots, b_{n,m})$:

$$\mathrm{Ad}_{b_n} T^a = \sum_{i,j} t^a_{ij} \frac{b_{n,i}}{b_{n,j}} E_{ij}\,. \tag{7.136}$$

Up to conjugation with a sequence within a compact subset of $\mathrm{PGL}_m\mathbb{R}$, we find for any $i, j$ with $t_{ij}^a \neq 0$ [309]:

$$\frac{b_{n,i}}{b_{n,j}} \to \begin{cases} 0\,, \\ 1\,, \\ \infty\,. \end{cases} \tag{7.137}$$

If the limit is finite and non-zero for all $i, j$ appearing with non-zero coefficients, denote the limiting generator by $S^a$.

If the limit becomes zero, multiply $T^a$ with the appearing quotient $b_{n,\tilde{i}}/b_{n,\tilde{j}}$ converging slowest to zero as $n \to \infty$, i.e., for which there exists $N$, such that for all $n > N$: $b_{n,\tilde{i}}/b_{n,\tilde{j}} \leq b_{n,i}/b_{n,j}$ for any other $i, j$ with $E_{ij}$ appearing with non-zero coefficient in the decomposition of $T^a$. Call the novel generator $S^a$.

Assume now that an index pair $(i, j)$ exists for which the limit $b_{n,i}/b_{n,j} \to \infty$ appears as $n \to \infty$. Let $(\tilde{i}, \tilde{j})$ be the index pair for which the quotient $b_{n,i}/b_{n,j}$ diverges fastest as $n \to \infty$, i.e., for which there exists $N$, such that for all $n > N$: $b_{n,\tilde{i}}/b_{n,\tilde{j}} \geq b_{n,i}/b_{n,j}$ for any other $i, j$ with $E_{ij}$ appearing with non-zero coefficient in the decomposition of $T^a$. We then define a novel generator $S^a := \lim_{n\to\infty}(b_{n,\tilde{j}}/b_{n,\tilde{i}})(b_n T^a b_n^{-1})$. Due to the limit $n \to \infty$ some of the $E_{ij}$ appear in $S^a$ now with zero coefficient instead of a non-zero one, though not all.

Since the generators $S^a$ can mutually not agree by construction, we have shown that

$$\dim_{n\to\infty} \mathrm{Ad}_{b_n}\mathfrak{h} \geq \dim\mathfrak{h}\,, \tag{7.138}$$

concluding the proof. $\qquad\qquad\qquad\qquad\qquad\qquad\qquad\qquad\qquad\qquad\qquad\square$

### 7.A.2 Conjugacy limits as contractions

Lie algebras of conjugacy limits are isomorphic as Lie algebras to Lie algebra contractions, which first an example demonstrates, subsequently giving the proof. We define a contraction as in [326]. For this consider a Lie subalgebra $\mathfrak{t}$ of a Lie algebra $\mathfrak{g}$, the latter with underlying vector space $\mathcal{V}$. Let $\mathfrak{t}'$ denote the subspace of $\mathcal{V}$ complementary to $\mathfrak{t}$, such that $X \in \mathcal{V}$ can be uniquely written as $X = X_\mathfrak{t} + X_{\mathfrak{t}'}$. For $\varepsilon > 0$ define $\phi_\varepsilon(X) := X_\mathfrak{t} + \varepsilon X_{\mathfrak{t}'}$. Then $[X, Y]' := \lim_{\varepsilon\to 0} \phi_\varepsilon^{-1}([\phi_\varepsilon(X), \phi_\varepsilon(Y)])$ exists for all $X, Y \in \mathcal{V}$. The vector space $\mathcal{V}$ equipped with the commutator $[\cdot, \cdot]'$ is called a contraction with respect to $\mathfrak{t}$. Other definitions exist, see e.g. [347].

**Example 7.A.2.** *The Lie algebra $\mathfrak{o}(3)$ has generators*

$$X^1 = \begin{pmatrix} 0 & 1 & 0 \\ -1 & 0 & 0 \\ 0 & 0 & 0 \end{pmatrix}, \quad X^2 = \begin{pmatrix} 0 & 0 & -1 \\ 0 & 0 & 0 \\ 1 & 0 & 0 \end{pmatrix}, \quad X^3 = \begin{pmatrix} 0 & 0 & 0 \\ 0 & 0 & 1 \\ 0 & -1 & 0 \end{pmatrix}, \tag{7.139}$$

*with explicit commutators $[X^1, X^2] = X^3$, $[X^1, X^3] = -X^2$, $[X^2, X^3] = X^1$. We may take a first conjugacy limit via $b_n = \mathrm{diag}(\exp(-2n), \exp(n), \exp(n))$, yielding after un-projectivization*

*the Euclidean motion group in two dimensions, $O(2) \ltimes \mathbb{R}^2$, with generators*

$$Y^1 = \begin{pmatrix} 0 & 0 & 0 \\ -1 & 0 & 0 \\ 0 & 0 & 0 \end{pmatrix}, \quad Y^2 = \begin{pmatrix} 0 & 0 & 0 \\ 0 & 0 & 0 \\ 1 & 0 & 0 \end{pmatrix}, \tag{7.140}$$

*and $X^3$. We may contract $O(3)$ along $X^3$ (in commutators $\varepsilon X^1, \varepsilon X^2$ appear), yielding the contracted commutators $[X^1, X^2] = 0$, $[X^1, X^3] = -X^2$, $[X^2, X^3] = X^1$. The contracted algebra is isomorphic to the Lie algebra of the conjugacy limit $O(2) \ltimes \mathbb{R}^2$.*

*We can take a final conjugacy limit of $O(2) \ltimes \mathbb{R}^2$ via $b_n = \mathrm{diag}(\exp(-n), \exp(-n), \exp(2n))$, giving after un-projectivization the Heisenberg group $H_3$, with generators $Y^1, Y^2$ and*

$$Y^3 = \begin{pmatrix} 0 & 0 & 0 \\ 0 & 0 & 0 \\ 0 & -1 & 0 \end{pmatrix}, \tag{7.141}$$

*such that $[Y^1, Y^2] = 0$, $[Y^1, Y^3] = -Y^2$ and $[Y^2, Y^3] = 0$. We obtain an isomorphic Lie algebra via contraction of $O(2) \ltimes \mathbb{R}^2$ along $X^1$ (mapping $Y^2 \mapsto \varepsilon Y^2$ and $X^3 \mapsto \varepsilon X^3$ in commutators).*

**Lemma 7.A.3.** *Let $H < \mathrm{PGL}_m \mathbb{R}$ be a symmetric subgroup. Let $X \in \mathfrak{b}$ with $\mathfrak{b}$ consisting of traceless diagonal matrices as in [309] and take the limit $L = \lim_{t \to \infty} \exp(\mathrm{i}tX) H \exp(-\mathrm{i}tX)$. Then, $\mathfrak{l} = \mathrm{Lie}(L)$ is isomorphic as a Lie algebra to a contraction of $\mathfrak{h} = \mathrm{Lie}(H)$.*

*Proof.* In the proof of Proposition 7.A.1 we constructed an explicit set of limiting generators $S^a$ from the generators $T^a$ of $\mathfrak{h}$. Each of the generators $S^a$ is of the type $S^a = \lim_{n \to \infty} c_{a,n} \mathrm{Ad}_{b_n} T^a$ for $c_{a,n}$ a sequence of real numbers. Commutators of $\mathfrak{l}$ are then given by matrix commutators of elements generated by the $S^a$:

$$[S^a, S^b] = \lim_{n \to \infty} [c_{a,n} \mathrm{Ad}_{b_n} T^a, c_{b,n} \mathrm{Ad}_{b_n} T^b] = \lim_{n \to \infty} c_{a,n} c_{b,n} \mathrm{Ad}_{b_n} [T^a, T^b]. \tag{7.142}$$

With $f^{abc}$ the structure constants of $\mathfrak{h}$ and $g^{abc}$ the structure constants of $\mathfrak{l}$, we find this way

$$[S^a, S^b] = \sum_c g^{abc} S^c = \sum_c g^{abc} \lim_{n \to \infty} c_{c,n} \mathrm{Ad}_{b_n} T^c = \sum_c \lim_{n \to \infty} f^{abc} c_{a,n} c_{b,n} \mathrm{Ad}_{b_n} T^c. \tag{7.143}$$

Since all of the involved limits and structure constants are finite, the quantity

$$g_n^{abc} = \frac{c_{a,n} c_{b,n}}{c_{c,n}} f^{abc}, \tag{7.144}$$

has as finite limit the structure constants

$$g^{abc} = \lim_{n \to \infty} g_n^{abc}. \tag{7.145}$$

Up to conjugacy of the $S^a$ by $\mathrm{PGL}_m \mathbb{R}$ elements, these are either equal to $f^{abc}$, or zero for specific $a, b, c$. Thus, Equation (7.144) defines a contraction, corresponding to the conjugacy limit $\mathfrak{h} \to \mathfrak{l}$. $\qquad \square$

The converse, that every contraction corresponds to a conjugacy limit on the level of Lie groups, is not true, as the following example shows.

**Example 7.A.4.** *The group* $\mathrm{PO}(3)$ *has inside of* $\mathrm{PGL}_3\mathbb{R}$ *a conjugacy limit conjugate to the Heisenberg group* $H_3$, *whose Lie algebra reads* $[X, Y] = Z$, $[X, Z] = [Y, Z] = 0$. *We contract with respect to* $\mathrm{Span}(Z)$, *the center of* $H_3$. *To this end, the contracted commutators read* $[X, Z]' = [Y, Z]' = 0$ *and*

$$[X, Y]' = \lim_{\varepsilon \to 0} [\varepsilon X, \varepsilon Y] = 0\,.$$

*Thus, the contracted Lie algebra is isomorphic to the abelian* $\mathbb{R}^3$, *but not isomorphic anymore to* $H_3$. *The latter, however, appears up to conjugacy by elements in* $\mathrm{PGL}_3\mathbb{R}$ *as a final conjugacy limit of* $\mathrm{PO}(3)$ *after un-projectivization. No further conjugacy limit refinement appears* [309]. *The contracted algebra* $\mathbb{R}^3$ *does not correspond to a conjugacy limit of* $\mathrm{PO}(3)$ *inside of* $\mathrm{PGL}_3\mathbb{R}$.

### 7.A.3 Limits of universal enveloping algebras

A commutative diagram for universal enveloping algebras can be given. The universal enveloping algebra of a Lie algebra $\mathfrak{g}$ is denoted by $\mathrm{UEA}(\mathfrak{g})$. Let $U : \mathrm{PGL}_5\mathbb{R} \to \mathcal{U}(\mathcal{H})$ be a projective unitary $\mathrm{PGL}_5\mathbb{R}$ representation.

**Lemma 7.A.5.** *Consider the limit* $\mathrm{O} \to \mathrm{O}'$, $\mathfrak{o} := \mathrm{Lie}(\mathrm{O})$, $\mathfrak{o}' := \mathrm{Lie}(\mathrm{O}')$. *Then,* $\mathrm{UEA}(\mathfrak{o}') = \lim_{n\to\infty} \mathrm{Ad}_{b_n} \mathrm{UEA}(\mathfrak{o})$ *and the diagram*

$$
\begin{array}{ccc}
\lim_{n\to\infty} \mathrm{Ad}_{b_n} : & \mathrm{O} \xrightarrow{\hspace{2cm}} \mathrm{O}' & \\
& \downarrow{\scriptstyle U|_\mathrm{O}} \qquad\qquad \downarrow{\scriptstyle U|_{\mathrm{O}'}} & \qquad (7.146) \\
\lim_{n\to\infty} \mathrm{Ad}_{U(b_n)} : & \mathrm{UEA}(\tilde{U}(\mathfrak{o})) \longrightarrow \mathrm{UEA}(\tilde{U}(\mathfrak{o}')) &
\end{array}
$$

*commutes. The same results hold for* $\tilde{\rho}$ *replacing* $U$.

*Proof.* We have by Proposition 7.A.1: $\mathfrak{o}' = \lim_{n\to\infty} \mathrm{Ad}_{b_n} \mathfrak{o}$. For any Lie algebra $\mathfrak{g}$ we set $\mathrm{UEA}_p(\mathfrak{g})$ to be the subspace of $\mathrm{UEA}(\mathfrak{g})$ spanned by products $X_1 \cdots X_k$, $X_j \in \mathfrak{g}$, $k \leq p$. We note by insertion of finitely many $1 = b_n b_n^{-1}$: $\mathrm{Ad}_{b_n} \mathrm{UEA}_p(\mathfrak{o}) = \mathrm{UEA}_p(\mathrm{Ad}_{b_n} \mathfrak{o})$. Thus, for all $p$:

$$\lim_{n\to\infty} \mathrm{Ad}_{b_n} \mathrm{UEA}_p(\mathfrak{o}) = \mathrm{UEA}_p(\mathfrak{o}')\,. \qquad (7.147)$$

$\mathrm{UEA}(\mathfrak{o}') = \lim_{n\to\infty} \mathrm{Ad}_{b_n} \mathrm{UEA}(\mathfrak{o})$ follows with

$$\mathrm{UEA}(\mathfrak{g}) = \bigcup_{p\in\mathbb{N}} \mathrm{UEA}_p(\mathfrak{g})\,. \qquad (7.148)$$

The extension to Lie algebra representations follows from the same arguments applied to the Lie algebra $\tilde{U}(\mathfrak{o})$ and the sequence $U(b_n)$. $\qquad\square$

## 7.B  Ambient representations and conjugacy limits

Let $G$ be a Lie group. While setting $G = \mathrm{PGL}_m\mathbb{R}$, $m \geq 5$, suffices for our purposes, we keep the statements of this appendix general. Denote by $\mathrm{GL}(\mathcal{H})$ the space of invertible linear operators on a Hilbert space $\mathcal{H}$.

**Proposition 7.B.1.** *Let $U : G \to \mathrm{GL}(\mathcal{H})$ be a complex projective representation of $G$ on $\mathcal{H}$. Let $H < G$ be a closed subgroup and $L$ a conjugacy limit of $H$ in $G$. Then $U(L)$ is up to multipliers of $U$ a conjugacy limit of $U(H)$ in $U(G)$.*

*Proof.* Let $c_n \in G$ be a sequence, such that $c_n H c_n^{-1}$ converges geometrically to the closed subgroup $L < G$. Let $\tilde{h}_n = c_n h_n c_n^{-1} \in c_n H c_n^{-1}$ such that $\tilde{h}_n \to g \in L$. Then $[U(\tilde{h}_n)] = [U(c_n)U(h_n)U(c_n)^{-1}]$ with $U(c_n) \in U(G)$, equivalence classes modulo $\mathbb{C}_{\neq 0}$ prefactors, and $U(\tilde{h}_n) \to U(g) \in U(L)$ by continuity of $U$. Every accumulation point of $\tilde{h}_n$ lies in $L$, so every accumulation point of $U(\tilde{h}_n)$ lies in $U(L)$. Indeed, $U(L)$ is a conjugacy limit of $U(H)$ in $U(G)$ up to limits of multipliers of $U$. $\qquad\square$

Chabauty topology is the subspace topology on the set $\mathcal{C}(G)$ of closed subgroups of $G$. $\mathcal{C}(G)$ with the Chabauty topology is a compact Hausdorff topological space [309, 325, 348]. A subgroup $L < G$ is a conjugacy limit of $H < G$ via a sequence $c_n \in G$ if and only if $H_n = c_n H c_n^{-1} \to L$ in the Chabauty topology [309]. This leads to the following proposition.

**Proposition 7.B.2.** *Every conjugacy limit of $U(H)$ in $U(G)$ is of the form $U(L)$ for a conjugacy limit $L$ of $H$ in $G$, up to limits of multipliers of $U$.*

*Proof.* Let $L'$ be a conjugacy limit of $U(H)$ in $U(G)$. Then, any $g' \in L'$ is the limit of some sequence $h'_n \in c'_n U(H)(c'_n)^{-1}$ with

$$h'_n = U(c_n)U(h_n)U(c_n)^{-1} = \omega(c_n, h_n)\omega(c_n h_n, c_n^{-1})U(c_n h_n c_n^{-1}) \qquad (7.149)$$

for $c_n \in G, h_n \in H$. We define $\tilde{h}_n := c_n h_n c_n^{-1}$, such that $h'_n = \omega(c_n, h_n)\omega(c_n h_n, c_n^{-1})U(\tilde{h}_n)$. $L'$ is a subgroup of $U(G)$, i.e., to any $g' \in L'$ there exists $g \in G$: $g' = U(g)$. Assume that $U$ is faithful. Then, given that $h'_n \to g'$ in $U(G)$, we obtain $\tilde{h}_n \to g$. The same argument applies to accumulation points of $h'_n \in U(G)$, which are induced from $\tilde{h}_n \in G$. Thus, $c_n H c_n^{-1}$ converges to a conjugacy limit $L < G$ up to limits of multipliers of $U$, with its group structure induced via $U$. The set $\mathcal{C}(G)$ of closed subgroups equipped with the Chabauty topology being Hausdorff, limits are unique. Thus, $[L'] = [U(L)]$ for a limit $L$ of $H$ in $G$.

The case of a non-faithful representation $U$ remains. Let $\ker(U) \neq \{1\}$ be the non-trivial kernel of $U$. $\ker(U)$ is a normal closed subgroup of $G$, such that we obtain the exact sequence of groups

$$1 \to \ker(U) < G \to G/\ker(U) \to 1\,. \qquad (7.150)$$

A limit $L'$ of $U(c_n)U(H)U(c_n)^{-1} = \omega(c_n, h)\omega(c_n h, c_n^{-1})U(c_n H c_n^{-1}) < U(G)$ for a sequence $c_n \in G$ induces the same limit $[L'] < [U(G/\ker(U))]$, since conjugation preserving $1$, it preserves $\ker(U)$. $U$ acting on $G/\ker(U)$ is a faithful projective representation, such that

$[L'] = [U(\ker(U) \cdot L)] = [U(L)]$ for a limit $L$ of $H < G$. Conjugacy limits of subgroups of $U(G)$ and $U(G/\ker(U))$ coincide trivially. Indeed, for a general representation $U$ we find $[L'] = [U(L)]$ for a limit $L$ of $H < G$. $\square$

**Theorem 7.B.3.** *For $H < G$ a closed Lie subgroup and $L$ a conjugacy limit of $H$ in $G$, and $U$ a projective complex representation of $G$, the diagram*

$$
\begin{array}{ccc}
H & \longrightarrow & L \\
\downarrow & & \downarrow \\
U(H) & \longrightarrow & [U(L)]
\end{array}
\tag{7.151}
$$

*commutes.*

*Proof.* The implied equality of morphism concatenations follows from Propositions 7.B.1 and 7.B.2. $\square$

By virtue of Theorem 7.B.3 limits of projective representations are the same as projective representations of limits up to limits of multipliers, within an ambient projective representation. Unitarity is preserved, as the following lemma shows.

**Lemma 7.B.4.** *Let $U : G \to \mathrm{GL}(\mathcal{H})$ be a unitary projective complex representation of $G$ on $\mathcal{H}$, $L$ a conjugacy limit of a subgroup $H < G$ within $G$. Then the projective representation $U|_L$ is unitary.*

*Proof.* Unitarity of $U$ implies that an inner product $\langle \cdot | \cdot \rangle$ exists on $\mathcal{H}$, such that for any $g \in G$, $v, w \in \mathcal{H}$: $\langle U(g)v | U(g)w \rangle = \langle v|w \rangle$. In particular, with $c_n \in G$:

$$
\langle U(c_n g c_n^{-1})v | U(c_n g c_n^{-1})w \rangle = \langle v|w \rangle ,
\tag{7.152}
$$

the limit $n \to \infty$ thus preserving unitarity. $\square$

## 7.C   Smeared operator algebras, closures and limits

We consider a quantum field $\hat{\mathcal{O}}$ on a four-dimensional geometry $(\mathsf{X}, \mathsf{O}) < (\mathbb{RP}^4, \mathrm{PGL}_5\mathbb{R})$. Assume the field operators $\hat{\mathcal{O}}([x])$ are Hilbert space operator-valued distributions on $\mathbb{RP}^4$. Let $f \in \mathscr{S}(\mathbb{RP}^4)$ be a test function, $\mathscr{S}(\mathbb{RP}^4)$ the space of Schwartz functions on $\mathbb{RP}^4$, and define the smeared field operator

$$
\hat{\mathcal{O}}^{(\dagger)}(f, \mathsf{X}) := \int_{\mathsf{X}} \mathrm{d}^4[y] \hat{\mathcal{O}}^{(\dagger)}([y]) f([y]) .
\tag{7.153}
$$

Define the operator algebra of smeared fields on $\mathsf{X}$ as

$$
\mathfrak{A}_{\mathrm{s}}(\mathsf{X}) := \left\{ \sum_{\ell} \sum_{j_k} a_{j_1 \cdots j_\ell} \hat{\mathcal{O}}^{(\dagger)}(f_{j_1}^{(\ell)}, \mathsf{X}) \cdots \hat{\mathcal{O}}^{(\dagger)}(f_{j_\ell}^{(\ell)}, \mathsf{X}) \,|\, f_{j_k}^{(\ell)} \in \mathscr{S}(\mathbb{RP}^4) \right\} \cap \mathcal{B}(\tilde{\mathcal{H}}) ,
\tag{7.154}
$$

with $\mathcal{B}(\mathcal{H})$ the space of bounded operators on the Hilbert space $\mathcal{H}$, and the occurring sums containing finitely many non-zero summands.

A sequence $\hat{C}_n \in \mathfrak{A}_s(\mathsf{X})$ converges weakly to $\hat{C} \in \mathcal{B}(\mathcal{H})$ if for all $v, w \in \mathcal{H}$ and $n \to \infty$:

$$|\langle v|\hat{C}_n|w\rangle - \langle v|\hat{C}|w\rangle| \to 0\,. \tag{7.155}$$

We denote the closure of $\mathfrak{A}_s(\mathsf{X})$ in the weak topology by $\overline{\mathfrak{A}_s(\mathsf{X})}$.

**Remark 7.C.1.** *By construction closed under the adjoint* $^\dagger$, $\overline{\mathfrak{A}_s(\mathsf{X})}$ *is a von Neumann algebra. A corresponding net of von Neumann algebras can be constructed from restricting the test functions employed in the involved smeared operators to functions with support in given bounded subsets of* $\mathsf{X}$.

For von Neumann algebras, closure with respect to the weak operator topology implies closure with respect to the strong operator topology [318].

To study the interplay of the ambient geometry with smeared operator algebras, set $[g]_*\hat{\mathcal{O}}(f, \mathsf{X}) := U([g])\hat{\mathcal{O}}(f, \mathsf{X})U^\dagger([g])$.

**Proposition 7.C.2.** *For* $[g] \in \mathrm{PGL}_5\mathbb{R}$, $f \in \mathscr{S}(\mathbb{RP}^4)$:

$$[g]_*\hat{\mathcal{O}}(f, \mathsf{X}) = \int_{\mathsf{X}} \mathrm{d}^4[y]\, U([g])\hat{\mathcal{O}}([y])U^\dagger([g])f([y])$$
$$= \int_{\mathsf{X}} \mathrm{d}^4[y]\, \rho([g^{-1}])\hat{\mathcal{O}}([g \cdot y])\, f([y])\,. \tag{7.156}$$

*The element* $[g]$ *acts on the algebra* $\mathfrak{A}_s(\mathsf{X})$ *analogous to* $\mathfrak{A}(\mathsf{X})$ *as in Proposition 7.3.5, denoted* $[g]_*$, *too.*

*Proof.* The claim is clear. $\qquad\square$

**Lemma 7.C.3.** *Let* $[b_n] \in \mathrm{PGL}_5\mathbb{R}$, *such that* $(\mathsf{X}, \mathsf{O}) \to (\mathsf{X}', \mathsf{O}')$ *is the geometry limit via* $[b_n]$. *If for any two states* $v, w \in \mathcal{H}$ *and any* $f \in \mathscr{S}(\mathbb{RP}^4)$:

$$\int_{\mathbb{RP}^4} \mathrm{d}^4[y]\, |\langle v|\hat{\mathcal{O}}([y])|w\rangle|\, f([y]) < \infty\,, \tag{7.157}$$

*and* $\rho([b_n]) = 1_{\dim \rho \times \dim \rho}$ *for all* $n \in \mathbb{N}$, *then the diagram*

$$
\begin{array}{ccc}
\lim_{n\to\infty} \mathrm{Ad}_{[b_n]}: & \mathsf{O} \longrightarrow \mathsf{O}' & \\
& \downarrow{\scriptstyle \mathrm{Ad}_{U|_\mathsf{O}}} \qquad \downarrow{\scriptstyle \mathrm{Ad}_{U|_{\mathsf{O}'}}} & \\
\lim_{n\to\infty}[b_n]_*: & \overline{\mathfrak{A}_s(\mathsf{X})} \longrightarrow \overline{\mathfrak{A}_s(\mathsf{X}')} &
\end{array}
\tag{7.158}
$$

*commutes.*

*Proof.* For any $[g] \in \mathrm{PGL}_5\mathbb{R}$ write $f_{[g]}([-]) := f([g \cdot -])$. Dominated convergence implies with Proposition 7.C.2:

$$\lim_{n\to\infty}[b_n]_*\hat{\mathcal{O}}(f_{[b_n]}, \mathsf{X}) = \lim_{n\to\infty} \hat{\mathcal{O}}(f, [b_n] \cdot \mathsf{X}) = \hat{\mathcal{O}}(f, \mathsf{X}')\,. \tag{7.159}$$

We obtain by the previous considerations the commutative diagram

$$
\begin{array}{ccc}
O & \longrightarrow & O' \\
\downarrow & & \downarrow \\
\mathfrak{A}_{\mathrm{s}}(\mathsf{X}) & \longrightarrow & \mathfrak{A}_{\mathrm{s}}(\mathsf{X}') \,,
\end{array}
\tag{7.160}
$$

with the same maps as for (7.158). Assuming that the involved limit operators exist, this naturally carries over to limits with respect to the weak operator topology. $\qquad\square$

# Chapter 8

# Conclusions

In this dissertation topological data analysis and geometric techniques have been developed to provide new perspectives on non-perturbative quantum field-theoretic phenomena. We conclusively summarize and discuss the obtained results, and provide a broader outlook on related future research prospects.

## 8.1  Discussion

In Chapter 3 we have investigated the emergence of collective phenomena such as long-range coherence and superfluidity during the time evolution of a spinor Bose gas. The high degree of control has allowed us to experimentally observe the thermalization process of an easy-plane ferromagnet, which we have verified with a comparison to Bogoliubov theory. From an experimental viewpoint, the employed methods and obtained results provide a step towards a quantitative understanding of the condensation dynamics in large magnetic spin systems and the study of the role of entanglement and topological excitations for their thermalization. The robust generation of a spin superfluid is a prerequisite for spin Josephson junctions, where finite temperature effects and spin-density separation can now be studied on a new quantitative level due to the direct access to the order parameter.

Understanding the collective processes during the thermalization of quantum many-body systems often rests on effective degrees of freedom. Topological data analysis can provide versatile order parameters, which are sensitive to a variety of collective phenomena. In Chapter 4 we have studied a simulated gluonic plasma through the lens of topology. We have examined energy and topological density correlations in an over-occupied regime, which has given rise to universal self-similar behavior. The scaling exponents could be understood from the energy cascade and the energy-momentum conservation Ward identity. Topological observables based on persistent homology have shown self-similarity related to the energy cascade, too. Providing a signature of the time-independent lattice volume, the occurring scaling exponents have been linked by a packing relation.

The packing relation itself has been proven in Chapter 5 and exemplifies that applications of persistent homology in physics can call for thorough investigations of related mathematical phenomena. The recent mathematical advances in the fields of computational geometry and random topology can allow for their transparent derivation. The devised probabilistic framework appears applicable to many further studies of persistent

homology in statistical and quantum physics settings. Beyond self-similar time evolutions, this particularly includes the introduced notion of ergodicity and the well-defined large-volume asymptotics for intensive persistent homology observables.

Returning to Chapter 4, we have demonstrated that the packing relation applies to self-similar dynamics in persistent homology as soon as there is *any* bound on the filtration. It need not be a spatial bound through a time-independent volume in which point clouds reside. Explicitly, we have shown that the packing relation also holds for cubical complex filtrations without spatial metric information entering, which goes beyond the findings for alpha complexes in Section 4.3 and [6]. This can be of relevance to any persistent homology study of self-similar phenomena, e.g. both for critical phenomena in equilibrium and non-thermal fixed points out of equilibrium.

In Chapter 6 we have investigated confining and deconfining phases in $\mathrm{SU}(2)$ lattice gauge theory via topological data analysis. Specifically, we have examined traced Polyakov loop and Polyakov loop topological density filtrations, the angle-difference filtration of Polyakov loop algebra element norms, and filtrations of traced electric and magnetic field strengths and topological densities. The respective Betti numbers of all filtrations potentially represent a novel type of order parameter for the confinement phase transition, showing kinks at the critical inverse coupling.

The employed cooling in general dampens quantum fluctuations beyond a cutoff scale. It has to be made sure that the physics of interest does not depend on the cutoff when taking the continuum limit. Our observations suggest that the relevant features are stable against the removal of high-frequency modes, with cooling merely enhancing the associated signatures. Nevertheless, a careful continuum extrapolation and study of the cutoff dependence seems appropriate to confirm that the limit can be taken consistently. Ideally, extracting the features of interest via topological data analysis should not require any smoothing at all. This aspect deserves further investigation and will be the subject of future work, alongside studying the dependence on the ratio of temporal and spatial lattice extents.

Space-time geometries set the ground for quantum field theories and their microscopic and macroscopic dynamics. Chapter 7 has been devoted to four-dimensional space-time geometries within real projective geometry and related quantum field-theoretical constructions, also taking particle statistics into account. We have considered quantum fields through the lens of representation theory, and have extended the space-time symmetry transformation behavior of quantum fields to the ambient projective geometry $(\mathbb{RP}^4, \mathrm{PGL}_5\mathbb{R})$. Then, quantum fields have behaved naturally under deformations and limits of geometries.

Connections of the projective frame bundle have given $\mathrm{PGL}_5\mathbb{R}$ gauge fields. Causality has yielded an effective gauge group reduction to $\mathrm{P}(\mathrm{GL}_2\mathbb{R} \times \mathrm{GL}_3\mathbb{R})$ for Poincaré and other geometries, which admit a notion of causality. Since this reduction has been on operator level, we have conjectured that it persists in classical limits and manifests in classical actions as the Standard Model gauge group $G_{\mathrm{SM}} \cong \mathrm{S}(\mathrm{U}(2) \times \mathrm{U}(3))$. We have shown that physical scale invariance is broken in the projective formulation by gauge

bosons corresponding to the gauge subgroup $P(GL_2\mathbb{R} \times 1) \cong \mathbb{R}_{\neq 0} \times PGL_2\mathbb{R}$, which is reminiscent of the Higgs mechanism in the Standard Model.

The consideration of irreducible fermionic quantum fields has led to representations of the reduced gauge group $P(GL_2\mathbb{R} \times GL_3\mathbb{R})$, which are analogous to the gauge transformation behavior of the Standard Model fermions. We have conjectured that the projective setting relates for quantum fields to their renormalizability. A formalization and proof of this conjecture could enhance the geometric understanding of renormalizability for quantum field theories.

## 8.2   Outlook

We provide further future research questions, which can be interesting from the physical viewpoint, and embed them in the broader research perspective. Proceeding mathematical questions building up on Chapter 5 have been stated at its end.

The observation of thermalization for an ultracold quantum gas off equilibrium along with a number of dynamically appearing phenomena showcases the importance of emergent collective dynamics for the time evolution of quantum many-body systems. It sets the foundations for further studies in quantum field settings, which address the microscopic processes of relevance for thermalization as well as its absence due to e.g. long-lived topological defects. The work exemplifies the need for a thorough theoretical understanding of non-perturbative phenomena in strongly correlated systems based on quantum field theories, optimally via derivations from first principles. In particular, this includes parameter regimes which are barely accessible with established quantum field-theoretical methods, e.g. classical-statistical simulations or two-particle-irreducible effective action techniques in perturbative or resummed $1/N$ expansions [81, 82]. Amongst others, non-perturbative regimes such as the low-energy limit of QCD at finite baryon densities or the strongly correlated dynamics of mobile interacting ultracold atoms throughout thermalization are of key interest [38].

Analog and digital quantum simulators offer promising perspectives in this regard, using microscopically engineered quantum devices to controllably emulate the dynamics of other quantum systems, which can be hardly accessible with established theoretical methods [349, 350]. Notably, in the past decade interest rose in quantum simulating the quantum field theories of high-energy physics [351–353]. There is vivid progress to resolve outstanding challenges such as the scalability of synthetic quantum matter to large systems [354, 355] or the simulation of lattice gauge theories in more than one spatial dimension [356]. Concerning the potential combination with TDA, it is interesting to note that the computation of persistent homology can benefit from the application of quantum algorithms [290].

Further progress in the understanding of collective phenomena out of equilibrium can be anticipated from devising suitable effective theories, which in particular take non-local excitations into account. For the gluonic plasma discussed in Chapter 4 this would especially include topological defects. While in the simulated over-occupied and weakly

coupled regime the influence of defects such as sphalerons on the macroscopic dynamics appears negligible (see Section 4.2.2), this need not be the case anymore if chiral quarks are included, as the CME suggests [61–64]. In addition, it is expected that topological defects can play a more dominant role in under-occupied scenarios. This is exemplified by the self-similar dynamics related to the phase ordering kinetics of defects [357], observed for one and two spatial dimensions [6, 66, 238, 358–360]. TDA can presumably provide valuable insights into the presence and macroscopic dynamical influence of non-local excitations such as topological defects in QCD and beyond. Particularly appealing is the potential access to topological information without the necessity of cooling, since the latter unavoidably removes physical information. Aiming for the detection of topological defects in over-occupied scenarios, a first study in relativistic scalar field theory using existing classical-statistical reweighing techniques is currently under way. This can pave the way to an enhanced understanding of the far-from-equilibrium universality classes related to non-thermal fixed points, which is of relevance for a wide range of applications in complex many-body systems.

A natural step beyond the study of non-Abelian confinement with TDA, described in Chapter 6, is its extension to the confinement-deconfinement phase transition in $SU(3)$ lattice gauge theory as well as QCD with dynamical quarks. The extraction of critical exponents by means of finite-size scaling [361] can be promising, based on previous related persistent homology studies [78–80]. This can help identifying signatures of certain correlation functions in persistent homology observables, which can further establish persistent homology as a probe for collective phenomena.

The approach to the topological structure of phase transitions with persistent homology may support or benefit from the application of machine learning techniques. Both supervised and unsupervised learning approaches have been explored for analyzing phase structure [362–369]. The representation of quantum states in variational approaches via neural networks can also be possible [370, 371]. Although studies have addressed the issue of extracting explicit expressions for learned order parameters [372–375], interpreting neural networks remains challenging. Explainable machine learning techniques as employed in [374] are ideally suited for a combined application with persistent homology. Furthermore, gauge-equivariant neural network architectures [376–379] could make use of the high sensitivity of persistent homology to non-local structures by means of adding appropriate topological layers.

On the more fundamental level, in Chapter 7 we have discussed potential origins of part of the structure of the Standard Model, based on projective geometry, causality and the spin-statistics relation. While the particle content of one generation of the Standard Model has been rigorously derived with regard to the gauge and Poincaré transformation behavior, an explanation for the appearance of three generations and their mixing is lacking. Regarding the deduced physical scale invariance breaking, its relation to the Standard Model Higgs mechanism is to be discussed.

In the devised framework Poincaré and gauge transformations both act for a quantum field $\hat{\mathcal{O}}$ via the representation $\rho$. In the Standard Model they act via a tensor product of Poincaré and gauge group representations, consistent with the Coleman-Mandula

theorem [346]. The latter is formulated using asymptotic states and Poincaré geometry. In our model gauge interactions take place on arbitrary geometries, and asymptotic states need not be well-defined. While the applicability of the Coleman-Mandula theorem to our framework thus appears questionable, implications of the peculiar relation between space-time and internal symmetries in our framework are to be worked out. Specifically, we expect that the gauge boson propagators with matter fields absent as well as the free propagators of the matter fields themselves are the same for our model and the Standard Model, since the two models differ only for correlators containing both gauge and matter field operators acting on each other. This suggests that at least perturbatively correlators of one generation of the Standard Model particles and correlators computed for our framework are indistinguishable.

In our approach the gauge group conjugate to $\mathrm{P}(\mathrm{GL}_2\mathbb{R} \times \mathrm{GL}_3\mathbb{R})$ appears as a subgroup of local projective frame transformations. These intersect non-trivially with the group of local Lorentz transformations of frames, which are the local symmetries of gravity. It would be interesting to investigate whether gravitational interactions can be included in the model to show that all quantum fields considered in Chapter 7 gravitate, as this suggests. Further, in the projective setting geometry deformations and limits act without coordinate singularities. This raises the question if gravity can be suitably described in projective geometry. For torsion-free gravity such a projective description has been developed, known as Thomas-Whitehead gravity [327, 329, 380–382]. Studies on the related generalization to projective connections with torsion and its relation to our approach to quantum fields can be promising.

Conjugacy limits of Lie groups are limits with respect to the Chabauty topology. While Chabauty topology barely appears in the physics literature, it can thus be central to studies of quantum theories and beyond, as Chapter 7 exemplifies. For instance, discrete subgroups of Lie groups can converge to the full groups with respect to Chabauty topology. This can be of use for the discussion of quantum simulators, whose construction often rests upon finite approximations of continuous symmetry groups.

In summary, understanding how macroscopic collective phenomena emerge from microscopic quantum field theories, and understanding their geometric origins provides versatile challenges across physical disciplines. Topological data analysis and geometry can provide valuable tools in this regard, as discussed in this dissertation.

# *Acknowledgments*

Many people contributed in widely different ways to the work and time that went into this thesis. While here I need to choose an anyway inadequate ordering, let me say that all of you made my doctoral time as unique as it was, including the countless things that I could learn from all of you.

First of all, I would like to express my gratitude to my long-term supervisor Jürgen Berges, which whom I have been collaborating since my Bachelor's thesis in 2016. I value a lot the confidence that you put in me and the freedom that you gave me to choose part of my research projects, even if they sometimes deviate from established directions. I am particularly grateful for the diverse insights into quantum field theory out of equilibrium, and for the stimulating research environment you provided.

I sincerely would like to thank Anna Wienhard for giving me the opportunity to build bridges between physics and mathematics. Thank you very much for your patience, even if I as a non-mathematician from time to time do not see the mathematically obvious. In addition, I am thankful for the possibilities that you gave me within the STRUCTURES EP Mathematics and Data.

As further mentors and collaborators I am indebted to Jan Pawlowski and Markus Oberthaler. I value a lot all the open-minded discussions that we had, which taught me a lot about physics and beyond. I would like to thank Tina Kuka, Gabriella Kälin, and all the secretaries of the ITP for their care in every organizational regard.

The research work discussed in this thesis has mostly been part of collaborative efforts. Especially, I would like to thank Maximilian Prüfer for his inspiring rational approach to projects even if they seem stuck. I furthermore would like to thank my collaborators Kirill Boguslavski, Julian Urban and, prospectively, Steffen Schmidt.

The activities within the EP Mathematics and Data have contributed a lot to the fruitful environment that I encountered during my doctoral studies. I would like to thank Michael Bleher, Maximilian Schmahl and Lukas Hahn for the many joint seminar sessions, organizational meetings and discussions on TDA and beyond.

A special thanks to the Berges group is in order, which shaped my doctoral time. Notably, I would like to thank my office mates over the doctoral years, Fabian, Gregor, Jannis, Jendrik, Robert and Thimo, for their always open ears and the interesting discussions. I appreciate a lot the lively environment and interactions we all have been facing every workday, to which also Aleksandr, Aleksandr, Aleksas, Alex, Daniel, Erekle, Frederick, Laura, Lillian, Louis, Michael, Torsten, Victoria and Yunxin have contributed.

For proofreading parts of this dissertation I would like to thank Jan, Julian, Lukas, Robert and Thimo.

Compensating the sometimes exhaustive challenges that theoretical physics poses is crucial. I would like to thank the Akademische Philharmonie Heidelberg for all the shining musical moments even in viral times, and all the exchange with its fascinating, open members. I should further thank my climbing partners (and the mountains), since all sorts of joint mountain activities gave further opportunities to distract and find a balance between work and personal life.

The project work described in this thesis has been conducted during both easy and hard, personally disruptive times that I faced in my life. I would wholeheartedly like to thank my family and Feli. Without your support, your occasional pieces of advice and your tender presence, may it be at a distance or nearby, I would not have been able to complete this thesis.

# List of abbreviations

**a.s.** Almost surely

**BEC** Bose-Einstein Condensate

**BRST** Becchi-Rouet-Stora-Tyutin

**CME** Chiral magnetic effect

**HMC** Hybrid/Hamiltonian Monte Carlo

**i.i.d.** Independent and identically distributed

**LHC** Large Hadron Collider

**ODLRO** Off-diagonal long-range order

**POVM** Positive operator-valued measure

**QCD** Quantumchromodynamics

**QED** Quantumelectrodynamics

**QFT** Quantum field theory

**QGP** Quark-gluon plasma

**rf** Radio-frequency

**RHIC** Relativistic Heavy Ion Collider

**s.d.** Standard deviation

**TDA** Topological data analysis

**TOF** Time-of-flight

# List of Figures

# Declaration of authorship

I, Daniel SPITZ, declare that this thesis titled, *"Topological data analysis and geometry in quantum field dynamics"* and the work presented in it are my own. I confirm that:

- Where any part of this thesis has previously been submitted for a degree or any other qualification at this University or any other institution, this has been clearly stated.

- Where I have consulted the published work of others, this is always clearly attributed.

- Where I have quoted from the work of others, the source is always given. With the exception of such quotations, this thesis is entirely my own work.

- Parts of this dissertation have been published in the following articles:

  1. Spitz, D. and Wienhard, A., "The self-similar evolution of stationary point processes via persistent homology", arXiv: 2012.05751 [math.PR].

  2. Prüfer, M., Spitz, D., Lannig, S., Strobel, H., Berges, J., and Oberthaler, M. K., "Condensation and thermalization of an easy-plane ferromagnet in a spinor Bose gas", *Nat. Phys.*, vol. 18, no. 12, pp. 1459–1463, 2022. arXiv: 2205.06188 [cond-mat.quant-gas].

  3. Spitz, D., Urban, J. M., and Pawlowski, J. M., "Confinement in non-Abelian lattice gauge theory via persistent homology", *Phys. Rev. D*, vol. 107, no. 3, p. 034 506, 2023. arXiv: 2208.03955 [hep-lat].

  4. Spitz, D., Boguslavski, K., and Berges, J., "Probing universal dynamics with topological data analysis in a gluonic plasma", *under review in Phys. Rev. D*, arXiv: 2303.08618 [hep-ph].

  5. Spitz, D., "Standard Model gauge theory from projective geometries", *in preparation*, 2023.

- During my doctoral studies I was involved in the following publications that are not part of this dissertation:

  6. Spitz, D., Berges, J., Oberthaler, M. K., and Wienhard, A., "Finding self-similar behavior in quantum many-body dynamics via persistent homology", *SciPost Phys.*, vol. 11, no. 3, p. 060, 2021. arXiv: 2001.02616 [cond-mat.quant-gas].

  7. Prüfer, M., Spitz, D., and Strobel, H., "Suprafluüssigkeit mit Spin", *Physik in unserer Zeit*, vol. 54, no. 2, pp. 58–59, 2023.

Signed:
_____

Date:
_____

# Bibliography

[1]   Spitz, D. and Wienhard, A., "The self-similar evolution of stationary point processes via persistent homology", arXiv: 2012.05751 [math.PR] (cit. on pp. ix, 65, 191).

[2]   Prüfer, M., Spitz, D., Lannig, S., Strobel, H., Berges, J., and Oberthaler, M. K., "Condensation and thermalization of an easy-plane ferromagnet in a spinor Bose gas", *Nat. Phys.*, vol. 18, no. 12, pp. 1459–1463, 2022. arXiv: 2205.06188 [cond-mat.quant-gas] (cit. on pp. ix, 21, 191).

[3]   Spitz, D., Urban, J. M., and Pawlowski, J. M., "Confinement in non-Abelian lattice gauge theory via persistent homology", *Phys. Rev. D*, vol. 107, no. 3, p. 034 506, 2023. arXiv: 2208.03955 [hep-lat] (cit. on pp. ix, 42, 101, 191).

[4]   Spitz, D., Boguslavski, K., and Berges, J., "Probing universal dynamics with topological data analysis in a gluonic plasma", *under review in Phys. Rev. D*, arXiv: 2303.08618 [hep-ph] (cit. on pp. ix, 41, 191).

[5]   Spitz, D., "Standard Model gauge theory from projective geometries", *in preparation*, 2023 (cit. on pp. ix, 191).

[6]   Spitz, D., Berges, J., Oberthaler, M. K., and Wienhard, A., "Finding self-similar behavior in quantum many-body dynamics via persistent homology", *SciPost Phys.*, vol. 11, no. 3, p. 060, 2021. arXiv: 2001.02616 [cond-mat.quant-gas] (cit. on pp. ix, 2, 42, 52, 54, 63, 66, 72, 74, 76, 79, 80, 86–88, 102, 180, 182, 191).

[7]   Prüfer, M., Spitz, D., and Strobel, H., "Supraflüssigkeit mit Spin", *Physik in unserer Zeit*, vol. 54, no. 2, pp. 58–59, 2023 (cit. on pp. ix, 21, 191).

[8]   Weinberg, S., *The quantum theory of fields. Vol. 1: foundations*. Cambridge University Press, Jun. 2005 (cit. on pp. 1, 6, 140, 142, 145).

[9]   Peskin, M. E. and Schroeder, D. V., *An introduction to quantum field theory*. Reading, USA: Addison-Wesley, 1995 (cit. on pp. 1, 6, 9, 11).

[10]  Liddle, A. R. and Lyth, D. H., *Cosmological inflation and large-scale structure*. Cambridge University Press, 2000 (cit. on p. 1).

[11]  Altland, A. and Simons, B. D., *Condensed matter field theory*, 2nd ed. Cambridge University Press, 2010 (cit. on p. 1).

[12]  Shankar, R., *Quantum field theory and condensed matter: an introduction*. Cambridge University Press, 2017 (cit. on p. 1).

[13]  Manohar, A. V., "Introduction to effective field theories", S. Davidson, P. Gambino, M. Laine, M. Neubert, and C. Salomon, Eds., Apr. 2018. arXiv: 1804.05863 [hep-ph] (cit. on p. 1).

[14] Donoghue, J. F., Golowich, E., and Holstein, B. R., *Dynamics of the Standard Model*. Oxford University Press, 2014 (cit. on pp. 1, 131).

[15] Schwartz, M. D., *Quantum field theory and the Standard Model*. Cambridge University Press, Mar. 2014 (cit. on pp. 1, 131).

[16] Langacker, P., *The Standard Model and beyond*. Taylor & Francis, 2017 (cit. on pp. 1, 131).

[17] Martin, S. P., "A supersymmetry primer", in *Perspectives on supersymmetry*, pp. 1–98 (cit. on p. 1).

[18] Langacker, P., "Grand unified theories and proton decay", *Phys. Rept.*, vol. 72, p. 185, 1981 (cit. on pp. 1, 131).

[19] Weinberg, S., "A new light boson?", *Phys. Rev. Lett.*, vol. 40, pp. 223–226, 1978 (cit. on p. 1).

[20] Wilczek, F., "Problem of strong $P$ and $T$ invariance in the presence of instantons", *Phys. Rev. Lett.*, vol. 40, pp. 279–282, 1978 (cit. on p. 1).

[21] Dasgupta, B. and Kopp, J., "Sterile neutrinos", *Phys. Rept.*, vol. 928, pp. 1–63, 2021. arXiv: 2106.05913 [hep-ph] (cit. on p. 1).

[22] Green, M. B., Schwarz, J. H., and Witten, E., *Superstring theory vol. 1: 25th anniversary edition* (Cambridge Monographs on Mathematical Physics). Cambridge University Press, Nov. 2012 (cit. on p. 1).

[23] Green, M. B., Schwarz, J. H., and Witten, E., *Superstring theory vol. 2: 25th anniversary edition* (Cambridge Monographs on Mathematical Physics). Cambridge University Press, Nov. 2012 (cit. on p. 1).

[24] Workman, R. L. *et al.*, "Review of particle physics", *PTEP*, vol. 2022, p. 083C01, 2022 (cit. on p. 1).

[25] Connes, A. and Lott, J., "Particle models and noncommutative geometry (expanded version)", *Nucl. Phys. B Proc. Suppl.*, vol. 18, pp. 29–47, 1991 (cit. on pp. 1, 131).

[26] Chamseddine, A. H. and Connes, A., "The spectral action principle", *Commun. Math. Phys.*, vol. 186, pp. 731–750, 1997. arXiv: hep-th/9606001 (cit. on pp. 1, 131).

[27] Dubois-Violette, M., "Exceptional quantum geometry and particle physics", *Nucl. Phys. B*, vol. 912, pp. 426–449, 2016. arXiv: 1604.01247 [math.QA] (cit. on pp. 1, 131).

[28] Furey, C., "$\mathrm{SU}(3)_C \times \mathrm{SU}(2)_L \times \mathrm{U}(1)_Y\ (\times \mathrm{U}(1)_X)$ as a symmetry of division algebraic ladder operators", *Eur. Phys. J. C*, vol. 78, no. 5, p. 375, 2018. arXiv: 1806.00612 [hep-th] (cit. on pp. 1, 131).

[29] Todorov, I. and Dubois-Violette, M., "Deducing the symmetry of the Standard Model from the automorphism and structure groups of the exceptional Jordan algebra", *Int. J. Mod. Phys. A*, vol. 33, no. 20, p. 1 850 118, 2018. arXiv: 1806.09450 [hep-th] (cit. on pp. 1, 131).

[30] Krasnov, K., "$\mathrm{SO}(9)$ characterization of the Standard Model gauge group", *J. Math. Phys.*, vol. 62, no. 2, p. 021 703, 2021. arXiv: 1912.11282 [hep-th] (cit. on pp. 1, 131).

[31] Woit, P., "Euclidean twistor unification", Apr. 2021. arXiv: 2104.05099 [hep-th] (cit. on pp. 1, 131).

[32] Baym, G., Hatsuda, T., Kojo, T., Powell, P. D., Song, Y., and Takatsuka, T., "From hadrons to quarks in neutron stars: a review", *Rept. Prog. Phys.*, vol. 81, no. 5, p. 056 902, 2018. arXiv: 1707.04966 [astro-ph.HE] (cit. on p. 2).

[33] Blaschke, D. and Chamel, N., "Phases of dense matter in compact stars", in *The Physics and Astrophysics of Neutron Stars*, L. Rezzolla, P. Pizzochero, D. I. Jones, N. Rea, and I. Vidaña, Eds. Cham: Springer International Publishing, 2018, pp. 337–400. arXiv: 1803.01836 [nucl-th] (cit. on p. 2).

[34] Wen, X.-G., "Zoo of quantum-topological phases of matter", *Rev. Mod. Phys.*, vol. 89, no. 4, p. 041 004, 2017. arXiv: 1610.03911 [cond-mat.str-el] (cit. on p. 2).

[35] Kofman, L., Linde, A. D., and Starobinsky, A. A., "Reheating after inflation", *Phys. Rev. Lett.*, vol. 73, pp. 3195–3198, 1994. arXiv: hep-th/9405187 (cit. on pp. 2, 14).

[36] Berges, J. and Serreau, J., "Parametric resonance in quantum field theory", *Phys. Rev. Lett.*, vol. 91, p. 111 601, 2003. arXiv: hep-ph/0208070 (cit. on pp. 2, 14).

[37] Berges, J., "Nonequilibrium quantum fields: from cold atoms to cosmology", Mar. 2015. arXiv: 1503.02907 [hep-ph] (cit. on pp. 2, 5, 8, 14).

[38] Berges, J., Heller, M. P., Mazeliauskas, A., and Venugopalan, R., "QCD thermalization: ab initio approaches and interdisciplinary connections", *Rev. Mod. Phys.*, vol. 93, no. 3, p. 035 003, 2021. arXiv: 2005.12299 [hep-th] (cit. on pp. 2, 13, 14, 41–43, 181).

[39] Micha, R. and Tkachev, I. I., "Relativistic turbulence: a long way from preheating to equilibrium", *Phys. Rev. Lett.*, vol. 90, p. 121 301, 2003. arXiv: hep-ph/0210202 (cit. on pp. 2, 15, 42).

[40] Berges, J., Rothkopf, A., and Schmidt, J., "Non-thermal fixed points: effective weak-coupling for strongly correlated systems far from equilibrium", *Phys. Rev. Lett.*, vol. 101, p. 041 603, 2008. arXiv: 0803.0131 [hep-ph] (cit. on pp. 2, 15, 42).

[41] Berges, J., Boguslavski, K., Schlichting, S., and Venugopalan, R., "Universal attractor in a highly occupied non-Abelian plasma", *Phys. Rev. D*, vol. 89, no. 11, p. 114 007, 2014. arXiv: 1311.3005 [hep-ph] (cit. on pp. 2, 15, 42, 43, 47).

[42] Berges, J., Boguslavski, K., Schlichting, S., and Venugopalan, R., "Universality far from equilibrium: from superfluid Bose gases to heavy-ion collisions", *Phys. Rev. Lett.*, vol. 114, no. 6, p. 061 601, 2015. arXiv: 1408.1670 [hep-ph] (cit. on pp. 2, 15, 42).

[43] Berges, J., Boguslavski, K., Schlichting, S., and Venugopalan, R., "Nonequilibrium fixed points in longitudinally expanding scalar theories: infrared cascade, Bose condensation and a challenge for kinetic theory", *Phys. Rev. D*, vol. 92, no. 9, p. 096 006, 2015. arXiv: 1508.03073 [hep-ph] (cit. on pp. 2, 15, 16).

[44] Orioli, A. Piñeiro, Boguslavski, K., and Berges, J., "Universal self-similar dynamics of relativistic and nonrelativistic field theories near nonthermal fixed points", *Phys. Rev. D*, vol. 92, no. 2, p. 025 041, 2015. arXiv: 1503.02498 [hep-ph] (cit. on pp. 2, 15, 16, 42).

[45] Mace, M., Schlichting, S., and Venugopalan, R., "Off-equilibrium sphaleron transitions in the glasma", *Phys. Rev. D*, vol. 93, no. 7, p. 074 036, 2016. arXiv: 1601.07342 [hep-ph] (cit. on pp. 2, 15, 42, 49).

[46] Berges, J., Mace, M., and Schlichting, S., "Universal self-similar scaling of spatial Wilson loops out of equilibrium", *Phys. Rev. Lett.*, vol. 118, no. 19, p. 192 005, 2017. arXiv: 1703.00697 [hep-th] (cit. on pp. 2, 15, 16, 42, 44).

[47] Prüfer, M., Kunkel, P., Strobel, H., Lannig, S., Linnemann, D., Schmied, C.-M., Berges, J., Gasenzer, T., and Oberthaler, M. K., "Observation of universal dynamics in a spinor Bose gas far from equilibrium", *Nature*, vol. 563, no. 7730, pp. 217–220, 2018. arXiv: 1805.11881 [cond-mat.quant-gas] (cit. on pp. 2, 15, 42).

[48] Erne, S., Bücker, R., Gasenzer, T., Berges, J., and Schmiedmayer, J., "Universal dynamics in an isolated one-dimensional Bose gas far from equilibrium", *Nature*, vol. 563, no. 7730, pp. 225–229, 2018. arXiv: 1805.12310 [cond-mat.quant-gas] (cit. on pp. 2, 15, 42).

[49] Glidden, J. A. P., Eigen, C., Dogra, L. H., Hilker, T. A., Smith, R. P., and Hadzibabic, Z., "Bidirectional dynamic scaling in an isolated Bose gas far from equilibrium", *Nature Phys.*, vol. 17, no. 4, pp. 457–461, 2021. arXiv: 2006.01118 [cond-mat.quant-gas] (cit. on pp. 2, 15, 42).

[50] Berges, J. and Sexty, D., "Bose condensation far from equilibrium", *Phys. Rev. Lett.*, vol. 108, p. 161 601, 2012. arXiv: 1201.0687 [hep-ph] (cit. on pp. 2, 16).

[51] Berges, J., Boguslavski, K., Mace, M., and Pawlowski, J. M., "Gauge-invariant condensation in the nonequilibrium quark-gluon plasma", *Phys. Rev. D*, vol. 102, no. 3, p. 034 014, 2020. arXiv: 1909.06147 [hep-ph] (cit. on pp. 2, 16, 42).

[52] Berges, J. and Cox, J., "Thermalization of quantum fields from time reversal invariant evolution equations", *Phys. Lett. B*, vol. 517, pp. 369–374, 2001. arXiv: hep-ph/0006160 (cit. on pp. 2, 16).

[53] Berges, J., Borsanyi, S., and Serreau, J., "Thermalization of fermionic quantum fields", *Nucl. Phys. B*, vol. 660, pp. 51–80, 2003. arXiv: hep-ph/0212404 (cit. on pp. 2, 16).

[54] Berges, J., Borsanyi, S., and Wetterich, C., "Prethermalization", *Phys. Rev. Lett.*, vol. 93, p. 142 002, 2004. arXiv: hep-ph/0403234 (cit. on pp. 2, 16).

[55] Shen, L., Berges, J., Pawlowski, J. M., and Rothkopf, A., "Thermalization and dynamical spectral properties in the quark-meson model", *Phys. Rev. D*, vol. 102, no. 1, p. 016 012, 2020. arXiv: 2003.03270 [hep-ph] (cit. on pp. 2, 16).

[56] Kaufman, A. M., Tai, M. E., Lukin, A., Rispoli, M., Schittko, R., Preiss, P. M., and Greiner, M., "Quantum thermalization through entanglement in an isolated many-body system", *Science*, vol. 353, no. 6301, pp. 794–800, 2016 (cit. on pp. 2, 17).

[57] Berges, J., Floerchinger, S., and Venugopalan, R., "Dynamics of entanglement in expanding quantum fields", *JHEP*, vol. 04, p. 145, 2018. arXiv: 1712.09362 [hep-th] (cit. on pp. 2, 17).

[58] Berges, J., Floerchinger, S., and Venugopalan, R., "Thermal excitation spectrum from entanglement in an expanding quantum string", *Phys. Lett. B*, vol. 778, pp. 442–446, 2018. arXiv: 1707.05338 [hep-ph] (cit. on pp. 2, 17).

[59] Busza, W., Rajagopal, K., and Schee, W. van der, "Heavy ion collisions: the big picture, and the big questions", *Ann. Rev. Nucl. Part. Sci.*, vol. 68, pp. 339–376, 2018. arXiv: 1802.04801 [hep-ph] (cit. on pp. 2, 41).

[60] Schlichting, S. and Teaney, D., "The first fm/c of heavy-ion collisions", *Ann. Rev. Nucl. Part. Sci.*, vol. 69, pp. 447–476, 2019. arXiv: 1908.02113 [nucl-th] (cit. on pp. 2, 41).

[61] Kharzeev, D. E., McLerran, L. D., and Warringa, H. J., "The effects of topological charge change in heavy ion collisions: 'event by event P and CP violation'", *Nucl. Phys. A*, vol. 803, pp. 227–253, 2008. arXiv: 0711.0950 [hep-ph] (cit. on pp. 2, 182).

[62] Fukushima, K., Kharzeev, D. E., and Warringa, H. J., "The chiral magnetic effect", *Phys. Rev. D*, vol. 78, p. 074 033, 2008. arXiv: 0808.3382 [hep-ph] (cit. on pp. 2, 182).

[63] Kharzeev, D. E., Liao, J., Voloshin, S. A., and Wang, G., "Chiral magnetic and vortical effects in high-energy nuclear collisions—a status report", *Prog. Part. Nucl. Phys.*, vol. 88, pp. 1–28, 2016. arXiv: 1511.04050 [hep-ph] (cit. on pp. 2, 182).

[64] Koch, V., Schlichting, S., Skokov, V., Sorensen, P., Thomas, J., Voloshin, S., Wang, G., and Yee, H.-U., "Status of the chiral magnetic effect and collisions of isobars", *Chin. Phys. C*, vol. 41, no. 7, p. 072 001, 2017. arXiv: 1608.00982 [nucl-th] (cit. on pp. 2, 182).

[65] Zhao, J. and Wang, F., "Experimental searches for the chiral magnetic effect in heavy-ion collisions", *Prog. Part. Nucl. Phys.*, vol. 107, pp. 200–236, 2019. arXiv: 1906.11413 [nucl-ex] (cit. on p. 2).

[66] Deng, J., Schlichting, S., Venugopalan, R., and Wang, Q., "Off-equilibrium infrared structure of self-interacting scalar fields: universal scaling, vortex-antivortex superfluid dynamics and Bose-Einstein condensation", *Phys. Rev. A*, vol. 97, no. 5, p. 053 606, 2018. arXiv: 1801.06260 [hep-th] (cit. on pp. 2, 182).

[67] Otter, N., Porter, M. A., Tillmann, U., Grindrod, P., and Harrington, H. A., "A roadmap for the computation of persistent homology", *EPJ Data Sci.*, vol. 6, pp. 1–38, 2017. arXiv: 1506.08903 [math.AT] (cit. on pp. 2, 41, 42, 50, 52, 65, 67).

[68] Cohen-Steiner, D., Edelsbrunner, H., and Harer, J., "Stability of persistence diagrams", *Discrete Comput. Geom.*, vol. 37, no. 1, pp. 103–120, 2007 (cit. on pp. 2, 52, 88, 102, 110).

[69]  Cohen-Steiner, D., Edelsbrunner, H., Harer, J., and Mileyko, Y., "Lipschitz functions have $L_p$-stable persistence", *Found. Comut. Math.*, vol. 10, no. 2, pp. 127–139, 2010 (cit. on pp. 2, 52, 66, 88, 89, 102, 110).

[70]  Bubenik, P. *et al.*, "Statistical topological data analysis using persistence landscapes." *J. Mach. Learn. Res.*, vol. 16, no. 1, pp. 77–102, 2015. arXiv: 1207.6437 [math.AT] (cit. on pp. 2, 89).

[71]  Hiraoka, Y., Shirai, T., and Trinh, K. D., "Limit theorems for persistence diagrams", *Ann. Appl. Prob.*, vol. 28, no. 5, pp. 2740–2780, 2018. arXiv: 1612.08371 [math.PR] (cit. on pp. 2, 4, 52, 65–67, 73, 82, 94–98, 102, 110).

[72]  Donato, I., Gori, M., Pettini, M., Petri, G., De Nigris, S., Franzosi, R., and Vaccarino, F., "Persistent homology analysis of phase transitions", *Phys. Rev. E*, vol. 93, no. 5, p. 052 138, 2016. arXiv: 1601.03641 [cond-mat.stat-mech] (cit. on pp. 2, 42, 102).

[73]  Speidel, L., Harrington, H. A., Chapman, S. J., and Porter, M. A., "Topological data analysis of continuum percolation with disks", *Phys. Rev. E*, vol. 98, no. 1, p. 012 318, 2018. arXiv: 1804.07733 [cond-mat.stat-mech] (cit. on pp. 2, 42, 102).

[74]  Santos, F. A., Raposo, E. P., Coutinho-Filho, M. D., Copelli, M., Stam, C. J., and Douw, L., "Topological phase transitions in functional brain networks", *Phys. Rev. E*, vol. 100, no. 3, p. 032 414, 2019 (cit. on pp. 2, 42, 102).

[75]  Olsthoorn, B., Hellsvik, J., and Balatsky, A. V., "Finding hidden order in spin models with persistent homology", *Phys. Rev. Res.*, vol. 2, no. 4, p. 043 308, 2020. arXiv: 2009.05141 [cond-mat.stat-mech] (cit. on pp. 2, 42, 102).

[76]  Tran, Q. H., Chen, M., and Hasegawa, Y., "Topological persistence machine of phase transitions", *Phys. Rev. E*, vol. 103, no. 5, p. 052 127, 2021. arXiv: 2004.03169 [cond-mat.stat-mech] (cit. on pp. 2, 42, 102).

[77]  Cole, A., Loges, G. J., and Shiu, G., "Quantitative and interpretable order parameters for phase transitions from persistent homology", *Phys. Rev. B*, vol. 104, no. 10, p. 104 426, 2021. arXiv: 2009.14231 [cond-mat.stat-mech] (cit. on pp. 2, 42, 102).

[78]  Sehayek, D. and Melko, R. G., "Persistent homology of $\mathbb{Z}_2$ gauge theories", *Phys. Rev. B*, vol. 106, no. 8, p. 085 111, 2022. arXiv: 2201.09856 [cond-mat.stat-mech] (cit. on pp. 2, 42, 79, 182).

[79]  Sale, N., Giansiracusa, J., and Lucini, B., "Quantitative analysis of phase transitions in two-dimensional XY models using persistent homology", *Phys. Rev. E*, vol. 105, no. 2, p. 024 121, 2022. arXiv: 2109.10960 [cond-mat.stat-mech] (cit. on pp. 2, 42, 79, 102, 115, 116, 182).

[80]  Sale, N., Lucini, B., and Giansiracusa, J., "Probing center vortices and deconfinement in $\mathrm{SU}(2)$ lattice gauge theory with persistent homology", *Phys. Rev. D*, vol. 107, no. 3, p. 034 501, 2023. arXiv: 2207.13392 [hep-lat] (cit. on pp. 2, 42, 79, 102, 121, 182).

[81]    Berges, J., "Introduction to nonequilibrium quantum field theory", *AIP Conf. Proc.*, vol. 739, no. 1, M. Bracco, M. Chiapparini, E. Ferreira, and T. Kodama, Eds., pp. 3–62, 2004. arXiv: hep-ph/0409233 (cit. on pp. 5, 14, 181).

[82]    Calzetta, E. A. and Hu, B.-L. B., *Nonequilibrium quantum field theory*. Oxford University Press, 2009 (cit. on pp. 5, 181).

[83]    Reeh, H. and Schlieder, S., "Bemerkungen zur Unitäräquivalenz von Lorentzinvarianten Feldern", *Nuovo Cim.*, vol. 22, no. 5, pp. 1051–1068, 1961 (cit. on p. 5).

[84]    Witten, E., "APS medal for exceptional achievement in research: invited article on entanglement properties of quantum field theory", *Rev. Mod. Phys.*, vol. 90, no. 4, p. 045 003, 2018. arXiv: 1803.04993 [hep-th] (cit. on pp. 5, 142, 155).

[85]    Mautner, F., "Unitary representations of locally compact groups I", *Ann. Math.*, pp. 1–25, 1950 (cit. on pp. 6, 166).

[86]    Breuer, H.-P. and Petruccione, F., *The theory of open quantum systems*. Oxford, England: Oxford University Press, Jan. 2007 (cit. on p. 6).

[87]    Breuer, H.-P., Laine, E.-M., Piilo, J., and Vacchini, B., "Colloquium: non-Markovian dynamics in open quantum systems", *Rev. Mod. Phys.*, vol. 88, p. 021 002, 2 2016 (cit. on p. 6).

[88]    Inönü, E. and Wigner, E. P., "On the contraction of groups and their representations", in *The Collected Works of Eugene Paul Wigner*, Springer, 1993, pp. 488–502 (cit. on p. 6).

[89]    Göckeler, M. and Schücker, T., *Differential geometry, gauge theories, and gravity*. Cambridge, England: Cambridge University Press, 1989 (cit. on pp. 9, 139, 152).

[90]    Weinberg, S., *The quantum theory of fields. Vol. 2: modern applications*. Cambridge, England: Cambridge University Press, Aug. 2013 (cit. on pp. 10, 11, 165).

[91]    Baez, J. C. and Huerta, J., "The algebra of grand unified theories", *Bull. Am. Math. Soc.*, vol. 47, pp. 483–552, 2010. arXiv: 0904.1556 [hep-th] (cit. on pp. 12, 131, 165).

[92]    Aaij, R. *et al.*, "Observation of $J/\psi p$ resonances consistent with pentaquark states in $\Lambda_b^0 \to J/\psi K^- p$ decays", *Phys. Rev. Lett.*, vol. 115, p. 072 001, 2015. arXiv: 1507.03414 [hep-ex] (cit. on p. 12).

[93]    Elitzur, S., "Impossibility of spontaneously breaking local symmetries", *Phys. Rev. D*, vol. 12, pp. 3978–3982, 1975 (cit. on p. 12).

[94]    Jaffe, A. and Witten, E., "Quantum Yang-Mills theory", *The millennium prize problems*, vol. 1, p. 129, 2006 (cit. on p. 13).

[95]    Rothe, H. J., *Lattice gauge theories: an introduction (fourth edition)*. World Scientific Publishing Company, 2012, vol. 43 (cit. on pp. 13, 45, 102, 123).

[96]    Berges, J., Boguslavski, K., Schlichting, S., and Venugopalan, R., "Basin of attraction for turbulent thermalization and the range of validity of classical-statistical simulations", *JHEP*, vol. 05, p. 054, 2014. arXiv: 1312.5216 [hep-ph] (cit. on pp. 13, 42, 43).

[97]    Aarts, G., Seiler, E., and Stamatescu, I.-O., "The complex Langevin method: when can it be trusted?", *Phys. Rev. D*, vol. 81, p. 054 508, 2010. arXiv: 0912.3360 [hep-lat] (cit. on p. 13).

[98]    Cristoforetti, M., Di Renzo, F., and Scorzato, L., "New approach to the sign problem in quantum field theories: high density QCD on a Lefschetz thimble", *Phys. Rev. D*, vol. 86, p. 074 506, 2012. arXiv: 1205.3996 [hep-lat] (cit. on p. 13).

[99]    Heyl, M., Polkovnikov, A., and Kehrein, S., "Dynamical quantum phase transitions in the transverse-field ising model", *Phys. Rev. Lett.*, vol. 110, p. 135 704, 13 2013. arXiv: 1206.2505 [cond-mat.stat-mech] (cit. on p. 14).

[100]   Heyl, M., "Dynamical quantum phase transitions: a review", *Rept. Prog. Phys.*, vol. 81, no. 5, p. 054 001, 2018. arXiv: 1709.07461 [cond-mat.stat-mech] (cit. on p. 14).

[101]   Nagle, J. L. and Zajc, W. A., "Small system collectivity in relativistic hadronic and nuclear collisions", *Ann. Rev. Nucl. Part. Sci.*, vol. 68, pp. 211–235, 2018. arXiv: 1801.03477 [nucl-ex] (cit. on p. 14).

[102]   Micha, R. and Tkachev, I. I., "Turbulent thermalization", *Phys. Rev. D*, vol. 70, p. 043 538, 2004. arXiv: hep-ph/0403101 (cit. on pp. 15, 42).

[103]   Berges, J. and Sexty, D., "Strong versus weak wave-turbulence in relativistic field theory", *Phys. Rev. D*, vol. 83, p. 085 004, 2011. arXiv: 1012.5944 [hep-ph] (cit. on p. 15).

[104]   Hohenberg, P. C. and Halperin, B. I., "Theory of dynamic critical phenomena", *Rev. Mod. Phys.*, vol. 49, pp. 435–479, 1977 (cit. on p. 15).

[105]   Stoof, H. T. C., Gubbels, K. B., and Dickerscheid, D. B. M., *Ultracold quantum fields* (Theoretical and Mathematical Physics). Berlin, Germany: Springer, 2009 (cit. on p. 16).

[106]   Penrose, O. and Onsager, L., "Bose-Einstein condensation and liquid Helium", *Phys. Rev.*, vol. 104, pp. 576–584, 1956 (cit. on p. 16).

[107]   Yang, C. N., "Concept of off-diagonal long-range order and the quantum phases of liquid He and of superconductors", *Rev. Mod. Phys.*, vol. 34, pp. 694–704, 1962 (cit. on p. 16).

[108]   Glauber, R. J., "The quantum theory of optical coherence", *Phys. Rev.*, vol. 130, no. 6, pp. 2529–2539, 1963 (cit. on pp. 16, 25).

[109]   Kurkela, A. and Moore, G. D., "Ultraviolet cascade in classical Yang-Mills theory", *Phys. Rev. D*, vol. 86, p. 056 008, 2012. arXiv: 1207.1663 [hep-ph] (cit. on pp. 16, 41–43, 47).

[110]   Makeenko, Y. M. and Migdal, A. A., "Exact equation for the loop average in multicolor QCD", *Phys. Lett. B*, vol. 88, p. 135, 1979, [Erratum: Phys.Lett.B 89, 437 (1980)] (cit. on p. 16).

[111]   Makeenko, Y. and Migdal, A. A., "Quantum chromodynamics as dynamics of loops", *Sov. J. Nucl. Phys.*, vol. 32, p. 431, 1980 (cit. on p. 16).

[112]   Yaffe, L. G., "Large $N$ limits as classical mechanics", *Rev. Mod. Phys.*, vol. 54, p. 407, 1982 (cit. on pp. 16, 157).

[113]   Aleiner, I. L., Faoro, L., and Ioffe, L. B., "Microscopic model of quantum butterfly effect: out-of-time-order correlators and traveling combustion waves", *Annals Phys.*, vol. 375, pp. 378–406, 2016. arXiv: 1609.01251 [cond-mat.stat-mech] (cit. on p. 17).

[114]   Swingle, B., "Unscrambling the physics of out-of-time-order correlators", *Nature Phys.*, vol. 14, no. 10, pp. 988–990, 2018 (cit. on p. 17).

[115]   A. Griffin, D. W. Snoke, and S. Stringari, Eds., *Bose-Einstein condensation*, 1st ed. Cambridge University Press, 1995 (cit. on p. 21).

[116]   Bloch, I., Hänsch, T. W., and Esslinger, T., "Measurement of the spatial coherence of a trapped Bose gas at the phase transition", *Nature*, vol. 403, no. 6766, pp. 166–170, Jan. 2000 (cit. on pp. 21, 25).

[117]   Deng, H., Solomon, G. S., Hey, R., Ploog, K. H., and Yamamoto, Y., "Spatial coherence of a polariton condensate", *Phys. Rev. Lett.*, vol. 99, no. 12, p. 126 403, 2007 (cit. on p. 21).

[118]   Damm, T., Dung, D., Vewinger, F., Weitz, M., and Schmitt, J., "First-order spatial coherence measurements in a thermalized two-dimensional photonic quantum gas", *Nat. Comm.*, vol. 8, no. 1, p. 158, Dec. 2017 (cit. on p. 21).

[119]   Kollath, C., Giamarchi, T., and Rüegg, C., "Bose-Einstein condensation in quantum magnets", in *Universal Themes of Bose-Einstein Condensation*, N. P. Proukakis, D. W. Snoke, and P. B. Littlewood, Eds., 1st ed., Cambridge University Press, Jan. 2017, pp. 549–568 (cit. on p. 21).

[120]   Jepsen, P. N., Amato-Grill, J., Dimitrova, I., Ho, W. W., Demler, E., and Ketterle, W., "Spin transport in a tunable Heisenberg model realized with ultracold atoms", *Nature*, vol. 588, no. 7838, pp. 403–407, Dec. 2020 (cit. on p. 21).

[121]   Geier, S., Thaicharoen, N., Hainaut, C., Franz, T., Salzinger, A., Tebben, A., Grimshandl, D., Zürn, G., and Weidemüller, M., "Floquet Hamiltonian engineering of an isolated many-body spin system", *Science*, vol. 374, no. 6571, pp. 1149–1152, 2021 (cit. on p. 21).

[122]   Scholl, P. *et al.*, "Microwave-engineering of programmable XXZ Hamiltonians in arrays of Rydberg atoms", *arXiv:2107.14459*, vol. 3, p. 020 303, 2 Mar. 2022, arXiv: 2107.14459 (cit. on p. 21).

[123]   Bloch, I., Dalibard, J., and Nascimbène, S., "Quantum simulations with ultracold quantum gases", *Nat. Phys.*, vol. 8, no. 4, pp. 267–276, 2012 (cit. on p. 22).

[124]   Gross, C. and Bloch, I., "Quantum simulations with ultracold atoms in optical lattices", *Science*, vol. 357, no. 6355, pp. 995–1001, 2017 (cit. on p. 22).

[125]   Rigol, M., Dunjko, V., and Olshanii, M., "Thermalization and its mechanism for generic isolated quantum systems", *Nature*, vol. 452, no. 7189, pp. 854–858, 2008, arXiv: 0708.1324 (cit. on p. 22).

[126]   Eisert, J., Friesdorf, M., and Gogolin, C., "Quantum many-body systems out of equilibrium", *Nat. Phys.*, vol. 11, no. 2, pp. 124–130, 2015 (cit. on p. 22).

[127]   Reimann, P., "Typical fast thermalization processes in closed many-body systems", *Nat. Comm.*, vol. 7, no. 1, p. 10 821, 2016 (cit. on p. 22).

[128]   Gogolin, C. and Eisert, J., "Equilibration, thermalisation, and the emergence of statistical mechanics in closed quantum systems", *Rep. Prog. Phys.*, vol. 79, no. 5, p. 056 001, 2016 (cit. on p. 22).

[129]   Mori, T., Ikeda, T. N., Kaminishi, E., and Ueda, M., "Thermalization and prethermalization in isolated quantum systems: A theoretical overview", *J. Phys. B*, vol. 51, no. 11, p. 112 001, 2018, arXiv: 1712.08790 (cit. on p. 22).

[130]   Kaufman, A. M., Tai, M. E., Lukin, A., Rispoli, M., Schittko, R., Preiss, P. M., and Greiner, M., "Quantum thermalization through entanglement in an isolated many-body system", *Science*, vol. 353, no. 6301, pp. 794–800, 2016 (cit. on p. 22).

[131]   Neill, C. *et al.*, "Ergodic dynamics and thermalization in an isolated quantum system", *Nat. Phys.*, vol. 12, no. 11, pp. 1037–1041, 2016 (cit. on p. 22).

[132]   Clos, G., Porras, D., Warring, U., and Schaetz, T., "Time-resolved observation of thermalization in an isolated quantum system", *Phys. Rev. Lett.*, vol. 117, no. 17, p. 170 401, 2016 (cit. on p. 22).

[133]   Evrard, B., Qu, A., Dalibard, J., and Gerbier, F., "From many-body oscillations to thermalization in an isolated spinor gas", *Phys. Rev. Lett.*, vol. 126, no. 6, p. 063 401, Feb. 2021, arXiv: 2010.13832 (cit. on p. 22).

[134]   Stamper-Kurn, D. M. and Ueda, M., "Spinor Bose gases: symmetries, magnetism, and quantum dynamics", *Rev. Mod. Phys.*, vol. 85, no. 3, pp. 1191–1244, 2013 (cit. on pp. 22, 38).

[135]   Uchino, S., "Spinor Bose gas in an elongated trap", *Phys. Rev. A*, vol. 91, no. 3, p. 033 605, 2015 (cit. on p. 22).

[136]   Navon, N., Smith, R. P., and Hadzibabic, Z., "Quantum gases in optical boxes", *Nat. Phys.*, vol. 17, no. 12, pp. 1334–1341, 2021 (cit. on p. 22).

[137]   Gerbier, F., Widera, A., Fölling, S., Mandel, O., and Bloch, I., "Resonant control of spin dynamics in ultracold quantum gases by microwave dressing", *Phys. Rev. A*, vol. 73, no. 4, p. 041 602, 2006 (cit. on p. 22).

[138]   Kunkel, P., Prüfer, M., Lannig, S., Rosa-Medina, R., Bonnin, A., Gärttner, M., Strobel, H., and Oberthaler, M. K., "Simultaneous readout of noncommuting collective spin observables beyond the standard quantum limit", *Phys. Rev. Lett.*, vol. 123, no. 6, p. 063 603, 2019 (cit. on pp. 23, 26).

[139]   Prüfer, M., Kunkel, P., Strobel, H., Lannig, S., Linnemann, D., Schmied, C.-M., Berges, J., Gasenzer, T., and Oberthaler, M. K., "Observation of universal dynamics in a spinor Bose gas far from equilibrium", *Nature*, vol. 563, no. 7730, pp. 217–220, 2018 (cit. on p. 23).

[140] Prüfer, M., Zache, T. V., Kunkel, P., Lannig, S., Bonnin, A., Strobel, H., Berges, J., and Oberthaler, M. K., "Experimental extraction of the quantum effective action for a non-equilibrium many-body system", *Nat. Phys.*, vol. 16, no. 10, pp. 1012–1016, 2020 (cit. on p. 23).

[141] Kunkel, P., Prüfer, M., Lannig, S., Strohmaier, R., Gärttner, M., Strobel, H., and Oberthaler, M. K., "Detecting entanglement structure in continuous many-dody quantum systems", *Phys. Rev. Lett.*, vol. 128, no. 2, p. 020 402, 2022 (cit. on pp. 23, 26).

[142] Sadler, L. E., Higbie, J. M., Leslie, S. R., Vengalattore, M., and Stamper-Kurn, D. M., "Spontaneous symmetry breaking in a quenched ferromagnetic spinor Bose–Einstein condensate", *Nature*, vol. 443, no. 7109, pp. 312–315, 2006 (cit. on p. 23).

[143] Kawaguchi, Y. and Ueda, M., "Spinor Bose-Einstein condensates", *Phys. Rep.*, vol. 520, no. 5, pp. 253–381, 2012, arXiv: 1001.2072 (cit. on pp. 24, 27, 28, 32).

[144] Köhl, M., Davis, M. J., Gardiner, C. W., Hänsch, T. W., and Esslinger, T., "Growth of Bose-Einstein condensates from thermal vapor", *Phys. Rev. Lett.*, vol. 88, no. 8, p. 080 402, 2002 (cit. on p. 25).

[145] Ritter, S., Öttl, A., Donner, T., Bourdel, T., Köhl, M., and Esslinger, T., "Observing the formation of long-range order during Bose-Einstein condensation", *Phys. Rev. Lett.*, vol. 98, no. 9, p. 090 402, 2007 (cit. on p. 25).

[146] Naraschewski, M. and Glauber, R. J., "Spatial coherence and density correlations of trapped Bose gases", *Phys. Rev. A*, vol. 59, no. 6, pp. 4595–4607, 1999 (cit. on p. 26).

[147] Öttl, A., Ritter, S., Köhl, M., and Esslinger, T., "Correlations and counting statistics of an atom laser", *Phys. Rev. Lett.*, vol. 95, no. 9, p. 090 404, 2005 (cit. on p. 26).

[148] Hodgman, S. S., Dall, R. G., Manning, A. G., Baldwin, K. G. H., and Truscott, A. G., "Direct measurement of long-range third-order coherence in Bose-Einstein condensates", *Science*, vol. 331, no. 6020, pp. 1046–1049, 2011 (cit. on p. 26).

[149] Perrin, A., Bücker, R., Manz, S., Betz, T., Koller, C., Plisson, T., Schumm, T., and Schmiedmayer, J., "Hanbury Brown and Twiss correlations across the Bose–Einstein condensation threshold", *Nat. Phys.*, vol. 8, no. 3, pp. 195–198, 2012 (cit. on p. 26).

[150] Cayla, H., Butera, S., Carcy, C., Tenart, A., Hercé, G., Mancini, M., Aspect, A., Carusotto, I., and Clément, D., "Hanbury-Brown and Twiss bunching of phonons and of the quantum depletion in a strongly-interacting Bose gas", *Phys. Rev. Lett.*, vol. 125, no. 16, p. 165 301, 2020, arXiv: 2006.11792 (cit. on p. 26).

[151] Landau, L., "Theory of the superfluidity of Helium II", *Phys. Rev.*, vol. 60, no. 4, pp. 356–358, 1941 (cit. on p. 26).

[152] Raman, C., Köhl, M., Onofrio, R., Durfee, D. S., Kuklewicz, C. E., Hadzibabic, Z., and Ketterle, W., "Evidence for a critical velocity in a Bose-Einstein condensed gas", *Phys. Rev. Lett.*, vol. 83, no. 13, pp. 2502–2505, 1999 (cit. on p. 26).

[153]  Weimer, W., Morgener, K., Singh, V. P., Siegl, J., Hueck, K., Luick, N., Mathey, L., and Moritz, H., "Critical velocity in the BEC-BCS crossover", *Phys. Rev. Lett.*, vol. 114, no. 9, p. 095 301, 2015 (cit. on p. 26).

[154]  Kim, J. H., Hong, D., and Shin, Y., "Observation of two sound modes in a binary superfluid gas", *Phys. Rev. A*, vol. 101, no. 6, p. 061 601, 2020 (cit. on p. 26).

[155]  Recati, A. and Piazza, F., "Breaking of Goldstone modes in a two-component Bose-Einstein condensate", *Phys. Rev. B*, vol. 99, no. 6, p. 064 505, 2019 (cit. on p. 26).

[156]  Cominotti, R., Berti, A., Farolfi, A., Zenesini, A., Lamporesi, G., Carusotto, I, Recati, A., and Ferrari, G., "Observation of massless and massive collective excitations with Faraday patterns in a two-component superfluid", *Phys. Rev. Lett.*, vol. 128, p. 210 401, 21 2022 (cit. on p. 26).

[157]  Uchino, S., Kobayashi, M., and Ueda, M., "Bogoliubov theory and Lee-Huang-Yang corrections in spin-1 and spin-2 Bose-Einstein condensates in the presence of the quadratic Zeeman effect", *Phys. Rev. A*, vol. 81, no. 6, p. 063 632, 2010 (cit. on pp. 27–30, 34, 38).

[158]  Symes, L. M., Baillie, D., and Blakie, P. B., "Static structure factors for a spin-1 Bose-Einstein condensate", *Phys. Rev. A*, vol. 89, no. 5, p. 053 628, 2014 (cit. on p. 31).

[159]  Manz, S. *et al.*, "Two-point density correlations of quasicondensates in free expansion", *Phys. Rev. A*, vol. 81, no. 3, p. 031 610, 2010 (cit. on p. 34).

[160]  Betz, T. *et al.*, "Two-point phase correlations of a one-dimensional bosonic Josephson junction", *Phys. Rev. Lett.*, vol. 106, no. 2, p. 020 407, 2011 (cit. on p. 34).

[161]  Bogoliubov, N, "On the theory of superfluidity", *J. Phys.*, vol. 11, no. 1, p. 23, 1947 (cit. on p. 34).

[162]  Phuc, N. T., Kawaguchi, Y., and Ueda, M., "Effects of thermal and quantum fluctuations on the phase diagram of a spin-1 87 Rb Bose-Einstein condensate", *Phys. Rev. A*, vol. 84, no. 4, p. 043 645, 2011 (cit. on p. 35).

[163]  Kawaguchi, Y., Phuc, N. T., and Blakie, P. B., "Finite-temperature phase diagram of a spin-1 Bose gas", *Phys. Rev. A*, vol. 85, no. 5, p. 053 611, 2012 (cit. on p. 35).

[164]  Yu, X. and Blakie, P. B., "Propagating ferrodark solitons in a superfluid: Exact solutions and anomalous dynamics", *Phys. Rev. Lett.*, vol. 128, p. 125 301, 12 2022 (cit. on p. 35).

[165]  Guzman, J., Jo, G.-B., Wenz, A. N., Murch, K. W., Thomas, C. K., and Stamper-Kurn, D. M., "Long-time-scale dynamics of spin textures in a degenerate F = 1 87 Rb spinor Bose gas", *Phys. Rev. A*, vol. 84, no. 6, p. 063 625, 2011 (cit. on p. 36).

[166]  Lannig, S., Schmied, C.-M., Prüfer, M., Kunkel, P., Strohmaier, R., Strobel, H., Gasenzer, T., Kevrekidis, P. G., and Oberthaler, M. K., "Collisions of three-component vector solitons in Bose-Einstein condensates", *Phys. Rev. Lett.*, vol. 125, no. 17, p. 170 401, 2020, arXiv: 2005.13278 (cit. on p. 37).

[167] Kunkel, P., Prüfer, M., Strobel, H., Linnemann, D., Frölian, A., Gasenzer, T., Gärttner, M., and Oberthaler, M. K., "Spatially distributed multipartite entanglement enables EPR steering of atomic clouds", *Science*, vol. 360, no. 6387, pp. 413–416, 2018 (cit. on p. 38).

[168] Gribov, L. V., Levin, E. M., and Ryskin, M. G., "Semihard processes in QCD", *Phys. Rept.*, vol. 100, pp. 1–150, 1983 (cit. on p. 41).

[169] Gelis, F., Iancu, E., Jalilian-Marian, J., and Venugopalan, R., "The color glass condensate", *Ann. Rev. Nucl. Part. Sci.*, vol. 60, pp. 463–489, 2010. arXiv: 1002.0333 [hep-ph] (cit. on p. 41).

[170] Baier, R., Mueller, A. H., Schiff, D., and Son, D. T., "'Bottom up' thermalization in heavy ion collisions", *Phys. Lett. B*, vol. 502, pp. 51–58, 2001. arXiv: hep-ph/0009237 (cit. on p. 41).

[171] Aarts, G. and Berges, J., "Classical aspects of quantum fields far from equilibrium", *Phys. Rev. Lett.*, vol. 88, p. 041 603, 2002. arXiv: hep-ph/0107129 (cit. on pp. 41, 43).

[172] Mueller, A. H. and Son, D. T., "On the equivalence between the Boltzmann equation and classical field theory at large occupation numbers", *Phys. Lett. B*, vol. 582, pp. 279–287, 2004. arXiv: hep-ph/0212198 (cit. on pp. 41, 43).

[173] Skullerud, J.-I., Smit, J., and Tranberg, A., "W and Higgs particle distributions during electroweak tachyonic preheating", *JHEP*, vol. 08, p. 045, 2003. arXiv: hep-ph/0307094 (cit. on pp. 41, 43).

[174] Jeon, S., "The Boltzmann equation in classical and quantum field theory", *Phys. Rev. C*, vol. 72, p. 014 907, 2005. arXiv: hep-ph/0412121 (cit. on pp. 41, 43).

[175] Arrizabalaga, A., Smit, J., and Tranberg, A., "Tachyonic preheating using 2PI-1/$N$ dynamics and the classical approximation", *JHEP*, vol. 10, p. 017, 2004. arXiv: hep-ph/0409177 (cit. on pp. 41, 43).

[176] Bjorken, J. D., "Highly relativistic nucleus-nucleus collisions: the central rapidity region", *Phys. Rev. D*, vol. 27, pp. 140–151, 1983 (cit. on p. 41).

[177] Chazal, F. and Michel, B., "An introduction to topological data analysis: fundamental and practical aspects for data scientists", *Front. Artif. Intell. Appl.*, vol. 4, 2021. arXiv: 1710.04019 [math] (cit. on pp. 41, 42, 50).

[178] Edelsbrunner, H. and Harer, J. L., *Computational topology: an introduction*. American Mathematical Society, 2022 (cit. on pp. 41, 42, 50, 65, 67).

[179] Berges, J., Boguslavski, K., Schlichting, S., and Venugopalan, R., "Turbulent thermalization process in heavy-ion collisions at ultrarelativistic energies", *Phys. Rev. D*, vol. 89, no. 7, p. 074 011, 2014. arXiv: 1303.5650 [hep-ph] (cit. on p. 42).

[180] Heller, M. P. and Spalinski, M., "Hydrodynamics beyond the gradient expansion: resurgence and resummation", *Phys. Rev. Lett.*, vol. 115, no. 7, p. 072 501, 2015. arXiv: 1503.07514 [hep-th] (cit. on p. 42).

[181] Romatschke, P., "Relativistic fluid dynamics far from local equilibrium", *Phys. Rev. Lett.*, vol. 120, no. 1, p. 012 301, 2018. arXiv: 1704.08699 [hep-th] (cit. on p. 42).

[182]   Soloviev, A., "Hydrodynamic attractors in heavy ion collisions: a review", *Eur. Phys. J. C*, vol. 82, no. 4, p. 319, 2022. arXiv: 2109.15081 [hep-th] (cit. on p. 42).

[183]   Berges, J., Scheffler, S., and Sexty, D., "Turbulence in non-Abelian gauge theory", *Phys. Lett. B*, vol. 681, pp. 362–366, 2009. arXiv: 0811.4293 [hep-ph] (cit. on p. 42).

[184]   Kurkela, A. and Moore, G. D., "Thermalization in weakly coupled non-Abelian plasmas", *JHEP*, vol. 12, p. 044, 2011. arXiv: 1107.5050 [hep-ph] (cit. on p. 42).

[185]   Berges, J., Schlichting, S., and Sexty, D., "Over-populated gauge fields on the lattice", *Phys. Rev. D*, vol. 86, p. 074 006, 2012. arXiv: 1203.4646 [hep-ph] (cit. on p. 42).

[186]   Schlichting, S., "Turbulent thermalization of weakly coupled non-Abelian plasmas", *Phys. Rev. D*, vol. 86, p. 065 008, 2012. arXiv: 1207.1450 [hep-ph] (cit. on pp. 42, 47, 49).

[187]   Abraao York, M. C., Kurkela, A., Lu, E., and Moore, G. D., "UV cascade in classical Yang-Mills theory via kinetic theory", *Phys. Rev. D*, vol. 89, no. 7, p. 074 036, 2014. arXiv: 1401.3751 [hep-ph] (cit. on pp. 42, 47).

[188]   Boguslavski, K., Kurkela, A., Lappi, T., and Peuron, J., "Spectral function for overoccupied gluodynamics from real-time lattice simulations", *Phys. Rev. D*, vol. 98, no. 1, p. 014 006, 2018. arXiv: 1804.01966 [hep-ph] (cit. on pp. 42–44, 47, 58).

[189]   Boguslavski, K., Kurkela, A., Lappi, T., and Peuron, J., "Highly occupied gauge theories in 2+1 dimensions: a self-similar attractor", *Phys. Rev. D*, vol. 100, no. 9, p. 094 022, 2019. arXiv: 1907.05892 [hep-ph] (cit. on p. 42).

[190]   Florkowski, W., Heller, M. P., and Spalinski, M., "New theories of relativistic hydrodynamics in the LHC era", *Rept. Prog. Phys.*, vol. 81, no. 4, p. 046 001, 2018. arXiv: 1707.02282 [hep-ph] (cit. on p. 42).

[191]   Romatschke, P. and Romatschke, U., *Relativistic fluid dynamics in and out of equilibrium* (Cambridge Monographs on Mathematical Physics). Cambridge University Press, May 2019. arXiv: 1712.05815 [nucl-th] (cit. on p. 42).

[192]   Hirakida, T., Kashiwa, K., Sugano, J., Takahashi, J., Kouno, H., and Yahiro, M., "Persistent homology analysis of deconfinement transition in effective Polyakov-line model", *Int. J. Mod. Phys. A*, vol. 35, no. 10, p. 2 050 049, 2020. arXiv: 1810.07635 [hep-lat] (cit. on pp. 42, 102).

[193]   Kashiwa, K., Hirakida, T., and Kouno, H., "Persistent homology analysis for dense QCD effective model with heavy quarks", *Symmetry*, vol. 14, no. 9, p. 1783, 2022. arXiv: 2103.12554 [hep-lat] (cit. on pp. 42, 102).

[194]   Moore, G. D., "Motion of Chern-Simons number at high temperatures under a chemical potential", *Nucl. Phys. B*, vol. 480, pp. 657–688, 1996. arXiv: hep-ph/9603384 (cit. on p. 44).

[195]   Berges, J., Gelfand, D., Scheffler, S., and Sexty, D., "Simulating plasma instabilities in SU(3) gauge theory", *Phys. Lett. B*, vol. 677, pp. 210–213, 2009. arXiv: 0812.3859 [hep-ph] (cit. on p. 44).

[196] Ipp, A., Rebhan, A., and Strickland, M., "Non-Abelian plasma instabilities: $SU(3)$ vs. $SU(2)$", *Phys. Rev. D*, vol. 84, p. 056 003, 2011. arXiv: 1012.0298 [hep-ph] (cit. on p. 44).

[197] Moore, G. D., "Improved Hamiltonian for Minkowski Yang-Mills theory", *Nucl. Phys. B*, vol. 480, pp. 689–728, 1996. arXiv: hep-lat/9605001 (cit. on p. 44).

[198] Di Vecchia, P., Fabricius, K., Rossi, G. C., and Veneziano, G., "Preliminary evidence for $U(1)_A$ breaking in QCD from lattice calculations", *Nucl. Phys. B*, vol. 192, J. Julve and M. Ramón-Medrano, Eds., p. 392, 1981 (cit. on p. 45).

[199] Coriano, C., Maglio, M. M., and Mottola, E., "TTT in CFT: trace identities and the conformal anomaly effective action", *Nucl. Phys. B*, vol. 942, pp. 303–328, 2019. arXiv: 1703.08860 [hep-th] (cit. on p. 47).

[200] Carlsson, G., "Topology and data", *Bulletin of the American Mathematical Society*, vol. 46, no. 2, pp. 255–308, 2009 (cit. on pp. 50, 102).

[201] May, J. P., *A concise course in algebraic topology*. University of Chicago press, 1999 (cit. on pp. 50, 67, 108).

[202] Munkres, J. R., *Elements of algebraic topology*. Boca Raton, Florida: CRC press, 2018 (cit. on pp. 50, 67).

[203] Maria, C., Boissonnat, J.-D., Glisse, M., and Yvinec, M., "The GUDHI library: simplicial complexes and persistent homology", in *International congress on mathematical software*, Springer, 2014, pp. 167–174 (cit. on pp. 52, 61, 110).

[204] Divol, V. and Chazal, F., "The density of expected persistence diagrams and its kernel based estimation", *J. Comput. Geom.*, vol. 10, no. 2, pp. 127–153, 2019 (cit. on pp. 52, 65, 72, 90).

[205] Bobrowski, O. and Skraba, P., "On the universality of random persistence diagrams", arXiv: 2207.03926 [math] (cit. on pp. 53, 55, 56, 59, 60).

[206] Edelsbrunner, H., Letscher, D., and Zomorodian, A., "Topological persistence and simplification", in *Proceedings of the 41st Annual Symposium on Foundations of Computer Science*, 2000, pp. 454–463 (cit. on p. 57).

[207] Zomorodian, A. and Carlsson, G., "Computing persistent homology", in *Proceedings of the 20th Annual Symposium on Computational Geometry*, ser. SCG '04, 2004, 347–356 (cit. on p. 57).

[208] Wagner, H., Chen, C., and Vuçini, E., "Efficient computation of persistent homology for cubical data", in *Topological methods in data analysis and visualization II*, Springer, 2012, pp. 91–106 (cit. on p. 61).

[209] Chazal, F., De Silva, V., Glisse, M., and Oudot, S., *The structure and stability of persistence modules*. Springer, 2016 (cit. on p. 65).

[210] Edelsbrunner, H., Letscher, D., and Zomorodian, A., "Topological persistence and simplification", in *Proceedings of the 41st annual symposium on foundations of computer science*, IEEE, 2000, pp. 454–463 (cit. on p. 65).

[211]    Ghrist, R., "Barcodes: the persistent topology of data", *Bull. Am. Math. Soc.*, vol. 45, no. 1, pp. 61–75, 2008 (cit. on p. 65).

[212]    Zomorodian, A. and Carlsson, G., "Computing persistent homology", *Discrete Comput. Geom.*, vol. 33, no. 2, pp. 249–274, 2005 (cit. on pp. 65, 68).

[213]    Bobrowski, O. and Borman, M. S., "Euler integration of Gaussian random fields and persistent homology", *J. Topol. Anal.*, vol. 4, no. 01, pp. 49–70, 2012 (cit. on p. 65).

[214]    Bobrowski, O., Kahle, M., Skraba, P., *et al.*, "Maximally persistent cycles in random geometric complexes", *Ann. Appl. Prob.*, vol. 27, no. 4, pp. 2032–2060, 2017 (cit. on p. 65).

[215]    Bobrowski, O. and Weinberger, S., "On the vanishing of homology in random Čech complexes", *Random Struct. Algorithms*, vol. 51, no. 1, pp. 14–51, 2017 (cit. on p. 65).

[216]    Edelsbrunner, H., Nikitenko, A., and Reitzner, M., "Expected sizes of Poisson–Delaunay mosaics and their discrete Morse functions", *Adv. Appl. Prob.*, vol. 49, no. 3, pp. 745–767, 2017 (cit. on p. 65).

[217]    Kahle, M., "Random geometric complexes", *Discrete Comput. Geom.*, vol. 45, no. 3, pp. 553–573, 2011 (cit. on p. 65).

[218]    Owada, T., Adler, R. J., *et al.*, "Limit theorems for point processes under geometric constraints (and topological crackle)", *Ann. Probab.*, vol. 45, no. 3, pp. 2004–2055, 2017 (cit. on p. 65).

[219]    Yogeshwaran, D and Adler, R. J., "On the topology of random complexes built over stationary point processes", *Ann. Appl. Prob.*, vol. 25, no. 6, pp. 3338–3380, 2015 (cit. on p. 65).

[220]    Yogeshwaran, D, Subag, E., and Adler, R. J., "Random geometric complexes in the thermodynamic regime", *Probab. Theory Relat. Fields*, vol. 167, no. 1-2, pp. 107–142, 2017 (cit. on p. 65).

[221]    Kahle, M., "Topology of random simplicial complexes: A survey", *AMS Contemp. Math*, vol. 620, pp. 201–222, 2014 (cit. on p. 65).

[222]    Goel, A., Trinh, K. D., and Tsunoda, K., "Strong law of large numbers for Betti numbers in the thermodynamic regime", *J. Stat. Phys.*, vol. 174, no. 4, pp. 865–892, 2019 (cit. on pp. 65, 74).

[223]    Krebs, J. T. and Polonik, W., "On the asymptotic normality of persistent Betti numbers", 2019. arXiv: 1903.03280 [math.PR] (cit. on pp. 65, 74).

[224]    Owada, T. and Thomas, A. M., "Limit theorems for process-level Betti numbers for sparse and critical regimes", *Adv. Appl. Prob.*, vol. 52, no. 1, pp. 1–31, 2020 (cit. on pp. 65, 74).

[225]    Roycraft, B., Krebs, J., and Polonik, W., "Bootstrapping persistent Betti numbers and other stabilizing statistics", 2020. arXiv: 2005.01417 [math.PR] (cit. on pp. 65, 74).

[226] Jaquette, J. and Schweinhart, B., "Fractal dimension estimation with persistent homology: a comparative study", *Commun. Nonlinear. Sci.*, vol. 84, p. 105 163, 2020 (cit. on pp. 66, 77).

[227] Bauer, U. and Edelsbrunner, H., "The Morse theory of Čech and Delaunay complexes", *Trans. Amer. Math. Soc.*, vol. 369, no. 5, pp. 3741–3762, 2017 (cit. on pp. 67, 70).

[228] Daley, D. J. and Vere-Jones, D., *An introduction to the theory of point processes. Vol. I: probability and its applications*. Springer Science & Business Media, 2003 (cit. on pp. 67, 80).

[229] Daley, D. J. and Vere-Jones, D., *An introduction to the theory of point processes. Vol. II: general theory and structure*. Springer Science & Business Media, 2007 (cit. on pp. 67, 69, 80, 90).

[230] Last, G. and Penrose, M., *Lectures on the Poisson process*. Cambridge University Press, 2017, vol. 7 (cit. on pp. 67, 80).

[231] Hatcher, A., *Algebraic topology*. Cambridge University Press, 2005 (cit. on p. 67).

[232] Gruber, P. M., *Convex and discrete geometry*. Springer Science & Business Media, 2007, vol. 336 (cit. on pp. 69, 94, 95).

[233] Penrose, M. D. and Yukich, J. E., "Central limit theorems for some graphs in computational geometry", *Ann. Appl. Prob.*, pp. 1005–1041, 2001 (cit. on p. 69).

[234] Ball, K., "Volume ratios and a reverse isoperimetric inequality", *J. London Math. Soc.*, vol. 2, no. 2, pp. 351–359, 1991 (cit. on p. 69).

[235] Amenta, N., Attali, D., and Devillers, O., "A tight bound for the Delaunay triangulation of points on a polyhedron", *Discrete Comput. Geom.*, vol. 48, no. 1, pp. 19–38, 2012 (cit. on p. 70).

[236] Mattila, P., *Geometry of sets and measures in Euclidean spaces: fractals and rectifiability*. Cambridge University Press, 1999 (cit. on p. 71).

[237] Gauthier, G., Reeves, M. T., Yu, X., Bradley, A. S., Baker, M., Bell, T. A., Rubinsztein-Dunlop, H., Davis, M. J., and Neely, T. W., "Giant vortex clusters in a two-dimensional quantum fluid", *Science*, vol. 364, no. 6447, pp. 1264–1267, Jan. 2018. arXiv: 1801.06951 [cond-mat.quant-gas] (cit. on p. 73).

[238] Johnstone, S. P., Groszek, A. J., Starkey, P. T., Billington, C. J., Simula, T. P., and Helmerson, K., "Evolution of large-scale flow from turbulence in a two-dimensional superfluid", *Science*, vol. 364, no. 6447, pp. 1267–1271, 2019 (cit. on pp. 73, 182).

[239] Thomas, A. M. and Owada, T., "Functional limit theorems for the Euler characteristic process in the critical regime", *Adv. Appl. Prob.*, vol. 53, no. 1, pp. 57–80, 2021 (cit. on p. 74).

[240] Björner, A., "Topological methods", *Handbook of combinatorics*, vol. 2, pp. 1819–1872, 1995 (cit. on p. 75).

[241] Niyogi, P., Smale, S., and Weinberger, S., "Finding the homology of submanifolds with high confidence from random samples", *Discrete Comput. Geom.*, vol. 39, no. 1-3, pp. 419–441, 2008 (cit. on p. 83).

[242] Bauer, U. and Lesnick, M., "Induced matchings and the algebraic stability of persistence barcodes", *J. Comput. Geom.*, vol. 6, pp. 162–191, 2015. arXiv: 1311.3681 [math.AT] (cit. on pp. 83, 88, 102, 110).

[243] Mileyko, Y., Mukherjee, S., and Harer, J., "Probability measures on the space of persistence diagrams", *Inverse Probl.*, vol. 27, no. 12, p. 124 007, 2011 (cit. on p. 89).

[244] Berry, E., Chen, Y.-C., Cisewski-Kehe, J., and Fasy, B. T., "Functional summaries of persistence diagrams", *J. Appl. Comput. Topol.*, vol. 4, no. 2, pp. 211–262, 2020 (cit. on pp. 89, 90).

[245] Biscio, C. A. and Møller, J., "The accumulated persistence function, a new useful functional summary statistic for topological data analysis, with a view to brain artery trees and spatial point process applications", *J. Comput. Graph. Stat.*, vol. 28, no. 3, pp. 671–681, 2019 (cit. on p. 89).

[246] Chazal, F., Fasy, B. T., Lecci, F., Rinaldo, A., and Wasserman, L., "Stochastic convergence of persistence landscapes and silhouettes", in *Proceedings of the 30th annual symposium on Computational geometry*, 2014, pp. 474–483 (cit. on p. 89).

[247] Chen, Y.-C., Wang, D., Rinaldo, A., and Wasserman, L., "Statistical analysis of persistence intensity functions", 2015. arXiv: 1510.02502 [stat.ME] (cit. on p. 89).

[248] Divol, V. and Polonik, W., "On the choice of weight functions for linear representations of persistence diagrams", *J. Appl. Comput. Topol.*, vol. 3, no. 3, pp. 249–283, 2019 (cit. on p. 90).

[249] McMullen, P., "Inequalities between intrinsic volumes", *Mon. Hefte Math.*, vol. 111, no. 1, pp. 47–53, 1991 (cit. on p. 94).

[250] Harrington, B. J. and Shepard, H. K., "Periodic Euclidean solutions and the finite temperature Yang-Mills gas", *Phys. Rev. D*, vol. 17, p. 2122, 1978 (cit. on p. 101).

[251] Kraan, T. C. and Van Baal, P., "Periodic instantons with non-trivial holonomy", *Nucl. Phys. B*, vol. 533, pp. 627–659, 1998. arXiv: hep-th/9805168 (cit. on pp. 101, 106).

[252] Kraan, T. C. and Van Baal, P., "Monopole constituents inside $SU(N)$ calorons", *Phys. Lett. B*, vol. 435, pp. 389–395, 1998. arXiv: hep-th/9806034 (cit. on pp. 101, 106).

[253] Lee, K. and Lu, C., "$SU(2)$ calorons and magnetic monopoles", *Phys. Rev. D*, vol. 58, p. 025 011, 1998. arXiv: hep-th/9802108 (cit. on pp. 101, 106).

[254] Ford, C., Pawlowski, J. M., Tok, T., and Wipf, A., "ADHM construction of instantons on the torus", *Nucl. Phys. B*, vol. 596, pp. 387–414, 2001. arXiv: hep-th/0005221 (cit. on p. 101).

[255] Ford, C. and Pawlowski, J. M., "Constituents of doubly periodic instantons", *Phys. Lett. B*, vol. 540, pp. 153–158, 2002. arXiv: hep-th/0205116 (cit. on p. 101).

[256] Ford, C. and Pawlowski, J. M., "Doubly periodic instantons and their constituents", *Phys. Rev. D*, vol. 69, p. 065 006, 2004. arXiv: hep-th/0302117 (cit. on p. 101).

[257] Ford, C. and Pawlowski, J. M., "Doubly periodic instanton zero modes", *Phys. Lett. B*, vol. 626, pp. 139–146, 2005. arXiv: hep-th/0505214 (cit. on p. 101).

[258] Pérez, M. G., Gonzalez-Arroyo, A., Montero, A., and Van Baal, P., "Calorons on the lattice - a new perspective", *JHEP*, vol. 06, p. 001, 1999. arXiv: hep-lat/9903022 (cit. on p. 101).

[259] Ilgenfritz, E.-M., Martemyanov, B., Veselov, A., Müller-Preussker, M, and Shcheredin, S, "Topological content of $SU(2)$ gauge fields below $T_c$", *Phys. Rev. D*, vol. 66, p. 074 503, 2002. arXiv: hep-lat/0206004 (cit. on p. 101).

[260] Bornyakov, V., Ilgenfritz, E.-M., Martemyanov, B., Mitrjushkin, V., and Müller-Preussker, M, "Topology across the finite temperature transition studied by overimproved cooling in gluodynamics and QCD", *Phys. Rev. D*, vol. 87, no. 11, p. 114 508, 2013. arXiv: 1304.0935 [hep-lat] (cit. on p. 101).

[261] Bornyakov, V., Ilgenfritz, E.-M., Martemyanov, B., and Müller-Preussker, M, "Dyons near the transition temperature in lattice QCD", *Phys. Rev. D*, vol. 93, no. 7, p. 074 508, 2016. arXiv: 1512.03217 [hep-lat] (cit. on p. 101).

[262] Bornyakov, V. G., Boyda, D. L., Goy, V. A., Ilgenfritz, E. M., Martemyanov, B. V., Molochkov, A. V., Nakamura, A., Nikolaev, A. A., and Zakharov, V. I., "Dyons and Roberge - Weiss transition in lattice QCD", Y. Foka, N. Brambilla, and V. Kovalenko, Eds., vol. 137, 2017, p. 03 002. arXiv: 1611.07789 [hep-lat] (cit. on p. 101).

[263] Gerhold, P., Ilgenfritz, E.-M., and Müller-Preussker, M, "An $SU(2)$ KvBLL caloron gas model and confinement", *Nucl. Phys. B*, vol. 760, pp. 1–37, 2007. arXiv: hep-ph/0607315 (cit. on p. 101).

[264] Diakonov, D. and Petrov, V., "Confining ensemble of dyons", *Phys. Rev. D*, vol. 76, p. 056 001, 2007. arXiv: 0704.3181 [hep-th] (cit. on pp. 101, 124).

[265] Bruckmann, F., Dinter, S., Ilgenfritz, E.-M., Maier, B., Müller-Preussker, M., and Wagner, M., "Confining dyon gas with finite-volume effects under control", *Phys. Rev. D*, vol. 85, p. 034 502, 2012. arXiv: 1111.3158 [hep-ph] (cit. on p. 101).

[266] Larsen, R. and Shuryak, E., "Interacting ensemble of the instanton-dyons and the deconfinement phase transition in the $SU(2)$ gauge theory", *Phys. Rev. D*, vol. 92, no. 9, p. 094 022, 2015. arXiv: 1504.03341 [hep-ph] (cit. on pp. 101, 117).

[267] Liu, Y., Shuryak, E., and Zahed, I., "Confining dyon-antidyon Coulomb liquid model. I." *Phys. Rev. D*, vol. 92, no. 8, p. 085 006, 2015. arXiv: 1503.03058 [hep-ph] (cit. on p. 101).

[268] Lopez-Ruiz, M. A., Jiang, Y., and Liao, J., "Confinement, holonomy, and correlated instanton-dyon ensemble: $SU(2)$ Yang-Mills theory", *Phys. Rev. D*, vol. 97, no. 5, p. 054 026, 2018. arXiv: 1611.02539 [hep-ph] (cit. on pp. 101, 106).

[269] Pepe, M. and Wiese, U.-J., "Exceptional deconfinement in G(2) gauge theory", *Nucl. Phys. B*, vol. 768, pp. 21–37, 2007. arXiv: hep-lat/0610076 (cit. on p. 101).

[270]  Diakonov, D., "Topology and confinement", *Nucl. Phys. B Proc. Suppl.*, vol. 195, pp. 5–45, 2009. arXiv: 0906.2456 [hep-ph] (cit. on pp. 101, 106, 113, 117).

[271]  Diakonov, D. and Petrov, V., "Confinement and deconfinement for any gauge group from dyons viewpoint", in *AIP Conf. Proc.*, F. J. Llanes-Estrada and J. R. Peláez, Eds., vol. 1343, 2011, pp. 69–74. arXiv: 1011.5636 [hep-th] (cit. on p. 101).

[272]  Larsen, R. N., Sharma, S., and Shuryak, E., "Correlating confinement to topological fluctuations near the crossover transition in QCD", *Phys. Rev. D*, vol. 105, no. 7, p. L071501, 2022. arXiv: 2112.04537 [hep-lat] (cit. on p. 102).

[273]  Liu, Y., Shuryak, E., and Zahed, I., "Light quarks in the screened dyon-antidyon Coulomb liquid model. II." *Phys. Rev. D*, vol. 92, no. 8, p. 085 007, 2015. arXiv: 1503.09148 [hep-ph] (cit. on p. 102).

[274]  Larsen, R. and Shuryak, E., "Instanton-dyon ensemble with two dynamical quarks: The chiral symmetry breaking", *Phys. Rev. D*, vol. 93, no. 5, p. 054 029, 2016. arXiv: 1511.02237 [hep-ph] (cit. on p. 102).

[275]  DeMartini, D. and Shuryak, E., "Chiral symmetry breaking and confinement from an interacting ensemble of instanton dyons in two-flavor massless QCD", *Phys. Rev. D*, vol. 104, no. 9, p. 094 031, 2021. arXiv: 2108.06353 [hep-ph] (cit. on p. 102).

[276]  Franzosi, R. and Pettini, M., "Theorem on the origin of phase transitions", *Phys. Rev. Lett.*, vol. 92, no. 6, p. 060 601, 2004. arXiv: 0312361 [cond-mat] (cit. on p. 102).

[277]  Franzosi, R., Pettini, M., and Spinelli, L., "Topology and phase transitions I. Preliminary results", *Nucl. Phys. B*, vol. 782, pp. 189–218, 2007 (cit. on p. 102).

[278]  Franzosi, R. and Pettini, M., "Topology and phase transitions II. Theorem on a necessary relation", *Nucl. Phys. B*, vol. 782, pp. 219–240, 2007. arXiv: math-ph/0505057 (cit. on p. 102).

[279]  Gori, M., Franzosi, R., and Pettini, M., "Topological origin of phase transitions in the absence of critical points of the energy landscape", *J. Stat. Mech.*, vol. 1809, no. 9, p. 093 204, 2018. arXiv: 1706.01430 [cond-mat] (cit. on p. 102).

[280]  Tirelli, A. and Costa, N. C., "Learning quantum phase transitions through topological data analysis", *Phys. Rev. B*, vol. 104, no. 23, p. 235 146, 2021. arXiv: 2109.09555 [cond-mat.str-el] (cit. on p. 102).

[281]  He, Y., Xia, S., Angelakis, D. G., Song, D., Chen, Z., and Leykam, D., "Persistent homology analysis of a generalized Aubry-André-Harper model", Apr. 2022. arXiv: 2204.13276 [cond-mat.dis-nn] (cit. on p. 102).

[282]  Olsthoorn, B., "Persistent homology of quantum entanglement", *Phys. Rev. B*, vol. 107, no. 11, p. 115 174, 2023. arXiv: 2110.10214 [cond-mat.stat-mech] (cit. on p. 102).

[283]  Duponchel, L., "Exploring hyperspectral imaging data sets with topological data analysis", *Analytica chimica acta*, vol. 1000, pp. 123–131, 2018 (cit. on p. 102).

[284] Nakamura, T., Hiraoka, Y., Hirata, A., Escolar, E. G., and Nishiura, Y., "Persistent homology and many-body atomic structure for medium-range order in the glass", *Nanotechnology*, vol. 26, no. 30, p. 304 001, 2015. arXiv: 1502.07445 [cond-mat.soft] (cit. on p. 102).

[285] Sousbie, T., "The persistent cosmic web and its filamentary structure–I. Theory and implementation", *Mon. Not. Roy. Astron. Soc.*, vol. 414, p. 350, 2011. arXiv: 1009.4015 [astro-ph.CO] (cit. on p. 102).

[286] Weygaert, R. v. d., Vegter, G., Edelsbrunner, H., Jones, B. J., Pranav, P., Park, C., Hellwing, W. A., Eldering, B., Kruithof, N., Bos, E., *et al.*, "Alpha, Betti and the megaparsec universe: on the topology of the cosmic web", in *Transactions on computational science XIV*, Springer, 2011, pp. 60–101. arXiv: 1306.3640 [astro-ph.CO] (cit. on p. 102).

[287] Pranav, P., Edelsbrunner, H., Weygaert, R. Van de, Vegter, G., Kerber, M., Jones, B. J., and Wintraecken, M., "The topology of the cosmic web in terms of persistent Betti numbers", *Mon. Not. Roy. Astron. Soc.*, vol. 465, no. 4, pp. 4281–4310, 2017. arXiv: 1608.04519 [astro-ph.CO] (cit. on p. 102).

[288] Pranav, P., Adler, R. J., Buchert, T., Edelsbrunner, H., Jones, B. J., Schwartzman, A., Wagner, H., and Weygaert, R. Van de, "Unexpected topology of the temperature fluctuations in the cosmic microwave background", *Astron. Astrophys.*, vol. 627, A163, 2019. arXiv: 1812.07678 [astro-ph.CO] (cit. on p. 102).

[289] Biagetti, M., Cole, A., and Shiu, G., "The persistence of large scale structures. Part I. Primordial non-Gaussianity", *JCAP*, vol. 2021, no. 04, p. 061, 2021. arXiv: 2009.04819 [astro-ph.CO] (cit. on p. 102).

[290] Lloyd, S., Garnerone, S., and Zanardi, P., "Quantum algorithms for topological and geometric analysis of data", *Nat. Commun.*, vol. 7, no. 10138, pp. 1–7, 2016. arXiv: 1408.3106 [quant-ph] (cit. on pp. 102, 181).

[291] Adams, H., Emerson, T., Kirby, M., Neville, R., Peterson, C., Shipman, P., Chepushtanova, S., Hanson, E., Motta, F., and Ziegelmeier, L., "Persistence images: a stable vector representation of persistent homology", *J. Mach. Learn. Res.*, vol. 18, 2017. arXiv: 1507.06217 [cs.CG] (cit. on p. 102).

[292] Pun, C. S., Lee, S. X., and Xia, K., "Persistent-homology-based machine learning: a survey and a comparative study", *Artificial Intelligence Review*, 2022. arXiv: 1811.00252 [math.AT] (cit. on p. 102).

[293] Larsen, R. N., Sharma, S., and Shuryak, E., "Towards a semiclassical description of QCD vacuum around $T_c$", *Phys. Rev. D*, vol. 102, no. 3, p. 034 501, 2020. arXiv: 1912.09141 [hep-lat] (cit. on p. 102).

[294] Duane, S., Kennedy, A., Pendleton, B. J., and Roweth, D., "Hybrid Monte Carlo", *Phys. Lett. B*, vol. 195, no. 2, pp. 216–222, 1987 (cit. on p. 102).

[295] Velytsky, A., "Finite temperature SU(2) gauge theory: critical coupling and universality class", *Int. J. Mod. Phys. C*, vol. 19, pp. 1079–1093, 2008. arXiv: 0711.0748 [hep-lat] (cit. on pp. 103, 104).

[296] Lüscher, M., "Properties and uses of the Wilson flow in lattice QCD", *JHEP*, vol. 08, p. 071, 2010, [Erratum: JHEP 03, 092 (2014)]. arXiv: 1006.4518 [hep-lat] (cit. on p. 103).

[297] Fukushima, K. and Skokov, V., "Polyakov loop modeling for hot QCD", *Prog. Part. Nucl. Phys.*, vol. 96, pp. 154–199, 2017. arXiv: 1705.00718 [hep-ph] (cit. on pp. 104–106).

[298] Engels, J., Mashkevich, S, Scheideler, T, and Zinovjev, G, "Critical behaviour of SU(2) lattice gauge theory. A complete analysis with the $\chi$2-method", *Phys. Lett. B*, vol. 365, pp. 219–224, 1996. arXiv: hep-lat/9509091 (cit. on p. 104).

[299] Fortunato, S. and Satz, H., "Polyakov loop percolation and deconfinement in su (2) gauge theory", *Phys. Lett. B*, vol. 475, pp. 311–314, 2000. arXiv: hep-lat/9911020 (cit. on pp. 106, 111).

[300] Langfeld, K. and Pawlowski, J. M., "Two-color QCD with heavy quarks at finite densities", *Phys. Rev. D*, vol. 88, no. 7, p. 071 502, 2013. arXiv: 1307.0455 [hep-lat] (cit. on p. 106).

[301] Ford, C, Mitreuter, U., Tok, T, Wipf, A, and Pawlowski, J., "Monopoles, Polyakov loops, and gauge fixing on the torus", *Annals Phys.*, vol. 269, pp. 26–50, 1998. arXiv: hep-th/9802191 (cit. on p. 112).

[302] Larsen, R. and Shuryak, E., "Classical interactions of the instanton-dyons with antidyons", *Nucl. Phys. A*, vol. 950, pp. 110–128, 2016. arXiv: 1408.6563 [hep-ph] (cit. on pp. 113, 117).

[303] Bonati, C. and D'Elia, M., "Comparison of the gradient flow with cooling in $SU(3)$ pure gauge theory", *Phys. Rev. D*, vol. 89, no. 10, p. 105 005, 2014. arXiv: 1401.2441 [hep-lat] (cit. on p. 122).

[304] Di Vecchia, P, Fabricius, K, Rossi, G., and Veneziano, G, "Preliminary evidence for $U_A(1)$ breaking in QCD from lattice calculations", *Nucl. Phys. B*, vol. 192, p. 392, 1981 (cit. on p. 123).

[305] Georgi, H. and Glashow, S. L., "Unity of all elementary particle forces", *Phys. Rev. Lett.*, vol. 32, pp. 438–441, 1974 (cit. on p. 131).

[306] Nath, P. and Fileviez Perez, P., "Proton stability in grand unified theories, in strings and in branes", *Phys. Rept.*, vol. 441, pp. 191–317, 2007. arXiv: hep-ph/0601023 (cit. on p. 131).

[307] Bergshoeff, E., Figueroa-O'Farrill, J., and Gomis, J., "A non-Lorentzian primer", Jun. 2022. arXiv: 2206.12177 [hep-th] (cit. on pp. 132, 135).

[308] Inönü, E. and Wigner, E. P., "On the contraction of groups and their representations", *PNAS*, vol. 39, no. 6, pp. 510–524, 1953 (cit. on pp. 132, 137).

[309] Cooper, D., Danciger, J., and Wienhard, A., "Limits of geometries", *Trans. Amer. Math. Soc.*, vol. 370, no. 9, pp. 6585–6627, 2018 (cit. on pp. 132, 134, 135, 171–175).

[310] Gutowski, J. B. and Reall, H. S., "Supersymmetric AdS(5) black holes", *JHEP*, vol. 02, p. 006, 2004. arXiv: hep-th/0401042 (cit. on p. 132).

[311] Kaul, R. K. and Sengupta, S., "Degenerate spacetimes in first order gravity", *Phys. Rev. D*, vol. 93, no. 8, p. 084 026, 2016. arXiv: 1602.04559 [gr-qc] (cit. on p. 132).

[312] Bagchi, A., Banerjee, A., and Muraki, H., "Boosting to BMS", *JHEP*, vol. 09, p. 251, 2022. arXiv: 2205.05094 [hep-th] (cit. on p. 132).

[313] Faedo, F., Klemm, S., and Mariotti, P., "Rotating black holes with Nil or $SL(2, \mathbb{R})$ horizons", Dec. 2022. arXiv: 2212.04890 [hep-th] (cit. on p. 132).

[314] Parker, L. E. and Toms, D., *Quantum field theory in curved spacetime: quantized field and gravity* (Cambridge Monographs on Mathematical Physics). Cambridge University Press, Aug. 2009 (cit. on p. 132).

[315] Wald, R. M., *Quantum field theory in curved space-time and black hole thermodynamics* (Chicago Lectures in Physics). Chicago, IL: University of Chicago Press, 1995 (cit. on p. 132).

[316] Hollands, S. and Wald, R. M., "Quantum fields in curved spacetime", *Phys. Rept.*, vol. 574, pp. 1–35, 2015. arXiv: 1401.2026 [gr-qc] (cit. on pp. 132, 153).

[317] Fredenhagen, K. and Rejzner, K., "Quantum field theory on curved spacetimes: axiomatic framework and examples", *J. Math. Phys.*, vol. 57, no. 3, p. 031 101, 2016. arXiv: 1412.5125 [math-ph] (cit. on p. 132).

[318] Haag, R., *Local quantum physics. Fields, particles, algebras*. Springer Berlin, Heidelberg, 1996 (cit. on pp. 132, 141, 142, 155, 177).

[319] Ovsienko, V. and Tabachnikov, S., *Projective differential geometry old and new: from the Schwarzian derivative to the cohomology of diffeomorphism groups*. Cambridge University Press, 2004, vol. 165 (cit. on p. 134).

[320] Gallier, J., "Basics of projective geometry", in *Geometric Methods and Applications: For Computer Science and Engineering*. New York, NY: Springer New York, 2011, pp. 103–175 (cit. on pp. 134, 138).

[321] Ciambelli, L., Leigh, R. G., Marteau, C., and Petropoulos, P. M., "Carroll structures, null geometry and conformal isometries", *Phys. Rev. D*, vol. 100, no. 4, p. 046 010, 2019. arXiv: 1905.02221 [hep-th] (cit. on p. 135).

[322] Fisher, S and Gartside, P, "On the space of subgroups of a compact group I", *Topol. Appl.*, vol. 156, no. 5, pp. 862–871, 2009 (cit. on p. 135).

[323] Fisher, S and Gartside, P, "On the space of subgroups of a compact group II", *Topol. Appl.*, vol. 156, no. 5, pp. 855–861, 2009 (cit. on p. 135).

[324] Biringer, I., "Metrizing the Chabauty topology", *Geom. Dedicata*, vol. 195, no. 1, pp. 19–22, 2018 (cit. on p. 135).

[325] Trettel, S. J., "Families of geometries, real algebras, and transitions", Ph.D. dissertation, UC Santa Barbara, 2019 (cit. on pp. 135, 171, 175).

[326] Dooley, A. H. and Rice, J., "On contractions of semisimple Lie groups", *Trans. Amer. Math. Soc.*, vol. 289, no. 1, pp. 185–202, 1985 (cit. on pp. 137, 172).

[327] Whitehead, J. H. C., "The representation of projective spaces", *Ann. Math.*, pp. 327–360, 1931 (cit. on pp. 137, 183).

[328] Tanaka, N., "Projective connections and projective transformations", *Nagoya Math. J.*, vol. 12, pp. 1–24, 1957 (cit. on p. 137).

[329] Eastwood, M., "Notes on projective differential geometry", in *Symmetries and Overdetermined Systems of Partial Differential Equations*, M. Eastwood and W. Miller, Eds. New York, NY: Springer New York, 2008, pp. 41–60 (cit. on pp. 137, 183).

[330] Aghanim, N. *et al.*, "Planck 2018 results. VI. Cosmological parameters", *Astron. Astrophys.*, vol. 641, A6, 2020, [Erratum: Astron.Astrophys. 652, C4 (2021)]. arXiv: 1807.06209 [astro-ph.CO] (cit. on p. 140).

[331] O'Neill, B., *Semi-Riemannian geometry with applications to relativity*. San Diego, California: Academic Press, 1983 (cit. on p. 141).

[332] Borchers, H. J., "On revolutionizing quantum field theory with Tomita's modular theory", *J. Math. Phys.*, vol. 41, pp. 3604–3673, 2000 (cit. on pp. 142, 155).

[333] Mackey, G. W., *Induced representations of groups and quantum mechanics*. WA Benjamin, 1968 (cit. on p. 142).

[334] Weibel, C. A., *An introduction to homological algebra*. Cambridge, England: Cambridge University Press, 1994 (cit. on p. 145).

[335] Roger, C., "Extensions centrales d'algèbres et de groupes de Lie de dimension infinie, algèbre de Virasoro et généralisations", *Rep. Math. Phys.*, vol. 35, no. 2-3, pp. 225–266, 1995 (cit. on p. 145).

[336] Streater, R. F. and Wightman, A. S., *PCT, spin and statistics, and all that*. Princeton, New Jersey: Princeton University Press, 2000, vol. 30 (cit. on p. 148).

[337] Verch, R., "A spin statistics theorem for quantum fields on curved space-time manifolds in a generally covariant framework", *Commun. Math. Phys.*, vol. 223, pp. 261–288, 2001. arXiv: math-ph/0102035 (cit. on p. 148).

[338] Tung, W.-K., *Group theory in physics*. Singapore: World Scientific, 1985, vol. 1 (cit. on pp. 149, 150).

[339] Fulton, W. and Harris, J., *Representation theory: a first course*. New York, New York: Springer Science & Business Media, 2013, vol. 129 (cit. on pp. 149, 150).

[340] Bekaert, X. and Boulanger, N., "The unitary representations of the Poincaré group in any spacetime dimension", *SciPost Phys. Lect. Notes*, vol. 30, p. 1, 2021. arXiv: hep-th/0611263 (cit. on p. 149).

[341] Molnár, E., "The projective interpretation of the eight 3-dimensional homogeneous geometries." *Beiträge zur Algebra und Geometrie*, vol. 38, pp. 261–288, 1997 (cit. on p. 152).

[342] Thiel, B., *Einheitliche Beschreibung der acht Thurstonschen Geometrien*. Diplomarbeit, Universitat zu Göttingen, 1997 (cit. on p. 152).

[343] Ortin, T., *Gravity and strings* (Cambridge Monographs on Mathematical Physics), 2nd ed. Cambridge University Press, Jul. 2015 (cit. on p. 154).

[344] Floerchinger, S. and Grossi, E., "Conserved and nonconserved Noether currents from the quantum effective action", *Phys. Rev. D*, vol. 105, no. 8, p. 085 015, 2022. arXiv: 2102.11098 [hep-th] (cit. on p. 154).

[345] Gardiner, C. and Zoller, P., *Quantum noise: a handbook of Markovian and non-Markovian quantum stochastic methods with applications to quantum optics*. Springer Science & Business Media, 2004 (cit. on p. 157).

[346] Coleman, S. R. and Mandula, J., "All possible symmetries of the $S$ matrix", *Phys. Rev.*, vol. 159, A. Zichichi, Ed., pp. 1251–1256, 1967 (cit. on pp. 170, 183).

[347] Nesterenko, M. and Popovych, R., "Contractions of low-dimensional Lie algebras", *J. Math. Phys.*, vol. 47, no. 12, p. 123 515, 2006 (cit. on p. 172).

[348] Leitner, A., "Limits under conjugacy of the diagonal subgroup in $SL_n\mathbb{R}$", *Proc. Amer. Math. Soc.*, vol. 144, no. 8, pp. 3243–3254, 2016 (cit. on p. 175).

[349] Cirac, J. I. and Zoller, P., "Goals and opportunities in quantum simulation", *Nature Phys.*, vol. 8, no. 4, pp. 264–266, 2012 (cit. on p. 181).

[350] Georgescu, I. M., Ashhab, S., and Nori, F., "Quantum simulation", *Rev. Mod. Phys.*, vol. 86, p. 153, 2014. arXiv: 1308.6253 [quant-ph] (cit. on p. 181).

[351] Wiese, U.-J., "Ultracold quantum gases and lattice systems: quantum simulation of lattice gauge theories", *Ann. Phys.*, vol. 525, no. 10-11, pp. 777–796, 2013. arXiv: 1305.1602 [quant-ph] (cit. on p. 181).

[352] Zohar, E., Cirac, J. I., and Reznik, B., "Quantum simulations of lattice gauge theories using ultracold atoms in optical lattices", *Rept. Prog. Phys.*, vol. 79, no. 1, p. 014 401, 2016. arXiv: 1503.02312 [quant-ph] (cit. on p. 181).

[353] Bañuls, M. C. *et al.*, "Simulating lattice gauge theories within quantum technologies", *Eur. Phys. J. D*, vol. 74, no. 8, p. 165, 2020. arXiv: 1911.00003 [quant-ph] (cit. on p. 181).

[354] Kokail, C. *et al.*, "Self-verifying variational quantum simulation of lattice models", *Nature*, vol. 569, no. 7756, pp. 355–360, 2019. arXiv: 1810.03421 [quant-ph] (cit. on p. 181).

[355] Yang, B., Sun, H., Ott, R., Wang, H.-Y., Zache, T. V., Halimeh, J. C., Yuan, Z.-S., Hauke, P., and Pan, J.-W., "Observation of gauge invariance in a 71-site Bose–Hubbard quantum simulator", *Nature*, vol. 587, no. 7834, pp. 392–396, 2020. arXiv: 2003.08945 [cond-mat.quant-gas] (cit. on p. 181).

[356] Zohar, E., "Quantum simulation of lattice gauge theories in more than one space dimension—requirements, challenges and methods", *Phil. Trans. A. Math. Phys. Eng. Sci.*, vol. 380, no. 2216, p. 20 210 069, 2021. arXiv: 2106.04609 [quant-ph] (cit. on p. 181).

[357] Bray, A. J., "Theory of phase-ordering kinetics", *Adv. Phys.*, vol. 43, p. 357, 1994. arXiv: cond-mat/9501089 (cit. on p. 182).

[358]  Karl, M. and Gasenzer, T., "Strongly anomalous non-thermal fixed point in a quenched two-dimensional Bose gas", *New J. Phys.*, vol. 19, no. 9, p. 093 014, 2017. arXiv: 1611.01163 [cond-mat.quant-gas] (cit. on p. 182).

[359]  Schmied, C.-M., Prüfer, M., Oberthaler, M. K., and Gasenzer, T., "Bidirectional universal dynamics in a spinor Bose gas close to a nonthermal fixed point", *Phys. Rev. A*, vol. 99, no. 3, p. 033 611, 2019. arXiv: 1812.08571 [cond-mat.quant-gas] (cit. on p. 182).

[360]  Lannig, S., "Vector solitons and different scenarios of universal dynamics in a spin-1 Bose-Einstein condensate.", Ph.D. dissertation, University of Heidelberg, 2022 (cit. on p. 182).

[361]  Goldenfeld, N., *Lectures on phase transitions and the renormalization group*. CRC Press, 2018 (cit. on p. 182).

[362]  Wang, L., "Discovering phase transitions with unsupervised learning", *Phys. Rev. B*, vol. 94, no. 19, p. 195 105, 2016. arXiv: 1606.00318 [cond-mat.stat-mech] (cit. on p. 182).

[363]  Van Nieuwenburg, E. P., Liu, Y.-H., and Huber, S. D., "Learning phase transitions by confusion", *Nature Phys.*, vol. 13, no. 5, pp. 435–439, 2017. arXiv: 1610.02048 [cond-mat.dis-nn] (cit. on p. 182).

[364]  Carrasquilla, J. and Melko, R. G., "Machine learning phases of matter", *Nature Phys.*, vol. 13, no. 5, pp. 431–434, 2017 (cit. on p. 182).

[365]  Venderley, J., Khemani, V., and Kim, E.-A., "Machine learning out-of-equilibrium phases of matter", *Phys. Rev. Lett.*, vol. 120, no. 25, p. 257 204, 2018. arXiv: 1711.00020 [dis-nn] (cit. on p. 182).

[366]  Giannetti, C., Lucini, B., and Vadacchino, D., "Machine learning as a universal tool for quantitative investigations of phase transitions", *Nucl. Phys. B*, vol. 944, p. 114 639, 2019. arXiv: 1812.06726 [cond-mat.stat-mech] (cit. on p. 182).

[367]  Rodriguez-Nieva, J. F. and Scheurer, M. S., "Identifying topological order through unsupervised machine learning", *Nature Phys.*, vol. 15, no. 8, pp. 790–795, 2019. arXiv: 1805.05961 [cond-mat.stat-mech] (cit. on p. 182).

[368]  Carrasquilla, J., "Machine learning for quantum matter", *Adv. Phys. X*, vol. 5, no. 1, p. 1 797 528, 2020. arXiv: 2003.11040 [physics.comp-ph] (cit. on p. 182).

[369]  Bachtis, D., Aarts, G., and Lucini, B., "Mapping distinct phase transitions to a neural network", *Phys. Rev. E*, vol. 102, no. 5, p. 053 306, 2020. arXiv: 2007.00355 [cond-mat.stat-mech] (cit. on p. 182).

[370]  Carleo, G. and Troyer, M., "Solving the quantum many-body problem with artificial neural networks", *Science*, vol. 355, no. 6325, pp. 602–606, 2017. arXiv: 1606.02318 [cond-mat.dis-nn] (cit. on p. 182).

[371] Carleo, G., Cirac, I., Cranmer, K., Daudet, L., Schuld, M., Tishby, N., Vogt-Maranto, L., and Zdeborová, L., "Machine learning and the physical sciences", *Rev. Mod. Phys.*, vol. 91, no. 4, p. 045 002, 2019. arXiv: 1903.10563 [physics.comp-ph] (cit. on p. 182).

[372] Wetzel, S. J. and Scherzer, M., "Machine learning of explicit order parameters: From the Ising model to SU(2) lattice gauge theory", *Phys. Rev. B*, vol. 96, no. 18, p. 184 410, 2017. arXiv: 1705.05582 [cond-mat.stat-mech] (cit. on p. 182).

[373] Hu, W., Singh, R. R., and Scalettar, R. T., "Discovering phases, phase transitions, and crossovers through unsupervised machine learning: a critical examination", *Phys. Rev. E*, vol. 95, no. 6, p. 062 122, 2017. arXiv: 1704.00080 [cond-mat.stat-mech] (cit. on p. 182).

[374] Blücher, S., Kades, L., Pawlowski, J. M., Strodthoff, N., and Urban, J. M., "Towards novel insights in lattice field theory with explainable machine learning", *Phys. Rev. D*, vol. 101, no. 9, p. 094 507, 2020. arXiv: 2003.01504 [hep-lat] (cit. on p. 182).

[375] Wetzel, S. J., Melko, R. G., Scott, J., Panju, M., and Ganesh, V., "Discovering symmetry invariants and conserved quantities by interpreting siamese neural networks", *Phys. Rev. Res.*, vol. 2, no. 3, p. 033 499, 2020. arXiv: 2003.04299 [physics.comp-ph] (cit. on p. 182).

[376] Kanwar, G., Albergo, M. S., Boyda, D., Cranmer, K., Hackett, D. C., Racaniere, S., Rezende, D. J., and Shanahan, P. E., "Equivariant flow-based sampling for lattice gauge theory", *Phys. Rev. Lett.*, vol. 125, no. 12, p. 121 601, 2020. arXiv: 2003.06413 [hep-lat] (cit. on p. 182).

[377] Boyda, D., Kanwar, G., Racanière, S., Rezende, D. J., Albergo, M. S., Cranmer, K., Hackett, D. C., and Shanahan, P. E., "Sampling using SU($N$) gauge equivariant flows", *Phys. Rev. D*, vol. 103, no. 7, p. 074 504, 2021. arXiv: 2008.05456 [hep-lat] (cit. on p. 182).

[378] Favoni, M., Ipp, A., Müller, D. I., and Schuh, D., "Lattice gauge equivariant convolutional neural networks", *Phys. Rev. Lett.*, vol. 128, no. 3, p. 032 003, 2022. arXiv: 2012.12901 [hep-lat] (cit. on p. 182).

[379] Abbott, R. *et al.*, "Gauge-equivariant flow models for sampling in lattice field theories with pseudofermions", 2022. arXiv: 2207.08945 [hep-lat] (cit. on p. 182).

[380] Thomas, T. Y., "On the projective and equi-projective geometries of paths", *Proc. Natl. Acad. Sci.*, vol. 11, no. 4, pp. 199–203, 1925 (cit. on p. 183).

[381] Hall, G. S. and Lonie, D., "The principle of equivalence and projective structure in spacetimes", *Class. Quantum Gravity*, vol. 24, no. 14, p. 3617, 2007. arXiv: 0703104 [gr-qc] (cit. on p. 183).

[382] Brensinger, S., Heitritter, K., Rodgers, V. G. J., and Stiffler, K., "General structure of Thomas−Whitehead gravity", *Phys. Rev. D*, vol. 103, no. 4, p. 044 060, 2021. arXiv: 2009.06730 [hep-th] (cit. on p. 183).